A Theoretical Analysis of Interstitial Hydrogen: Pressure-Composition-Temperature, Chemical Potential, Enthalpy and Entropy

by

Peter Omondi Orondo

B.Sc., Electrical Science and Engineering
Massachusetts Institute of Technology, 1995

M.Eng., Electrical Engineering and Computer Science
Massachusetts Institute of Technology, 1997

Submitted to the Department of Electrical Engineering and Computer Science in Partial Fulfillment of the Requirements for the Degree of

DOCTOR OF PHILOSOPHY IN ELECTRICAL ENGINEERING AND COMPUTER SCIENCE

at the Massachusetts Institute of Technology

September 2012

Signature of Author:_____
Department of Electrical Engineering and Computer Science
June 22, 2012

Certified by:_____
Peter L. Hagelstein
Associate Professor of Electrical Engineering and Computer Science
Thesis Supervisor

Accepted by:_____
Leslie A. Kolodziejski
Professor of Electrical Engineering and Computer Science
Chair, Committee for Graduate Students

Dedication

This thesis is dedicated to the current (Amisi, Odundo and Quintabella) and future members of the Omondi Family. It is my sincere hope that this work plays a part, however small, in inspiring a passion for learning, knowledge and discovery.

I would also like to dedicate the thesis to my mother, Penina Odundo Omolo, and late father, Caleb Orondo Omolo.

Acknowledgements

I would like to acknowledge all my teachers for their inspiration and wisdom:

All my Nyaoke Primary School (1979-1986) teachers helped me form a strong foundation. I thank **all** of you, and especially – Mrs. Ojijo, Mr. Ngani, Mr. Omari, Mr. Odondi, Mr. Omolo, and above all my dad Mr. C. O. Omolo.

All my Alliance High School (1987-1990) teachers challenged me to achieve my full potential. Thank you **all**, but especially Mr. F. Geke, Mr. Mwangi, Mr. Ondong, Mrs. Murila and above all, Mr. Khaemba.

All my MIT professors (1991-1997,1998-2000,2009-2012). I would especially like to thank Prof. C. Warde, Prof. T. P. Orlando, Prof. J. Kong, Dr. B. Little, Dr. V. Shrauger and above all my thesis advisor Prof. Hagelstein.

A Theoretical Analysis of Interstitial Hydrogen: Pressure-Composition-Temperature, Chemical Potential, Enthalpy and Entropy

by

Peter Omondi Orondo

Submitted to the Department of Electrical Engineering and Computer Science in Partial Fulfillment of the Requirements for the Degree of

DOCTOR OF PHILOSOPHY IN ELECTRICAL ENGINEERING AND COMPUTER SCIENCE

ABSTRACT

We provide a first principles analysis of the physics and thermodynamics of interstitial hydrogen in metal. By utilizing recent advances in Density Functional Theory (DFT) to get state energies of the metal-hydrogen system, we are able to model the absorption process fairly accurately. A connection to experiment is made via Pressure-Composition-Temperature (PCT) isotherms, and thermodynamic molar quantities.

In the model, we understand the excess entropy of absorbed hydrogen in terms of the change in its accessible microstates. A connection is also made between the entropy and electronic states of interstitial hydrogen. However, our model indicates that this connection is too small to account for experimental results. Therefore, a conclusion is made that the entropy of absorbed hydrogen is mostly (non-ideal) configurational in nature.

To model the latter in a manner consistent with experiment, we have explored a new model that posits a weak binding between clusters of hydrogen atoms at neighboring sites. We have developed a formulation and fitted the results to experimental data. We find a least squares fitting of the model to the entropy and enthalpy results in model parameters which seem physically reasonable. The resulting model appears to provide a natural physical explanation for the dependence of the excess entropy on loading.

Prof. Peter L. Hagelstein, Associate Professor of Electrical Engineering and Computer Science

Prof. Cardinal Warde, Professor of Electrical Engineering and Computer Science

Dr. Louis F. Dechiaro, Scientist, United States Navy

II – Preface / How to Read This Thesis

This work is organized approximately in the chronological order of research. We have included the main results at each point, even if those results are improved upon subsequently. As a consequence, the flow of ideas is not generally linear because some investigative paths were not found to be fruitful. A consistent theme through the work is to keep the model grounded firmly on first principles. Thus, wherever possible, foundational results are derived rather than stated, and the thesis is organized in such a way as to make its results easily reproducible.

In Chapter 1, we give a brief overview of the main topics of investigation, beginning with a very broad statement of the problem. This is followed by a summary of DFT theory and a preliminary analysis of a related problem of a water dipole. Finally we present some preliminary results from first principles DFT calculations.

Chapter 2 presents the basic statistical mechanics formulation to derive the chemical potential of interstitial hydrogen. The basic model is extended to include tetrahedral occupation using a basic excitation type model (which we derive and solve for *ab initio*). A connection to DFT is made within the grand partition function formalism, leading to (PCT) isotherms that we compare to experiment via a metal/gas boundary condition match. This chapter also introduces an interaction energy solution that was successfully used to validate initial versions of the PCT model.

Chapter 3 presents a preliminary Phase Diagram calculation for the PdH system using the Rule of Equal Areas.

Chapters 4, 5, 6 and 8 detail probative investigations that we used to determine whether results of DFT would be good enough for use as state energies within our basic model. We do this by using DFT to solve for well known problems. We also presented a summary of the underlying theory of DFT with a view to interpreting contracted quantities.

In Chapters 7 we present a first principles analytical model for enthalpy and entropy based on a connection to the basic model from Chapter 2. We use the results to model enthalpy changes during the absorption process, and attempt to understand the entropy in terms of the excess accessible microstates of the absorbed hydrogen. Each time, a comparison is made to experiment.

In Chapter 9, we present a new model of interstitial hydrogen in terms of a simple binding energy model. The result is a clumping type isotherm that we connect to thermodynamic molar quantities from experiment.

In Chapter 10, we attempt another model refinement by adding a nearest neighbor exclusion component, whereby the absorption process is modeled to occur in isolated clumps. The results are compared to prior models. Additionally, we make an attempt at understanding the electronic

states of the absorbed hydrogen, distinct from those of the protium. We explore two such electronic approximations and compare their contributions to the protons'.

Finally in Chapter 11, we derive the phase diagram from the improved models of Chapters 9 and 10. Additionally, we add temperature dependence as a key part of the model.

♦

A chronological reading of the above chapters will deliver the best understanding of the work presented. However , for those already familiar with the material, the beginning of the thesis (Chapters 1-6, 8) may be skimmed followed by a poring over the latter chapters (7, 9-11).

III – Contents

IV – Figures

Chapter 1 - Introduction & Preliminary Analysis

Introduction

Electrochemical loading of metals in base has been known for a long time. Palladium hydride, for example, is metallic palladium with a large number of hydrogen atoms within its crystalline lattice. Such metallic hydrides have many applications, including hydrogen storage, energy conversion, and even catalytic conversion, such that a fundamental understanding of the process is of significant interest.

Hydrogen loading of metals is thought to occur primarily through the following three processes (Green & Britz, 1996):

Volmer Process

Volmer is the primary process whereby hydrogen loads palladium. During a Volmer reaction, one hydrogen atom gets adsorbed on the surface of palladium to begin the loading process.

For each adsorbed hydrogen atom, a single electrochemical charge exchange takes place according to the following:

$$H_2O + e^- + M \rightleftharpoons MH_{ads} + OH^- \quad (1)$$

It is thought that the adsorbed hydrogen, H_{ads}, then diffuses into the metal lattice and occupies either an octahedral site (energetically preferred – see preliminary results below) or a tetrahedral site under the influence of electrochemical potential.

Tafel Process

Tafel is another process to consider in metallic loading by hydrogen in base. Tafel process is believed to be the primary process by which adsorbed hydrogen leaves the surface:

$$MH_{ads} + MH_{ads} \rightleftharpoons M + H_2\ (gas) \quad (2)$$

Again, there is a corresponding electrochemical charge for each hydrogen atom that leaves the adsorbed state.

Heyrovsky Process

In the high loading regime, adsorbed hydrogen is lost through the Heyrovsky Process:

$$H_2O + MH_{ads} \rightleftharpoons M + H_2 + OH^- \quad (3)$$

Heyrovsky leads to loss of hydrogen from the lattice at high loading.

Adsorbed-Absorption Exchange

We will also consider one last reaction, namely the exchange between adsorbed and diffused hydrogen according to the following

$$H_{ads} \rightleftharpoons H_{abs} \quad (4)$$

This process is electrochemically neutral since there is no charge exchange.

Gas Pressure Loading

Even though we have formulated the loading process in electrochemical terms, loading may also be achieved under gas pressure as described in following chapters. Regardless of the loading method, the thermodynamics and solid state physics of the absorbed hydrogen are the same.

A First Principles Look at Volmer, Tafel & Heyrovsky

Introduction

Our aim in this work is to conduct a systematic study of the three processes above from first principles.

Quantum Physics Formulation

At a fundamental level, the problem of electrochemical interface may be modeled quantum mechanically. This involves solving the Schrodinger Equation whereby constituent particles of the system are described by a wave function $\Psi(r)$ which describes the probability of finding the particle at a given position r. In our case the particles are electrons & protons of the metallic electrode and ionic electrolyte. In its time independent form (when discussing bound states), the Schrodinger Equation is:

$$\hat{H}(r)\Psi(r) = E\Psi(r) \quad (5)$$

where $\hat{H}(\mathrm{r})$ is the Hamiltonian operator and E is the total N-particle system energy.

The Hamiltonian operator is generally decomposed into its potential and kinetic energy components, thus

$$\hat{H}(\mathrm{r}) = \hat{T} + \hat{V} + \hat{U} \quad (6)$$

$$\hat{T} = -\sum_{i=1}^{N} \frac{\hbar^2}{2m_i} \nabla_i^2 \quad (7)$$

for kinetic energy and

$$\hat{V} = \sum_{i=1}^{N} V(r_i) \quad (8)$$

for potential energy, representing the potential energy experienced by the electrons due to the positively charged nuclei, and

$$\hat{U} = \sum_{i=1}^{N} U(r_i) = \frac{1}{2} \sum_{i \neq j}^{N} \frac{e^2}{|r_i - r_j|} \quad (9)$$

is the electron-electron interaction term.

For the system of interest here (a number of electrons and protons – details of which we will discuss later), Equation 5 is generally very difficult to solve exactly or even approximately. We therefore need some simplifying assumptions to make the problem slightly less difficult.

The Born-Oppenheimer Approximation

In the system we model (electrons and protons) the mass of the electron is much lighter than that of the proton. This makes it possible to separate electronic and nuclear dynamics, to a good approximation. Essentially, the Born-Oppenheimer approximation posits that we can compute electronic wave function while assuming a fixed nuclear geometry:

$$\Psi(\boldsymbol{r}, \boldsymbol{R}) = \Phi(\boldsymbol{R})\psi(\boldsymbol{r}; \boldsymbol{R}) \quad (10)$$

where $\boldsymbol{R}$ denotes a particular nuclear geometry, and $\psi(\boldsymbol{r}; \boldsymbol{R})$ is the resulting electronic orbital assuming $\boldsymbol{R}$. As is customary, we will make $\boldsymbol{R}$ dependence implicit and write $\psi(\boldsymbol{r}; \boldsymbol{R})$ simply as $\psi(\boldsymbol{r})$.

Using this approximation, we can calculate the electronic energy of the system, to which we can add the classical nuclear energy (since wave-component of the nuclear energy can be neglected to a very good approximation) to obtain the total system energy. We can imagine repeating this for a large number of nuclear geometry configurations. Obviously such configurations would be

connected to our hypothesis of the physical system, but nonetheless, we would then obtain a Potential Energy Surface (PES). The PES then forms the basis for solving the nuclear dynamics.

Density Functional Theory

To calculate electronic energies, we have chosen the Density Functional Theory (DFT) as an *ab initio* method. DFT was introduced in 1964 by Kohn and Sham (Hohenberg & Kohn, 1964), (Kohn & Sham, 1965), and supplants the related but older Hartree-Slater theory which was found to be very computationally expensive and inaccurate at predicting physical solid state properties.

The basic idea behind DFT is that, based solely on fundamental properties of constituent atoms (their atomic number), we should be able to determine physical properties using quantum mechanics. Specifically, DFT provides a theoretical framework whereby physical features of an ensemble system may be determined from the ground state electronic density only (Kohn & Sham, 1965), (Fall, 1999). We shall outline the key elements of DFT here (and also in Chapter 5), following the treatment and formulation of Martin and Baer (Martin, 2004), (Baer, 2009), while referring the reader to the cited texts for the intricate details of the theory.

♦

From an experimental point of view, it turns out that we can extract physically meaningful quantities using contracted quantities, thereby averting the need to solve Equation 5 exactly. DFT uses the electron density, $\boldsymbol{n}(r)$ as a contracted quantity. In DFT, a rigorous theorem by Kohn and Sham (Kohn & Sham, 1965), which we will not present here in full detail, proves that the knowledge of the ground state electronic density is sufficient to determine all the physical properties of the system. In particular, we may write the electronic density $\boldsymbol{n}(r)$, as the expectation value of the density operator,

$$\hat{\boldsymbol{n}}(\boldsymbol{r}) = \sum_{i=1}^{N} \delta(r - r_i) \qquad 11$$

$$\boldsymbol{n}(\boldsymbol{r}) = \frac{\langle \Psi | \hat{\boldsymbol{n}}(\boldsymbol{r}) | \Psi \rangle}{\langle \Psi | \Psi \rangle} = N \frac{\int d^3r_2 \int d^3r_3 \cdots \int d^3r_N \, \Psi^*(r, r_2, r_3, \cdots, r_N)\Psi(r, r_2, r_3, \cdots, r_N)}{\int d^3r_1 \int d^3r_2 \cdots \int d^3r_N \, \Psi^*(r, r_1, r_2, r_3, \cdots, r_N)\Psi(r, r_2, r_3, \cdots, r_N)} \qquad 12$$

We may invert Equation 12 if we knew the ground state electronic density function, $\boldsymbol{n_0}(r)$, to get the ground state wave function $\Psi_0(r_2, \cdots, r_N)$:

$$\Psi_0(r_2, \cdots, r_N) = \Psi_0[\boldsymbol{n_0}(r)] \tag{13}$$

Equation 13 expresses the wave function as a *functional* of electron density, and from it we can get the ground state expectation value of any observable according to

$$O[n_0] = \langle \Psi_0[\boldsymbol{n_0}] | \hat{O}[n_0] | \Psi_0[\boldsymbol{n_0}] \rangle \tag{14}$$

Similarly, one may also obtain the ground state energy, thus:

$$E[n_0] = \langle \Psi_0[\boldsymbol{n_0}] | \hat{T} + \hat{U} + \hat{V} | \Psi_0[\boldsymbol{n_0}] \rangle \tag{15}$$

Equation 15 may be minimized to obtain ground state electron density $\boldsymbol{n_0}(r)$, i.e. Equation 15 is a minimum when $\boldsymbol{n}(r) = \boldsymbol{n_0}(r)$. More generally, we may express the total system energy as a functional of the electron density:

$$E[n(r)] = F[n] + \int v_{ext}(r) n(r) d^3r \tag{16}$$

where

$$F[n] = \langle \hat{T} \rangle + \langle \hat{U} \rangle \tag{17}$$

and we have expressed the potential energy due to nuclear interaction as a simple integral over electron density function. We have also labeled this potential "external" since it is considered external to the electronic interaction. Furthermore, as is traditionally done in DFT, we note that the functional $F[n]$ is universal in the sense that it does not change from one molecule to

A Preliminary Analysis

In this section, we will present some preliminary analysis that we have done in the course of our investigation. These analyses start at what we believe is the natural starting point, namely the surface chemistry of a metal.

Water Adsorption on a Metallic Surface

We will first look at the adsorption of water on Pd(111) surface. While this is a reasonably well studied problem (Cao & Chen, 2006), (Michaelides, Alavi, & King, 2003), (Michaelides, Alavi, & King, 2004), (Meng, Wang, & Gao, 2004), and others, it is a problem that closely relates to our original goals since it is a precursor of the Volmer Process.

Water is known to adsorb weakly on a clean Pd(111) surface (Cao & Chen, 2006). This has been confirmed by both theoretical calculations e.g. (Cao & Chen, 2006), but also experimentally (Mitsui, Rose, Fomin, Ogletree, & Salmeron, 2002). The theoretical studies using DFT have also revealed that H2O adsorption is aided by other co-adsorbates, for example OH (Cao & Chen, 2006), (Michaelides, Alavi, & King, 2003).

What remains less well understood are the precise processes leading to the H2O adsorption. For example, it is not clear which sites are favored for the adsorption and what orientation of the water molecule is favored. Previous works have clearly made an attempt at this e.g. (Michaelides, Alavi, & King, 2003), but there is still no consistent picture of where H2O adsorbs on the Pd(111) surface and with what orientation.

To gain better insight into this problem, we will begin by addressing a much simpler problem: the interaction of the H2O dipole with a uniform electric field.

The Microscopic Water Molecule

Macroscopically, water dipole tends to align with an external electric field since the external field creates an orienting torque given by

$$\boldsymbol{\tau} = \boldsymbol{p} \times \boldsymbol{E_0} \qquad 20$$

where $\boldsymbol{p}$ is the water molecule's dipole moment and $\boldsymbol{E_0}$ is the applied electric field.

another. As Baer puts it, "the identity of system is captured by the external potential $v_{ext}(r)$" (Baer, 2009).

The basic problem of DFT, and also its major theoretical breakthrough, is contained in minimizing Equation 17 for a given number of particles. A theorem of DFT due to Kohn (Kohn & Sham, 1965) states that the electron density that minimizes the energy of Equation 17 must be the exact ground state electronic energy. For a system of N-particles, we have

$$\int d^3r\, n(r) = N \tag{18}$$

therefore, the constrained Langragian of Equation 17 becomes

$$\mathcal{L}[n] = E[n] - \lambda\left[\int d^3r\, n(r) - N\right] \tag{19}$$

where λ is a variational parameter.

We note that the DFT theory does not prescribe any methods for calculating $F[n]$ as would be of interest to us in any *ab initio* effort. The approximations in DFT mainly deal with choosing the functionals $F[n]$ that lead to the solution of the minimization in Equation 19, and the path to achieving that minimum.

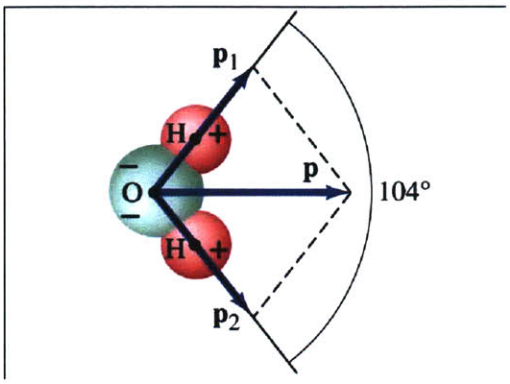

Figure 1:Water Molecule Dipole Moment

We are however dealing with water at a microscopic level, so while the classical picture of Equation 20 is still valid, we have to re-evaluate the actual field that the water molecule experiences.

Local Field Experienced by a Water Molecule

In the following analysis, we will closely follow the arguments and approximations laid out in (Haus & Melcher, 1989), (Kittel, Introduction to Solid State Physics, 7th Edition, 1996) and (Purcell, 1985). Our starting point is the total dipole moment in a unit cell, which is given simply as

$$\boldsymbol{p} = \sum_{n=1}^{N} q_n \boldsymbol{r_n} \qquad 21$$

where $\boldsymbol{r_n}$ is the position vector for charge q_n, and we understand N to be the total number of water molecules in the unit cell.

We would like to understand the electric field local to water molecule. Thus, the localized electric field at a general position $\boldsymbol{r}$ due to a dipole moment $\boldsymbol{p}$ is then given by

$$\boldsymbol{e}(\boldsymbol{r}) = \frac{3(\boldsymbol{p}.\boldsymbol{r}).\boldsymbol{r} - r^2\boldsymbol{p}}{4\pi\epsilon_0 r^5} \qquad 22$$

To get the total microscopic field, we simply add individual vector contributions represented by Equation 22. We would then arrive at the total dipole field. To get the total field, we need to add the externally applied field:

$$\boldsymbol{E} = \boldsymbol{E_o} + \sum_i \boldsymbol{e_i}(\boldsymbol{r_i}) = \boldsymbol{E_o} + \frac{1}{4\pi\epsilon_0}\sum_i \frac{3(\boldsymbol{p_i}.\boldsymbol{r_i}).\boldsymbol{r_i} - r_i^2\boldsymbol{p_i}}{r_i^5} \qquad 23$$

Equation 23 is an exact relationship, but it is not immediately clear how to proceed towards a solution other than through an approximation. The most accessible approximation, and the one given below, has been developed by (Purcell, 1985), and is summarized as follows.

♦

We will consider the induced dipole moment, and alignment of the polar water molecules independently in this approximate treatment.

First, we look at the induced dipole moment in water molecules when an external electric field $\boldsymbol{E_0}$ is applied. We let N be the number of molecules per unit volume and α be the molecular polarizability of water. The induced dipole moment for each water molecule is given simply by (magnitude)

$$p = \alpha E \qquad 24$$

where E is the effective field experienced by the water molecule. Now, the neighboring molecule will be, on average, a distance of about

$$\tilde{a} \approx \frac{1}{N^{\frac{1}{3}}} \qquad 25$$

According to Equation 23 therefore, the field at this neighboring molecule from the induced dipole moment will have a magnitude of approximately

$$E' \approx \frac{\alpha E}{2\pi\epsilon_0 \tilde{a}^3} = \frac{\alpha N}{2\pi\epsilon_0} E \qquad (26)$$

We next get an approximate value of the electric field due to the permanent dipole moment of the water molecule. We denote the permanent dipole moment of water molecule as p_0, such that in a unit volume with N molecules, the total polarization density is potentially

$$P = Np_0 \qquad (27)$$

if we assume perfect alignment (and thus ignore thermal agitations). For water molecules, Equation 27 leads to a very large microscopic electric field. However, at a particular nonzero temperature T, we expect that each water molecule will have a mean rotational or translational energy that is in the order of $k_B T$. We therefore expect that only a fraction of the polarization density in Equation 26 is realized at any finite temperature:

$$Np_0 \rightarrow Np_0 \left(\frac{p_0 E}{k_B T}\right) \qquad (28)$$

where $p_0 E$ is the rotational potential energy of the single dipole moment (and E is the total field), and the quantity in brackets is the "fractional occupation" of aligned dipoles at the dipole energy level pE.

From Equation 28, we get the approximate polarization density as

$$P \approx \left(\frac{Np_0{}^2}{k_B T}\right) E \qquad (29)$$

We may also calculate the approximate fractional alignment at room temperature when a unit electric field per cm (1 unit is equivalent to about 300V/cm) is applied

$$f \approx \left(\frac{p_0 E_0}{k_B T}\right) = \frac{1.8x10^{-18}\ esu.\ cm\ x\ 1\ statvolt/cm}{4x10^{-14}\ erg} = 0.45x10^{-4} \qquad (30)$$

where we have used CGS units (1 erg=6.24x10^11 eV). In SI units, we can easily see that Equation 30 has the correct dimensions, vis. a vis.:

$$\frac{C.M\,x\,V.M^{-1}}{J.K^{-1}xK} = \frac{Cx\,V}{J} = \frac{C.V}{J} = \frac{C.J.C^{-1}}{J} = 1 \qquad 31$$

Equation 30 indicates that at an electric field of 300 V/cm, only one half in 10,000 water dipoles will be aligned with the electric field.

From the above analysis, we conclude that water molecule orientation will not be affected appreciably by the applied electric field. Thus in our model, the best orientation of water in the bulk will be nearly random and independent of the applied electric field. However, near the metal interface, we expect them to prefer some orientation and surface sites. We tackle this issue next before presenting some initial results.

Preferred Orientation and Preferred Surface Sites for Adsorption of Water Molecule on Metal Surface

The surface science of water adsorption is extensive and complicated. A review of existing literature however reveals several well established factors that characterize chemisorption of water on metallic surfaces.

Water monomer (molecule) is weakly adsorption on metallic surfaces, with theoretical adsorption energies in the 0.1-0.4 eV range (Michaelides, Alavi, & King, 2003), (Thiel & Madey, 1987). These adsorption energies are so low that they are competitive with inter-molecular forces acting between individual monomers, making it rather difficult to model and experiment on water monomers since water molecules tend to exist in cluster formations (Thiel & Madey, 1987).

Water is traditionally thought to bond to surfaces through the oxygen atom (Thiel & Madey, 1987). This may be explained simply from basic electronic bonding considerations, namely that the oxygen atom contains unpaired electronic states that result in a charge transfer to the metal surface.

Our next consideration is to determine the most energetically favorable site on the metallic surface. There are several possibilities for the water monomer to adsorb on palladium surface.

These include the on-top site whereby the water monomer sits atop a metal atom as shown clearly below:

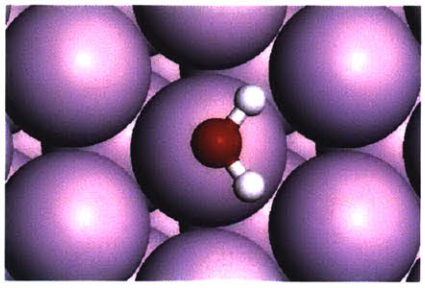

Figure 2: On-Top Site Occupation (from (Michaelides, Alavi, & King, 2003))

Water monomer may also adsorb via a bridge site (two-fold shown below from (Thiel & Madey, 1987))

Figure 3: Two-fold bridge site (From (Thiel & Madey, 1987))

Lastly, we may also have a three- and four-fold bridge sites as shown below.

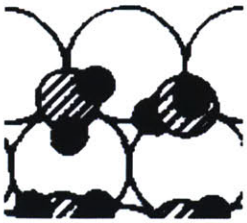

Figure 4: Three-fold bridge site (From (Thiel & Madey, 1987))

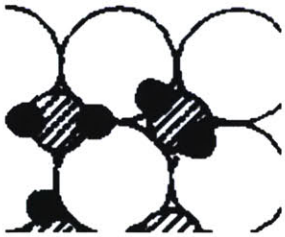

Figure 5: Four-fold bridge site (From (Thiel & Madey, 1987))

The simplest model to explain the most preferred adsorption site that we can find in the literature is that of a simple acid-base reaction whereby the oxygen atom donates an electron to the metal, whereas the metal acts as an electron acceptor. According to this model, when analyzing a smooth metal surface, the most electronically deficient site, and hence the most energetically favorable electron acceptor site is the on-top site (Starr, 1982). Indeed recent *ab initio* DFT calculations have also shown the on-top site to be the most preferred adsorption site for a variety of metals and metallic surfaces (Michaelides, Alavi, & King, 2003).

The other consideration is the orientation of the water molecule at any given site. Unfortunately, the picture here is a little bit murky. Several investigators have predicted an upright orientation (perpendicular to the metal surface) [(Michaelides, Alavi, & King, 2003), (Michaelides, Alavi, & King, 2004) and references therein] while others have predicted a parallel orientation (Michaelides, Alavi, & King, 2003), (Michaelides, Alavi, & King, 2004) and references therein.

Predicting Dissociative Adsorption of Water on Pd

Dissociation is another model factor that we have to account for. In general, water may adsorb molecularly on the metal surface or it may dissociate into its constituent parts, hydroxyl or hydrogen. In the following analysis, we follow (Benzinger, 1980) to approximately predict thermodynamically whether or not water will dissociatively adsorb on Pd. Since what follows is a well known result, we will simply outline the simple model from literature and state qualitative assumptions made therein, so we can compare our first principles calculation with theory.

In his 1980 paper (Benzinger, 1980), Benzinger was interested in modeling whether diatomic molecules dissociatively adsorbed on metallic surfaces or not, based on thermodynamic considerations only. The basic result is stated below, without the ensuing analysis.

The model proceeds by comparing the relative enthalpies of dissociative adsorption, ΔH_d vs. that of molecular adsorption, ΔH_m. A more positive ΔH_d than ΔH_m suggests non-dissociative adsorption while a more negative ΔH_d than ΔH_m suggests dissociation (Benzinger, 1980), (Thiel

& Madey, 1987) - (secondary ref). For H_2O on Pd (100), (Thiel & Madey, 1987) reports the following:

ΔH_d (Complete Dissociation)	ΔH_d (Partial Dissociation)	ΔH_m
+58 kJ/Mol	-5 kJ/Mol	-50 kJ/Mol

Table 1: Pd(100) - Enthalpy Changes for Dissociation (From (Thiel & Madey, 1987))

From the above table, the predicted pathway is non-dissociative adsorption. This is a somewhat surprising result since we would expect dissociative adsorption for H_2O on Pd (100) based on experiment (we would not have any loading without dissociative adsorption).

We however note the following:

- Increasing temperature shifts the prediction above away from molecular to dissociative adsorption (Benzinger, 1980). In fact, the break point temperature for this to occur is in the range of 250-325K, which is very close to room temperature.

- The above model ignores kinetic effects, as well as coverage effects.

- The above model ignores morphological effects. In fact, it is known that surface effects are enough to shift the balance from molecular to dissociative adsorption (Thiel & Madey, 1987).

We expect to shed some more light on this prediction in our *ab initio* simulation.

Preparatory Results

We now briefly present some preliminary results that we have used to prove that simple DFT calculations of well known problems match those from experiment. These results also show that we have made the necessary progress to set up and understand the computational environment where analysis of more complex systems may be performed in later chapters.

Overview of the Methodology

All calculations below are done in the context of Density Functional Theory (DFT) using the electron exchange correlation functional introduced by Perdew, Zunger (PZ). We use ultrasoft pseudopotential, with a wavefunction cut-off of 40 Ry and charge density expansion cut off of 400 Ry. All the calculations utilized the Quantum Espresso's (QE) DFT PWscf package (Giannozzi, 2010), while the geometrical and physical modeling of surfaces and molecules was done using various software tools including Xcrysden and Material Studio.

Calculation of Equilibrium Lattice Constant of PdH

Palladium exists in FCC lattice with an experimentally reported lattice constant of 3.89 Angstroms (7.351 a.u.). With an incorporated Hydrogen atom in its lattice, we expect the lattice constant for PdH to increase slightly from the additional stress (Hagelstein P. , Private Conversation, 2009), but we need to verify this numerically using DFT. Because this is a sufficiently simple calculation, it will also offer us the opportunity to gain confidence in the future, more complicated calculated performed by QE.

To calculate the equilibrium lattice constant for PdH in the ground state, we will manually relax the geometry around the reported value, each time calculating the ground state Self Consistent Field (SCF) total energy. We expect that the equilibrium lattice constant value will have minimum energy, and we should be able to verify this numerically.

We carry out such a relaxation, and get the following results for an octahedral site H occupation:

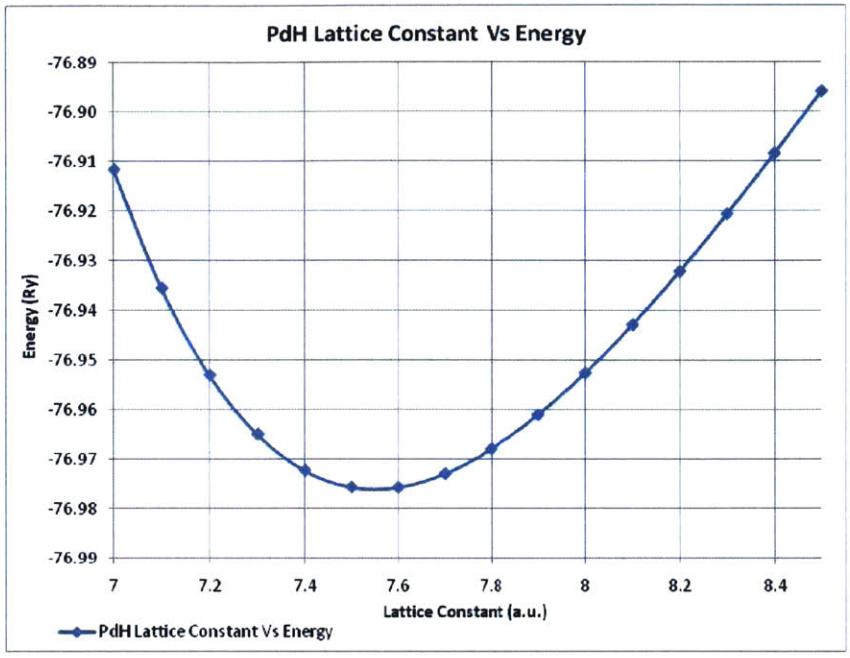

Figure 6: PdH Lattice Constant vs. Energy

From these results, we see that the calculated *ab initio* equilibrium lattice constant for PdH is about 7.6 a.u.

Energy Cut-off and k-Points Convergence

In DFT, a crystal structure is modeled as an infinite system via the periodic boundary condition (PBC) formalism. We can therefore use Bloch Theorem to solve Schrodinger's Equation, thus:

$$\Psi_{n,\bar{k}}(\bar{r}) = e^{i\bar{k}.\bar{r}}\, u_{n,\bar{k}}(\bar{r}) \qquad 32$$

where $\Psi_{n,\bar{k}}(\bar{r})$ is the wave function we are solving for, $u_{n,\bar{k}}(\bar{r})$ captures the periodicity of the crystal and is given by an infinite Fourier expansion in reciprocal lattice space:

$$u_{n,\bar{k}}(\bar{r}) = \sum_{G} c_G\, e^{i\vec{G}.\bar{r}} \qquad 33$$

$\bar{G}$ are reciprocal lattice vectors and c_G are expansion coefficients. In theory, we would expand Equation 33 to infinity, but in practice, we have to stop somewhere. In DFT, this cut-off is often specified in energy terms corresponding to the kinetic energy of the highest $\bar{G}$ included in Equation 33.

Analogously, to get the total self consistent crystal energy, we need to integrate the resultant wave function over the Brillouin Zone. This integral is approximated by a finite number of k-values (k-mesh actually since we are in 3 dimensions). It is therefore critical that any energy calculation we do is based on converged k-space i.e., the k-mesh should be dense enough for the problem at hand.

We first test the energy cut-off of PdH by starting with a reasonable value of 10 Ry and manually testing convergence. The results are shown below.

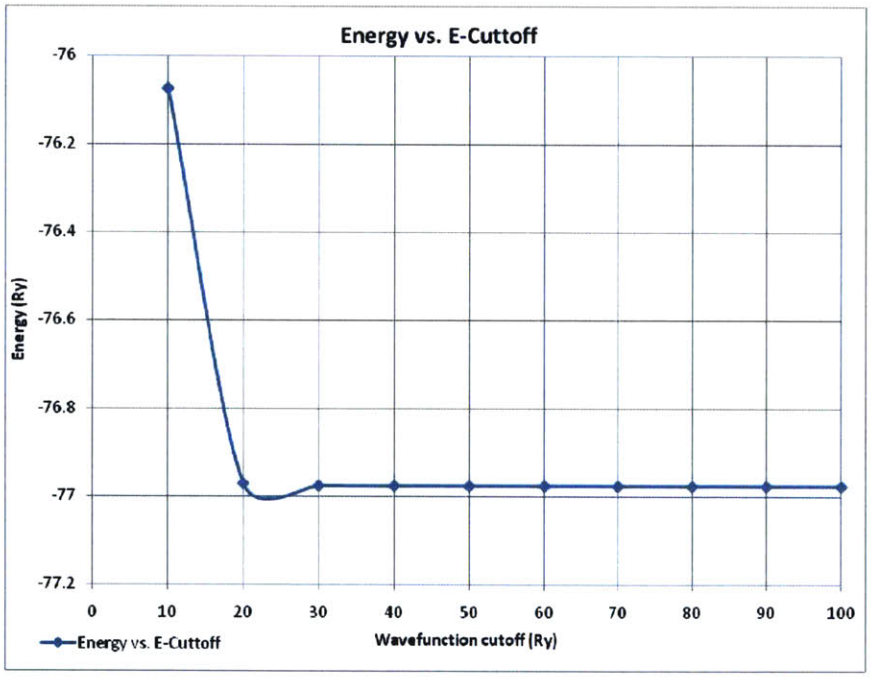

Figure 7: Energy Cut-Off Relaxation

We see that convergence is achieved at a plane-wave cut-off corresponding to about 30 Ry. It remains to be answered if this cut-off energy depends on other systematic parameters, and what the nature of such dependence is.

Note: Determining E-cut-off is useful numerically due to computational savings.

Using the above cut-off, we will next investigate the k-point convergence, starting with a 1x1x1 grid:

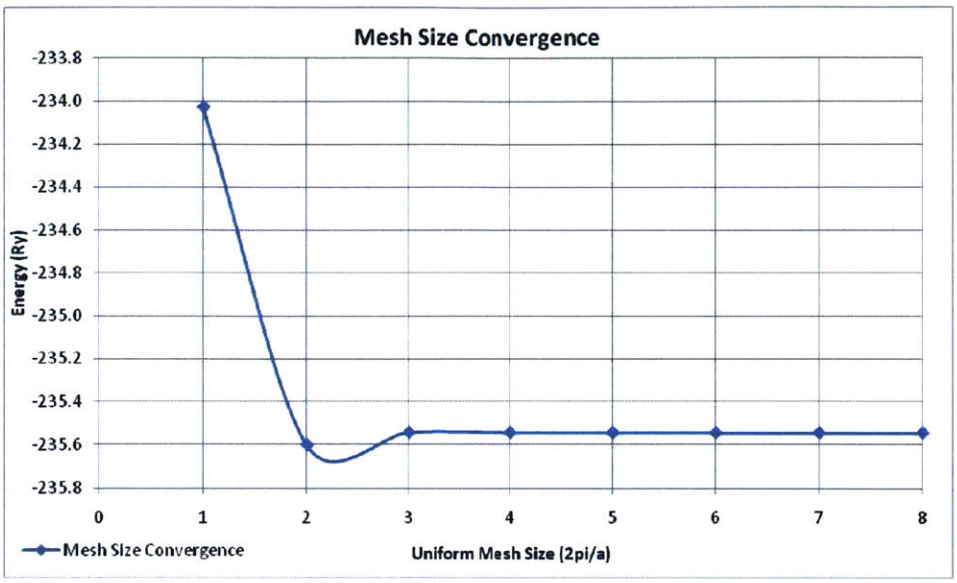

Figure 8: Mesh Size Convergence

A k-point mesh size of 4x4x4, therefore, seems appropriate for the PdH calculations we will be performing.

Octahedral vs. Tetrahedral Site Occupation

We are also interested in calculating SCF energies for both tetrahedral and octahedral H-Site occupation. From literature, we expect the octahedral site to be preferred energetically.

In the following calculation, we have used the converged values of lattice parameter, plane wave energy cut-off, and k-point mesh size to calculate the total ground state energy of the PdH molecule as the H atom moves from a tetrahedral site (¼ ¼ ¼) to an octahedral site (½ ½ ½) along a straight line. As expected, the octahedral site is the more energetically stable occupation site, and we should thus expect it to be preferred as long as it is statistically available in the sense of section *Tetrahedral Site Occupation: O-to-T Excitation Model* of Chapter 2.

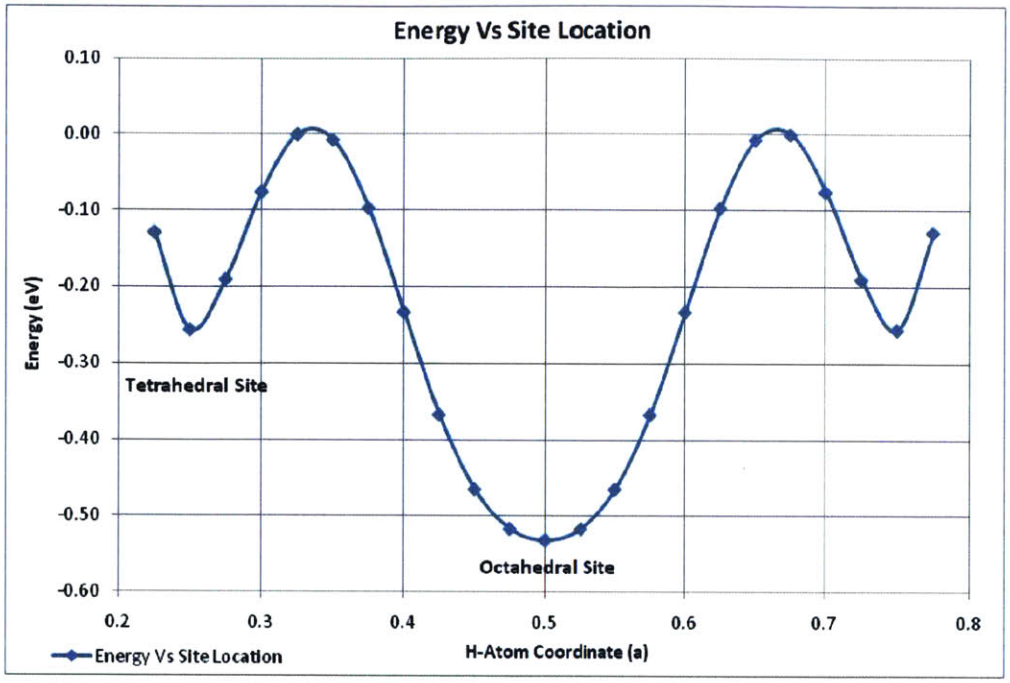

Figure 9: Potential Energy Surface (PdH Octahedral-to-Tetrahedral)

Volmer - The Physical Model

It may be useful to create a physical model before embarking on a detailed calculation. As you may recall, during a Volmer reaction water dissociatively adsorbs on the Pd surface according to the following (Equation 1)

$$H_2O + e^- + M \rightleftharpoons MH_{ads} + OH^-$$

34

We may visualize a water molecule approaching the Pd surface. At some point, it dissociates according to the following physical model:

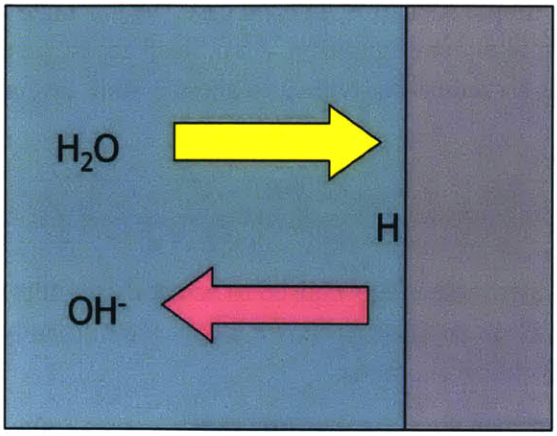

Figure 10: The Physical Volmer

The process is mediated by an electrochemical charge exchange (according to Equation 34) which completes the external electrical current. Undoubtedly, this is a rather simplistic picture, but we can imagine two systems, one consisting of a H_2O double layer representing the pre-Volmer state and the other consisting of H_2O-OH-H overlayer system, very similar to that considered by Michaelides and his coworkers (Michaelides, Alavi, & King, 2003). We can then determine the energetics of the two systems and hopefully shed some light into whether Volmer process can be predicted from first principles.

1-D PES

Initially, we may just be interested in determining the PES for simple cases, say 1-D PES for specific configurations that we know are of interest. In the following, we use some parameter results from literature while varying others as shown in the following table:

Orientation	**Layering**	**Preferred Adsorption surface**	**H-up vs. H-down (for overlayer)**	**Bond Distances**
Lower Layer parallel to surface (Michaelides, Alavi, & King, 2004)	Two layers (Thiel & Madey, 1987)	(111)[Several]	Unresolved in literature. Investigate (see below)	Experimental (Water). Other bond distances chosen arbitrarily (must be relaxed *ab initio*)

We can then consider several simple scenarios. In each case, we calculate the ground state energies to determine the most likely configuration. Also, in all cases, we use a 4 atom layer Pd{111} surface atop which is a vacuum equivalent to about 5 atom layers.

Bilayer H-Up Configuration

This is depicted below. The water molecule is chosen to be nearly parallel to the surface of the Pd, and the overlayer is in the H-up position as shown below. Traditionally (Thiel & Madey, 1987), this is the assumed adsorption geometry:

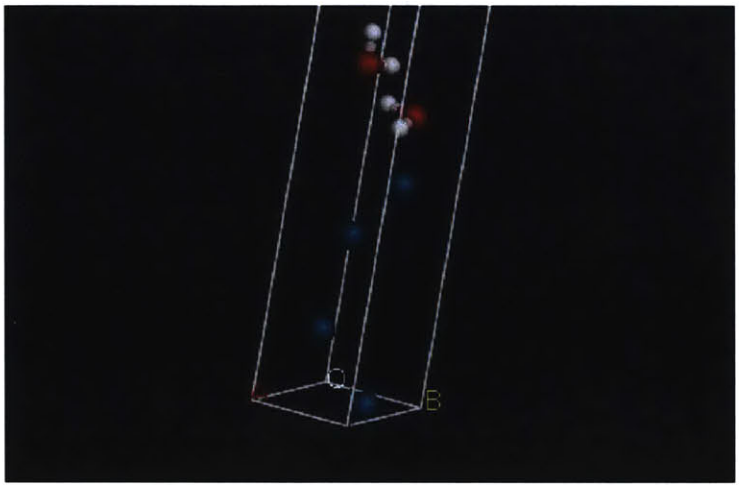

Figure 11: Bilayer, Parrallel Adsorption with H-Up overlayer (Blue=Pd, White=H, Red=O)

Bilayer H-Down Configuration

Recently however, some workers (Ogasawara, et al., 2002) have determined, using Pt{111} that the H-down configuration is more favored. This configuration is shown below:

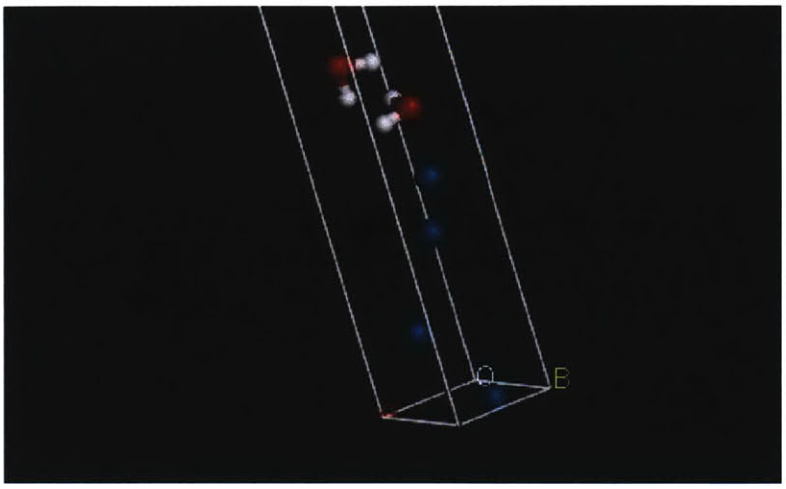

Figure 12: Bilayer, Parallel Adsorption with H-Down overlayer

Preliminary Results: H-Up vs. H-Down

Based on our first principles calculations for Pd{111}, we conclude that the H-Up configuration is slightly energetically favored over H-Down. All figures are given in eV per atom.

H-Down	H-Up	Difference
-213.133	-214.297	1.163767

We therefore confirm the long standing H-up adsorption configuration and use it in the following adsorption model.

Summary

In this chapter, we introduced the problem and provided some preliminary analysis of a water dipole. We also tested the DFT on some simple problems.

Chapter 2 – The Chemical Potential of Hydrogen in Palladium

Introduction

A natural beginning of our investigation is the determination of the chemical potential of H within the Pd lattice. Doing so will tell us the extent to which Hydrogen loading of Palladium occurs.

From first principles, chemical potential is one of the four fundamental thermodynamic quantities. It is a measure of the ease with which particles may be exchanged between systems whose contact allows for a particle exchange (Kittel, Thermal Physics, 1980). Chemical potential is indeed a form of potential energy – it is the energy needed to bring two systems into diffusive equilibrium while holding total volume and temperature constant [ibid].

Mathematically, chemical potential is defined as follows:

$$\mu(\tau, V, n) \equiv \left(\frac{\partial F}{\partial n}\right)_{\tau,V} \tag{35}$$

In Equation 35, F is the Helmholtz Free Energy, defined as an energy balance between minimum energy and maximum entropy:

$$F(\tau, V, n) \equiv U - \tau\sigma \tag{36}$$

where U is the total system energy, σ is the system entropy and $\tau = \kappa_B T$. In classical thermodynamics, it can be shown that $F(\tau, V, n)$ obtains a minimum with respect to all fundamental thermodynamic variables (τ, V, n).

Even with this brief subject matter introduction, we are almost ready with the basic formulation. Before that, we need to introduce one more basic concept, namely the Grand Partition Function, $\mathcal{Z}$:

$$\mathcal{Z}(\tau,\mu) = \sum_{ASN} e^{\frac{n\mu-\varepsilon_s}{\tau}}$$

37

In Equation 37, the summation is carried out over all states of the system for all numbers of particles, and $\varepsilon_s = \varepsilon(n)$ are (micro)state energies for the given number of particles, n. Intuitively, the partition function captures the configuration of the system by encoding the individual state probabilities based on their energies.

The Chemical Potential of Hydrogen in Palladium: A Basic Analysis

Introduction

We would like apply the foregoing simple classical thermodynamic analysis to the case of hydrogen atoms in a Pd lattice. Initially, we will consider octahedral sites only. We will generalize the analysis to tetrahedral occupations later in this chapter. For octahedral occupation only, then, we imagine them being in contact with a reservoir of H:

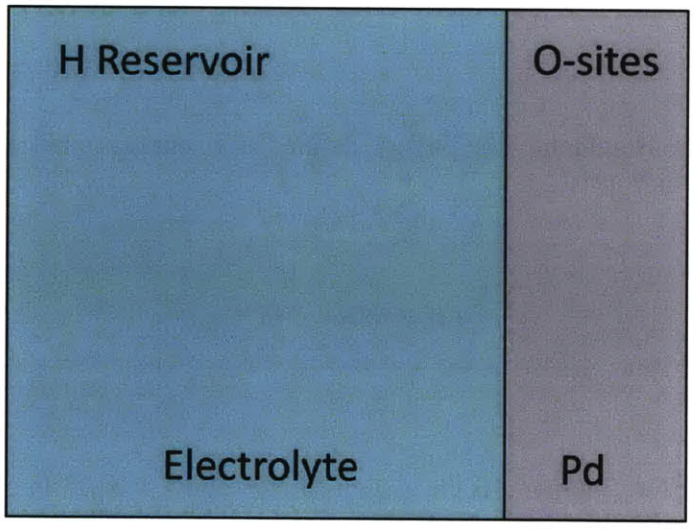

Figure 13: H Reservoir in contact with O-sites

Following (Fowler, 1936), (Lacher, 1937), (Christensen, Stoltze, Jacobsen, & Norskov, 1990) and others, we write the grand canonical partition function for the H atoms in the O-sites as

follows:

$$Z_H(\tau,\mu) = \sum_n \sum_{ASN} e^{\frac{n\mu-\varepsilon_h}{\tau}} z^n \qquad 38$$

In Equation 38,

n is the number of H atoms, distributed among N available O-sites, and the second sum has the same meaning as in Equation 37,

z is the isolated H-atom partition function within the O-sites, unspecified as of now, and

$\varepsilon_h = \varepsilon_h(n)$ is the total interaction energy of the configuration with n H atoms, distributed among N available O-sites.

Equation 38 has well known approximations that we will utilize here. In particular, we use the approximation adopted by (Lacher, 1937), who used previous work by Bragg and Williams (Bragg & Williams, 1934) to write it as:

$$Z_H(\tau,n) \cong \frac{N!}{n!\,(N-n)!} e^{\frac{-n\varepsilon_h}{\tau}} z^n \qquad 39$$

This approximation is also called Mean Field Approximation (Christensen, Stoltze, Jacobsen, & Norskov, 1990) or Self Consistent Field approximation. We will adopt the Bragg and Williams Approximation terminology in this work. While a full treatment of the Bragg Williams Approximation is not considered here, we note in passing that it essentially approximates the many-body interactions implicit in Equation 38 with an average effective interaction, essentially reducing the problem to one-body interaction with an effective field. (Buckley, Dobson, & Poyser, 1995) has performed Monte Carlo simulations that support the use of this approximation in the same context as ours, so we believe the approach we are taking is on solid theoretical foundation.

Chemical Potential Expression

We get the chemical potential by minimizing the free energy with respect to the number of particles:

$$\mu_H \equiv \frac{\partial F}{\partial n} = -\tau \frac{\partial \ln Z_H}{\partial n} \tag{40}$$

Equation 40 is typically used in conjunction with an uncorrelated partition function, but we think that as long as the energy ε_h in Equation 39 is the total interaction energy of H within Pd lattice, Equation 40 will be valid for the case of H in Pd.

We determine an expression for Equation 40 below, noting that the algebra that follows may be dispensed with, but we have included it here for reference purposes:

From Equation 39, using Equation 40, we get

$$\mu_H = -\tau \frac{\partial}{\partial n}\left\{ln \frac{N!}{n!\,(N-n)!} + ln\, z^n - \frac{n\varepsilon_h}{\tau}\right\} = -\tau \frac{\partial}{\partial n}\{T_1 + T_2 + T_3\} \tag{41}$$

Using the Stirling Approximation

$$N! \cong (2\pi N)^{\frac{1}{2}} N^N e^{\left[-N + \frac{1}{12N} + \cdots\right]} \tag{42}$$

we can write the first term as

$$T_1 = ln\frac{N!}{n!\,(N-n)!} = lnN! - ln(N-n)\,! - ln\,n!$$

$$\cong ln\sqrt{2\pi} + \left(N+\frac{1}{2}\right) lnN - N$$

$$- \left(ln\sqrt{2\pi} + \left(n+\frac{1}{2}\right)\ln n - n\right)$$

$$-\left(\, ln\sqrt{2\pi} + \left(N-n+\frac{1}{2}\right) ln\,(N-n) - (N-n)\right)$$

$$= \left(N+\frac{1}{2}\right) lnN - \left(\left(n+\frac{1}{2}\right) ln\,n\right) - \left(ln\sqrt{2\pi} + \left(N-n+\frac{1}{2}\right) ln\,(N-n)\right)$$

43

After the following algebra, we get

$$\frac{\partial}{\partial n} T_1 = -\frac{\partial}{\partial n}\left\{\left(n+\frac{1}{2}\right) ln\,n + \left(N-n+\frac{1}{2}\right) ln(N-n)\right\}$$

$$= -\left\{\left(n+\frac{1}{2}\right)\frac{1}{n} + ln\,n + \left(N-n+\frac{1}{2}\right)\left(\frac{1}{N-n}\right)(-1) + (-1)\,ln(N-n)\right\}$$

$$= -\left\{\left(n+\frac{1}{2}\right)\frac{1}{n} + ln\,n + \left(N-n+\frac{1}{2}\right)\left(\frac{1}{N-n}\right)(-1) + (-1)\,ln(N-n)\right\}$$

$$= -\left\{1 + \frac{1}{2n} + ln\,n - 1 - \frac{1}{2}\left(\frac{1}{N-n}\right) - ln(N-n)\right\} = -\left\{\frac{1}{2n} - \frac{1}{2}\left(\frac{1}{N-n}\right) + ln\frac{n}{N-n}\right\}$$

44

We get the other terms as

$$\frac{\partial}{\partial n} T_2 = ln\,z$$

45

and

$$\frac{\partial}{\partial n} T_3 = \frac{\partial}{\partial n}\left(-\frac{n\varepsilon_h(n)}{\tau}\right) = -\frac{n}{\tau}\frac{\partial\varepsilon_h(n)}{\partial n} - \frac{\varepsilon_h(n)}{\tau}$$

46

In Equation 46, we have emphasized that the total interaction energy will depend on the number of occupied O-sites, as previous workers have already noted, for example, (Lacher, 1937).

If we define the degree of loading as the ratio of the number of Hydrogen atoms to those of Palladium, i.e., $\theta = \frac{n}{N}$, we can re-write Equation 44 as:

$$\frac{\partial}{\partial n} T_1 = -\frac{1}{2N}\left(\frac{1}{\theta} - \frac{1}{1-\theta}\right) - ln\frac{\theta}{1-\theta} \qquad 47$$

In Equation 47, we note that with N very large, the second term will always dominate the first, even near $\theta = 0$, such that the final result, to a good approximation, is

$$\frac{\partial}{\partial n} T_1 \cong -ln\frac{\theta}{1-\theta} \qquad 48$$

Lastly,

$$\frac{\partial}{\partial n} T_3 = -\frac{\theta}{\tau}\frac{\partial}{\partial \theta}\varepsilon_h(\theta) - \frac{\varepsilon_h(\theta)}{\tau} \qquad 49$$

Putting Equation 41 together with Equations 45, 47 & 49, we arrive at an expression for the chemical potential of H in Pd for the case of single interstitial site occupation as follows:

$$\mu_H(\tau,\theta) = \tau\, ln\frac{\theta}{1-\theta} - \tau\, ln\, z + \theta\frac{\partial}{\partial \theta}\varepsilon_h(\theta) + \varepsilon_h(\theta) \qquad 50$$

This result has been derived by Christensen (Christensen, Stoltze, Jacobsen, & Norskov, 1990) and several others, who generally based their work on the earlier work by Lacher (Lacher, 1937) and Fowler (Fowler, 1936). It is considered accurate to within the approximations made in its derivation, namely the statistical mechanical description via the grand partition function formalism, and the Stirling approximation. We interpret Equation 50 as expressing the chemical potential of H within the Pd lattice to consist of its value without any lattice interaction, μ_0, plus

correction terms that depend on loading:

$$\mu_H(\theta) = -\tau \ln z + \tau \ln\frac{\theta}{1-\theta} + \theta\frac{\partial}{\partial\theta}\varepsilon_h(\theta) + \varepsilon_h(\theta)$$
$$= \mu_0 + \mu_1(\theta) + \mu_2(\theta) + \mu_3(\theta)$$

51

Single H-Particle Partition Function

It still remains to determine the partition function of the H atom in the absence of interaction, z.

For this, we use a 1D harmonic oscillator model, which, for simplicity, is modeled as an Einstein atom with vibrational energy $\epsilon_{0v} = \hbar\omega$. This model has been used by others, for example (Christensen, Stoltze, Jacobsen, & Norskov, 1990) & (Buckley, Dobson, & Poyser, 1995), to treat the same problem as ours. Basically, the isolated protium is assumed to vibrate at a frequency much higher than the lattice phonons, making their independence possible and resulting in a reasonably good approximation using a harmonic oscillator (Flanagan & Oates, 1991).

For a 1D harmonic oscillator, z is particularly simple since

$$E_n = \epsilon_{0v}\left(n + \frac{1}{2}\right)$$

52

where ϵ_{0v} is the ground state vibrational quantum. We obviously expect ϵ_{0v} to be loading dependent (see, for example, (Rush, Rowe, & Richter, 1984)), but to a first approximation, we will assume that it has a constant value independent of loading.

Therefore, for all three normal modes, we have

$$z = \left(\sum_{n=0}^{\infty} e^{-\frac{\epsilon_{0v}\left(n+\frac{1}{2}\right)}{\tau}}\right)^3 = \left(e^{-\frac{\epsilon_{0v}}{2\tau}}\sum_{n=0}^{\infty} e^{-\frac{\epsilon_{0v}n}{\tau}}\right)^3 = \left(\frac{e^{-\frac{\epsilon_{0v}}{2\tau}}}{1-e^{-\frac{\epsilon_{0v}}{\tau}}}\right)^3 = \left(2sinh\frac{\epsilon_{0v}}{2\tau}\right)^{-3}$$

53

Equation 53, together with Equation 51, provide a reasonable model for the chemical potential of H within the Pd Lattice whereby only one species of sites (octahedral) has been considered. The interaction energy as a function of loading, $\varepsilon_h(\theta)$, may be calculated directly from first principles, while ϵ_{0v} may be obtained from literature (Wicke & Brodowsky, 1978).

Including Tetrahedral Site Occupation

It is generally accepted that there will be tetrahedral site occupation, especially at high loading (Lacher, 1937). In this section, we start with the following potential energy diagram from our DFT results that shows that there is about a 276 meV excitation between the two energy levels. This is a very large energy barrier as we can easily show. Other workers have also found this energy difference to be very close to our calculation using other methods, for example, 295 meV using Molecular Dynamics methodology (Salomons, 1990).

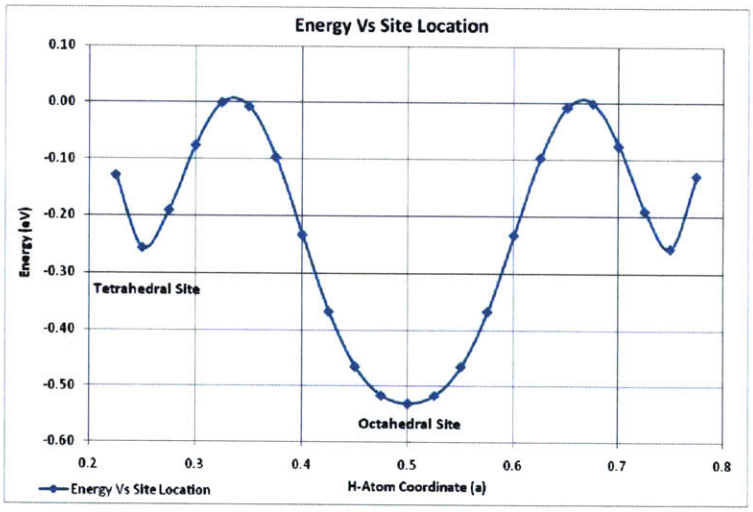

Figure 14: Low Loading Octahedral to Tetrahedral Site Excitation Energy

Our expectation is that, using statistical mechanics concepts that we started formulating above, we can determine what percentage of site occupations, n, will consist of O-site occupations and which ones will be T-site occupations.

Figure 14 is accurate only at low loading levels (and in fact the excitation energy from (Salomons, 1990) is from near zero loading). A question arises as to whether the O-to-T excitation energy is constant with loading or not.

To this question, we seek an answer from our first principles computational (DFT) framework. We performed some *ab initio* calculations whereby, for a specific loading and configuration, we randomly promoted one hydrogen atom from an O-site to a T-site. The results indicate a general increase in excitation energy with loading for both a single cell calculation and a 2x2x2 super cell calculation:

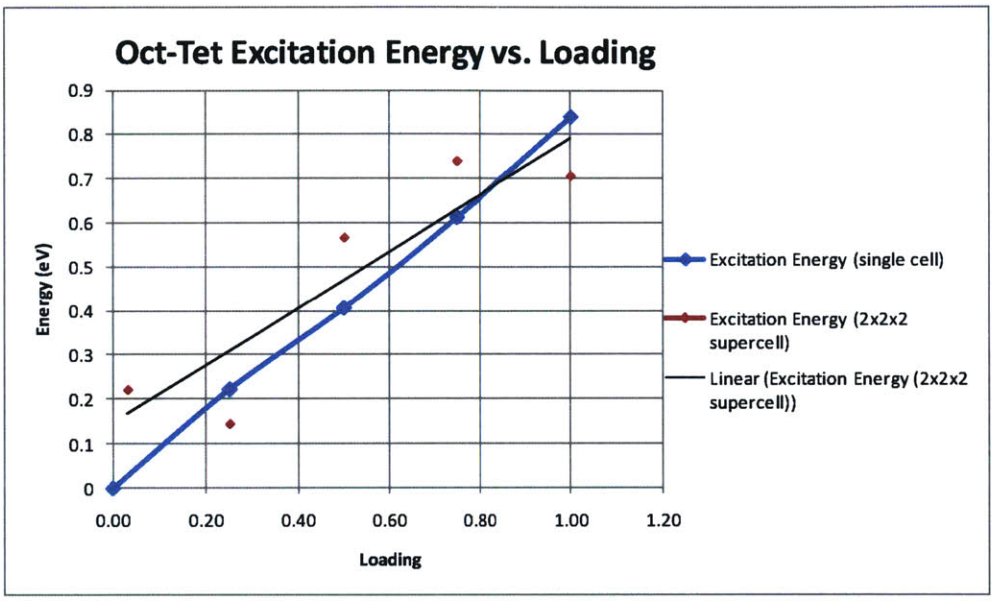

Figure 15: Octahedral to Tetrahedral site Excitation Energy as a function of loading

The first thing we note is that there is strong configurational dependence, which means that the energy is most likely to be strongly dependent on the particular configuration chosen. We also notice a big increase in excitation energy with loading. We speculate that this is due to a stronger H-H interaction (repulsion) when the tetrahedral sites are occupied.

Based on (Salomons, 1990)'s near zero loading results which closely match our low loading *ab initio* calculations, we believe that it is a good approximation to use the low loading results since our higher loading results will simply preclude tetrahedral sites even more severely. The formulation of the model follows below.

Tetrahedral Site Occupation: O-to-T Excitation Model

Once again, we begin with the partition function of the full configurational system:

$$Z_H(\tau,\mu) = \sum_{n_o}\sum_{n_t}\sum_{ASN} e^{\frac{(n_o+n_t)\mu-\varepsilon_h}{\tau}} z^{(n_o+n_t)} \qquad 54$$

In Equation 54,

n_o is the number of H atoms, distributed among N_o available O-sites, n_t is the number of H atoms, distributed among N_t available T-sites, and the last sum means all system configurations with $\{n_o, n_t\}$ H atoms,

z is the isolated H-atom partition function, already specified in Equation 53 above,

$\varepsilon_h = \varepsilon_h(n_o, n_t)$ is the total loading-dependent interaction energy of the configuration, with $n = n_o + n_t$ H atoms, distributed among $N = N_o + N_t$ available interstitial sites of both types, and,

μ is the chemical potential for the H atom, which must be the same for either O-site or T-site occupation.

We write Equation 54 using the previous approximation (Equation 39) and following (Hagelstein P. , Private Conversation, 2009)'s extension of (Lacher, 1937)'s treatment of Octahedral to Tetrahedral occupations:

$$Z_H(\tau,n_o,n_t) \cong \frac{N_o!}{n_o!\,(N_o-n_o)!}\frac{N_t!}{n_t!\,(N_t-n_t)!} e^{\frac{(n_o+n_t)\varepsilon_h(n_o,n_t)}{\tau}} z^{n_o+n_t} \qquad 55$$

We are aware of at least a couple of workers who have looked at this problem and come up with appropriate models, for example (Salomons, 1990), (Geerken & Griessen, 1983). Salomon's model considers the chemical potentials for each site separately, and using the fact that they must be equal, determines the relative O vs. T site occupations:

$$\mu_o(\tau,n_o,n_t) = \mu_t(\tau,n_o,n_t) \qquad 56$$

Using a previous (Geerken & Griessen, 1983) Mean Field Approximation to account for the hydrogen-hydrogen interaction, (Salomons, 1990) arrives at an expression very similar to our Equation 50 above:

$$\mu_i = \tau \, ln\frac{\theta_i}{1-\theta_i} + f(\theta_i) + \varepsilon_i \qquad i = \{o, t\} \tag{57}$$

In Equation 57, $f(\theta_i)$ represents the interaction term, and ε_i are site energies which we do not define here more precisely since we are only interested in their difference (below), and

$$\theta_o = \frac{n_o}{N_o} \tag{58}$$

$$\theta_t = \frac{n_t}{N_t} \tag{59}$$

are, respectively, the partial octahedral and tetrahedral contributions to the overall loading.

Combining Equation 56 and 57 yields (Salomons, 1990):

$$\varepsilon_o + \tau \, ln\frac{\theta_o}{1-\theta_o} = \varepsilon_t + \tau \, ln\frac{\theta_t}{1-\theta_t} \tag{60}$$

We may use Equation 60 to determine the relative fractional site occupations. (Salomons, 1990) has calculated the activation energy $\Delta\varepsilon = \varepsilon_t - \varepsilon_o = 295 \; meV$ at near zero loading, such that at room temperature, Equation 60 predicts a very small tetrahedral fractional occupation:

$$\theta_t = \begin{cases} 8.54 * 10^{-4} \; (\theta_o = .99) \\ 8.63 * 10^{-6} \; (\theta_o = 0.5) \end{cases} \tag{61}$$

♦

While Equations 60 & 61 give us some indication regarding the relative fractional occupations of octahedral and tetrahedral sites, we are still not any closer to a complete tetrahedral+octahedral model in the *ab-initio* framework (where the interaction energy of the system now includes both occupations).

In this work, we take a slightly different view. From the full configuration (octahedral and tetrahedral) partition function, Equation 55, we calculate the chemical potential two ways:

$$\mu_o(\tau, n_o, n_t) = -\tau \frac{\partial \ln Z_H(\tau, n_o, n_t)}{\partial n_o} \tag{62}$$

$$\mu_t(\tau, n_o, n_t) = -\tau \frac{\partial \ln Z_H(\tau, n_o, n_t)}{\partial n_t} \tag{63}$$

where

$$\mu_o(\tau, n_o, n_t) = -\tau \frac{\partial}{\partial n_o}\left\{ ln \frac{N_o!}{n_o!\,(N_o - n_o)!} + ln \frac{N_t!}{n_t!\,(N_t - n_t)!} - \frac{(n_o + n_t)\varepsilon_h(n_o, n_t)}{\tau} + (n_o + n_t)\, ln(z) \right\} \tag{64}$$

Once again, we use the Stirling Approximation

$$ln(x!) \cong \frac{1}{2} ln(2\pi) + \left(x + \frac{1}{2}\right) ln\, x - x \tag{65}$$

for x a large integer, and organize the terms according to (using previous results):

$$\mu_o(\tau, n_o, n_t) = \tau \left\{ ln \frac{n_o}{N_o - n_o} - ln(z) + \frac{(n_o + n_t)}{\tau} \frac{\partial \varepsilon_h(n_o, n_t)}{\partial n_o} + \frac{\varepsilon_h(n_o, n_t)}{\tau} \right\} \tag{66}$$

Similarly:

$$\mu_t(\tau, n_o, n_t) = \tau\left\{ ln\frac{n_t}{N_t - n_t} - ln(z) + \frac{(n_o + n_t)}{\tau}\frac{\partial \varepsilon_h(n_o, n_t)}{\partial n_t} + \frac{\varepsilon_h(n_o, n_t)}{\tau}\right\} \quad 67$$

Furthermore, using the ratio of Octahedral to Tetrahedral sites, which for an FCC lattice is equal to ½:

$$\frac{N_o}{N_t} = \frac{1}{2} \quad 68$$

and

$$\partial\theta_o = \frac{1}{N_o}\partial n_o \quad 69$$

etc, we write

$$\varepsilon_h(\tau, n_o, n_t) \rightarrow \varepsilon_h(\tau, \theta_o, \theta_t) \quad 70$$

and

$$\mu_o(\tau, \theta_o, \theta_t) = \tau\, ln\frac{\theta_o}{1 - \theta_o} - \tau\, l\, n(z) + (\theta_o + 2\theta_t)\frac{\partial \varepsilon_h(\theta_o, \theta_t)}{\partial \theta_o} + \varepsilon_h(\theta_o, \theta_t) \quad 71$$

$$\mu_t(\tau, \theta_o, \theta_t) = \tau\, ln\frac{\theta_t}{1 - \theta_t} - \tau\, l\, n(z) + (\theta_t + \frac{1}{2}\theta_o)\frac{\partial \varepsilon_h(\theta_o, \theta_t)}{\partial \theta_t} + \varepsilon_h(\theta_o, \theta_t) \quad 72$$

This completes our expression for the chemical potential where both interstitial sites may be occupied.

Connecting O-to-T Excitation Formulation To DFT: A Computational Model

We would like to connect the above formulation to our DFT model.

First, we need to assign a meaning to $\varepsilon_h(\theta_o, \theta_t)$. According to the Grand Partition Function (Equation 54), $\varepsilon_h(\theta_o, \theta_t)$ is the total interaction energy in the configuration whereby both interstitial site types may be occupied, and can be calculated from first principles directly using DFT.

Second, we need to relate $\theta_o$and θ_t to the loading level that we have used previously, θ, defined as the number of hydrogen atoms per palladium atom. From their definitions above, we can make a simple connection:

$$\theta' = \frac{n_o + n_t}{N_o + N_t} = \frac{1}{3}\theta_o + \frac{2}{3}\theta_t \tag{73}$$

We note that for an FCC unit cell, there are a total of 12 interstitial sites, i.e., $N_o + N_t = 12/cell$, therefore, Equation 73 does not define the ratio of hydrogen to palladium atoms. We can connect the two using:

$$3\theta' = \theta = \theta_o + 2\theta_t \tag{74}$$

From Equation 74, we can simplify the model further using

$$\frac{\partial \varepsilon_h(\theta_o, \theta_t)}{\partial \theta_o} = \frac{\partial \varepsilon_h(\theta)}{\partial \theta}\frac{\partial \theta}{\partial \theta_o} = \frac{\partial \varepsilon_h(\theta)}{\partial \theta} \tag{75}$$

and

$$\frac{\partial \varepsilon_h(\theta_o, \theta_t)}{\partial \theta_t} = \frac{\partial \varepsilon_h(\theta)}{\partial \theta}\frac{\partial \theta}{\partial \theta_t} = 2\frac{\partial \varepsilon_h(\theta)}{\partial \theta} \tag{76}$$

such that Equations 71 and 72 become

$$\mu_o(\tau, \theta_o, \theta_t) = \tau\, ln\frac{\theta_o}{1-\theta_o} - \tau\, ln(z) + \theta\frac{\partial \varepsilon_h(\theta)}{\partial \theta} + \varepsilon_h(\theta_o, \theta_t) \quad (77)$$

$$\mu_t(\tau, \theta_o, \theta_t) = \tau\, ln\frac{\theta_t}{1-\theta_t} - \tau\, ln(z) + \theta\frac{\partial \varepsilon_h(\theta)}{\partial \theta} + \varepsilon_h(\theta_o, \theta_t) \quad (78)$$

Finally, we have to find a way to calculate the relative distribution of O vs. T-sites as a function of loading. We cannot use (Salomons, 1990)'s result described above, Equation 60, because it is independent of loading.

As a first attempt at a model, we may imagine a state of the system with n_i^o O-sites filled, and whose total energy is ε_i^o. The approximate relative probability of the system being in this state may be approximated by the Gibbs factor:

$$P_{rel}^o(n_i^o, \tau) \propto e^{\frac{n_i^o \mu - \varepsilon_i^o}{\tau}} \quad (79)$$

Similarly, for T-Site occupation whose energy is ε_j^t,

$$P_{rel}^t(n_j^t, \tau) \propto e^{\frac{n_j^t \mu - \varepsilon_j^t}{\tau}} \quad (80)$$

Therefore, the relative occupation of O- to T-sites is expected to be

$$\frac{P_{rel}^o(n_o, \tau)}{P_{rel}^t(n_t, \tau)} = e^{\frac{\left(n_i^o - n_j^t\right)\mu - \left(\varepsilon_i^o - \varepsilon_j^t\right)}{\tau}} \quad (81)$$

It is not immediately apparent how to proceed from Equation 81 within our computational framework. We may however use an alternative model formulation which may be readily connected to our computational model, and which we believe lends itself to a statistical mechanics interpretation. We tackle that next.

♦

We compare two systems, both with n interstitial sites of both types that may be filled. In the first system, only Octahedral sites are filled. As before, the relative probability of the system being in this state is

$$P_{rel}^{1}(n,\tau) \propto e^{\frac{n\mu-\epsilon_1}{\tau}} \quad 82$$

The second system is exactly the same as the first except one of the interstitials is now a T-site. The relative probability of this state, with some energy $\epsilon_2 \neq \epsilon_1$, is

$$P_{rel}^{2}(n,\tau) \propto e^{\frac{n\mu-\epsilon_2}{\tau}} \quad 83$$

$\epsilon_2 - \epsilon_1$ is available from the computational model, and from it we can get the relative occupation as

$$\frac{P_{rel}^{o}(n,\tau)}{P_{rel}^{t}(n,\tau)} = e^{\frac{\epsilon_2-\epsilon_1}{\tau}} \quad 84$$

Equation 84 is most certainly an approximation, but agrees with the intuition that as the loading increases, an increasingly higher number of T-sites will be occupied. However, it does not depend on loading so it is difficult to interpret it (and it is rather doubtful if it captures the full physics of the problem). Furthermore, it lacks any connection to entropy, so its efficacy is very much in doubt.

Even though Equation 84 does not depend on loading as it should, it may be used as a boundary condition (near loading of zero). Using the experimental, near zero loading value of O-to-T-site excitation energy of 295 meV (Salomons, 1990), at room temperature, it predicts a very high O-site occupation relative to that of T-site:

$$\frac{P_{rel}^{o}(n,\tau)}{P_{rel}^{t}(n,\tau)} = .9937 \quad 85$$

This means that if we are using a 2x2x2 supercell to represent our PdH system, there will be configurational T-site occupation only after unity loading. But this is not a limitation on the model, however, since we can use statistical interpolation at any loading level once we have an overall model.

A Simple O-to-T Excitation Model

We may refine the above estimates, which are primarily for computational purposes, from the results of (Salomons, 1990), Equation 60, which includes entropy terms with the hope of capturing more physics of the problem. We write it as:

$$e^{-\frac{\epsilon_t-\epsilon_o}{\tau}} = \frac{\theta_t(1-\theta_o)}{\theta_o(1-\theta_t)} \qquad 86$$

We may put Equation 86 on a firmer footing within our framework using Equations 77 & 78 as a starting point, repeated below for convenience:

$$\mu_o(\tau,\theta_o,\theta_t) = \tau\, ln\frac{\theta_o}{1-\theta_o} - \tau\, l\, n(z) + (\theta_o + 2\theta_t)\frac{\partial\varepsilon_h(\theta_o,\theta_t)}{\partial\theta_o} + \varepsilon_h(\theta_o,\theta_t) \qquad 87$$

$$\mu_t(\tau,\theta_o,\theta_t) = \tau\, ln\frac{\theta_t}{1-\theta_t} - \tau\, l\, n(z) + (\theta_t + \frac{1}{2}\theta_o)\frac{\partial\varepsilon_h(\theta_o,\theta_t)}{\partial\theta_t} + \varepsilon_h(\theta_o,\theta_t) \qquad 88$$

We define the O-to-T excitation energy via a matching of the Octahedral and Tetrahedral site chemical potentials, equating Equations 87 & 88,

$$\Delta\varepsilon_{O-T}(\theta) = (\theta_t + \frac{1}{2}\theta_o)\frac{\partial\varepsilon_h(\theta_o,\theta_t)}{\partial\theta_t} - (\theta_o + 2\theta_t)\frac{\partial\varepsilon_h(\theta_o,\theta_t)}{\partial\theta_o} \qquad 89$$

which, for the FCC lattice we are dealing with, and using Equation 74, becomes

$$\Delta\varepsilon_{O-T}(\theta) = \frac{1}{2}\theta\frac{\partial\varepsilon_h(\theta_o,\theta_t)}{\partial\theta_t} - \theta\frac{\partial\varepsilon_h(\theta_o,\theta_t)}{\partial\theta_o}$$

90

It is the zeroth order of this quantity that (Salomons, 1990) estimates to be 295 meV. We may actually estimate its full loading dependence, Equation 90, using our *ab initio* model. The result is shown below:

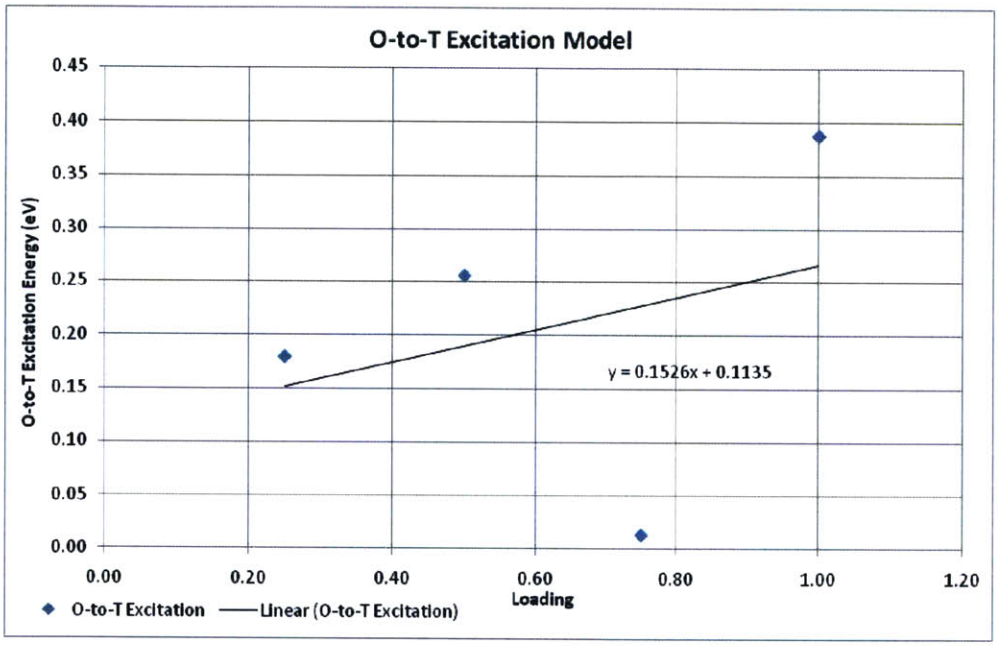

Figure 16: Model loading dependent O-to-T Excitatin Energy

Via a linear interpolation of the graphed data, we get the following simple but reasonable, linear Octahedral-to-Excitation model

$$\Delta\varepsilon_{O-T}(\theta) = 0.1526\theta + 0.1135\ (eV\ per\ H\ atom)$$

91

From this, we rewrite Equation 86 as

$$e^{-\frac{\Delta\varepsilon_{O-T}(\theta)}{\tau}} = \frac{\theta_t(1-\theta_o)}{\theta_o(1-\theta_t)}$$

92

Equations 91 and 92 together with Equations 56, 77 and 78 fully characterize the computational model, and may be used after state energies $\varepsilon_h(\theta_o, \theta_t)$, and the Excitation Energy, $\Delta\varepsilon_{O-T}(\theta)$ have been calculated *ab-initio,* and connected to experiment as detailed below.

In terms of computation, the final result means that Equations 62 and 63, now written as a function of fractional occupations using Equations 77 & 78, become:

$$\mu_H(\tau, \theta_o, \theta_t) = \mu_o(\tau, \theta_o, \theta_t) = \mu_t(\tau, \theta_o, \theta_t) \quad 93$$

Hydrogen in Metal Lattice: State Energies

We would like to determine the interaction energy when a number of Hydrogen atoms, n, are introduced in the metal lattice and occupy n of available N Pd interstitial sites of both O- and T-species. We take the view that the interaction energy is equivalent to the energy difference between an isolated H_2 molecule in its gas phase compared to the energy of the same molecule within the lattice. The energy difference provides us with a measure of the chemical potential energy required to bring an isolated H atom (proton) into the potential energy holes within the Pd Lattice.

Computationally, we use one particular definition of this interaction (Hagelstein P. , Private Communication, 2010) & (Fukai, 2005) as follows:

$$\varepsilon_h(n) = \varepsilon^{Pd}_{(n+1)H} - \left(\varepsilon^{Pd}_{nH} + \frac{1}{2}\varepsilon^{Vac}_{2H}\right) \quad 94$$

In Equation 94,

$\varepsilon^{Pd}_{(n+m)H}$ is the ground state energy of a Pd Lattice with $(n+m)$ of its N interstices filled with H-atoms, and

ε^{Vac}_{2H} is the ground state energy of an isolated H_2 molecule in its gas phase.

As defined, Equation 94 will give us the interaction energy of one H atom, which is precisely what we need for the determination of chemical potential in Equation 40. In the following sections, we will provide some results based on *ab initio* calculation on a 2x2x2 Pd supercell.

Connecting Total Interaction Energy to Enthalpy Change

To be able to compare our results to experiment, it is crucial that we make a correct translation of our calculated state energy as defined by Equation 94, to what is normally done in the literature by physical chemists. The interaction energy as defined in Equation 94 makes it clear that it is the energy change of a Hydrogen atom entering into the Pd lattice. Consequently, since it is a total energy change, it must consist of enthalpy AND entropy contributions, in line with the fundamental thermodynamic relationship in terms of total internal energy vs. entropy balance

(Equation 36):

$$F(\tau, V, n) \equiv U - \tau\sigma \tag{95}$$

In other words, the interaction energy as defined does not equal enthalpy change. It is in fact more closely related to the change in the total Internal Energy in a thermodynamic sense. See Chapter 9 for a more detailed discussion of this connection. At this stage in the model, all we can say is that enthalpy and entropy changes are related to the interaction energy in some way:

$$\Delta H(n) = f[\varepsilon_h(n)] \tag{96}$$

$$\Delta S(n) = g[\varepsilon_h(n)] \tag{97}$$

where, in physical chemistry terms, $\Delta H(n)$ is the enthalpy (heat) of solution, and $\Delta S(n)$ is the entropy of solution, see (Fukai, 2005), for example. Equations 96 & 97 may be expressed in terms of kJ per mole of H_2 gas, but we adopt an equivalent measure of eV per H atom here.

The other consequence of Equations 96 & 97 is that our model will only capture configurational entropy. The other entropy terms (optical, acoustic and image interaction) need to be added as correction terms (Kuji, Oates, Bowerman, & Flanagan, 1983) – see next section for a full discussion with parameters.

Energy Corrections

Zero-Point, Thermal Excitation Energies

The results from experiment include both zero point and thermal excitation energies of the free H2 molecule as well as the absorbed H. Our *ab initio* results do not include these energy terms, such that it is important to correct for them. These correction terms are well known from literature, (Christensen, Stoltze, Jacobsen, & Norskov, 1990) for example, so we only summarize them here.

For the gas phase, we need to include the translational thermal energy, rotational thermal energy, and vibrational zero point energy as, respectively (Christensen, Stoltze, Jacobsen, & Norskov, 1990):

$$\varepsilon_{Trans}^{H2} = \frac{5}{2}k_B T \tag{98}$$

$$\varepsilon_{Rot}^{H2} = k_B T \tag{99}$$

$$\varepsilon_{Zero}^{H2} = \frac{1}{2}\hbar\omega_{H-H} \tag{100}$$

The thermal energy of the absorbed Hydrogen atom is given by

$$\varepsilon_{Thermal}^{H/Pd} = 3k_B T \tag{101}$$

For the zero point energy, we ignore thermal contributions and take into account only the vibrational part (including all 3 modes) to arrive at

$$\varepsilon_{Vib}^{H/Pd} = \frac{3}{2}\hbar\omega_0 \tag{102}$$

Lastly, we add the work needed to compress Hydrogen into the Palladium bulk:

$$\varepsilon_{Comp}^{H/Pd} = \frac{1}{2}k_B T$$

103

On a per Hydrogen atom basis, therefore, we need to add the following correction term, from Equations 98-102:

$$\Delta E = \left(3k_B T + \tfrac{3}{2}\hbar\omega_0 + \frac{1}{2}k_B T\right) - \frac{1}{2}\left(\tfrac{5}{2}k_B T + k_B T + \tfrac{1}{2}\hbar\omega_{H-H}\right)$$

104

Using the following figures: $T = 300$, $\hbar\omega_{H-H} = 540\ meV$ (Christensen, Stoltze, Jacobsen, & Norskov, 1990), and $\hbar\omega_0 = 68.5\ meV$ (Wicke & Brodowsky, 1978), we get the energy correction for the Hydrogen atom at T=300K:

$$\Delta E = \left(3k_B T + \tfrac{3}{2}\hbar\omega_0 + \frac{1}{2}k_B T\right) - \frac{1}{2}\left(\tfrac{5}{2}k_B T + k_B T + \tfrac{1}{2}\hbar\omega_{H-H}\right) = -77\ meV$$

105

or about $\Delta E = -77\ meV$.

The correction term is thus very small and is will only be a small corrective factor in our results below.

Energy Pressure Correction

Finally, we consider the energy correction that is due to the isothermal change in pressure. As the volume changes isothermally from V to $V + \Delta V$ as a result of change in pressure from P to $P + \Delta P$, we would expect a free energy change given by:

$$dE = -\sigma d\tau + pdV$$

106

where σ here denotes entropy and p is pressure. In Equation 106, dV is understood to be positive (the usual formulation, $dE = \sigma d\tau - pdV$, assumes a *decrease* in volume as pressure is applied). For an isothermal change (assuming the volumetric change is slow enough), Equation 106

becomes nearly approximately

$$dE = p(\theta)dV \tag{107}$$

This represents the work done on the PdH system at a particular loading-dependent pressure. We take the view that Equation 107 corrects our interaction energy calculation (Equation 94) in the following manner:

$$\varepsilon_h' = \varepsilon_{(n+1)H}^{Pd} - \left(\varepsilon_{nH}^{Pd} + \frac{1}{2}\varepsilon_{2H}^{Vac}\right) + \left(dE_{(n+1)H} - dE_{nH}\right) \tag{108}$$

where

$$dE_{nH} = p(\theta = n/N)dV \tag{109}$$

and dV is the volumetric *increase* of the lattice per additional hydrogen atom.

It is a challenge to gain the value of $p(\theta = n/N)$ theoretically, so it has to be included here from experiment in a self consistent manner.

Configurational Correction

The calculated state energies are based on a simple model where there is no tetrahedral occupation below unity loading (and full octahedral occupation at or above unity loading). Based on our O-to-T model above, Equations 91 & 92, it is evident there will be occupation of both sites at all loading levels and temperatures (above model equations are repeated here):

$$e^{-\frac{\Delta\varepsilon_{O-T}(\theta)}{\tau}} = \frac{\theta_t(1-\theta_o)}{\theta_o(1-\theta_t)} \tag{110}$$

where

$$\Delta\varepsilon_{O-T}(\theta) = 0.1526\theta + 0.1135\ (eV\ per\ H\ atom) \qquad 111$$

Based on this model, we attempted to correct the calculated state energies using the fractional occupations predicted by Equations 110 and 111. The idea is to assume that, below unity loading, we can assign fractional energies based on the fractional O-occupation (as opposed to the full loading based on supercell configuration). The two figures are close but not identical due to Equations 110 and 111. We then assign the fractional T-occupation the higher state energy predicted by Equation 111. The real dependence is obviously more complex, but ours may be considered to be a first order linear approximation.

The results, shown below, indicate that the differences are negligible.

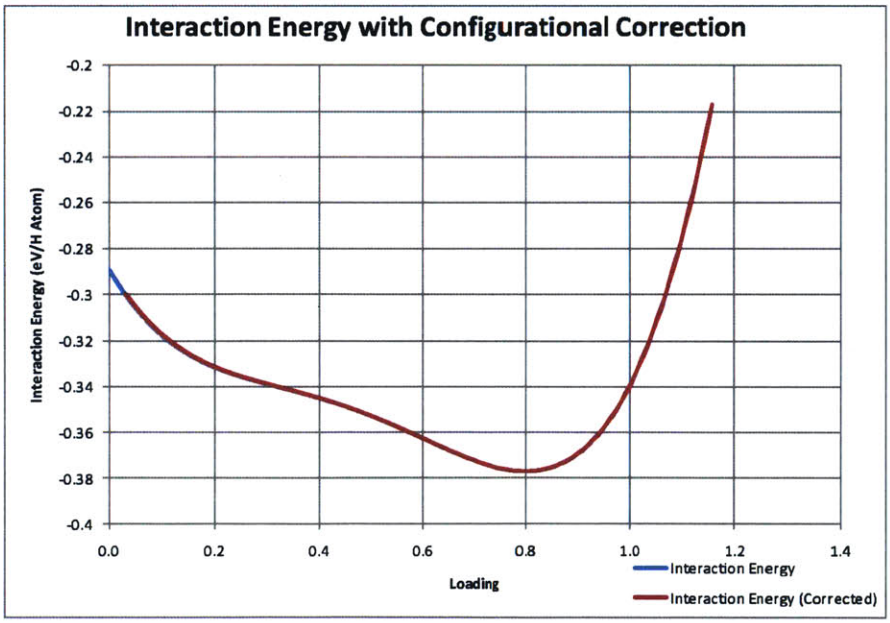

Figure 17: Interstitial Site Configurational Correction

Entropy Correction

From the discussion in section *Connecting Total Interaction Energy to Enthalpy Change* above, it is apparent that the calculated interaction energy for dissolved H in Pd, Equation 94, will contain electronic and configurational entropy terms, but not acoustical, option and image interaction terms. These need to be added as correction terms. We attempt to capture the corrections here following the treatment of (Kuji, Oates, Bowerman, & Flanagan, 1983).

For dissolved Hydrogen, we identify the following excess entropy terms (relative to zero loading):

$$\Delta S_{corr} = \Delta S_{opt} + \Delta S_{ac} + \Delta S_{el} + \Delta S_{im} + \Delta S_{nc} \quad 112$$

for optical, acoustic, electronic, image interaction, and non-ideal configurational entropy, respectively.

We ignore magnetic and translational contributions since we expect these to be small [ibid]. Next, we attempt to estimate each term as in [ibid]:

ΔS_{opt} is estimated to increase from 4.15E-05*T to 6.15E-05*T eV per H atom as the loading θ increases from $\theta = 0$ to $\theta = 1$. (Rush, 1982) in (Kuji, Oates, Bowerman, & Flanagan, 1983).

ΔS_{ac} is estimated to be zero ($\Delta S_{ac} \sim 0$) [ibid]

ΔS_{elec} may be estimated to rise from zero at zero loading to about $\Delta S_{el} = 4.15\text{E} - 05 * \text{T}$ eV per H atom

ΔS_{im} may be estimated to be $\Delta S_{im} = -3.01\text{E} - 05 * \theta * \text{T}$ eV per H atom

Of course ΔS_{nc} is already included in our model.

From these results, we estimate the total entropy correction to be

$$\Delta S_{corr} = 7.26 * 10^{-5} * T \left(\frac{eV}{Atom}\right) \quad 113$$

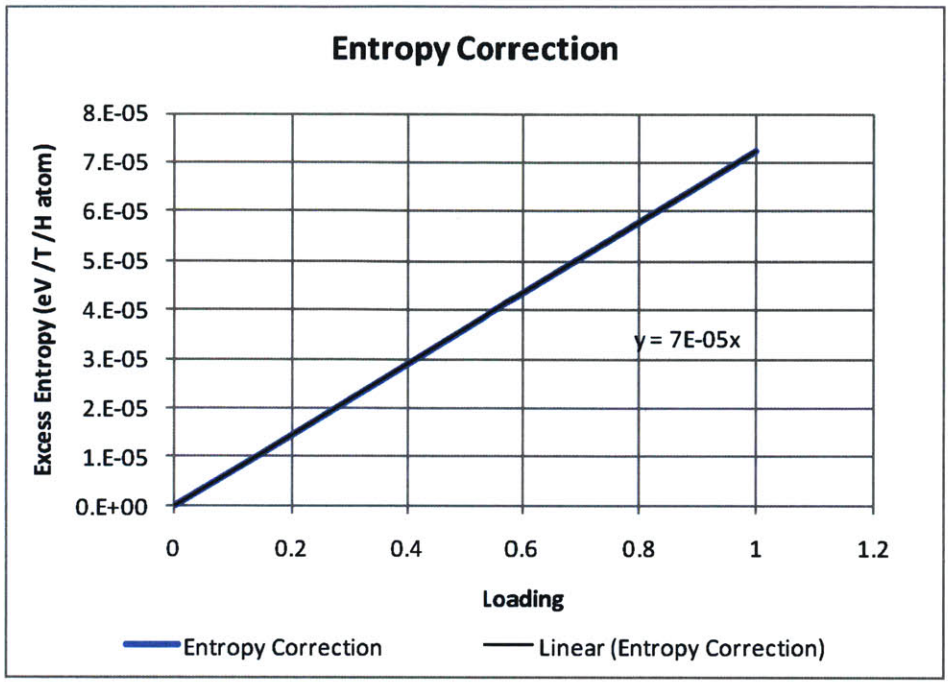

Figure 18: Entropy Corrections Model

DFT Energy Correction

Constant Correction

We expect the energy calculations from DFT to contain a constant shift by formulation. From the first Hohenberg-Kohn theorem, the electron density $n_0(\boldsymbol{r})$ uniquely determines the external potential $V_{ext}(\boldsymbol{r})$ to a constant. This implies the Hamiltonian, and hence the energy, is then also determined up to a constant. Based on this, we may attempt first to correct Equation 94 by a constant energy shift:

$$\varepsilon_h(n) = \varepsilon^{Pd}_{(n+1)H} - \left(\varepsilon^{Pd}_{nH} + \frac{1}{2}\varepsilon^{Vac}_{2H}\right) + \Delta\varepsilon_0 \qquad 114$$

where $\Delta\varepsilon_0$ is a constant correction term independent of loading. It may be determined by comparison to experimental data.

Polynomial Correction

However, we also know that DFT contains other errors and approximations that we need to account for. These include exchange/correlation errors and the errors due to the pseudo potential approximation.

There is no reason to believe these errors are constant with loading. Therefore, as a first approximation, if we assume the errors are small, we may use a linear expansion around a particular loading, i.e.

$$\Delta\varepsilon_0 = \varepsilon_1 + \varepsilon_\delta\theta \tag{115}$$

where ε_1 and ε_δ are determined based on an experimental fit.

We made an attempt to correct the interaction energy according to Equation 115. However, it does not appear as if there are any ε_1 or ε_δ that would make this scheme yield any reasonable results. We therefore discard this idea, and instead revisit a more robust model of DFT errors in Chapter 9.

The Equivalent Gas Pressure

We would eventually like to connect any results we get with experimental observables. The most accessible quantities in the types of loading experiments that we would like to connect to are Temperature (T) and Pressure (P), and especially the latter.

Previously in Equation 51, we found a connection between the chemical potential and loading. We would now like to make the connection between pressure (which we can readily measure experimentally) and loading, using the chemical potential as the bridge. To do so, we will assume the system is in equilibrium. If this is the case, then the chemical potential of hydrogen in the gas phase has to equal that of absorbed hydrogen:

$$\mu_H(absorbed) = \frac{1}{2}\mu_{H_2}(gas) \qquad 116$$

In Equation 116, we have used the $\frac{1}{2}$ factor to account for dissociation of the hydrogen molecule upon absorption. Equation 51 provides an expression for $\mu_H(absorbed)$. It remains to determine $\mu_{H_2}(gas)$.

Chemical Potential for Hydrogen Gas

As a first step, we shall model the hydrogen molecule as an ideal gas. For an ideal gas, we can use the ideal gas law:

$$PV = N\tau \qquad 117$$

This assumption treats individual molecules as independent point particles (i.e. that occupy zero volume). We will further assume that the gas molecules have the following types of energy: translational, rotational, vibrational and electronic (we have thus ignored any energy of a nuclear nature). Lastly, we will assume that the different energy types are independent of each other. Using these assumptions, we can get the molecular partition function as

$$Z_{H_2} = Z_t Z_v Z_r Z_e \qquad 118$$

where Z_t, Z_v, Z_r, Z_e are, respectively, the translational, vibrational, rotational and electronic partition functions of the molecule. The gas phase chemical potential is then

$$\mu_{H_2} = -\tau \, ln(Z_{H_2}) = \mu_t + \mu_v + \mu_r + \mu_e \tag{119}$$

In the following sections, we will derive the expressions for the terms in Equation 119 in terms of thermodynamic observables using basic statistical mechanics formulation in (Kittel, Thermal Physics, 1980) and (Silbey, Alberty, & Bawendi, 2004).

Translational Chemical Potential

For the translational component of the chemical potential, we use basic particle-in-a-box model with energy quanta (indexed by a positive integer n):

$$\epsilon_n = \frac{h^2 n^2}{8mV^{\frac{2}{3}}} \tag{120}$$

From basic thermodynamics, counting all degrees of freedom, we can build the single partition function as

$$z_t = \left[\sum_n exp\left(-\frac{h^2 n^2}{8mV^{\frac{2}{3}}}\right)\right]^3 = \left(\frac{2\pi m\tau}{h^2}\right)^{\frac{3}{2}} V \tag{121}$$

after turning the sum into an integral and evaluating. Because all molecules are taken to be identical, the total partition function representing N non-interacting particles is then

$$Z_t = \frac{1}{N!} {z_t}^N \tag{122}$$

Helmholtz free energy is then given by

$$F_t = -\tau \, ln(Z_t)$$

123

and the chemical potential follows as

$$\mu_t = \left(\frac{\partial F_t}{\partial N}\right)_{\tau,V} = -\tau \, ln\left[\left(\frac{2\pi m\tau}{h^2}\right)^{\frac{3}{2}} \frac{\tau}{P}\right]$$

124

after using the ideal gas law and the Stirling approximation.

Vibrational Chemical Potential

At or near the ground state, the hydrogen molecule may be modeled as a simple harmonic oscillator per Equation 53 above:

$$z_v = \sum_{n=0}^{\infty} e^{-\frac{\epsilon_{0v}\left(n+\frac{1}{2}\right)}{\tau}} = e^{-\frac{\epsilon_{0v}}{2\tau}} \sum_{n=0}^{\infty} e^{-\frac{\epsilon_{0v} n}{\tau}} = \frac{e^{-\frac{\epsilon_{0v}}{2\tau}}}{1 - e^{-\frac{\epsilon_{0v}}{\tau}}}$$

125

where we have picked a single mode, and explicitly included the zero point energy. For N non-interacting molecules,

$$Z_v = {z_v}^N$$

126

from which

$$F_v = -\tau \, ln(Z_v) = -N\tau \, ln \, (z_v)$$

127

and

$$\mu_v = \left(\frac{\partial F_v}{\partial N}\right)_{\tau,V} = -\tau \, ln \frac{e^{-\frac{\epsilon_{0v}}{2\tau}}}{1 - e^{-\frac{\epsilon_{0v}}{\tau}}} \tag{128}$$

Rotational Chemical Potential

The rotational energy for a diatomic molecule may be expressed in terms of its moment of inertia I and rotational quantum number J as follows

$$\epsilon_r = \frac{J(J+1)h^2}{8\pi^2 I} \tag{129}$$

We can arrive at the particle partition function by summing over all degeneracies of J (there are $(2J+1)$ of them for each energy level)

$$z_r = \sum_{J=0}^{\infty} (2J+1) e^{-\frac{J(J+1)h^2}{8\pi^2 I}} = \frac{8\pi^2 I\tau}{h^2} \tag{130}$$

after turning the summation into an integral (valid for the range of τ that we are interested in). We note that we need to add a "symmetry factor", σ, to Equation 130, to account for the fact that the properties of the hydrogen molecule are unchanged upon a 180 degree rotation:

$$z_r = \frac{8\pi^2 I\tau}{\sigma h^2} \tag{131}$$

For N non-interacting molecules,

$$Z_r = {z_r}^N \tag{132}$$

from which

$$F_t = -\tau\, ln(Z_r) = -N\tau\, ln\,(z_r)$$

133

and

$$\mu_r = \left(\frac{\partial F_r}{\partial N}\right)_{\tau,V} = -\tau\, ln\frac{8\pi^2 I\tau}{\sigma h^2}$$

134

Electronic Chemical Potential

We state here the chemical potential contribution from electronic states of a diatomic molecule without elaboration but in reference to (Silbey, Alberty, & Bawendi, 2004), (Christensen, Stoltze, Jacobsen, & Norskov, 1990):

$$\mu_e = -\tau\, ln[g_0 e^{\frac{\epsilon_D}{\tau}}]$$

135

where $g_0(=1)$ (singlet) is the ground state degeneracy and $-\epsilon_D$ is normally chosen as the spectroscopic dissociation energy of the hydrogen molecule, (Silbey, Alberty, & Bawendi, 2004)

$$\mu_e = -\epsilon_D$$

136

Note: According to our definition of the interaction energy, Equation 94, we are interested in the chemical potential of the hydrogen atom, and since our reference is the un-dissociated hydrogen gas, the electronic contribution to the chemical potential must be zero:

$$\mu_e = -\epsilon_D = 0$$

137

Contrast this to other investigators that reference the interaction energy against two dissociated

hydrogen atoms (e.g. (Fukai, 2005)). In that case, Equation 136 applies.

Total Chemical Potential for Hydrogen Gas

Putting together Equations 124, 128, 134 and 136, we get the gas phase chemical potential as

$$\mu_{H_2} = -\tau ln\left[\left(\frac{2\pi m\tau}{h^2}\right)^{\frac{3}{2}}\frac{\tau}{P}\right] - \tau ln\frac{e^{-\frac{\epsilon_{0v}}{2\tau}}}{1-e^{-\frac{\epsilon_{0v}}{\tau}}} - \tau\, ln\frac{8\pi^2 I\tau}{\sigma h^2} - \epsilon_D \qquad 138$$

Chemical Potential Continuity Condition

We may compare Equation 138 to Equation 51:

$$\mu_H(\theta) = -\tau \ln z + \tau \ln \frac{\theta}{1-\theta} + \theta \frac{\partial}{\partial \theta} \varepsilon_h(\theta) + \varepsilon_h(\theta) \tag{139}$$

and make the connection between Equation 138 and Equation 139 via Equation 116:

$$\mu_H(absorbed) = \tfrac{1}{2} \mu_{H_2}(gas) \tag{140}$$

Thus our initial model is:

$$-\tau \ln \frac{e^{-\frac{\epsilon_{0v}}{2\tau}}}{1-e^{-\frac{\epsilon_{0v}}{\tau}}} + \tau \ln \frac{\theta}{1-\theta} + \theta \frac{\partial}{\partial \theta} \varepsilon_h(\theta) + \varepsilon_h(\theta) = -\frac{\tau}{2}\left[\ln \left[\left(\frac{2\pi m \tau}{h^2} \right)^{\frac{3}{2}} \frac{\tau}{P} \right] + \ln \frac{e^{-\frac{\epsilon_{0v}}{2\tau}}}{1-e^{-\frac{\epsilon_{0v}}{\tau}}} + \ln \frac{8\pi^2 I \tau}{\sigma h^2} + \frac{\epsilon_D}{\tau} \right] \tag{141}$$

Simplifying, we get

$$-\frac{\tau}{2} \ln \frac{e^{-\frac{\epsilon_{0v}}{2\tau}}}{1-e^{-\frac{\epsilon_{0v}}{\tau}}} + \tau \ln \frac{\theta}{1-\theta} + \theta \frac{\partial}{\partial \theta} \varepsilon_h(\theta) + \varepsilon_h(\theta) = -\frac{\tau}{2}\left[\ln \left[\left(\frac{2\pi m \tau}{h^2} \right)^{\frac{3}{2}} \frac{\tau}{P} \right] + \ln \frac{8\pi^2 I \tau}{\sigma h^2} + \frac{\epsilon_D}{\tau} \right] \tag{142}$$

In terms of thermodynamic parameters, Equation 142 is a function of temperature and pressure only. We can therefore simply connect gas pressure to loading with temperature as a parameter.

Total Chemical Potential Continuity Condition Including Tetrahedral Occupation

From our analysis above, we may include tetrahedral occupation to the results of Equation 142 using Equations 77 & 78. The results are the following two relationships based on equality of chemical potentials for O- and T-sites:

$$\tau\, ln\frac{\theta_o}{1-\theta_o} - \tau\, ln(z) + \theta\frac{\partial \varepsilon_h(\theta)}{\partial \theta} + \varepsilon_h(\theta_o, \theta_t) = -\frac{\tau}{2}\left[ln\left[\left(\frac{2\pi m\tau}{h^2}\right)^{\frac{3}{2}}\frac{\tau}{P}\right] + ln\frac{e^{\frac{\epsilon_{0y}}{2\tau}}}{1-e^{\frac{\epsilon_{0y}}{\tau}}} + ln\frac{8\pi^2 I\tau}{\sigma h^2} + \frac{\epsilon_D}{\tau}\right] \quad (143)$$

and

$$\tau\, ln\frac{\theta_t}{1-\theta_t} - \tau\, ln(z) + \theta\frac{\partial \varepsilon_h(\theta)}{\partial \theta} + \varepsilon_h(\theta_o, \theta_t) = -\frac{\tau}{2}\left[ln\left[\left(\frac{2\pi m\tau}{h^2}\right)^{\frac{3}{2}}\frac{\tau}{P}\right] + ln\frac{e^{\frac{\epsilon_{0y}}{2\tau}}}{1-e^{\frac{\epsilon_{0y}}{\tau}}} + ln\frac{8\pi^2 I\tau}{\sigma h^2} + \frac{\epsilon_D}{\tau}\right] \quad (144)$$

Given pressure from experiment, either Equation 143 or 144 may be solved consistently with Equation 74:

$$\theta = \theta_o + 2\theta_t \quad (145)$$

and Equations 91 & 92:

$$\Delta\varepsilon_{O-T}(\theta) = 0.1526\theta + 0.1135\ (eV\ per\ H\ atom) \quad (146)$$

$$e^{-\frac{\Delta\varepsilon_{O-T}(\theta)}{\tau}} = \frac{\theta_t(1-\theta_o)}{\theta_o(1-\theta_t)} \quad (147)$$

Model of Non-Ideal H Gas: Fugacity

The gas phase chemical potential (Equation 138) is based on an ideal gas model (Equation 117). Unfortunately, the behavior of the gas phase will deviate significantly from its ideal characteristics especially at high pressures. Therefore, we cannot reliably use a model based on ideal gas law and expect it to match experiment. This is a well studied subject, and we will not rehash it here. Instead, we will work with a few key results.

To model a non-ideal gas, we may use the van de Waals Equation in place of the ideal gas equation:

$$\left(P + \frac{a}{V^2}\right)(V - Nb) = N\tau \qquad 148$$

where

a is a constant characteristic of the gas in question,

b is the exclusion volume (i.e., volume actually occupied by the gas molecules), and

N is the number of moles of the gas in volume V.

From this simple equation, we note that the "real pressure" or *fugacity* (Bockris, Chien, Hodko, & Minevski, 1992) is given by $P + \frac{a}{V^2}$. It is therefore appropriate to correct our total chemical potential for the gas phase (Equation 138), by replacing the pressure by fugacity, f:

$$\mu_{H_2} = -\tau\, ln\left[\left(\frac{2\pi m\tau}{h^2}\right)^{\frac{3}{2}}\frac{\tau}{f}\right] - \tau\, ln\frac{e^{-\frac{\epsilon_{0v}}{2\tau}}}{1 - e^{-\frac{\epsilon_{0v}}{\tau}}} - \tau\, ln\frac{8\pi^2 I\tau}{\sigma h^2} - \epsilon_D \qquad 149$$

The chemical potential continuity condition (Equation 141) then becomes

$$-\tau\, ln\frac{e^{-\frac{\epsilon_{0v}}{2\tau}}}{1 - e^{-\frac{\epsilon_{0v}}{\tau}}} + \tau\, ln\frac{\theta}{1-\theta} + \theta\frac{\partial}{\partial\theta}\varepsilon_h(\theta) + \varepsilon_h(\theta) = -\frac{\tau}{2}\left[ln\left[\left(\frac{2\pi m\tau}{h^2}\right)^{\frac{3}{2}}\frac{\tau}{f}\right] + ln\frac{e^{-\frac{\epsilon_{0v}}{2\tau}}}{1 - e^{-\frac{\epsilon_{0v}}{\tau}}} + ln\frac{8\pi^2 I\tau}{\sigma h^2} + \frac{\epsilon_D}{\tau}\right] \qquad 150$$

We interpret Equation 150 to connect fugacity to temperature and loading in a first principles manner. To connect experimentally measured pressure to temperature and loading, we need to first solve Equation 150 for fugacity then connect the resulting fugacity to the experimental pressure in the manner described below.

Note:

A question naturally arises as to whether the other terms making up the gas phase chemical potential should remain the same or be similarly corrected. Intuitively, only the kinetic (translational) contribution to the chemical potential is dependent on pressure, and the rotational, vibrational, and electronic contributions should remain independent of pressure. In fact this is exactly the conclusion that another worker (Hemmes, Driessen, & Griessen, 1986) came to.

Connecting Fugacity to Pressure: Model of Tkacz

It still remains to get a relationship between pressure and fugacity. There is an elementary analytical relationship between the two that we may use, namely

$$log\frac{f}{P} = -\frac{1}{\tau}\int_0^P \left(\frac{\tau}{V} - V\right) dP \qquad 151$$

The analytical expression must then be connected to experiment. Several such parameterizations are available, including (Hemmes, Driessen, & Griessen, 1986) and (Tkacz & Litwiniuk, 2002). The latter in particular, covers the high pressure region we are interested in (up to 100GPa), and has a simple dependence on temperature:

$$ln\, f = \frac{\left\{1.5 * A * P^{2/3} + 3 * B * P^{1/3} + (D + E * T) * ln(P) - 3 * C * P^{-1/3}\right\}}{R * T} \qquad 152$$

where, for hydrogen in gas phase,

A=176.330,

B=-633.675,

C=-304.574,

D=731.393,

E=8.59805,

and pressure and fugacity are in units of MPa. We plot the model below:

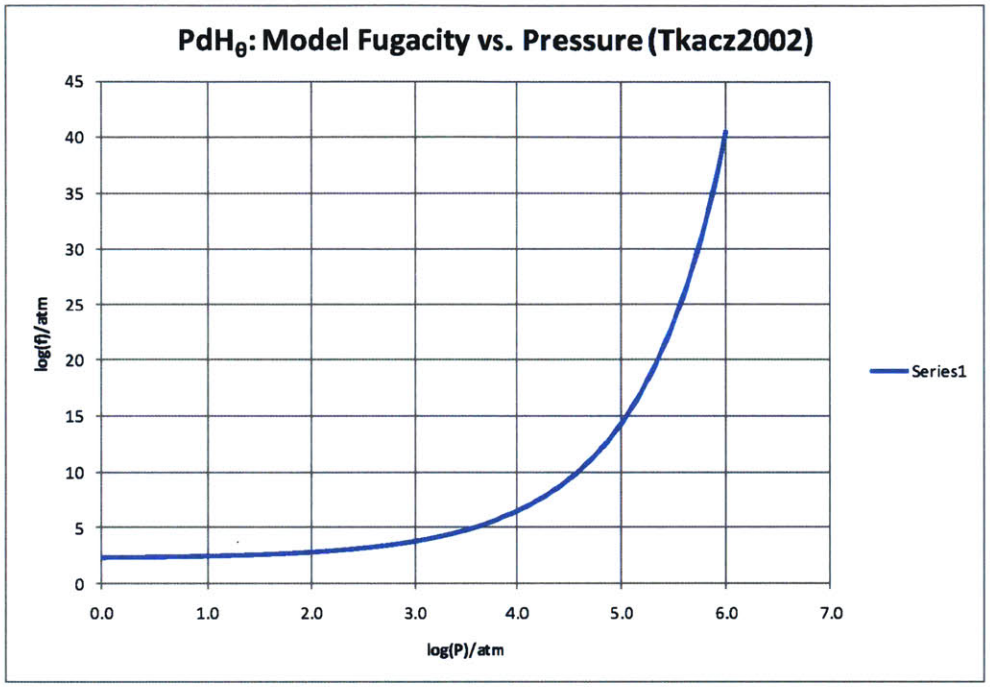

Figure 19: Model Fugacity vs. Pressure (Based on fugacity model by (Tkacz & Litwiniuk, 2002))

Connecting Fugacity to Pressure: The Bockris Model

We also looked at alternative fugacity models. In particular, (Bockris, Chien, Hodko, & Minevski, 1992) has a model around room temperature (300K). The results are shown below, and may be seen to be slightly different from those of (Tkacz & Litwiniuk, 2002).

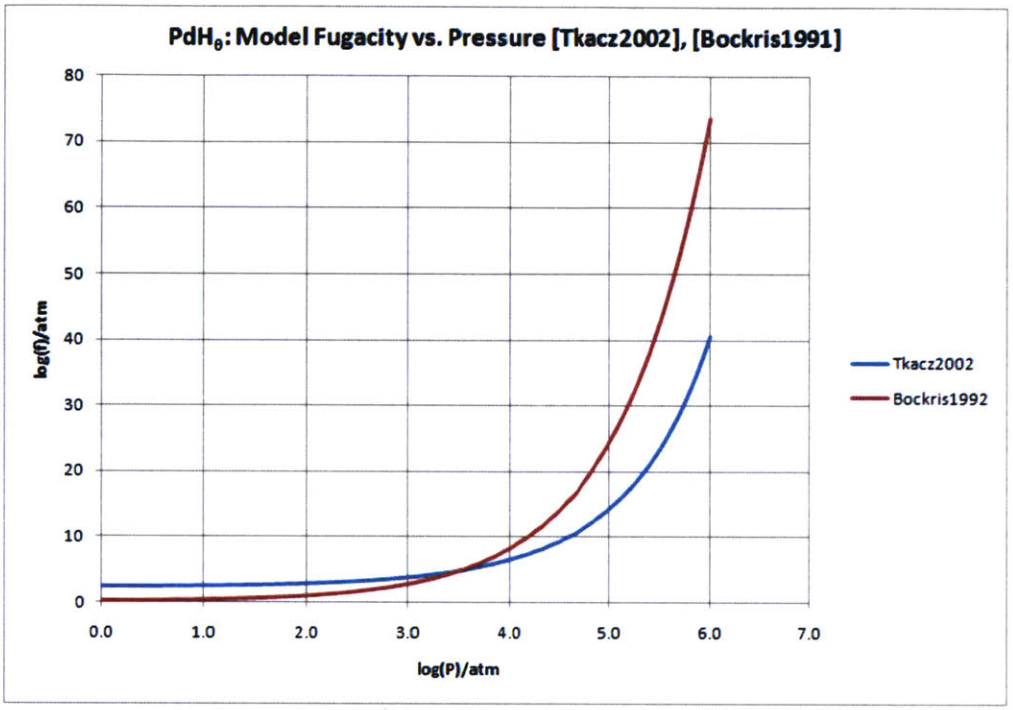

Figure 20: Comparison of fugacity models based on (Bockris, Chien, Hodko, & Minevski, 1992) and (Tkacz & Litwiniuk, 2002). Model fit done for computational purposes.

Putting the Entire Model Together: First Try

Here we put together the full model which contains all energy corrections, both tetrahedral and octahedral occupations, and correction for non-ideal gas.

The gas phase chemical potential is given by Equation 149:

$$\mu_{H_2} = -\tau\, ln\left[\left(\frac{2\pi m\tau}{h^2}\right)^{\frac{3}{2}}\frac{\tau}{f}\right] - \tau\, ln\frac{e^{-\frac{\epsilon_{0v}}{2\tau}}}{1-e^{-\frac{\epsilon_{0v}}{\tau}}} - \tau\, ln\frac{8\pi^2 I\tau}{\sigma h^2} - \epsilon_D \tag{153}$$

As a first try, we may assume what is readily accessible from our computational model, namely that there is no tetrahedral occupation below a loading of unity and vice versa. In other words, we may use the following estimate of the bulk hydrogen chemical potential:

$$\mu_H(\tau,\theta_o,\theta_t) = \begin{cases}\mu_o(\tau,\theta_o,\theta_t), & \theta \le 1\\ \mu_t(\tau,\theta_o,\theta_t), & \theta > 1\end{cases} \tag{154}$$

where

$$\mu_o(\tau,\theta_o,\theta_t) = \tau\, ln\frac{\theta_o}{1-\theta_o} - \tau\, ln(z) + \theta\frac{\partial\varepsilon_h(\theta)}{\partial\theta} + \varepsilon_h(\theta_o,\theta_t) \tag{155}$$

and

$$\mu_t(\tau,\theta_o,\theta_t) = \tau\, ln\frac{\theta_t}{1-\theta_t} - \tau\, ln(z) + \theta\frac{\partial\varepsilon_h(\theta)}{\partial\theta} + \varepsilon_h(\theta_o,\theta_t) \tag{156}$$

The continuity condition is given by Equation 140:

$$\mu_H(\text{absorbed}) = \tfrac{1}{2}\mu_{H_2}(\text{gas}) \tag{157}$$

Therefore, for, $\theta < 1$,

$$\tau\, ln\frac{\theta_o}{1-\theta_o} - \tau\, ln(z) + \theta\frac{\partial \varepsilon_h(\theta)}{\partial \theta} + \varepsilon_h(\theta_o, \theta_t) = -\frac{1}{2}\left[\tau ln\left[\left(\frac{2\pi m\tau}{h^2}\right)^{\frac{3}{2}}\frac{\tau}{f}\right] + \tau ln\frac{e^{-\frac{\epsilon_{0v}}{2\tau}}}{1-e^{-\frac{\epsilon_{0v}}{\tau}}} + \tau ln\frac{8\pi^2 I\tau}{\sigma h^2} + \epsilon_D\right] \quad 158$$

For, $\theta > 1$, incorporating entropy expression from (Powell, 1976) into Equation 158, we have

$$\tau\, ln\frac{\theta}{3-\theta} - \tau\, ln(z) + \theta\frac{\partial \varepsilon_h(\theta)}{\partial \theta} + \varepsilon_h(\theta) = -\frac{1}{2}\left[\tau ln\left[\left(\frac{2\pi m\tau}{h^2}\right)^{\frac{3}{2}}\frac{\tau}{f}\right] + \tau ln\frac{e^{-\frac{\epsilon_{0v}}{2\tau}}}{1-e^{-\frac{\epsilon_{0v}}{\tau}}} + \tau\, ln\frac{8\pi^2 I\tau}{\sigma h^2} + \epsilon_D\right] \quad 159$$

Equations 158 and 159 complete the model. From them, we can calculate fugacity as:

$$f(\theta) = Ae^{\frac{B(\theta)}{\tau}} \quad 160$$

where

$$A(\tau) = \tau\left(\frac{2\pi m\tau}{h^2}\right)^{\frac{3}{2}} \quad 161$$

$$B(\theta) = \begin{cases} 2\tau ln\frac{\theta_o}{1-\theta_o} - 2\tau\, ln(z) + 2\theta\frac{\partial \varepsilon_h(\theta)}{\partial \theta} + 2\varepsilon_h(\theta) + \tau ln\frac{e^{-\frac{\epsilon_{0v}}{2\tau}}}{1-e^{-\frac{\epsilon_{0v}}{\tau}}} + \tau ln\frac{8\pi^2 I\tau}{\sigma h^2} + \epsilon_D & \theta < 1 \\ 2\tau ln\frac{\theta}{3-\theta} - 2\tau\, ln(z) + 2\theta\frac{\partial \varepsilon_h(\theta)}{\partial \theta} + 2\varepsilon_h(\theta) + \tau ln\frac{e^{-\frac{\epsilon_{0v}}{2\tau}}}{1-e^{-\frac{\epsilon_{0v}}{\tau}}} + \tau ln\frac{8\pi^2 I\tau}{\sigma h^2} + \epsilon_D & \theta > 1 \end{cases} \quad 162$$

are both known.

Out of curiosity, we can actually verify that $A(\tau)$ has the units of pressure, thus

$$A(\tau) \rightarrow \frac{J^{\frac{5}{2}}Kg^{\frac{3}{2}}}{J^3s^3} \rightarrow \frac{Kg^{\frac{3}{2}}}{J^{\frac{1}{2}}s^3} \rightarrow \frac{sKg^{\frac{3}{2}}}{Kg^{\frac{1}{2}}ms^3} \rightarrow \frac{Kg}{ms^2}$$

163

which is the unit of a Pascal.

The results are shown below:

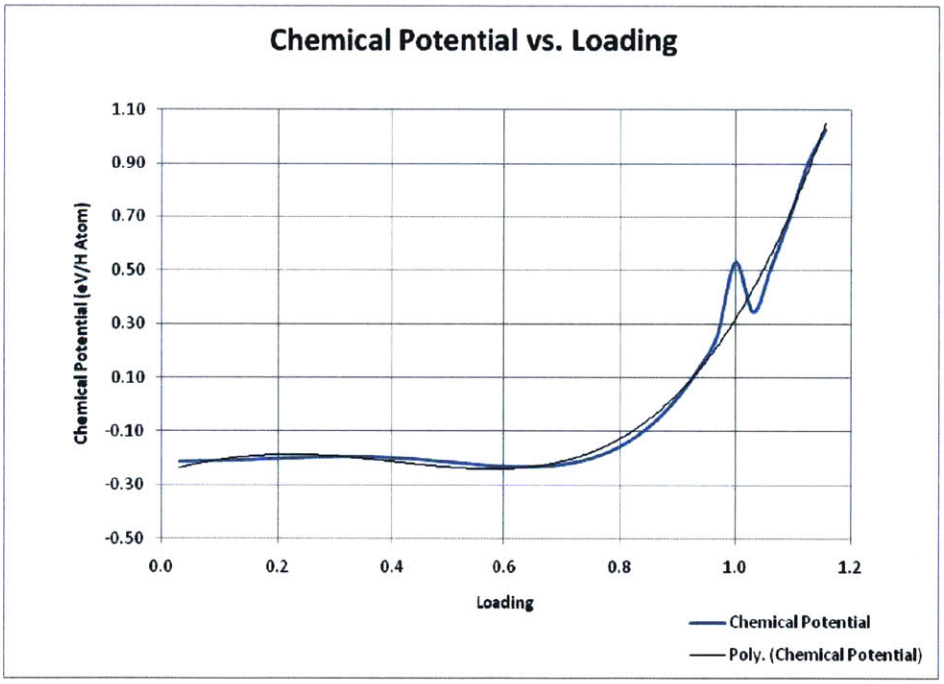

Figure 21: Chemical Potential vs. Loading (Based on Model+Offset)

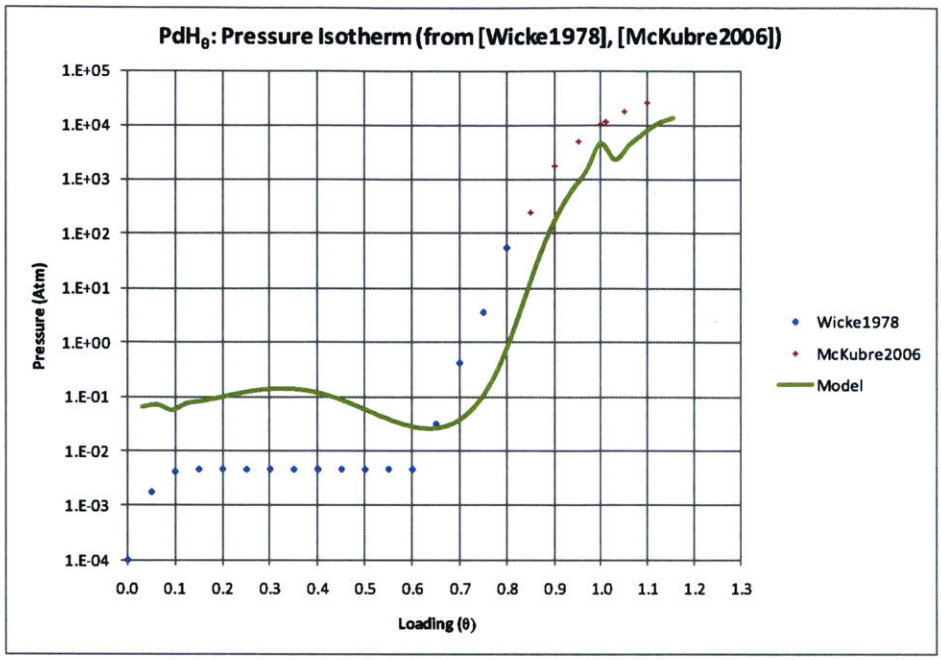

Figure 22: Pressure Composition Isotherm at room temperature: Model vs. Experiment (Pressure is on log scale). See above section on how pressure plotted here was derived from fugacity model of (Tkacz & Litwiniuk, 2002).

Putting the Entire Model Together: Discussion and Second Try

It turns out that the approximations leading to Equations 158 & 159 yield results which, while reasonably match experiments, fail to predict correct behavior around unity loading, which is a key concern of ours.

The chemical potential from these approximations is shown above whereby we note that there is a discontinuity around loading of unity, a clearly unphysical result. We attribute this to the incorrect treatment of the step in energy going from octahedral to tetrahedral site occupations.

We see a similar unphysical result in pressure around unity loading in the Figure 22 above.

Correct Unity Loading Treatment

To correct the unity loading values, we need the account for both octahedral and tetrahedral entropies at all loading levels, and especially around loading of unity. To do this, we use the above approximations to arrive at the interaction/state energy model as a function of loading. An example of such a model is given in Figure 23 below. This result is based on fractional loading approximations made leading to Equations 158 & 159.

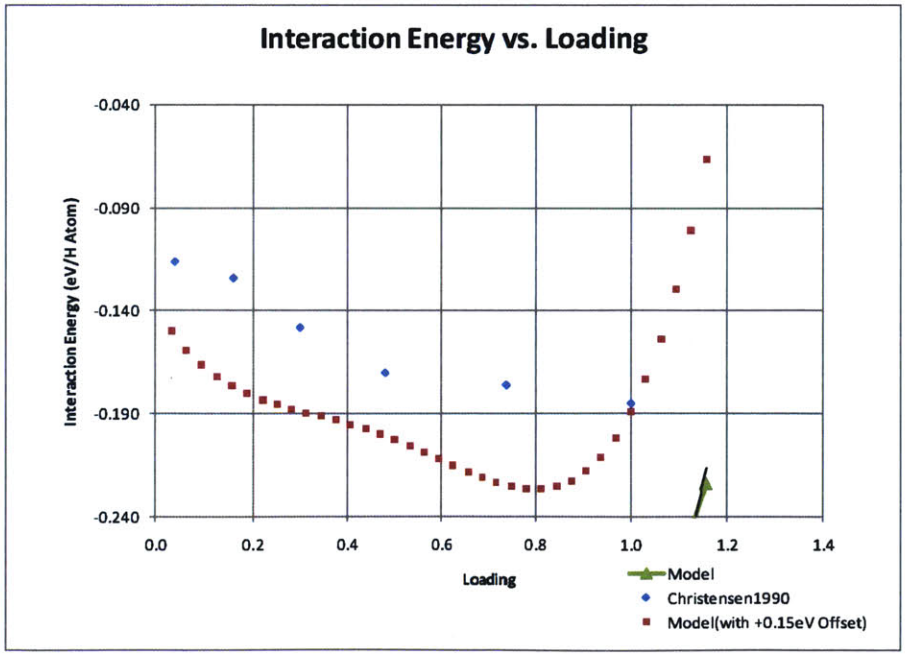

Figure 23: Interaction Energy vs. Loading (2x2x2 Super Cell) - with +.15 eV Offset vs. (Christensen, Stoltze, Jacobsen, & Norskov, 1990)

Once we arrive at the interaction/state energy model, we match the chemical potentials according to the analysis leading to Equation 147:

$$e^{\frac{\Delta\varepsilon_{O-T}(\theta)}{\tau}} = \frac{\theta_t(1-\theta_o)}{\theta_o(1-\theta_t)} \tag{164}$$

Unlike the approximations leading to Equations 158 & 159, Equation 164 predicts **both** octahedral and tetrahedral occupations at **all** loading levels. This means the full model used to derive the equivalent gas pressure and chemical potential may be re-written as follows (we have repeated previous equations for convenience):

The gas phase chemical potential is unchanged (Equation 153):

$$\mu_{H_2} = -\tau ln\left[\left(\frac{2\pi m\tau}{h^2}\right)^{\frac{3}{2}}\frac{\tau}{f}\right] - \tau ln\frac{e^{-\frac{\epsilon_{0y}}{2\tau}}}{1-e^{-\frac{\epsilon_{0y}}{\tau}}} - \tau ln\frac{8\pi^2 I\tau}{\sigma h^2} - \epsilon_D \tag{165}$$

The bulk hydrogen chemical is given by Equation 93:

$$\mu_H(\tau,\theta_o,\theta_t) = \mu_o(\tau,\theta_o,\theta_t) = \mu_t(\tau,\theta_o,\theta_t) \tag{166}$$

where

$$\mu_o(\tau,\theta_o,\theta_t) = \tau ln\frac{\theta_o}{1-\theta_o} - \tau\, ln(z) + \theta\frac{\partial\varepsilon_h(\theta)}{\partial\theta} + \varepsilon_h(\theta_o,\theta_t) \tag{167}$$

$$\mu_t(\tau,\theta_o,\theta_t) = \tau ln\frac{\theta_t}{1-\theta_t} - \tau\, ln(z) + \theta\frac{\partial\varepsilon_h(\theta)}{\partial\theta} + \varepsilon_h(\theta_o,\theta_t) \tag{168}$$

The continuity condition is given by Equation 116:

$$\mu_H(absorbed) = \frac{1}{2}\mu_{H_2}(gas)$$

169

Therefore, for all, θ

$$\tau\, ln\frac{\theta_o}{1-\theta_o} - \tau\, ln(z) + \theta\frac{\partial \varepsilon_h(\theta)}{\partial \theta} + \varepsilon_h(\theta_o, \theta_t) = \tau\, ln\frac{\theta_t}{1-\theta_t} - \tau\, l\, n(z) + \theta\frac{\partial \varepsilon_h(\theta)}{\partial \theta} + \varepsilon_h(\theta_o, \theta_t)$$

$$= -\frac{\tau}{2}\left[ln\left[\left(\frac{2\pi m\tau}{h^2}\right)^{\frac{3}{2}}\frac{\tau}{f(\theta)}\right] + ln\frac{e^{-\frac{\epsilon_{0v}}{2\tau}}}{1-e^{-\frac{\epsilon_{0v}}{\tau}}} + ln\frac{8\pi^2 I\tau}{\sigma h^2} + \frac{\epsilon_D}{\tau}\right]$$

170

and Equation 164 determines O vs. T site occupation. This completes our model.

♦

As before, we calculate fugacity as

$$f(\theta) = A(\tau)e^{\frac{B(\theta)}{\tau}}$$

171

where

$$A(\tau) = \tau\left(\frac{2\pi m\tau}{h^2}\right)^{\frac{3}{2}}$$

172

$$B(\theta) = 2\tau ln\frac{\theta_o}{1-\theta_o} - 2\tau\, ln(z) + 2\theta\frac{\partial \varepsilon_h(\theta)}{\partial \theta} + 2\varepsilon_h(\theta_o, \theta_t) + \tau ln\frac{e^{-\frac{\epsilon_{0v}}{2\tau}}}{1-e^{-\frac{\epsilon_{0v}}{\tau}}} + \tau\, ln\frac{8\pi^2 I\tau}{\sigma h^2} + \epsilon_D$$

173

are both known from the model or experiment.

Methodology

For the test results, we used a 2x2x2 supercell, and placed H atoms at O-sites at random. For the 2x2x2 supercell, there is an enormous number of configurations for the PdH system. However, we found out that, empirically, the difference in energy between adjacent loading levels ($\Delta\theta = \frac{1}{32}$) is on the order of 13.6 eV per atom, which is larger than most configurational differences.

We then carried out SCF *ab-initio* calculations using a plane wave basis. The exchange correlation function used in all cases was Generalized Gradient Approximation (GGA) utilizing the Perdew-Burke-Ernzehof exchange correlation which includes a nonlinear core correction.

To calculate the lattice constant, we used a single PdH cell. The cell was manually relaxed at several loading levels by minimizing the SCF energies at different values of the lattice constant around the expected value for the cell. These values were then fitted to a sixth order polynomial to arrive at a fairly accurate lattice constant that minimizes the ground state energy. We can see that the Pd lattice expands about 4% from its bulk unloaded to fully loaded, which is about 12.5% volumetric expansion (vs. 10% experimental).

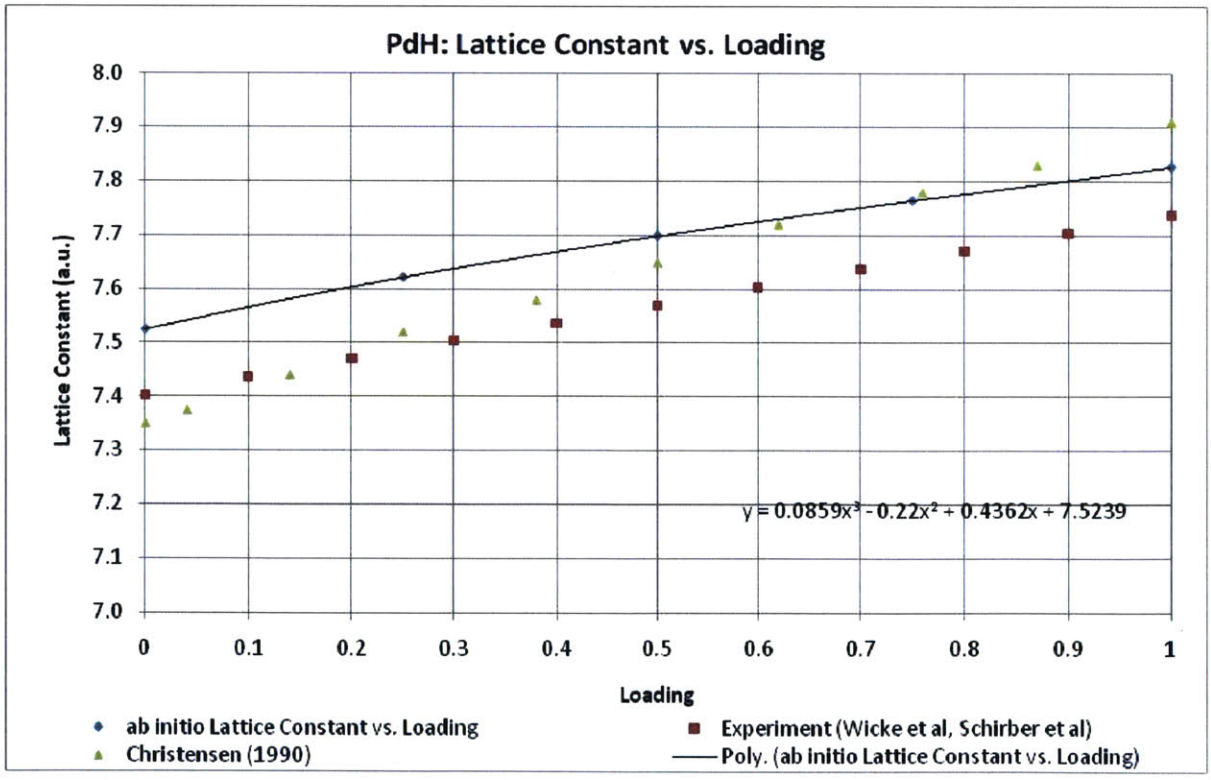

Figure 24: Lattice constant relaxation (Pd): *ab initio* model results compared to various experimental data.

We also used the same plane wave basis to calculate the SCF ground state energy of a hydrogen molecule. This is accomplished by placing the molecule inside a vacuum whose size is the same as the cell size used in the metallic bulk and loaded calculation. Additionally, the same energy and charge density cut-offs and mesh sizes were used in both cases. The H-H bond length was obtained from literature (74pm):

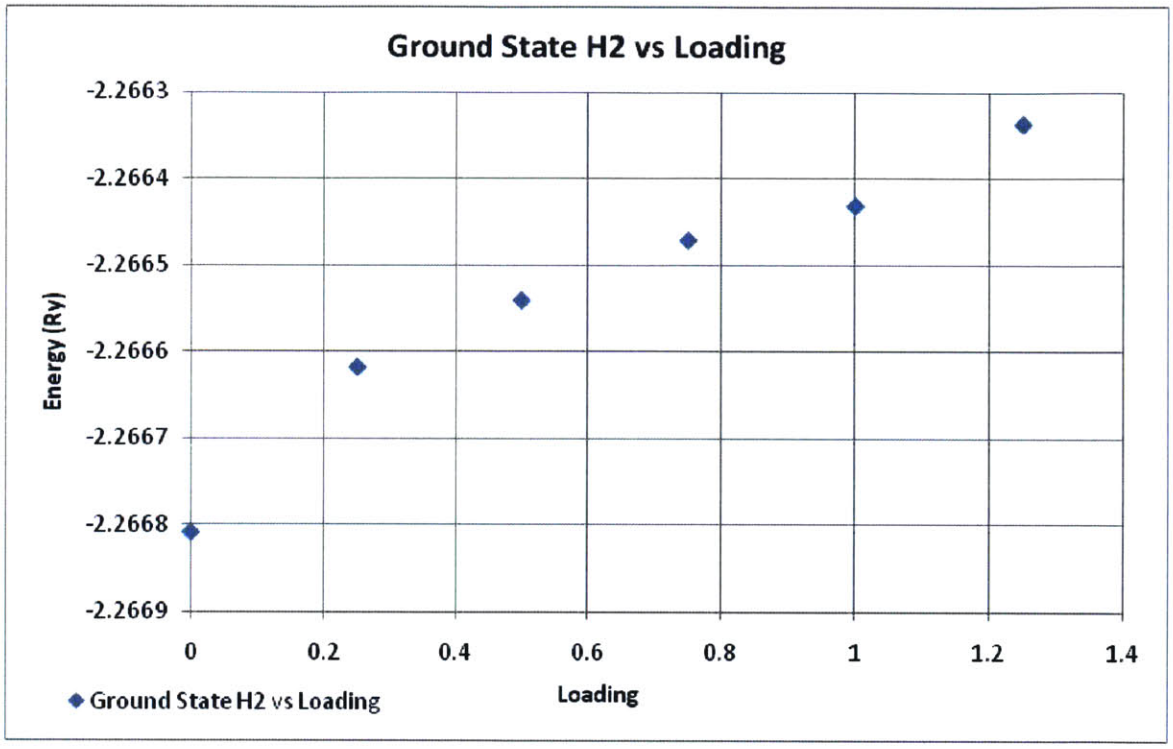

Figure 25: Hydrogen Molecule in a Box: energy vs. box size - based on loading (shown for Pd)

As can be seen from the above figure, there was no appreciable ground state energy difference as the box size was varied to coincide with the corresponding lattice constant (the energy difference is only around 0.01 eV).

Results

We use the following parameters:

Parameter	Value	Source	Comment
ϵ_{0v}	68.5 meV	(Christensen, Stoltze, Jacobsen, & Norskov, 1990)	
ϵ_h	2.65079 eV	(Silbey, Alberty, & Bawendi, 2004)	
m	$2 * 1.00794 * m_u$ kg	-	Use twice the mass of H
m_u	1.661e-27 kg	-	Atomic mass constant
σ	2	-	
I	$4.605 * 10^{-48} kg\ m^2$	(Silbey, Alberty, & Bawendi, 2004)	
P_0	$101.325 * 10^3$ Pa	-	Standard Pressure
ϵ_D	0 eV		Applies to H atom

Interaction Energy vs. Loading

We first present the results for Palladium. The interaction energy (Equation 94) is plotted below on a per hydrogen atom basis as a function of loading. In the literature, this energy is related (but not equivalent) to the absorption energy or heat of solution, and is a measure of the probability of hydrogen to occupying an interstitial site within Pd. We will go into further details about the connection in later chapters.

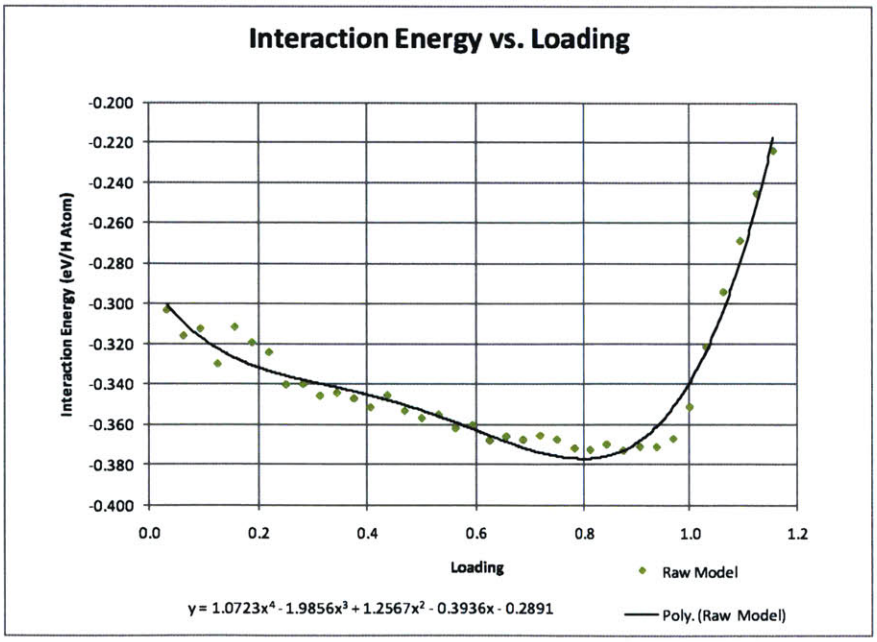

Figure 26: Interaction Energy vs. Loading (2x2x2 Super Cell). Raw, uncorrected model results.

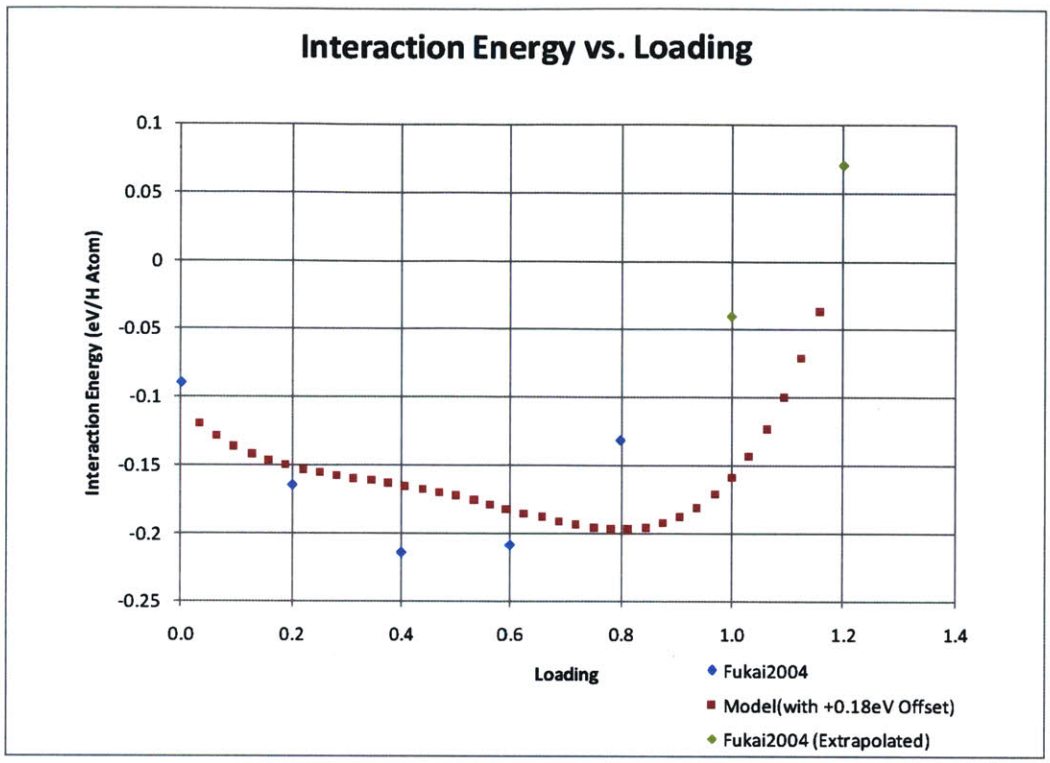

Figure 27: Interaction Energy vs. Loading (2x2x2 Super Cell) - with +.16 eV Offset vs. (Fukai, 2005). Note that Fukai's data is actually enthalpy.

We note that, if we make a constant 0.16 eV/atom correction, this result matches favorably other author's results (Fukai, 2005) as well as experiment (Mueller, Freeman, Dimmock, & Furdyna, 1970) in the loading range of 0.8-1.2. In particular, we note that the slope changes after a loading of around $\theta = 0.8$ in our results vs. $\theta = 0.6$ in the works cited. Since (Fukai, 2005)'s experimental data did not go beyond a loading of 0.8, we have extrapolated them beyond $\theta = 0.8$ by matching the slope from the data.

The correction is necessary to account for in-built computational error inherent in DFT (as distinct from relativity inherent in all pseudo-potential based calculations)

Chemical Potential vs. Loading

The chemical potential is also expected to increase with increasing absorption energy, and is shown below. We get this curve directly from Equations 94 and 96:

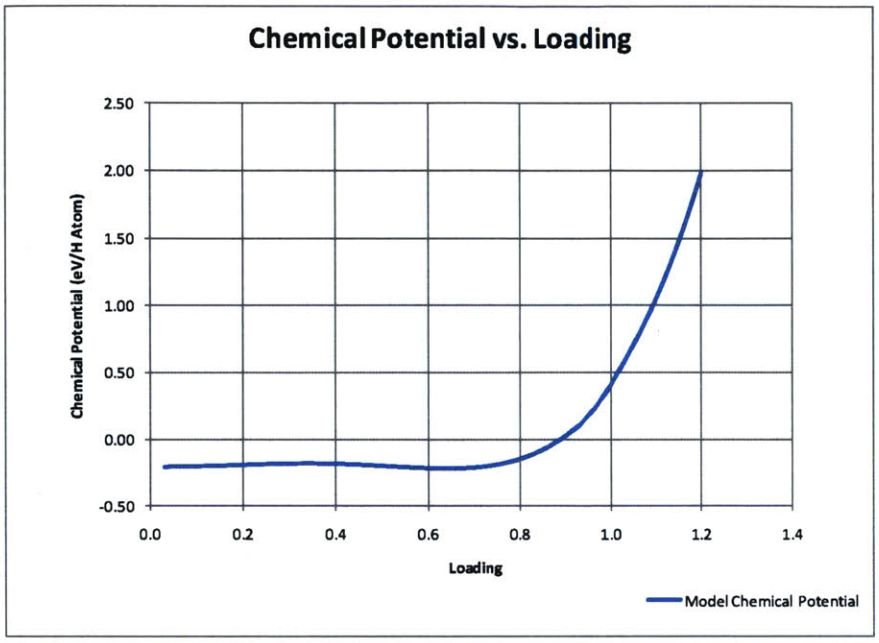

Figure 28: Chemical Potential vs. Loading (Based on Model+Offset)

Equivalent Pressure vs. Loading

The following result matches (Wicke & Brodowsky, 1978) data quite favorably after a +0.16 constant energy correction. Beyond unity loading, we see somewhat of a wider variance between model and data.

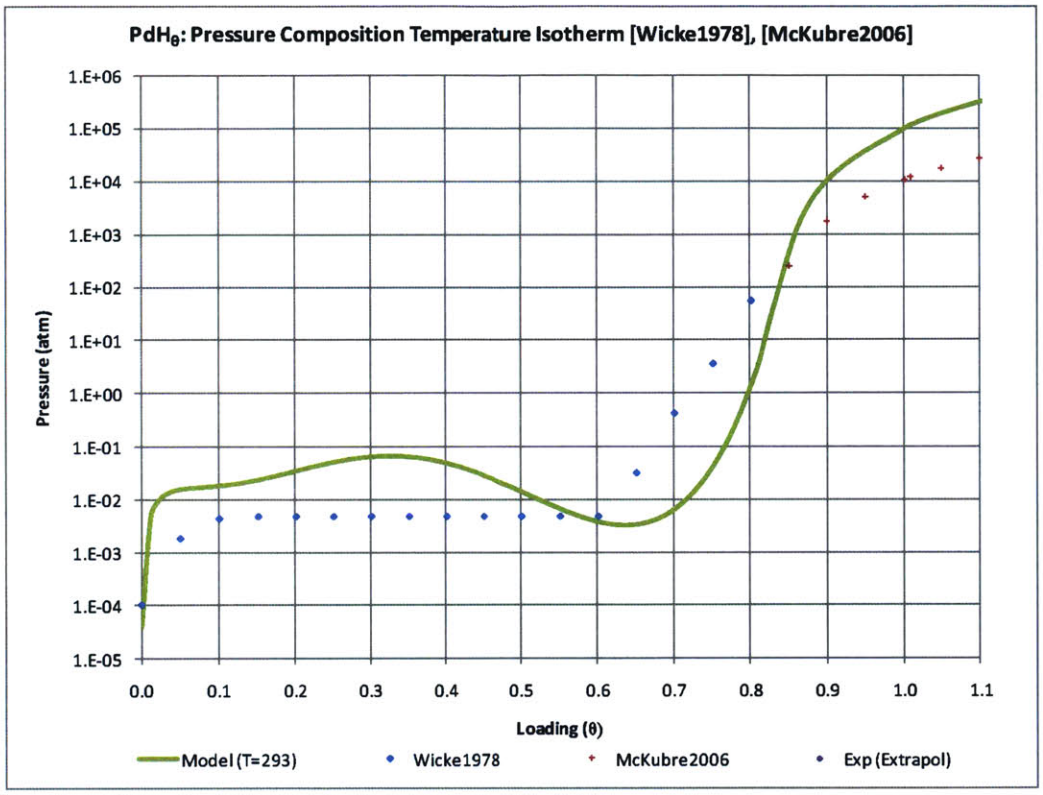

Figure 29: Pressure Composition Isotherm at room temperature: Model vs. Experiment (pressure is on log scale). See above section on how pressure plotted here was derived from fugacity model from (Tkacz & Litwiniuk, 2002)

Experimental reference: (Wicke & Brodowsky, 1978), (Tripodi, 2000) & (Baranowski, Filipek, Szustakowski, & Woryna, 1990) as analyzed by (McKubre & Tanzella, 2006).

Interaction Energy From Experiment: Integrated Energy Formulation

In this section, we will use experimental Pressure-Composition-Temperature (PCT) isotherms from experiment and, using our model, calculate the interaction energy that experiments suggest. This exercise will validate our model results by, in effect, running it backwards.

Model Equation (Octahedral Occupation)

We start with the chemical potential continuity condition, Equation 116

$$\mu_H(absorbed) = \frac{1}{2}\mu_{H_2}(gas) \tag{174}$$

From which (see above for complete derivation) we get Equation **142**:

$$-\tau ln\frac{e^{\frac{\epsilon_{0v}}{2\tau}}}{1-e^{\frac{\epsilon_{0v}}{\tau}}} + \tau ln\frac{\theta}{1-\theta} + \theta\frac{\partial}{\partial\theta}\varepsilon_h(\theta) + \varepsilon_h(\theta) = -\frac{\tau}{2}\left[ln\left[\left(\frac{2\pi m\tau}{h^2}\right)^{\frac{3}{2}}\frac{\tau}{P}\right] + ln\frac{e^{-\frac{\epsilon_{0v}}{2\tau}}}{1-e^{\frac{\epsilon_{0v}}{\tau}}} + ln\frac{8\pi^2 I\tau}{\sigma h^2} + \frac{\epsilon_D}{\tau}\right] \tag{175}$$

We recast Equation 175 into the following simpler partial ordinary differential equation form

$$\varepsilon_h'(\theta) + \varepsilon_h(\theta)F(\theta) = g(\theta) \tag{176}$$

where

$$\varepsilon_h'(\theta) = \frac{\partial}{\partial\theta}\varepsilon_h(\theta) \tag{177}$$

$$F(\theta) = \frac{1}{\theta} \tag{178}$$

and

$$g(\theta) = \frac{\tau}{\theta} ln(z) - \frac{\tau}{\theta} ln\frac{\theta}{1-\theta} - \frac{\tau}{2\theta}\left[ln\left[\left(\frac{2\pi m\tau}{h^2}\right)^{\frac{3}{2}}\frac{\tau}{P(\theta)}\right] + ln\frac{e^{-\frac{\epsilon_{0v}}{2\tau}}}{1-e^{-\frac{\epsilon_{0v}}{\tau}}} + ln\frac{8\pi^2 I\tau}{\sigma h^2} + \frac{\epsilon_h}{\tau}\right] \quad (179)$$

In Equation 179, we explicitly note that the pressure is a function of loading, and extract the following pressure isotherm from (Wicke & Brodowsky, 1978):

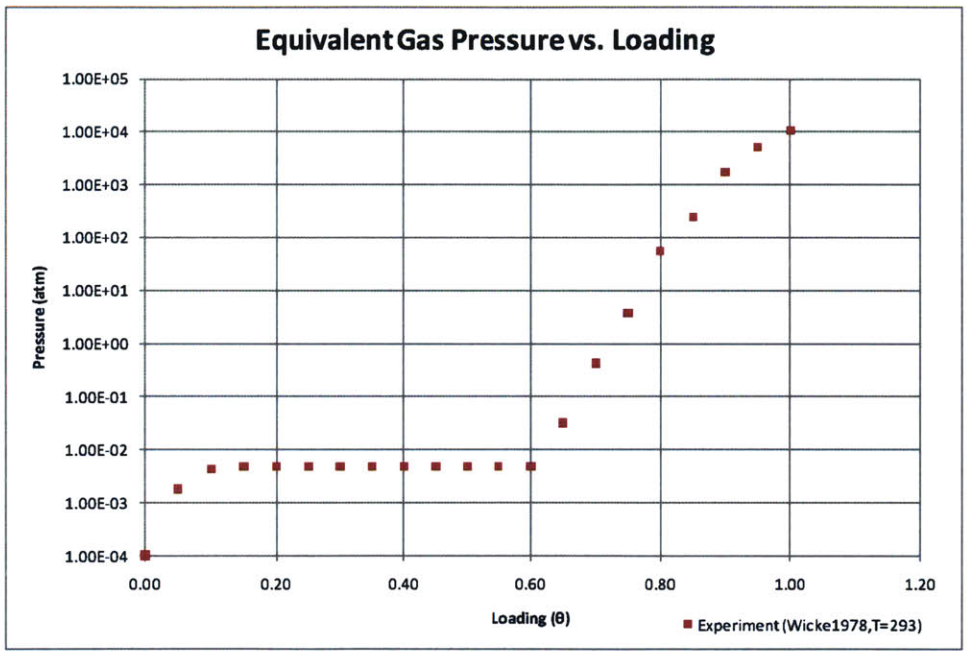

Figure 30: PdH: Pressure Composition Temperature isotherm (from (Wicke & Brodowsky, 1978))

Model Equation: Initial Conditions From Experiment

We assume that, given that it is an explicit function of loading only, Equation 176 may be solved numerically using ODE methods. In particular, we use a stiff ODE Matlab solver (ode23s) (Matlab, 2011), which is an implementation of the Rosenbrock formula, order 2, for solving stiff ODEs.

The solution will need some initial conditions, and for this we look to experimental data. Specifically, we need to find experimental data for Equation 176,

$$\varepsilon_{init} = \varepsilon_h(\theta = \theta_{init}) \tag{180}$$

There exists experimental data for the absorption energy per hydrogen atom from (Mueller, Freeman, Dimmock, & Furdyna, 1970). The data corresponds to $\theta = 0.037$ and the absorption energy was found to be -0.18 eV. It only remains to find the corresponding gas pressure at that loading level from (Wicke & Brodowsky, 1978) data. The full initial condition applicable to Equation 176 is thus

$$\varepsilon_{init} = -0.18\ eV\ per\ H\ atom = \varepsilon_h(\theta = 0.037) \tag{181}$$

and

$$P(\theta_{init}) = 10^{-2.488}\ atm \text{ (Wicke \& Brodowsky, 1978)} \tag{182}$$

The result is shown below, compared to our model:

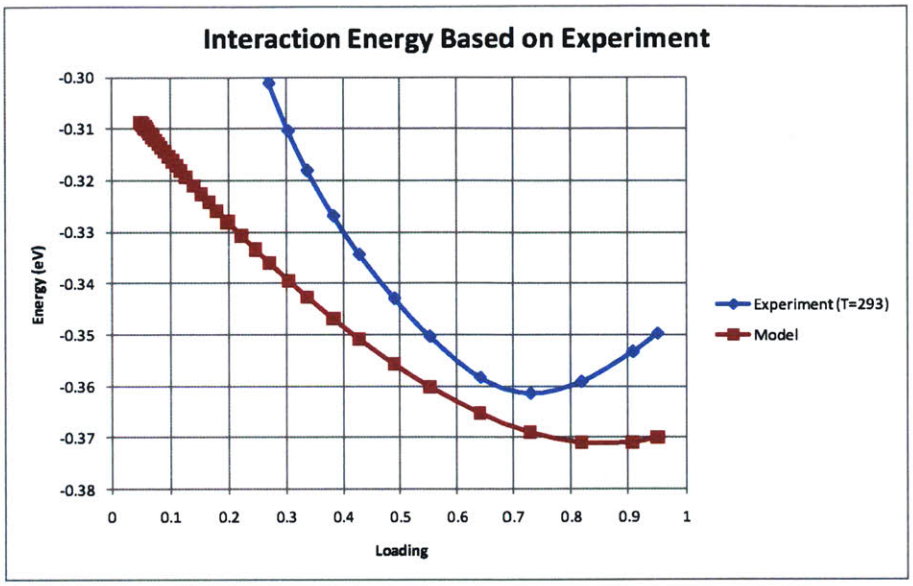

Figure 31: Initial Interaction Energy Curve Based on O-Site Occupation only.

Model Equation Including Tetrahedral Occupation

Once again, following the analysis of section *Connecting O-to-T Excitation Formulation To DFT: A Computational Model* we note that because the absorption energy for a tetrahedral occupation is much higher than that of an octahedral site, for occupations below unity, we have Equations 158 and 154:

$$\mu_o(\tau,\theta_o,\theta_t) \approx -\frac{\tau}{2}\left[ln\left[\left(\frac{2\pi m\tau}{h^2}\right)^{\frac{3}{2}}\frac{\tau}{P}\right] + ln\frac{e^{-\frac{\epsilon_{0V}}{2\tau}}}{1-e^{-\frac{\epsilon_{0V}}{\tau}}} + ln\frac{8\pi^2 I\tau}{\sigma h^2} + \frac{\epsilon_h}{\tau}\right] \quad 183$$

Beyond unity loading, we use Equations 159 and 154, repeated below for convenience:

$$\tau ln\frac{\theta}{3-\theta} - \tau\, ln(z) + \theta\frac{\partial\varepsilon_h(\theta)}{\partial\theta} + \varepsilon_h(\theta) = -\frac{1}{2}\left[\tau ln\left[\left(\frac{2\pi m\tau}{h^2}\right)^{\frac{3}{2}}\frac{\tau}{f}\right] + \tau ln\frac{e^{-\frac{\epsilon_{0V}}{2\tau}}}{1-e^{-\frac{\epsilon_{0V}}{\tau}}} + \tau\, ln\frac{8\pi^2 I\tau}{\sigma h^2} + \epsilon_D\right] \quad 184$$

The individual terms are already defined above. Based on this approximation, very similar to

Equations 176-179, we have:

$$\varepsilon_h'(\tau,\theta_o,\theta_t)+\varepsilon_h(\tau,\theta_o,\theta_t)F(\tau,\theta_o,\theta_t)=g(\tau,\theta_o,\theta_t) \tag{185}$$

where

$$\varepsilon_h'(\tau,\theta_o,\theta_t)=\frac{\partial}{\partial\theta_t}\varepsilon_h(\tau,\theta_o,\theta_t) \tag{186}$$

$$F(\theta_o,\theta_t)=\frac{2}{\theta_0+2\theta_t} \tag{187}$$

and

$$g(\tau,\theta_o,\theta_t)=\frac{2\tau}{\theta_0+2\theta_t}ln(z)-\frac{2\tau}{\theta_0+2\theta_t}ln\frac{\theta_t}{1-\theta_t}$$
$$-\frac{\tau}{\theta_0+2\theta_t}\left[ln\left[\left(\frac{2\pi m\tau}{h^2}\right)^{\frac{3}{2}}\frac{\tau}{P(\theta_o,\theta_t)}\right]+ln\frac{e^{-\frac{\epsilon_{0v}}{2\tau}}}{1-e^{-\frac{\epsilon_{0v}}{\tau}}}+ln\frac{8\pi^2I\tau}{\sigma h^2}+\frac{\epsilon_D}{\tau}\right] \tag{188}$$

Model Equation Including Tetrahedral Occupation, Non-Ideal Gas Correction and Full Entropy Calculation

We utilize the full model (Equation 170) to write the continuity condition as

$$\tau\, ln\frac{\theta_o}{1-\theta_o} - \tau\, ln(z) + \theta\frac{\partial\varepsilon_h(\theta)}{\partial\theta} + \varepsilon_h(\theta_o,\theta_t) = \tau\, ln\frac{\theta_t}{1-\theta_t} - \tau\, ln(z) + \theta\frac{\partial\varepsilon_h(\theta)}{\partial\theta} + \varepsilon_h(\theta_o,\theta_t)$$

$$= -\frac{1}{2}\left[\tau\, ln\left[\left(\frac{2\pi m\tau}{h^2}\right)^{\frac{3}{2}}\frac{\tau}{f}\right] + \tau\, ln\frac{e^{\frac{\epsilon_{0v}}{2\tau}}}{1-e^{\frac{\epsilon_{0v}}{\tau}}} + \tau\, ln\frac{8\pi^2 I\tau}{\sigma h^2} + \epsilon_D\right] \quad 189$$

Once again, we write Equation 189 as

$$\varepsilon_h'(\tau,\theta_o,\theta_t) + \varepsilon_h(\tau,\theta_o,\theta_t)F(\tau,\theta_o,\theta_t) = g(\tau,\theta_o,\theta_t) \quad 190$$

where now

$$\varepsilon_h'(\tau,\theta) = \frac{\partial}{\partial\theta}\varepsilon_h(\tau,\theta) \quad 191$$

$$F(\theta) = \frac{1}{\theta} \quad 192$$

$$g(\tau,\theta) = \frac{\tau}{\theta}l\,n(z) - \frac{\tau}{\theta}\, ln\frac{\theta_{o,t}}{1-\theta_{o,t}} - \frac{1}{2\theta}\left[\tau\, ln\left[\left(\frac{2\pi m\tau}{h^2}\right)^{\frac{3}{2}}\frac{\tau}{f(\theta)}\right] + \tau\, ln\frac{e^{\frac{\epsilon_{0v}}{2\tau}}}{1-e^{\frac{\epsilon_{0v}}{\tau}}} + \tau\, ln\frac{8\pi^2 I\tau}{\sigma h^2} + \epsilon_D\right] \quad 193$$

High Pressure, High Loading Results

In this section, we extend our results above to high loading regime ($\theta > 1$). Several authors have done experiments in the high pressure, high loading region using the resistance ratio method to determine loading levels of H/D in Pd [(Baranowski, Filipek, Szustakowski, & Woryna, 1990), (Zhang, Zhang, & Zhang, 2004), (Tripodi, 2000)]. Recently, (McKubre & Tanzella, 2006) brought together the results of these authors in one monograph (see Figure 32) below:

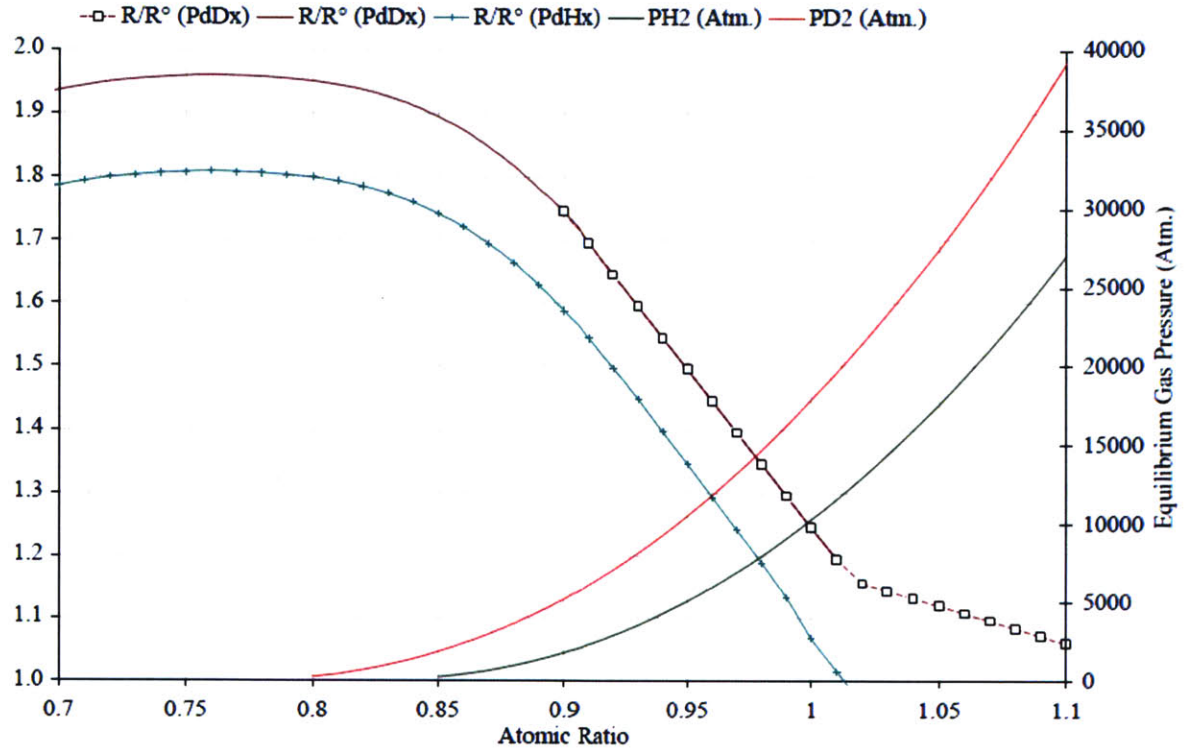

Figure 32: High Loading Data (From (McKubre & Tanzella, 2006))

The first thing we do is extend the (Wicke & Brodowsky, 1978) data (Figure 30 above) to loading beyond unity using the (McKubre & Tanzella, 2006) data. The result is shown below:

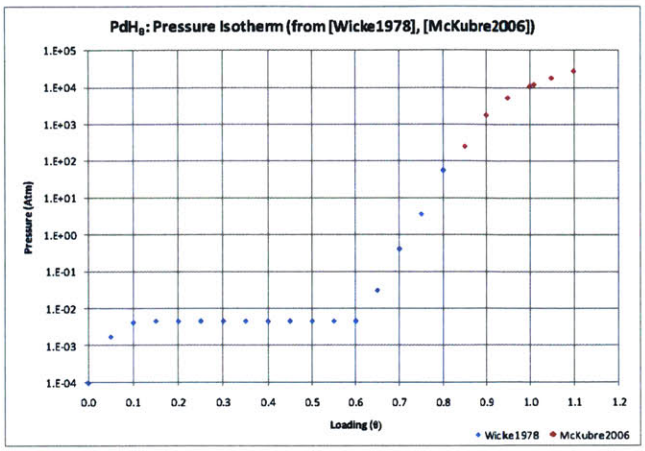

Figure 33: Room Temperature Pressure Composition Temperature Isotherm Extended to High Loading (Based on (Wicke & Brodowsky, 1978), (Baranowski, Filipek, Szustakowski, & Woryna, 1990), (Tripodi, 2000) and (McKubre & Tanzella, 2006))

Using the above P-C-T data, we use our model to predict the interaction energy as follows [Equations (189-193)]. The resulting interaction energy is given below, compared to experimental data (Fukai, 2005). We also include what our model would predict given the experimental loading level:

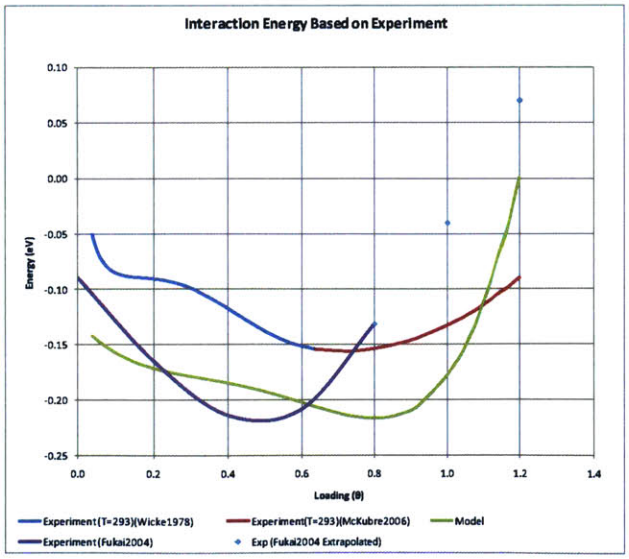

Figure 34: Interaction energy derived from using our model on Experimental P-C-T isotherms from (Wicke & Brodowsky, 1978) extended to higher loading by data from (McKubre & Tanzella, 2006). For consistency, model has a +0.16 eV offset.

Summary

In this foundational chapter, we have used the basic statistical model in the tradition of (Lacher, 1937) to derive the chemical potential of absorbed hydrogen. We provide the basic analysis and other important considerations (like the O-to-T model) that are used throughout the subsequent chapters.

Chapter 3 – Palladium Hydride (PdH): Modeling the Miscibility Gap & Phase

Introduction

This chapter deals with the modeling of the mixed phase region. We would specifically want to understand how our model framework may be used to correct or otherwise modify the observed experimental data. Lastly, we will also attempt to calculate the phase diagram of the PdH system using our *ab initio* model.

What is Miscibility Gap?

In physical chemistry, miscibility gap is defined as the region whereby two distinct phases of a compound exist simultaneously. In the case of PdH, the mixed phase region is defined as the region below {570K, 19atm, θ =0.257} (Flanagan & Oates, 1991), whereby the pressure is flat and independent of the loading level (Lacher, 1937), (Lewis, 1967). This region contains two distinct hydride phases (called the α and β phases, respectively) of varying hydrogen content.

In the mixed phase region the α-phase solid gradually decreases relative to β-phase solid while pressure stays constant until, at a loading level designated as β_{min}, only the β-phase solid exists and pressure starts to rise sharply with loading, and loading is related to pressure (again empirically) as (Wicke & Brodowsky, 1978):

$$\theta = a + b\,log\,(p) \tag{194}$$

Can we Model Miscibility Gap Theoretically?

A natural question arises as to whether our model framework can predict the presence of the miscibility gap in PdH. In particular, how can we conceivably come up with a theoretical model that matches the flat pressure isotherm in the miscibility gap phase region?

Rule of Equal Areas

To answer the previous question, we follow closely the theoretical analysis of (Lacher, 1937), which we believe applies to our problem. According to (Lacher, 1937), the theoretical chemical potential curve should obey the rule of equal areas. Under this scheme, in the mixed phase region, the area above and below the chemical potential curve should be equal. (Lacher, 1937) actually uses the $log\left(p^{\frac{1}{2}}\right)$ in his analysis, but the same applies to our case, up to a multiplicative constant, i.e.,

$$ln\, p^{\frac{1}{2}} = ln\frac{\theta'}{1-\theta'} - \frac{\chi_0 - \frac{1}{2}\chi_d + \chi\theta'}{\tau} + ln\frac{(\tau F_2')^{1/2}}{v(\tau)} \qquad 195$$

In Equation 195, in terms of the variables and terminology we have been using,

$\theta' = \theta/.59$,

χ_0 is the loading dependent interaction energy of H in Pd,

χ_d is the dissociation energy of the hydrogen molecule,

χ is a proportionality constant,

F_2' is the vibrational and rotational contributions to the chemical potential of hydrogen molecule in its gas phase, and,

$v(\tau) = z$ is the partition function of hydrogen in Pd.

Following the analysis of (Lacher, 1937), we rewrite Equation 195 as follows, after disregarding constant terms that merely shift the origin of the chemical potential coordinates:

$$ln\, p^{\frac{1}{2}} = f(\theta') = ln\frac{\frac{1}{2} + \left(\theta' - \frac{1}{2}\right)}{\frac{1}{2} - \left(\theta' - \frac{1}{2}\right)} - \frac{\chi}{\tau}\left(\theta' - \frac{1}{2}\right) \qquad 196$$

According to a proof given by (Fowler, 1936) and applied by (Lacher, 1937) to the same problem as ours, pairs of numerically equal roots of Equation 196 in θ' occur for values of θ_α'

and θ'_β that satisfy $\theta'_\alpha + \theta'_\beta = 1$. Because Equation 196 is symmetric around $\theta' = \frac{1}{2}$, it follows that the area above $log\left(p^{\frac{1}{2}}\right)$ axis is equal to that below. This is the rule of equal areas. Furthermore, (Lacher, 1937) has shown that in the miscibility gap, the equal areas rule must apply. We illustrate the rule below:

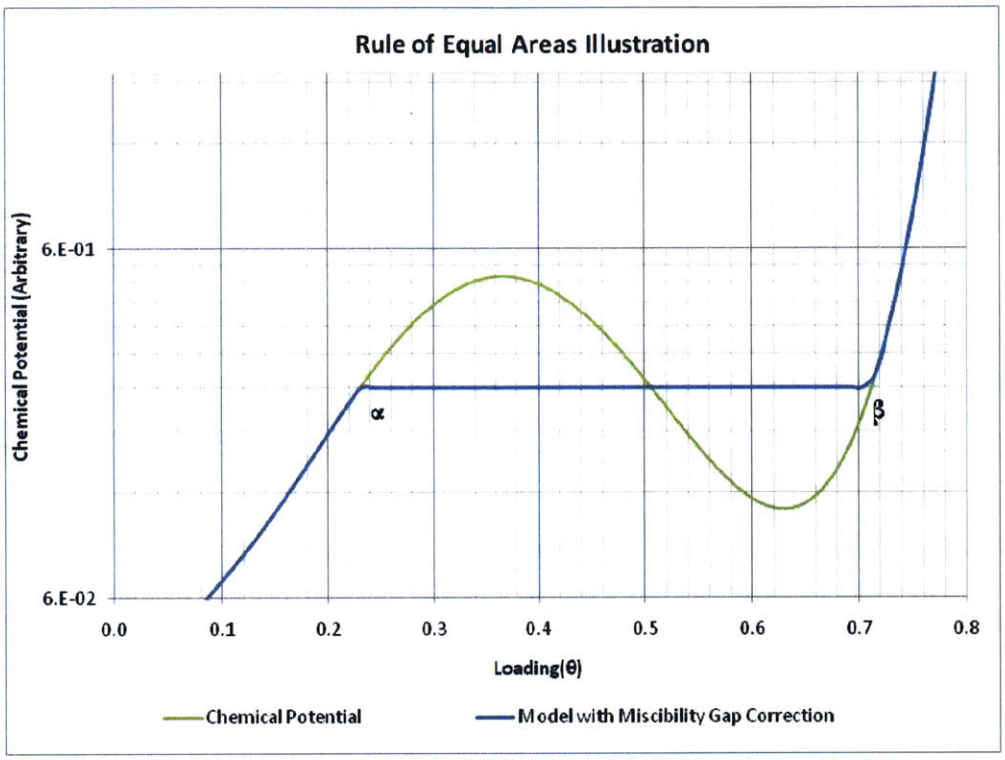

Figure 35: Rule of Equal Areas Illustration

The Rule of Equal Areas has a simple interpretation (Lacher, 1937), namely that, in θ-space, the smallest root corresponds to the alpha phase loading, θ'_α while the largest root corresponds to the beta phase, θ'_β loading. We use this interpretation below to derive the model phase boundary.

♦

We compare Equation 195 to our continuity condition for the chemical potential (Equation 170, Chapter 2):

$$\tau\, ln\frac{\theta_o}{1-\theta_o} - \tau\, ln(z) + \theta\frac{\partial \varepsilon_h(\theta)}{\partial\theta} + \varepsilon_h(\theta_o,\theta_t) = \tau\, ln\frac{\theta_t}{1-\theta_t} - \tau\, ln(z) + \theta\frac{\partial \varepsilon_h(\theta)}{\partial\theta} + \varepsilon_h(\theta_o,\theta_t)$$

$$= -\frac{\tau}{2}\left[ln\left[\left(\frac{2\pi m\tau}{h^2}\right)^{\frac{3}{2}}\frac{\tau}{f(\theta)}\right] + ln\frac{e^{\frac{\epsilon_{0v}}{2\tau}}}{1-e^{\frac{\epsilon_{0v}}{\tau}}} + ln\frac{8\pi^2 I\tau}{\sigma h^2} + \frac{\epsilon_D}{\tau}\right] \qquad 197$$

where we have used fugacity instead of pressure following arguments given in Chapter 2. If we apply the Rule of Equal Areas, it follows that our statistical mechanics based model may not be compared to flat chemical potential in the mixed phase region. Following (Lacher, 1937), we write Equation 197 as

$$ln\, f(\theta)^{\frac{1}{2}} = ln\frac{\theta_o}{1-\theta_o} + \frac{1}{\tau}\theta\frac{\partial \varepsilon_h(\theta)}{\partial\theta} + \frac{1}{\tau}\varepsilon_h(\theta) + C(T) \qquad 198$$

where

$$C(T) = -ln(z) + \frac{1}{\tau}ln\frac{e^{\frac{\epsilon_{0v}}{2\tau}}}{1-e^{\frac{\epsilon_{0v}}{\tau}}} + \frac{1}{\tau}ln\frac{8\pi^2 I\tau}{\sigma h^2} + \epsilon_D + \frac{1}{2}ln\left[\tau\left(\frac{2\pi m\tau}{h^2}\right)^{\frac{3}{2}}\right] \qquad 199$$

is independent of loading and thus does not affect the nature of the solutions in theta.

Instead, we need to take experimental chemical potential and, in the mixed phase region, make it conform to the Equal Areas Rule before matching it to the gas phase chemical potential as in Equation 197, in the manner formulated below.

Interaction Energy From Experiment: Miscibility Gap Correction

We write Equation 197 as

$$\varepsilon_h'(\tau,\theta_o,\theta_t)+\varepsilon_h(\tau,\theta_o,\theta_t)F(\tau,\theta_o,\theta_t)=g(\tau,\theta_o,\theta_t) \tag{200}$$

where

$$\varepsilon_h'(\tau,\theta)=\frac{\partial}{\partial\theta}\varepsilon_h(\tau,\theta) \tag{201}$$

$$F(\theta)=\frac{1}{\theta} \tag{202}$$

$$g(\tau,\theta)=\frac{\tau}{\theta}ln(z)-\frac{\tau}{\theta}ln\frac{\theta_{o,t}}{1-\theta_{o,t}}-\frac{1}{2\theta}\left[\tau\,ln\left[\left(\frac{2\pi m\tau}{h^2}\right)^{\frac{3}{2}}\frac{\tau}{f(\theta)}\right]+\tau\,ln\frac{e^{-\frac{\epsilon_{0v}}{2\tau}}}{1-e^{-\frac{\epsilon_{0v}}{\tau}}}+\tau\,ln\frac{8\pi^2I\tau}{\sigma h^2}+\epsilon_D\right] \tag{203}$$

As before, we seek to calculate the interaction energy given the experimental P-C-T data. The pressure data appears in Equation 203 in terms of fugacity, as discussed in Chapter 2.

We take the view that in order to apply the Rule of Equal Areas, we need to examine the gas phase chemical potential term (Equation 204 below) since that it is the term that contains the measured pressure isotherm:

$$\frac{1}{2}\mu_{gas}(\tau,\theta)=-\frac{\tau}{2}\left[ln\left[\left(\frac{2\pi m\tau}{h^2}\right)^{\frac{3}{2}}\frac{\tau}{f(\theta)}\right]+ln\frac{e^{-\frac{\epsilon_{0v}}{2\tau}}}{1-e^{-\frac{\epsilon_{0v}}{\tau}}}+ln\frac{8\pi^2I\tau}{\sigma h^2}+\frac{\epsilon_D}{\tau}\right] \tag{204}$$

We plot Equation 204, together with the P-C-T that is it based on below (room temperature data):

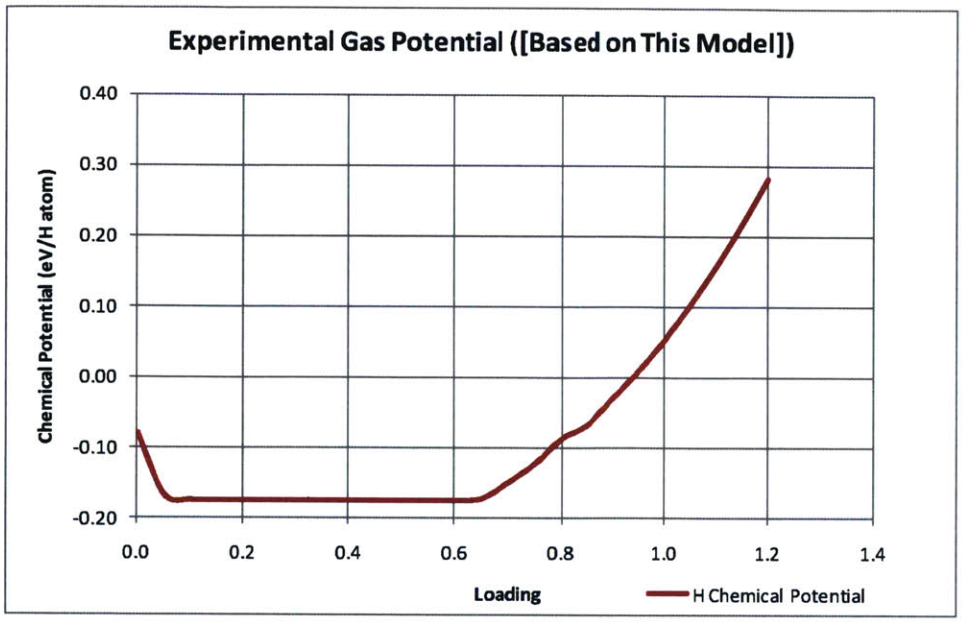

Figure 36: Chemical Potential Based on Experimental Pressure Isotherm (below)

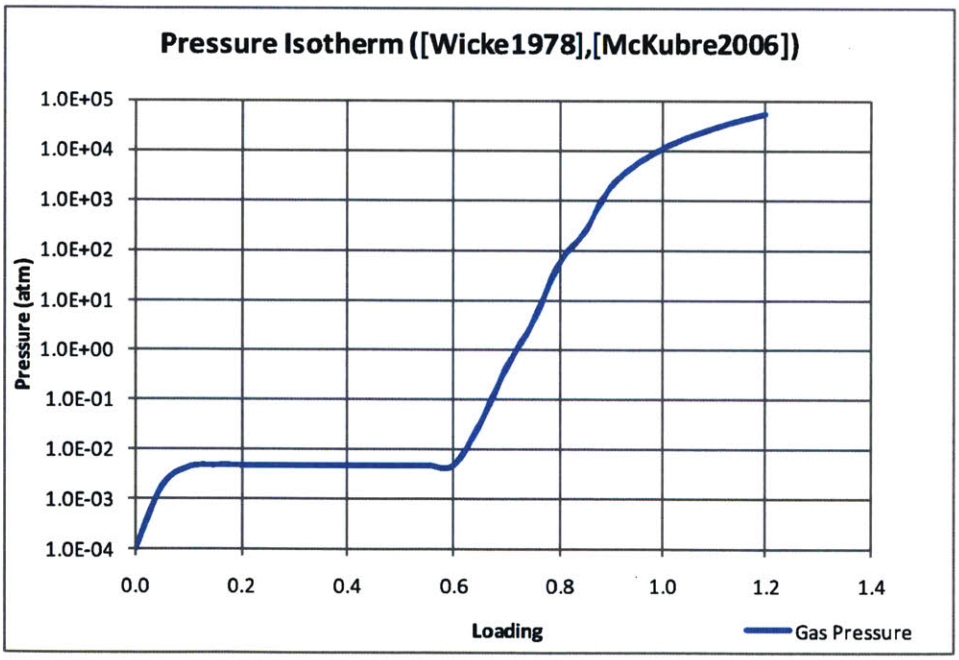

Figure 37: Experimental Pressure Isotherm (from (Wicke & Brodowsky, 1978) and (McKubre & Tanzella, 2006))

Applying Rule of Equal Areas

Starting from above Figure 36, we assume that the chemical potential is not flat, but rather obeys the Rule of Equal Areas according to the theory of (Lacher, 1937). To that end, we assume the chemical potential will take the following general shape in the miscibility gap region:

$$y(\theta) = a + b * sin(c * (\theta - \theta_0)) \tag{205}$$

where a, b, c and θ_0 are as yet undetermined constants, and, based on experimental data,

$$0.12 < \theta < 0.65 \tag{206}$$

We set the first zero of Equation 205 to match the alpha phase boundary. For the experimental data we are using, this boundary is at ($\theta = 0.12$) (Wicke & Brodowsky, 1978) even though other workers like (Flanagan & Oates, 1991) have found it around $\theta = 0.01$. Thus:

$$y(\theta = 0.12) = a = -0.17477\ eV/H\ atom \tag{207}$$

$$\theta_0 = -0.12 \tag{208}$$

The constant c is chosen to put the second zero at $\theta = 0.65$:

$$y(\theta = 0.65) = -0.17477\ eV/H\ atom \tag{209}$$

$$c\ (\theta - \theta_0)|_{\theta=0.65} = 2\pi \quad \rightarrow \quad c = \frac{2\pi}{0.65 - \theta_0} \tag{210}$$

At the third zero, we also want to match the slope from experiment, thereby determining the constant b, i.e.,

$$\left.\frac{dy(\theta)}{d\theta}\right|_{\theta=0.65} = b * c * \cos(c * (\theta - \theta_0)) = 0.5616\ eV/\ H\ atom/unit\ loading \quad (211)$$

$$b * c * cos(c * (0.65 - \theta_0))|_{\theta=0.65} = .5616 \quad \rightarrow \quad b = \frac{.5616}{c * cos(c * (0.65 - \theta_0))} \quad (212)$$

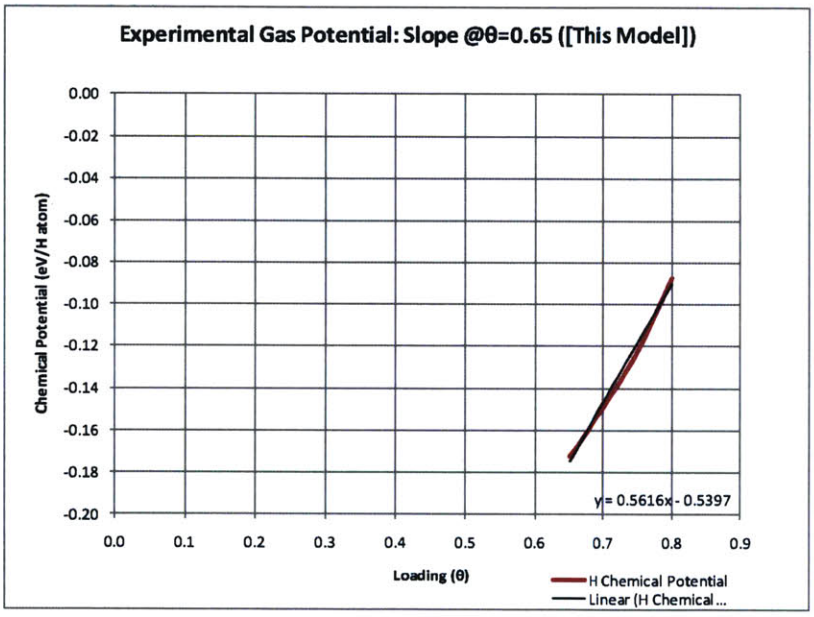

Figure 38: Estimated Experimental Chemical Potential Slope at Loading of 0.65

The result of the match is shown below:

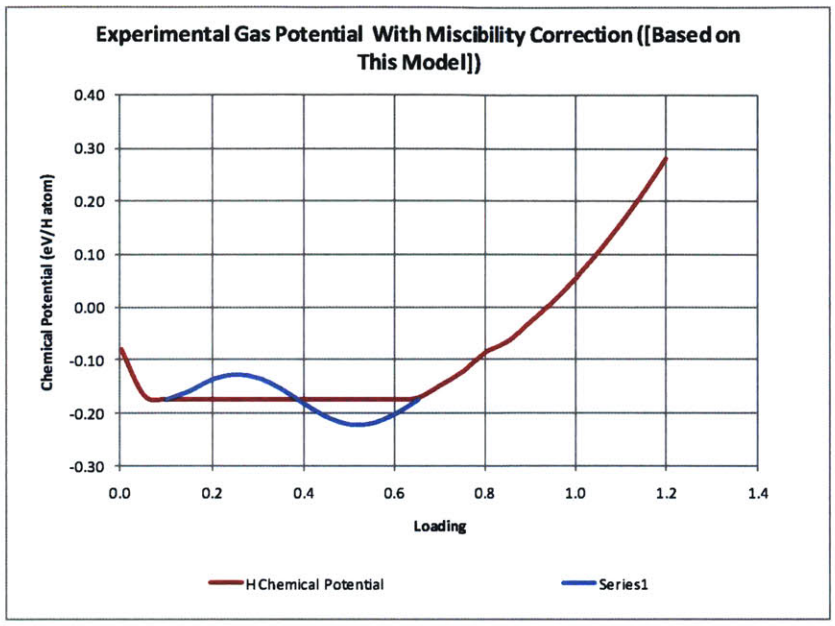

Figure 39: Miscibility Gap Correction (blue) vs. Experiment (red). Correction applies only to mixed phase region.

Interaction Energy With Miscibility Gap Correction

Using the above results, we can calculate the Interaction Energy from experiment. As before, we use Equation 203, where now the right hand side is corrected for miscibility gap as described in the prior section.

In the following figure, we also compare our results with experiment (Fukai, 2005):

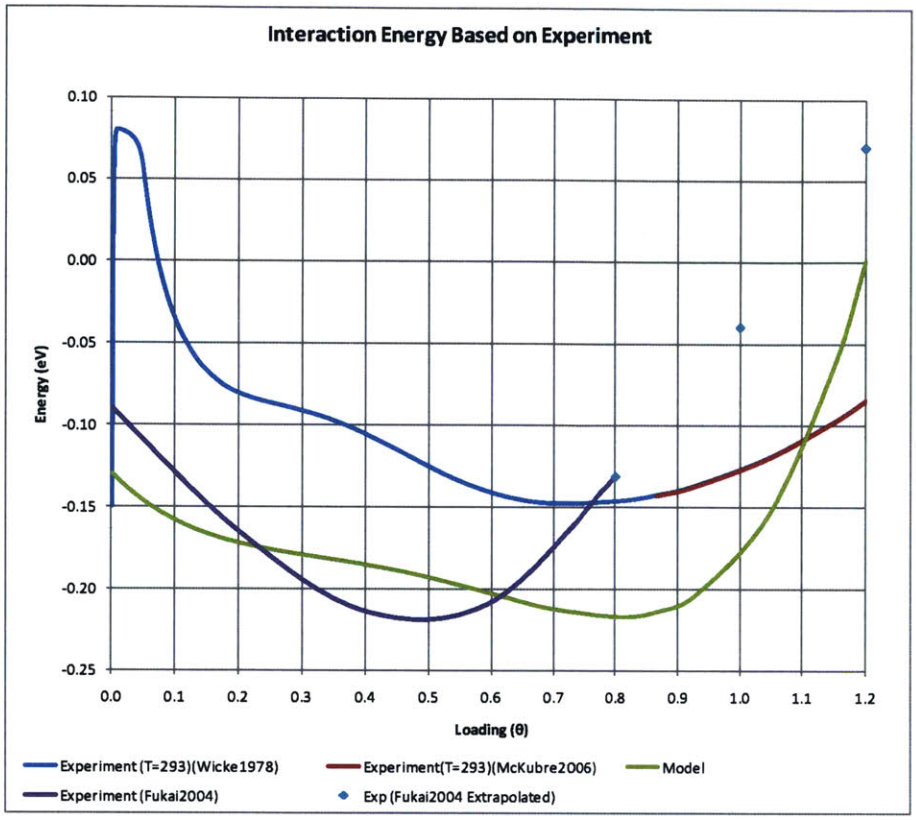

Figure 40: Interaction Energy, from top (a) model based on Experiment (b) model (c) Experiment (Fukai, 2005)

The agreement is reasonable, especially in the mixed phase region. Above the mixed phase region, there is less of an agreement.

Model P-C-T Isotherm Corrected for Miscibility Gap

We would like to correct our model P-C-T isotherm for miscibility gap. An example model isotherm without the miscibility gap correction is shown below:

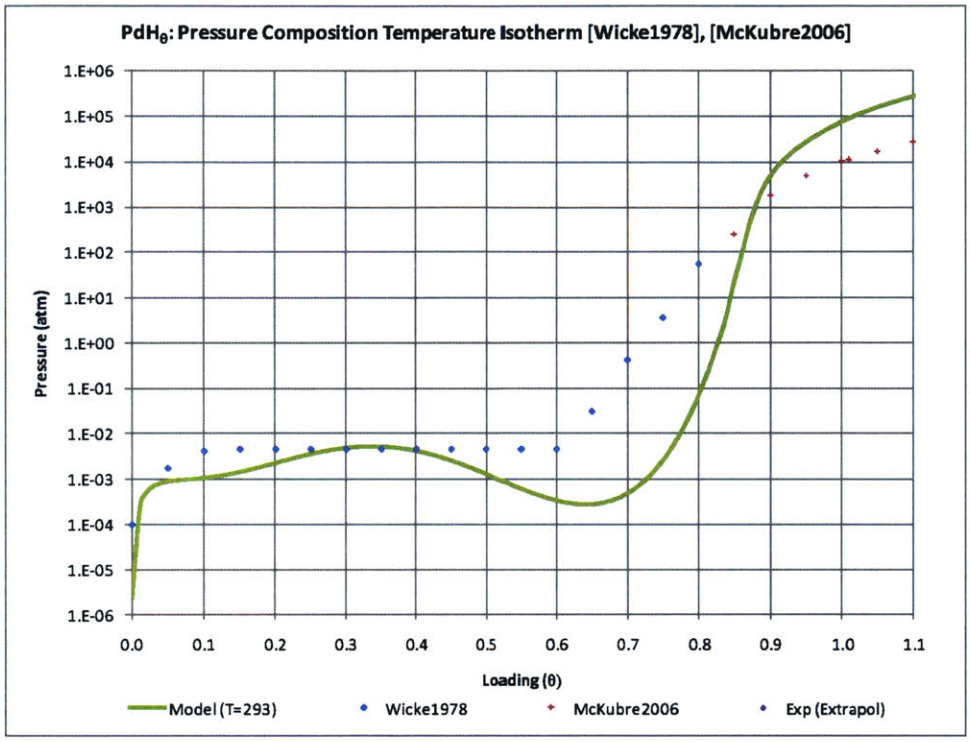

Figure 41: Pressure Composition Isotherm at room temperature: Model vs. Experiment (Pressure is on log scale). See above section on how pressure plotted here was derived from fugacity model from (Tkacz & Litwiniuk, 2002)

The first thing we notice is that we cannot readily apply the Rule of Equal Areas simply using a sinusoidal function since the model result is somewhat more complicated.

One way to apply the Rule of Equal Areas to our results is to pick θ_α, $\theta_{\alpha\beta}$, θ_β in such a way that

$$\int_{\theta=\theta_\alpha}^{\theta=\theta_{\alpha\beta}} ln\big(P(\theta')\big)\, d\theta' = \int_{\theta=\theta_{\alpha\beta}}^{\theta=\theta_\beta} ln\big(P(\theta')\big)\, d\theta'$$

213

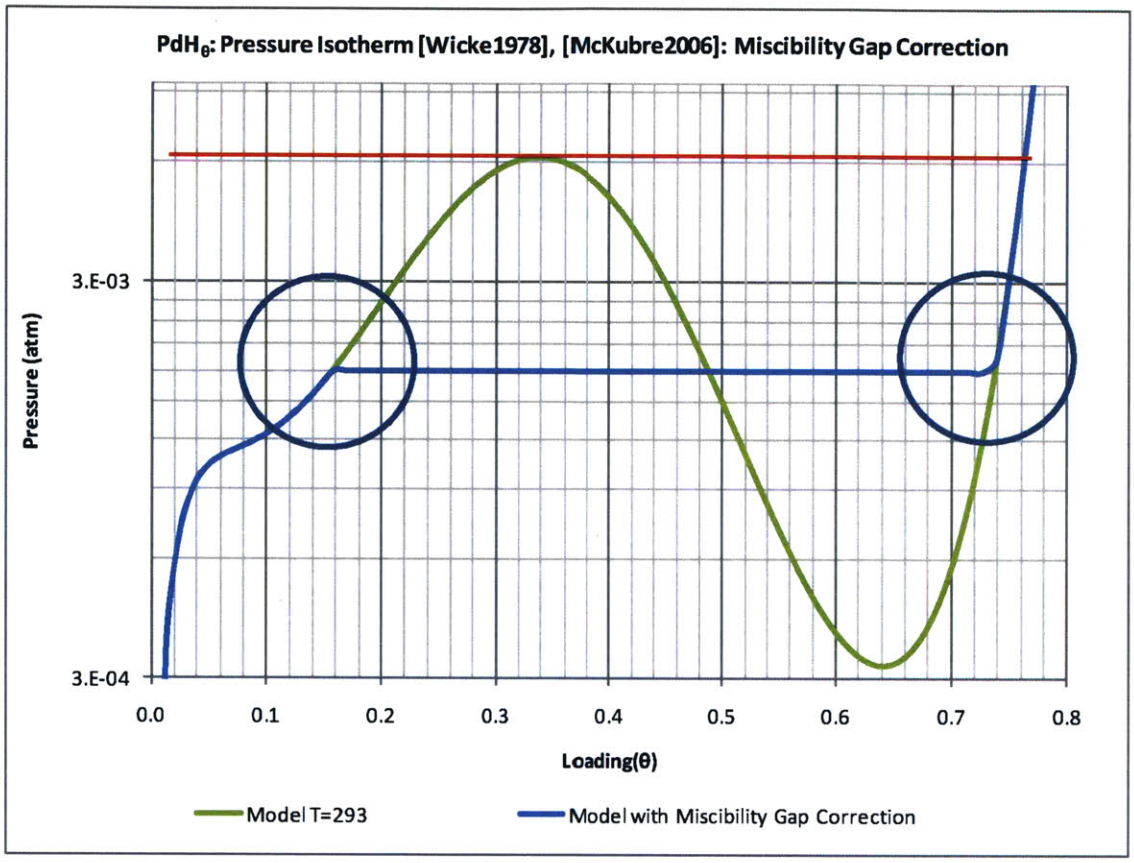

Figure 42: Loading extrema: the first extremum is determined arbitrarily using first data point and while the second is determined by a horizontal tangent as shown.

As shown in Figure 42, θ_α should be chosen as α_{max}, which equals 0.12 from experiment (Wicke & Brodowsky, 1978). However our model finds it closer to $\alpha_{max} = 0.16$ as the figure shows. This is the value we used in the Rule of Equal Areas calculation.

θ_β is chosen in such a way as to match the tangent of the local maximum of the (log of) pressure in the mixed phase region. $\theta_{\alpha\beta}$ may then be determined by numerically integrating Equations 213. Also note that when we work in log(p) space since that is the regime where the Rule of Equal Areas applies.

The results are shown below (Figure 43).

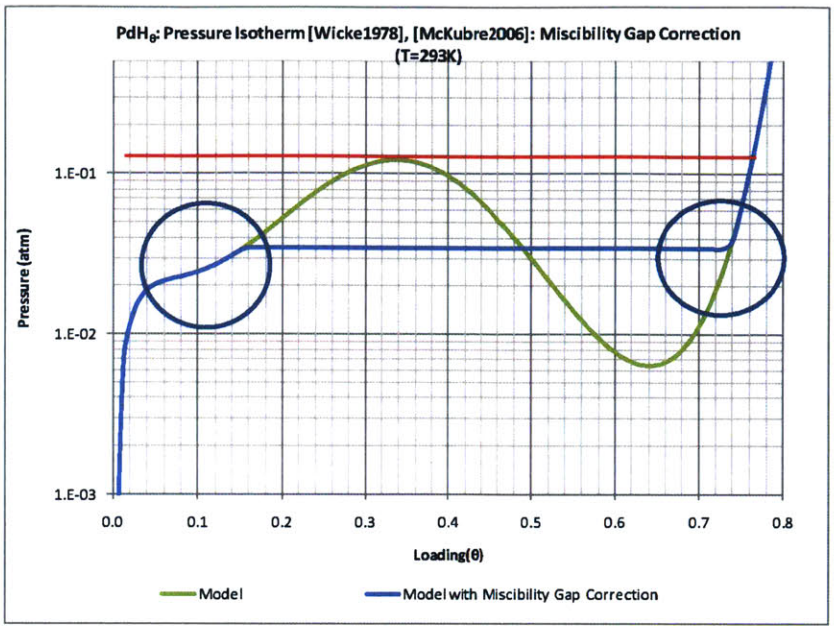

Figure 43: P-C-T Isotherm with Miscibility Gap. The cycles show correction to phase boundaries suggested by Miscibility gap correction

Based on the results of the Miscibility Gap correction, the suggested phase boundaries are changed slightly. The maximum alpha phase α_{max} loading increases while the β_{min} decreases slightly. The final results are shown below (room temperature results) vs. experiment.

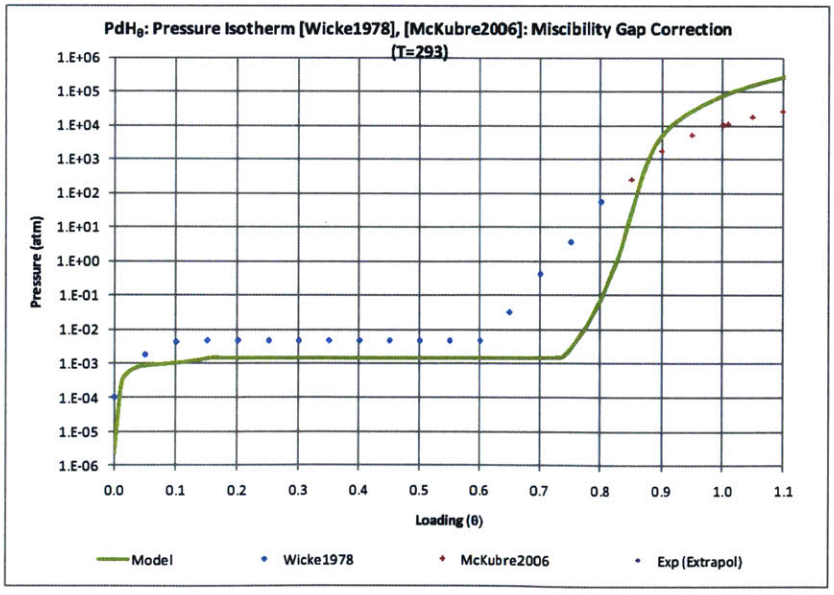

Figure 44: Final Miscibility Gap Results for Room Temperature.

Model Phase Diagram

We can repeat the above exercise for other temperatures. For T=473, for example, we have

$$\theta_0 = 0.27 \tag{214}$$

$$\theta_2 = 0.71 \tag{215}$$

In fact, in this regime, we may now use a simple averaging of logarithms technique that works fairly well, and provides results very close to the more exact integral technique above, i.e.,

$$log(p(\theta)) = \frac{1}{n}\int_{\theta=\theta_\alpha}^{\theta=\theta_\beta} log\big(P(\theta')\big)\, d\theta' \tag{216}$$

where n is the number of discrete points taken in the sum.

The results are shown below for various temperatures. We have kept the pressure scale identical in order to show that our model correctly predicts the miscibility gap decreasing as we move up along a temperature scale (1.5 decades).

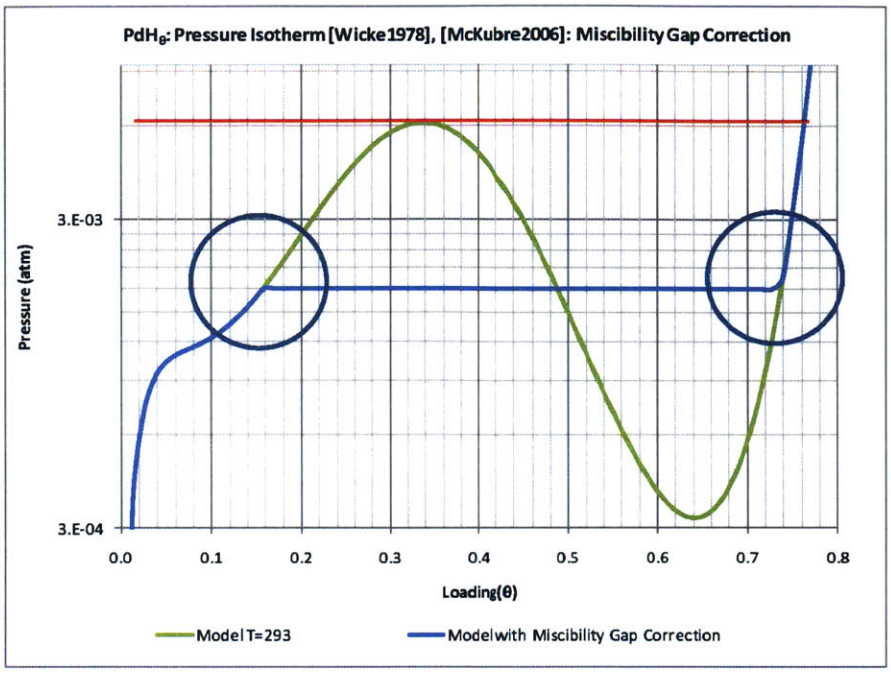

Figure 45: Miscibility Gap Correction, T=293

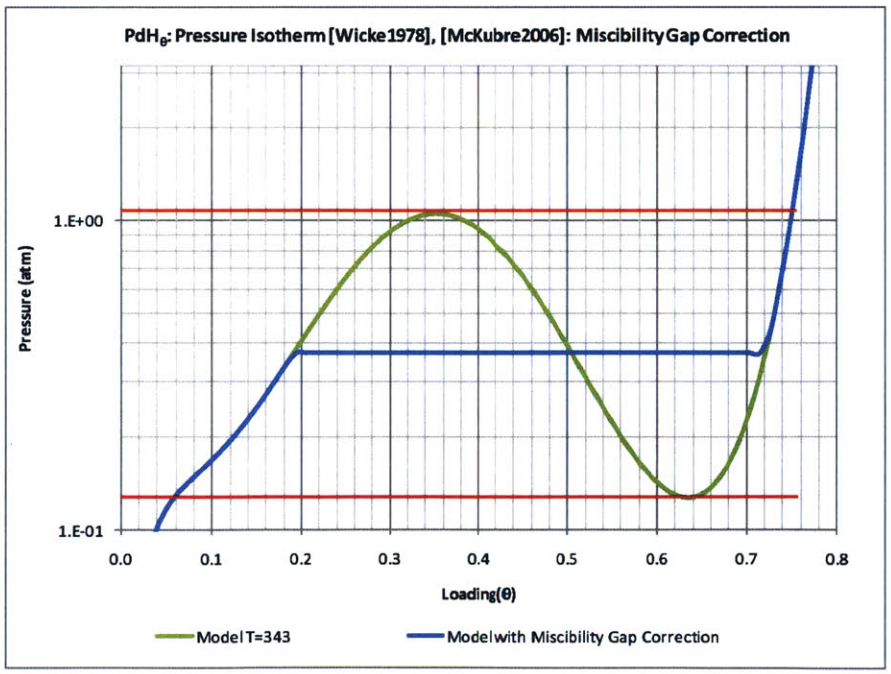

Figure 46: Miscibility Gap Correction, T=343

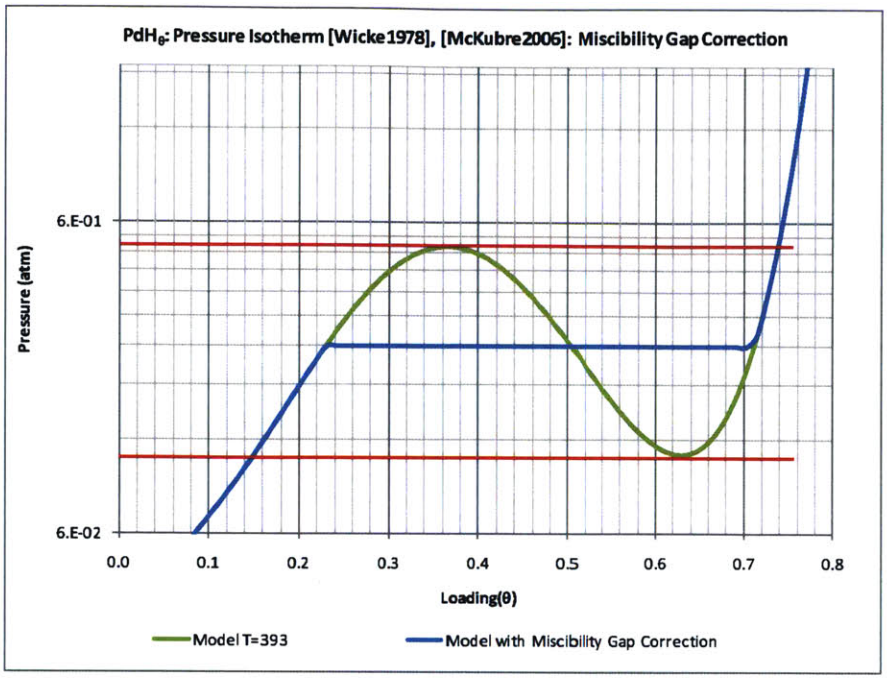

Figure 47: Miscibility Gap Correction, T=393

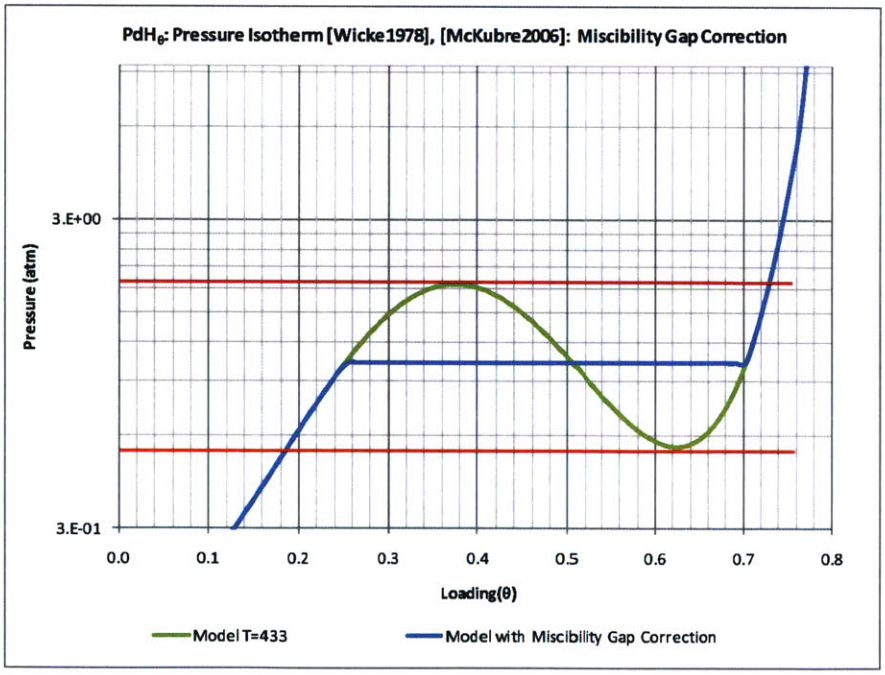

Figure 48: Miscibility Gap Correction, T=433

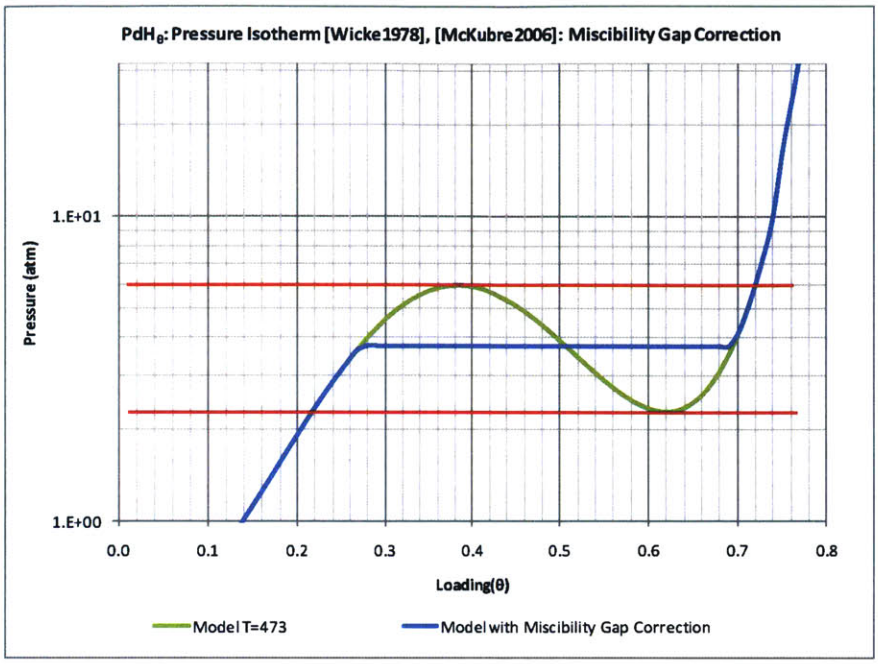

Figure 49: Miscibility Gap Correction, T=473

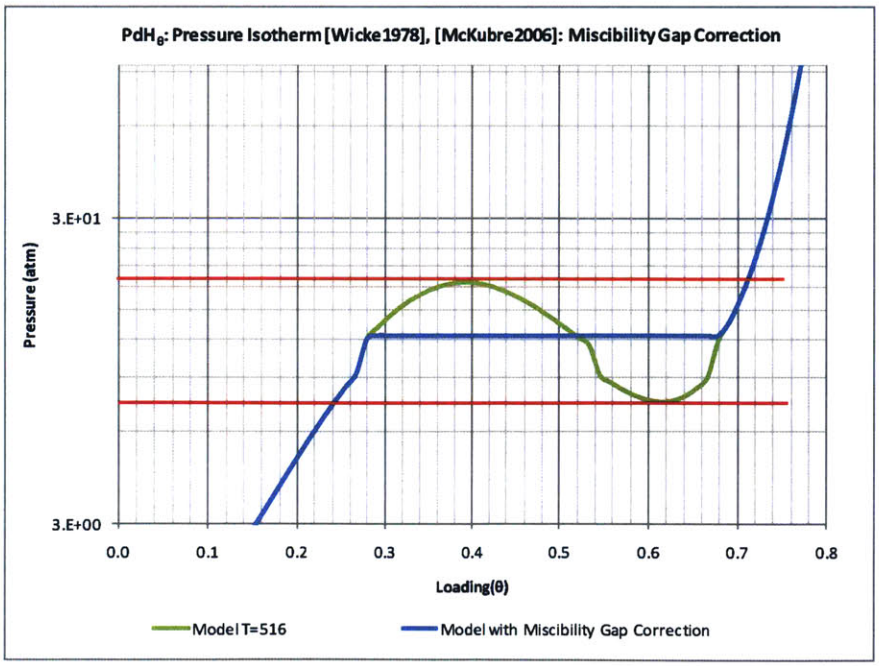

Figure 50: Miscibility Gap Correction, T=516

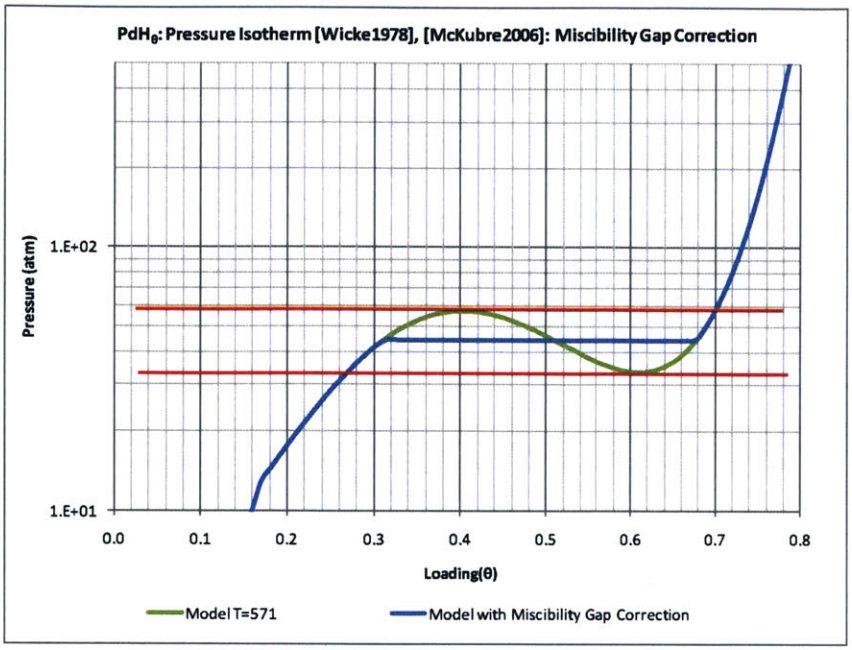

Figure 51: Miscibility Gap Correction, T=571

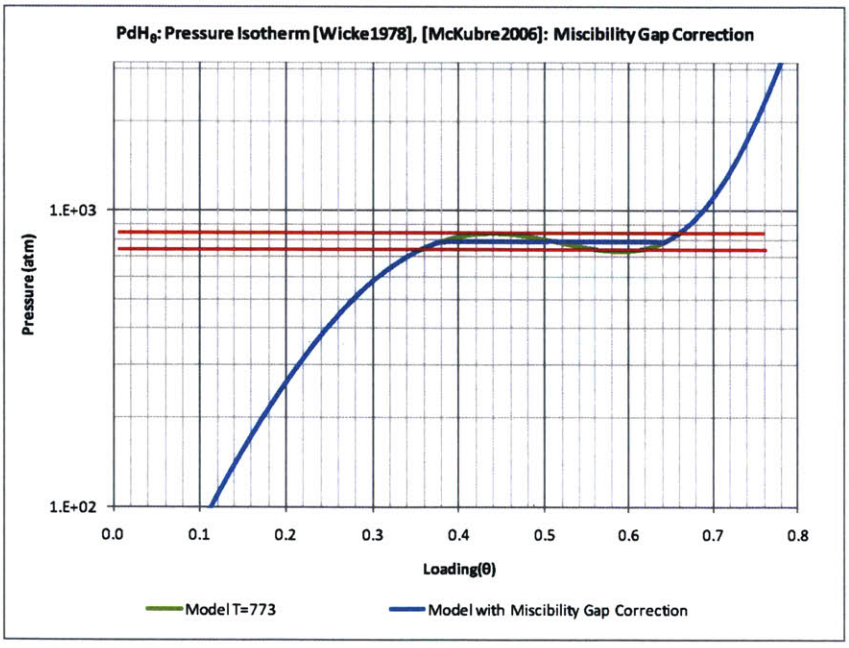

Figure 52: Miscibility Gap Correction, T=773

The full results are shown below. We have also included a couple of experimental P-C-T isotherms (at T=293 and T=571) . The match is quite reasonable.

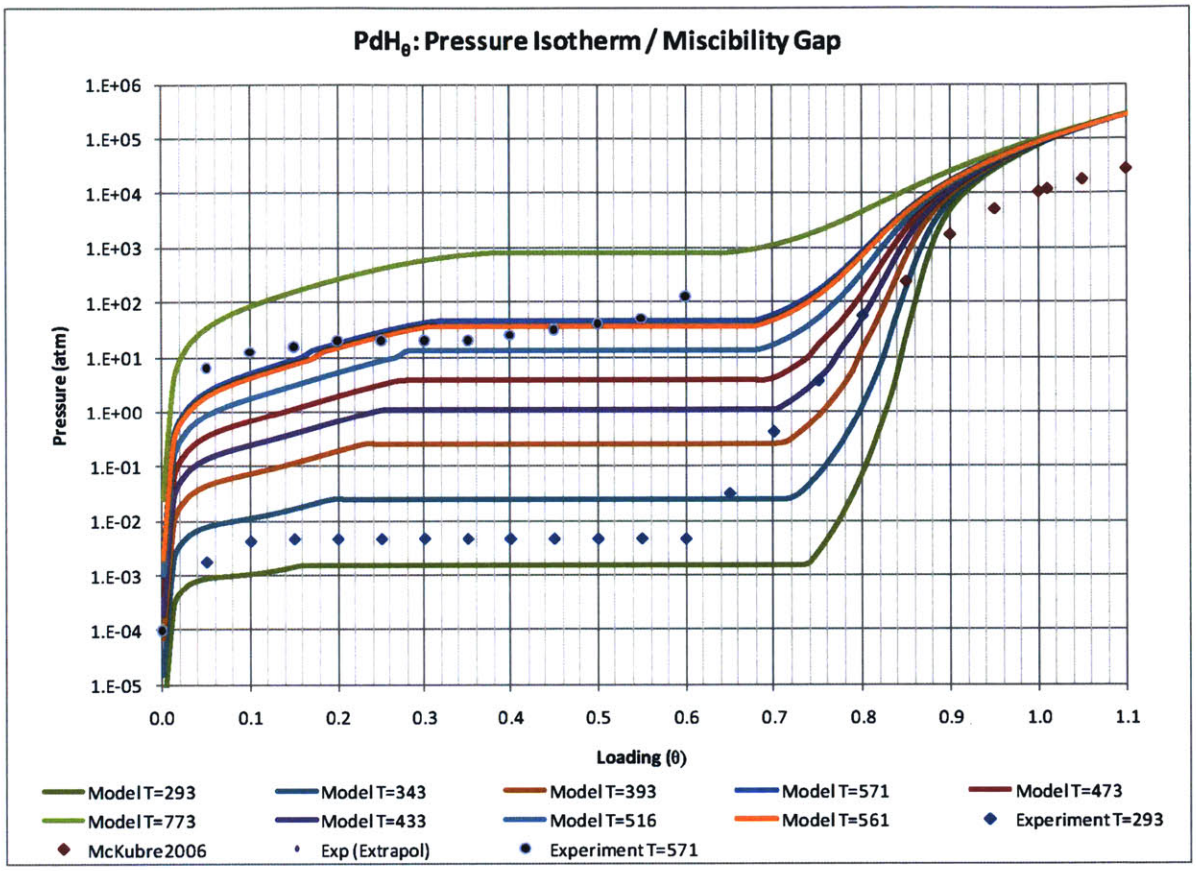

Figure 53: Model P-C-T corrected for Miscibility Gap vs. Experimental data at T=293 (dotted, blue) and T=571 (dotted, black) are also shown.

We calculate the phase diagram and compare to experimental phase diagram below as a function of temperature vs. loading (Wicke & Brodowsky, 1978). The low temperature phase diagram was estimated based on the highest temperature model results, in comparison with other workers' results (Wicke & Brodowsky, 1978), (Christensen, Stoltze, Jacobsen, & Norskov, 1990), for example.

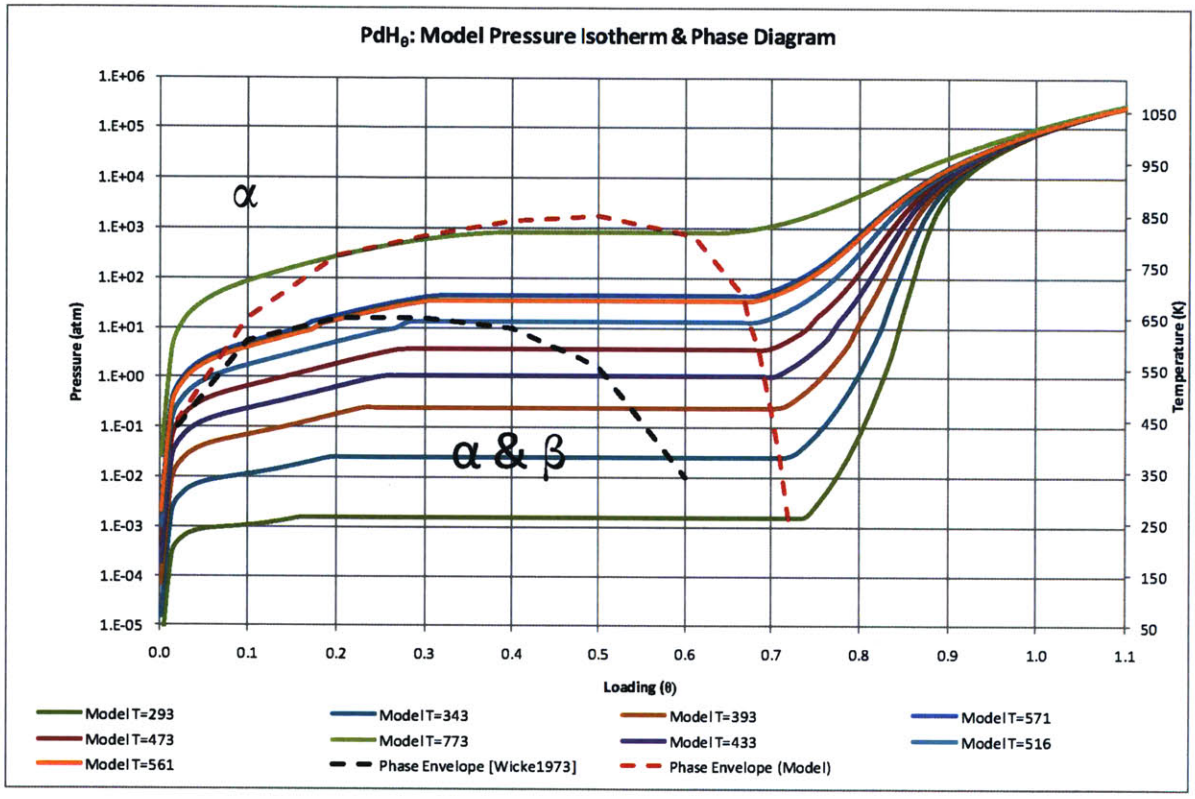

Figure 54: Model vs. Experimental Phase Diagram (After (Wicke & Brodowsky, 1978)). Model Phase diagram is derived graphically based on alpha/beta phase boundary, and is therefore approximate.

Summary

In this chapter, we have provided the analytical basis for the treatment of the miscibility gap within our model. We do this by applying the Rule of Equal Areas. Finally, we apply the analysis to derive P-C-T and phase diagram for the basic model of Chapter 2.

Chapter 4 - Models of Basic Properties of Palladium Hydride

Introduction

In this chapter, we will provide results of basic properties of Pd that we are able to model *ab initio*. This is intended to help us gain a basic and first principles understanding of the particular physics and chemistry of Pd phenomena. In all cases, a comparison is made to experiment or alternate model results from other workers.

Calculated Lattice Constant

One of the first tasks we have to do is determine the lattice constant for Pd within the DFT framework. We are interested specifically in how the lattice constant changes with loading since Pd is known to expand as it is loaded with hydrogen [several]. We cannot use experimentally determined values, except for comparison, since the DFT values are known to be slightly different, so the experimental values would not represent minimum energy configurations.

Initially, we have chosen a simple methodology whereby we slowly vary the lattice constant, first over a one (1) Angstrom range and calculating the total electronic energies. We then zero down the search further around the computed minimum with the range down to about 0.2 Angstrom.

The results of these calculations are shown below as a function of loading (using a single cell model):

Alat (a.u)	7.52	7.62	7.70	7.76	7.83
Alat (A)	**3.98**	**4.03**	**4.07**	**4.11**	**4.14**
Loading	0	0.25	0.5	0.75	1

We then fit the above data to a polynomial to be able to calculate the lattice dependence on loading for a 2x2x2 supercell:

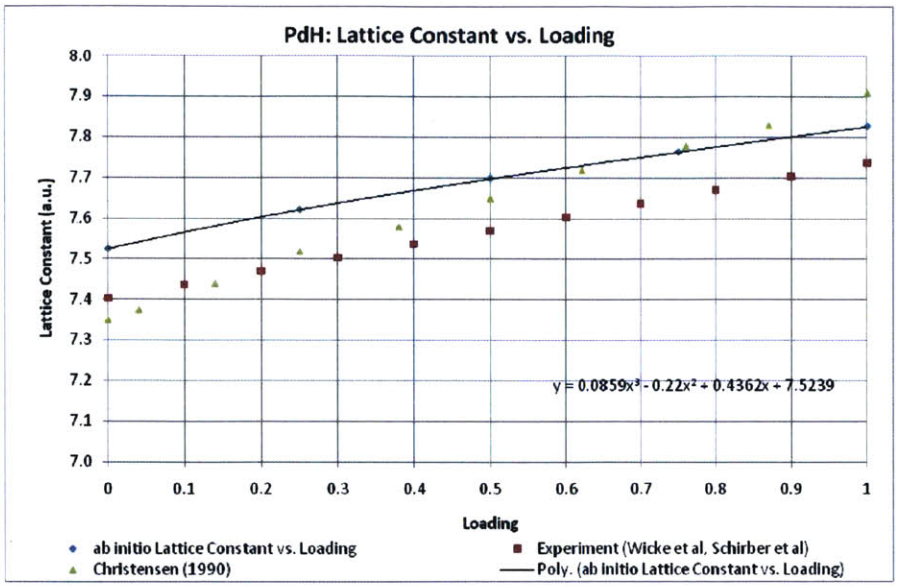

Figure 55: Model Lattice Constant vs. Loading Compared to Experiment

The lattice constant relaxations were done by minimizing the ground state energies around some reasonable starting points based on values reported in literature. We performed a wide scan followed by a narrow scan once the approximate value was calculated (hence the reason why the region around the minima in the following curves is sampled more frequently):

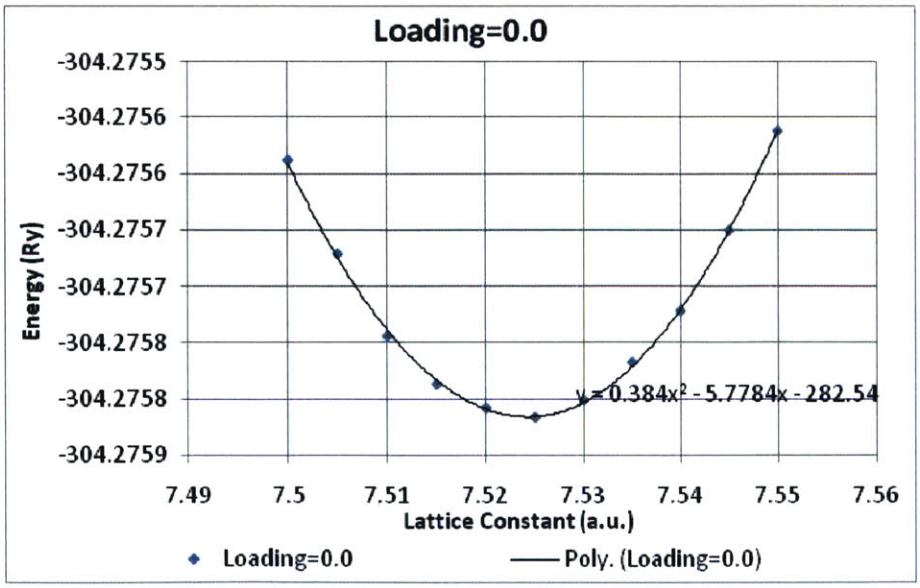

Figure 56: Model Lattice Constant - Bulk Pd

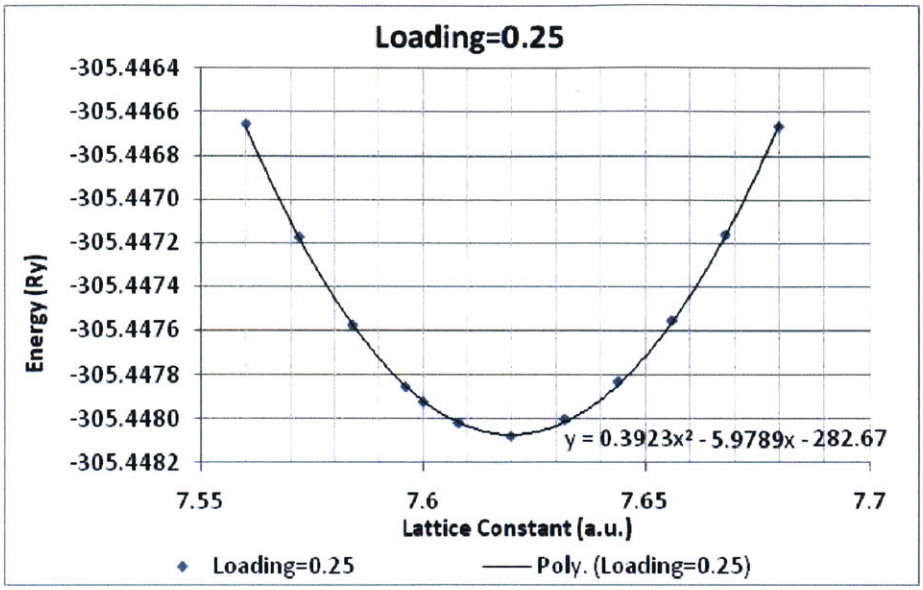

Figure 57: Model Lattice Constant - Loading=0.25

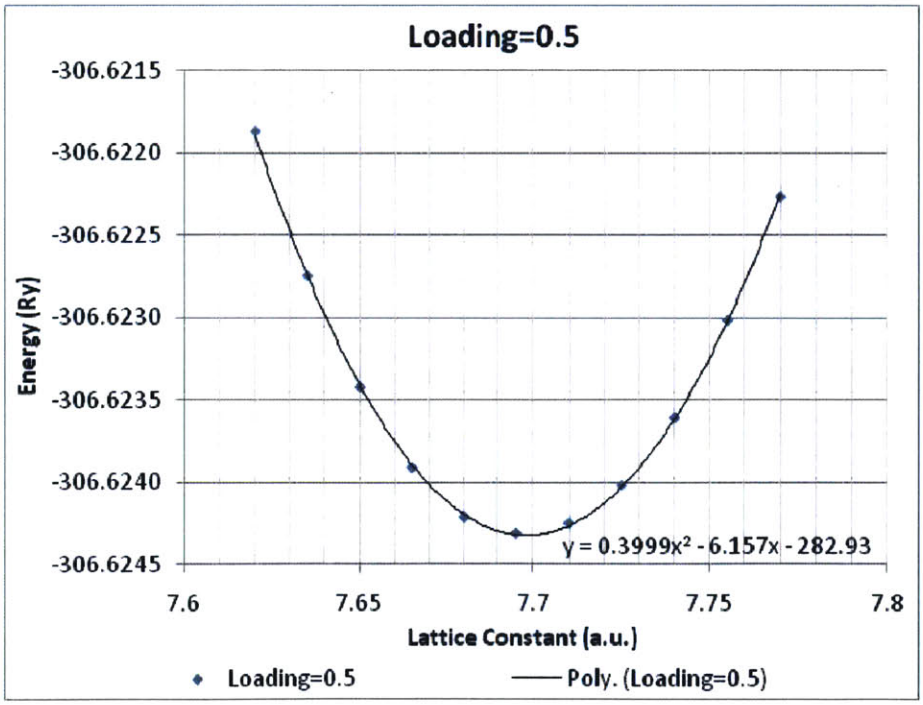

Figure 58: Model Lattice Constant - Loading=0.5

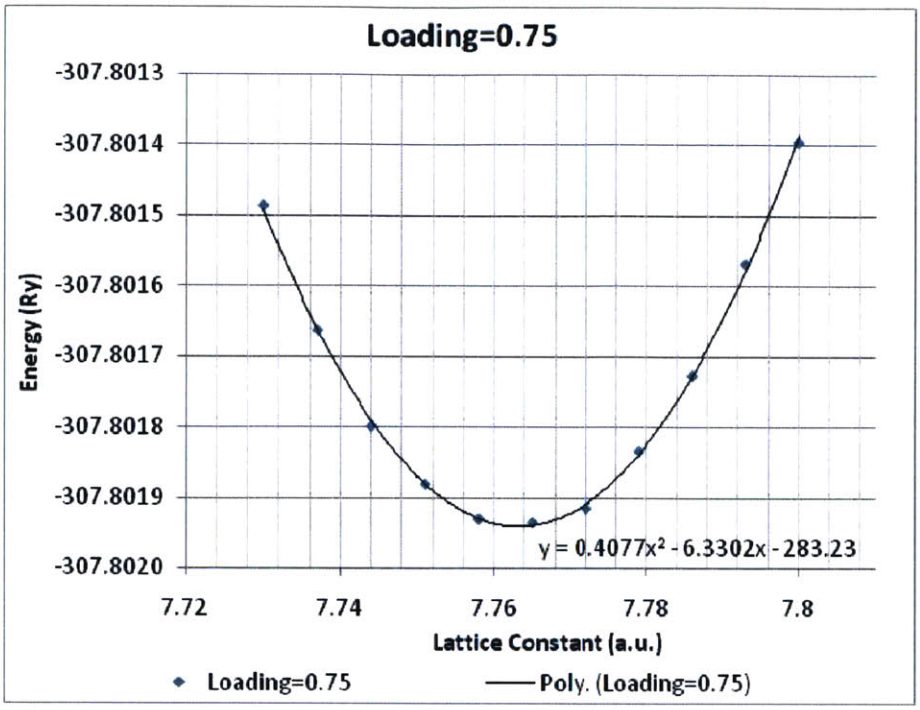

Figure 59: Model Lattice Constant - Loading=0.75

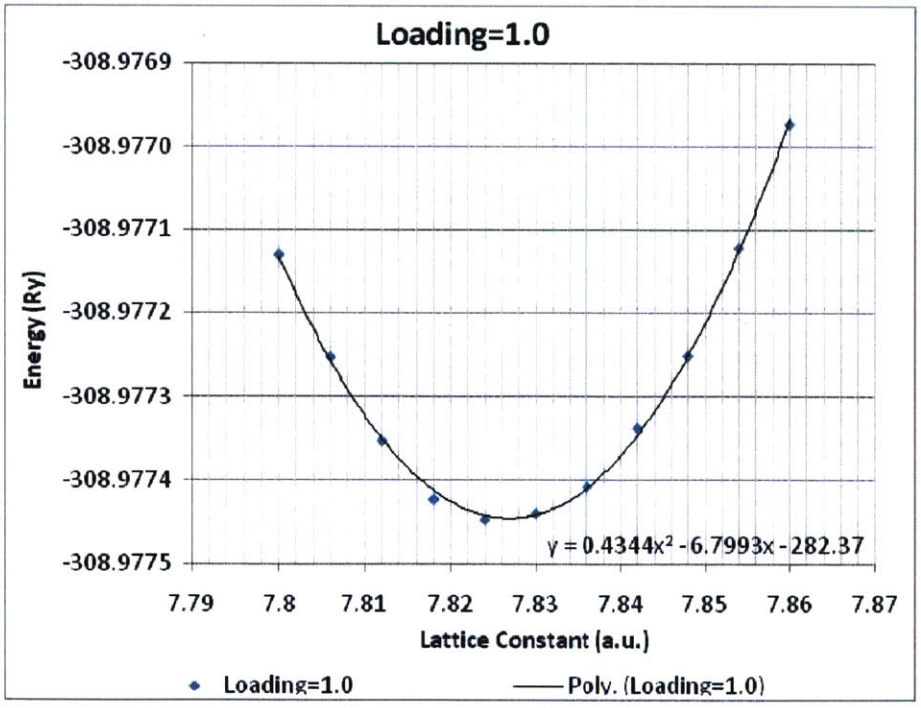

Figure 60: Model Lattice Constant - Loading=1.0

A simple minimization of the resulting quadratic gives an accurate global minimum lattice constant. For example, we can do the minimization as follows in Matlab:

```
>> sym('x')

 ans =

 x

>>  y0 = 0.384*x^2 - 5.7784*x - 282.54

 y0 =

 (48*x^2)/125 - (7223*x)/1250 - 14127/50

 >> subs(solve(diff(y0)))

ans =

   7.5240
```

Comparison to Experiment and Other *Ab Initio* Methods

In Figure 55, we have included experimental results for comparison, (Schirber & Morosin, 1975), (Wicke & Brodowsky, 1978). The experimental data was conducted using x-ray diffraction techniques, at 77K (Schirber & Morosin, 1975).

In general, we see that our calculations overestimate the lattice constant at all loading levels, but the match is fairly close (about 1.7% higher). Christensen has suggested that the *ab initio* model overestimates the lattice constant since it overestimates the Pd-H repulsion (Christensen, Stoltze, Jacobsen, & Norskov, 1990).

We have also compared our results with those obtained using other similar *ab initio* techniques, specifically the Effective Medium Theory (EMT) (Christensen, Stoltze, Jacobsen, & Norskov, 1990). The match is again fairly consistent even though EMT predicts more expansion at higher loading and less expansion at lower loading levels.

Electron Charge Density

We may expect electronic charge density to play a key role in any DFT calculation since the theory contemplates the total energy to be a unique functional of the electron charge density, $\rho(\bar{r})$.

It is therefore critical that we are able to accurately calculate the charge density for various configurations of interest for Pd, H & PdH.

Electron Charge Density: Isolated Pd Atom

The first case we will consider is the electron charge density for an isolated Pd atom. In particular, we are interested in the knowing the charge density around at the Pd-H bonding length, 1.67 Angstroms (Hagelstein P. , Private Communication, 2010). To make the calculation, we need to isolate a Pd atom, perform an SCF total energy calculation, and then use the resulting output files to calculate electronic charge densities.

From a computational perspective, the Pd atom is put in a large enough vacuum box to obviate any interaction due to periodic boundary conditions imposed by our DFT framework. Initially, we used a vacuum that was 5x the Pd lattice constant. However, we found out that the results did not change appreciably when the size of the box was reduced to 2x the lattice constant. The following results were thus done at 2x the lattice constant.

We show the results using both LDA and GGA functionals. For comparison, we also plot the results from a numerical HF calculation [ibid], Figure 61.

The results for LDA and GGA are fairly consistent. However, the numerical Hartree Fock (HF) result is significantly lower. We think this difference is most likely due to the 5S wave function that is present in the LDA and GGA pseudopotentials, but absent in the HF calculation.

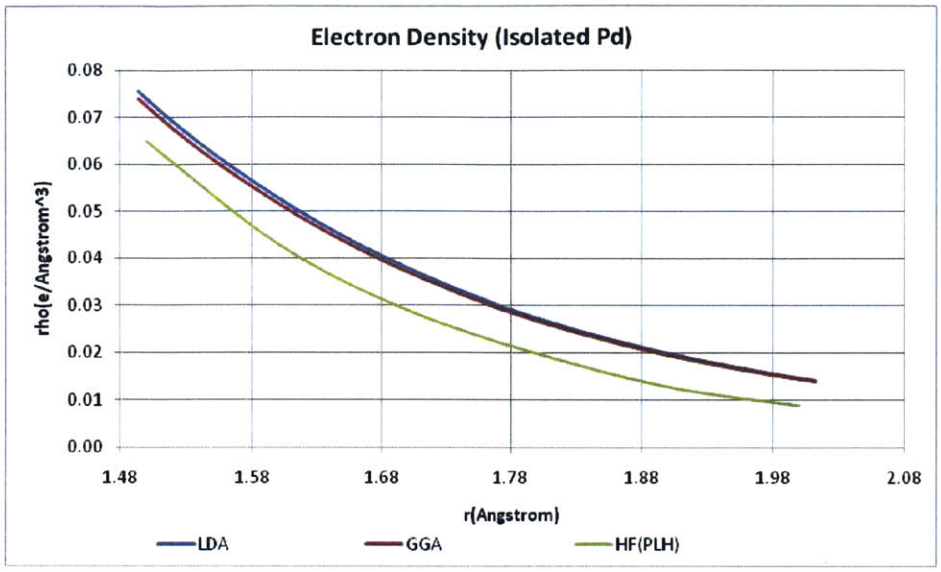

Figure 61: Electron Density Around an Isolated Pd Atom

Electron Charge Density: Bulk Pd [111] Atom

We are also interested in finding out the bulk charge density that the hydrogen atom will experience. We choose the [111] direction and perform several calculations that should yield equivalent results:

- We perform different calculations using LDA and GGA pseudopotentials.
- We perform the same calculation using different cell sizes (single cell versus 2x2x2 supercell)

For comparison, we have used two sets of results: one was done using DFT, but by another team (Hagelstein & deChiaro, 2009), while the other was done using an all electron numerical Hatree Fock (HF) method (Hagelstein & deChiaro, 2009).

Once again, there is a deviation from our results with those from (Hagelstein & deChiaro, 2009), but again this is explained by the different orbital descriptions used, while the other set of results are in excellent agreement:

- There is generally excellent agreement with (Hagelstein & deChiaro, 2009)'s DFT results, with the deviations at the PBC edges perhaps due to different DFT framework parameters employed (energy or charge density cut-offs are most likely)

- There is excellent agreement between results based on LDA and GGA approximations.

- There is also excellent agreement going from a single cell to the2x2x2 supercell.

The last point is especially important since it shows us that our description of the supercell (which we apply for more sophisticated calculations), is correct.

In terms of the calculation details, the single cell and bulk results were obtained using a simple QE representation of bulk Pd, with the experimental lattice constant of 7.3535 a.u. The resulting SCF calculation was used as a basis (input) for calculating the charge density using the QE post-processing programs (pp & plotrho), (Giannozzi, 2010).

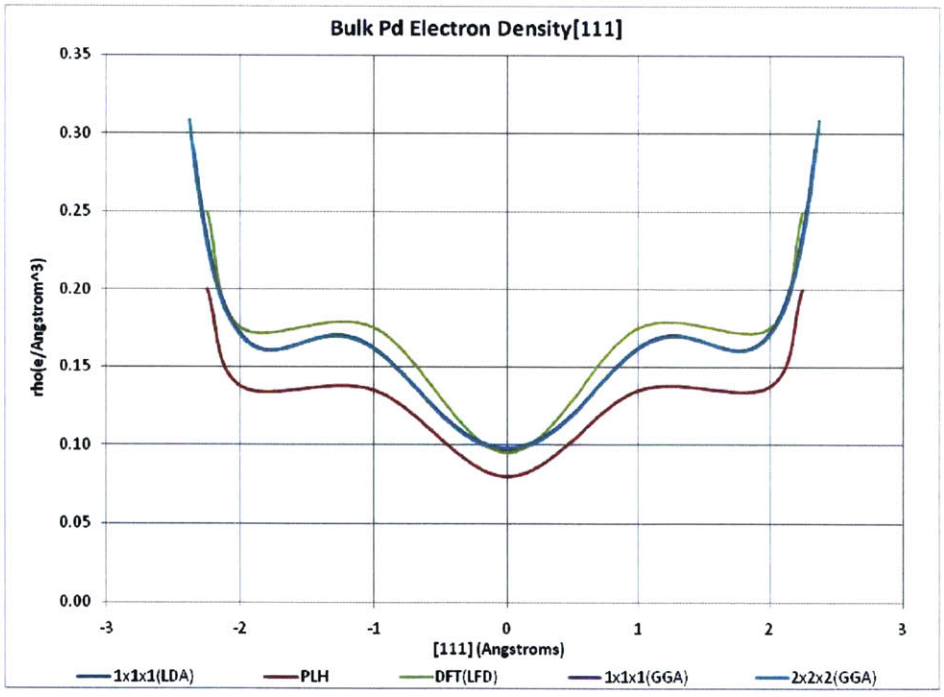

Figure 62: Electron Density in Bulk Pd [111]

k-Mesh Size Convergence

An important consideration when calculation the charge densities (and indeed while doing any DFT calculation) is that of convergence. In particular, we tested the wave function energy cut-off used in the k-vector Fourier expansion and we found that 40 Ry was sufficient for convergence. We did this by varying (increasing) this energy until there was no significant change to the total SCF, all other parameters being held constant. The charge density cut-off was then set at 10x the k-vector cut off (i.e. 400 Ry) to be consistent with the ultrasoft pseudopotentials we are employing (Giannozzi, 2010).

We were also interested in finding out what k-mesh size was sufficient. After optimizing the wave vector energy cut-off, we used charge density to optimize the mesh size. The results are shown below, and indicate that a uniform mesh size of 4x4x4 is sufficient.

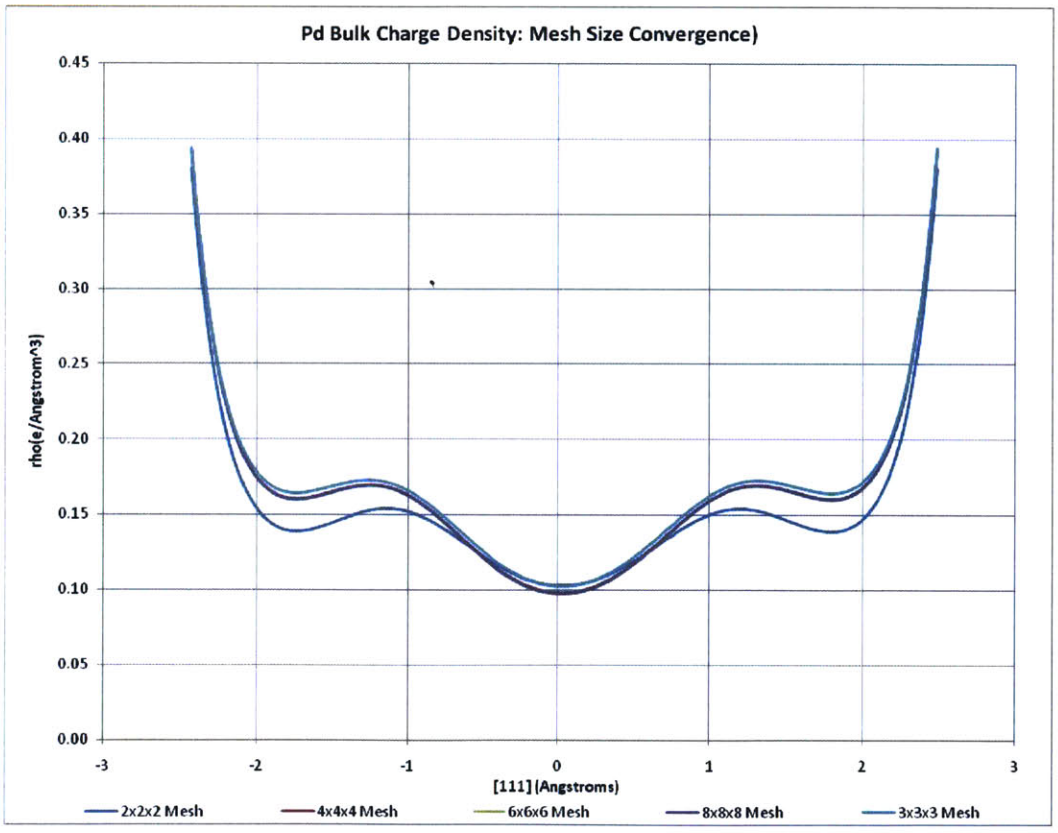

Figure 63: k-Mesh size convergence

PdH Ground State Potential Energy Curve

The potential energy curve for PdH has been investigated by many authors. Balasubra (Balasubramanian, Feng, & Liao, 1987), for example, have used FOCI calculations that closely matched experimental data for low lying ground states:

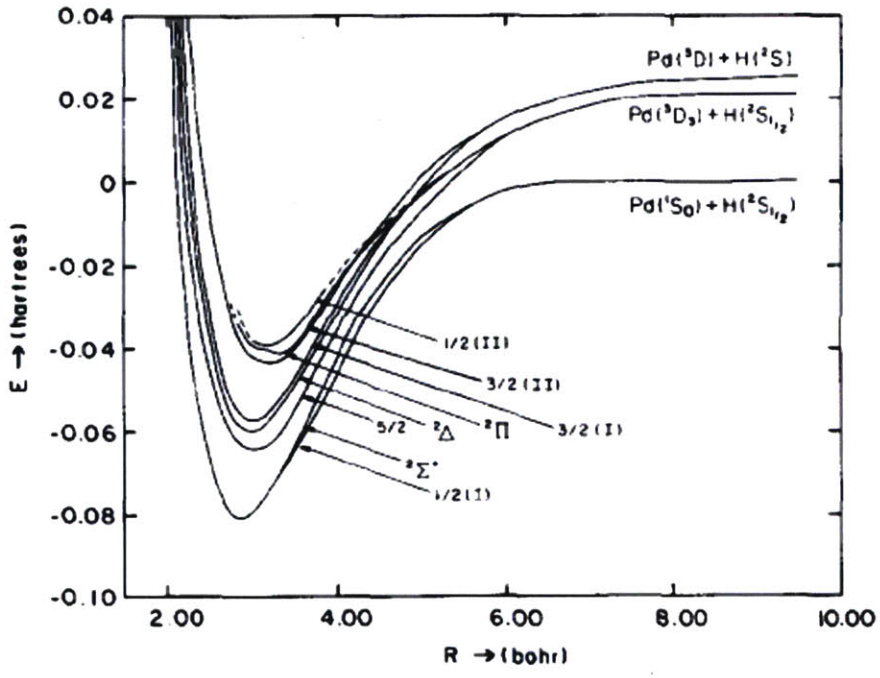

Figure 64: From (Balasubramanian, Feng, & Liao, 1987).

We investigated whether our DFT framework could predict the above results. Specifically, we are interested in replicating the equilibrium bonding length of 1.53 Angstroms. The experimental value was referenced from (Malmberg, Scullman, & Nylen, 1969).

(Computationally, we simply put PdH in a large enough vacuum box and calculate the total SCF energy as the Pd-H distance is varied)

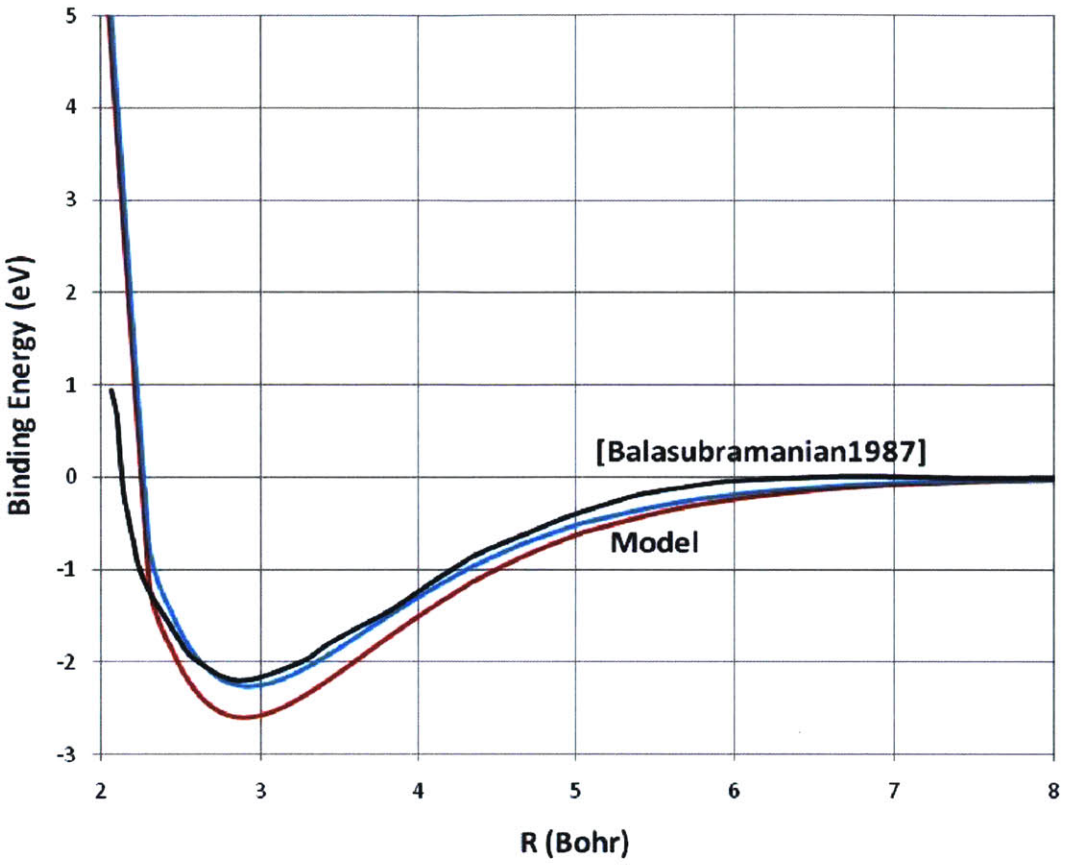

Figure 65: PdH Potential Energy Curve From DFT

Our results (2.9 Bohr) agree very well with experiment.

Lattice Expansion/Elastic Energy

The interaction energy of palladium is believed to be mostly due to the lattice expansion. In this section, we will compare the calculated vs. the experimental lattice elastic energy.

Experimentally, the volumetric change on expansion may be expressed as

$$\delta = \frac{V' - V}{V} = \epsilon_{xx} + \epsilon_{yy} + \epsilon_{zz} \tag{217}$$

For uniform dilation, we have

$$\epsilon_{xx} = \epsilon_{yy} = \epsilon_{zz} = \epsilon \tag{218}$$

or

$$\epsilon = \frac{\delta}{3} \tag{219}$$

The elastic energy density for a general crystal system is given by the tensor

$$U = \frac{1}{2} \sum_{\lambda=1}^{6} \sum_{\sigma=1}^{6} C_{\lambda\sigma} e_\lambda e_\sigma \tag{220}$$

where $C_{\lambda\sigma}$ are elastic constants.

For a cubic crystal like palladium, the energy density is given by

$$U = \frac{1}{6} (C_{11} + 2C_{12}) \delta^2 \tag{221}$$

where the elastic constants are measured experimentally.

The results below show a reasonable agreement with experiment, at low lattice constants, but we note that un-modeled thermal expansion effects in experiment but not model account for deviation at higher lattice expansion.

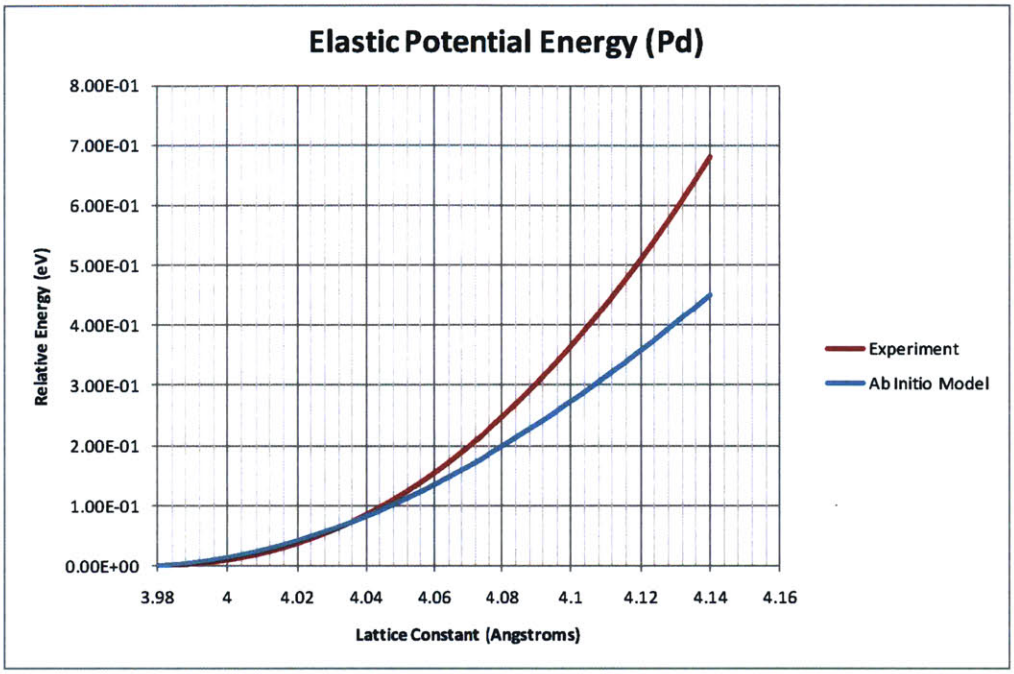

Figure 66: Elastic Potential Energy of bulk Pd: Model vs. Experiment

Summary

This is a 'stick model' chapter. We prove the suitability of DFT by applying it to well known problems. Deviations from experiment are discussed.

Chapter 5 - Understanding the Energies Calculated by DFT

Introduction

In this brief chapter, we will attempt to understand the output energies as reported by our Quantum Espresso (QE)(Giannozzi, 2010) DFT framework. We will start by reviewing the theoretical foundations of DFT for reference purposes, followed by an interpretation of calculated DFT output.

Fundamental Many-Body Problem

The starting point of the Density Functional Theory (DFT) is obviously the difficult many-body problem. Briefly, the fundamental problem is that of the many-body electrons and nuclei , represented by the Hamiltonian:

$$\hat{H} = -\frac{\hbar^2}{2m_e}\sum_i \nabla_i^2 - \sum_{i,I}\frac{Z_I e^2}{|\mathbf{r}_i - \mathbf{R}_I|} + \sum_{i\neq j}\frac{e^2}{|\mathbf{r}_i - \mathbf{r}_j|} - \frac{\hbar^2}{2M_I}\sum_{I\neq j}\nabla_I^2 + \frac{1}{2}\sum_{I\neq j}\frac{Z_I Z_J e^2}{|\mathbf{R}_I - \mathbf{R}_J|} \quad 222$$

We follow the notation and formulation presented in (Martin, 2004) to write Equation 222 thus:

$$\hat{H} = \hat{T} + \hat{V}_{ext} + \hat{V}_{int} + E_{II} + E_C \quad 223$$

In Equation 223, the operator terms are

$\hat{T} = -\frac{\hbar^2}{2m_e}\sum_i \nabla_i^2$ is the kinetic energy operator for the electrons,

$\hat{V}_{ext} = \sum_{i,I}\frac{Z_I e^2}{|\mathbf{r}_i - \mathbf{R}_I|}$ + const is the potential acting on the electrons due to the nuclei,

$\hat{V}_{int} = \sum_{i\neq j}\frac{e^2}{|\mathbf{r}_i - \mathbf{r}_j|}$ is the electron-electron interaction,

$E_{II} = \frac{1}{2}\sum_{I\neq J}\frac{Z_I Z_J e^2}{|\mathbf{R}_I - \mathbf{R}_J|}$ is the classical nuclei-nuclei interaction, and,

$E_C = \frac{1}{2}\sum_{i \neq j} \frac{Z_I Z_J}{|\mathbf{R}_I - \mathbf{R}_J|}$ is the kinetic energy of the nuclei.

Using the Born Oppenheimer approximation, the nuclear kinetic energy may be ignored, such that Equation 223 becomes

$$\hat{H} = \hat{T} + \hat{V}_{ext} + \hat{V}_{int} + E_{II} \tag{224}$$

To describe electronic structure, we may replace the external coulomb potential due to the nuclei, $\hat{V}_{ext}$, with a fixed pseudo-potential external to the electrons. The pseudo potential also captures the effects of core electrons.

The problem thus defined reduces the complexity of Equation 222 somewhat, but we still have electron-electron interaction to grapple with.

Hohenberg-Kohn Theorems

Hohenberg-Kohn Theorem is at the center of Density Functional Theory and applies to a system of interacting particles, as in Equation 222, namely (Martin, 2004):

Theorem I:

For any system of interacting particles in an external potential $V_{ext}(\boldsymbol{r})$, the potential $V_{ext}(\boldsymbol{r})$ is determined uniquely, except for a constant, by the ground state particle density $n_0(\boldsymbol{r})$.

The implication of Theorem I is that the Hamiltonian is fully determined by the ground state electron density, $n_0(\boldsymbol{r})$. But it also means any energy calculations we make may have a constant shift, all factors being the same.

Theorem II:

A universal functional of energy $E[n]$ in terms of the density $n(\boldsymbol{r})$ can be defined, valid for any external potential $V_{ext}(\boldsymbol{r})$. For any particular $V_{ext}(\boldsymbol{r})$, the exact ground state energy of the system is the global minimum value of this functional, and the density $n(\boldsymbol{r})$ that minimizes the functional is the exact ground state density, $n_0(\boldsymbol{r})$.

Summary of Basic DFT Formulation

We want to solve the stationary Schrodinger Equation subject to the Hamiltonian of Equation 222:

$$\left[-\frac{\hbar^2}{2m_e}\sum_i \nabla_i^2 - \sum_{i,I}\frac{Z_I e^2}{|\mathbf{r}_i - \mathbf{R}_I|} + \sum_{i\neq j}\frac{e^2}{|\mathbf{r}_i - \mathbf{r}_j|} - \frac{\hbar^2}{2M_I}\sum_I \nabla_I^2 + \frac{1}{2}\sum_{I\neq J}\frac{Z_I Z_J}{|\mathbf{R}_I - \mathbf{R}_J|}\right]\psi(\boldsymbol{r}_i) = E_i\psi(\boldsymbol{r}_i)$$

225

or

$$\hat{H}\psi(\boldsymbol{r}_i) = E_i\psi(\boldsymbol{r}_i)$$

226

where $\psi(\boldsymbol{r}_i)$ is the many body wave function that we want to solve for.

The total energy is the expectation value of the Hamiltonian:

$$E \equiv \langle\hat{H}\rangle = \langle\hat{T}\rangle + \langle\hat{V}_{int}\rangle + \int d^3r\, \hat{V}_{ext}(\boldsymbol{r})n(\boldsymbol{r}) + E_{II}$$

227

In Equation 227, we have expressed the expectation value of the external potential as a simple integral over the charge density, $n(\boldsymbol{r})$.

$$n(\boldsymbol{r}) = \frac{\langle\psi|\hat{n}(\boldsymbol{r})|\psi\rangle}{\langle\psi|\psi\rangle} = N\frac{\int d^3r_2 \ldots d^3r_N \sum_{\sigma_1}|\psi(\boldsymbol{r}, \boldsymbol{r_2}, \ldots \boldsymbol{r_N})|^2}{\int d^3r_2 \ldots d^3r_N |\psi(\boldsymbol{r}, \boldsymbol{r_2}, \ldots \boldsymbol{r_N})|^2}$$

228

In Equation 228, we have utilized the Pauli Exclusion principle, namely that all electrons are identical, to replace electron $\boldsymbol{r_i}$ by electron $\boldsymbol{r_1}$.

Furthermore,

σ denotes spin,

$\hat{n}(\boldsymbol{r})$ is the electron density operator,

$$\hat{n}(\boldsymbol{r}) = \sum_{i=1,N} \delta(\boldsymbol{r} - \boldsymbol{r}_i) \qquad 229$$

and

$$\int d^3\boldsymbol{r}\, n(\boldsymbol{r}) = N \qquad 230$$

According to the HK Theorems, therefore, we can in principle start with the ground state electron density, $n_o(\boldsymbol{r})$. From there, we can determine the external potential $V_{ext}(\boldsymbol{r})$, from which we can build the Hamiltonian and whence the wavefunction of any state may be determined. On the other hand, the ground state electronic density function may be obtained by minimizing Equation 228 with respect to ***all*** parameters. Of course this is a circular definition, but as we shall see below, it suggests an iterative, self consistent solution approach.

The minimization outlined above, however, is a daunting task. Furthermore, it would yield far more information that we are interested in (basically it will tell us pretty much the spatial location of all nucleus and electron at any given time).

Kohn-Sham Ansatz For the Ground State

Kohn and Sham realized that the many body problem, Equation 225, is extremely difficult to solve, and the HK Theorems do not offer any practical guidelines for solving the electronic states except in very simple systems (*N=1* for example). The Kohn-Sham ansatz, (Martin, 2004), (Hohenberg & Kohn, 1964), (Kohn & Sham, 1965), starts by assuming that the ground state electronic density of the system of real interacting system (the real world one whose solution we seek) is equivalent to that of some chosen non-interacting system.

The non-interacting system is an easier problem to solve. However, the interaction in the original system does not magically disappear; it is instead replaced by an exchange-correlation functional of electron density, which captures the interaction inherent in the original interacting system.

In practice, the exchange-correlation functional is an approximation (several of which exist today, including the Local Density Approximation, LDA, and various flavors of Generalized Gradient Approximations, GGA to which we have referred in previous chapters).

Auxiliary System Formulation

According to HK Theorem II, we should be able to express the total ground energy as a functional of the electronic density, i.e. Equation 227 may be recast in its density functional form as:

$$E_{HK}[n] = T[n] + E_{int}[n] + \int d^3r\, V_{ext}(\boldsymbol{r})n(\boldsymbol{r}) + E_{II} \tag{231}$$

where we have expressed the expectation of the external potential as an integral over the electronic density. We may also treat the second term (electron-electron interaction) as a self interacting classical charge density:

$$E_{Hartree}[n] = \frac{1}{2}\int d^3r\, d^3r'\, \frac{n(\boldsymbol{r})\, n(\boldsymbol{r}')}{|r - r'|} \tag{232}$$

The Kohn Sham ansatz (guess, but turns out to be a spark of genius) is to realize the following:

(1) The exact ground state density can be represented by the ground state density of an auxiliary system of non-interacting particles.

(2) The auxiliary Hamiltonian is chosen to have the usual kinetic energy operator and an effective local potential $V_{eff}^{\sigma}(\boldsymbol{r})$ acting on an electron of spin σ at position $\boldsymbol{r}$. A key simplification usually used in the formulation is that the potential is localized.

The auxiliary system Hamiltonian is then (in Hartree atomic units):

$$\hat{H}_{aux}^{\sigma} = -\frac{1}{2}\nabla^2 + V_{eff}^{\sigma}(\boldsymbol{r}) \tag{233}$$

where $V_{eff}^{\sigma}(\boldsymbol{r})$ is as yet unspecified.

For (the auxiliary) system of $N = N^{\uparrow} + N^{\downarrow}$ electrons, Equation 233 suggests that the ground state will have one electron in each of the N^{σ} orbitals $\psi_i^{\sigma}(\boldsymbol{r})$ with the lowest eigenvalues ϵ_i^{σ} of the Hamiltonian.

Still for the auxiliary system, we can calculate the particle density and kinetic energy as, respectively:

$$n(\boldsymbol{r}) = \sum_{\sigma} \sum_{i=1}^{N^{\sigma}} |\psi_i^{\sigma}(\boldsymbol{r})|^2 \tag{234}$$

$$T_s = \sum_{\sigma} \sum_{i=1}^{N} \langle \psi_i(\boldsymbol{r}) | \nabla^2 | \psi_i(\boldsymbol{r}) \rangle \tag{235}$$

The Kohn-Sham ansatz then is to realize that we can recast the ground state energy of the full interacting many-body problem Equations 231, 232, as follows:

$$E_{KS}[n] = T_s[n] + E_{Hartree}[n] + \int d^3r \, V_{ext}(\boldsymbol{r}) n(\boldsymbol{r}) + E_{II} + E_{xc}[n] \tag{236}$$

We note the following about Equation 236:

- It is an educated guess (but based on its success since it was proposed, it is a very good one),
- It is essentially an independent particle equation except that all the many-body effects have been lumped into the last term, the exchange-correlation energy, $E_{xc}[n]$.

But Equation 236 also begs the question: What is Exchange-Correlation Energy, $E_{xc}[n]$, anyway? We provide an algebraic answer that we hope sheds some light. Comparing Equation 231 and Equation 236 reveals that (noting that $E_{KS}[n] = E_{HK}[n]$ by formulation),

$$E_{xc}[n] = T[n] + E_{int}[n] - T_s[n] - E_{Hartree}[n] \quad (237)$$

We note from Equation 227 that the functionals are actually expectation values that evaluate to an energy component of the fully interacting many body system, i.e.,

$$E_{xc}[n] = \left(\langle \hat{T} \rangle - T_s[n]\right) + \left(\langle \hat{V}_{int} \rangle - E_{Hartree}[n]\right) \quad (238)$$

In other words, the Exchange Correlation Energy is the difference between the kinetic and self interaction energy of the true system, and those of the auxiliary one.

Kohn-Sham Equations

To arrive at the ground state of the real interacting system, we need to minimize the Kohn-Sham energy functional of Equation 236. To minimize the KS energy, we can vary either $n(\boldsymbol{r})$ or the wave function.

One way to perform the minimization is via the Lagrangian of the functional, subject to the constraint of wave function orthonormality:

$$\langle \psi_i(\boldsymbol{r}) | \psi_j(\boldsymbol{r}) \rangle = \delta_{i,j} \quad (239)$$

i.e.

$$L[n] = E_{KS}[n] - \epsilon_i \left[\langle \psi_i(\boldsymbol{r}) | \psi_j(\boldsymbol{r}) \rangle - \delta_{i,j} \right] \quad (240)$$

In Equation 240, we have fortuitously chosen the Lagrange multipliers in anticipation of the results below. Varying the Lagrangian leads to

$$\frac{\delta L[n]}{\delta \psi_i^*(\boldsymbol{r})} = \frac{\delta E_{KS}[n]}{\delta \psi_i^*(\boldsymbol{r})} - \epsilon_i \psi_i(\boldsymbol{r}) = 0$$

241

The variation of the KS energy $\frac{\delta E_{KS}[n]}{\delta \psi_i^*(r)}$, may be done straightforwardly by applying chain rule on terms that don't explicitly depend on the wave function, i.e.:

$$\frac{\delta E_{KS}[n]}{\delta \psi_i^*(\boldsymbol{r})} = \frac{\delta T_s[n]}{\delta \psi_i^*(\boldsymbol{r})} + \frac{\delta E_{Hartree}[n]}{\delta n(\boldsymbol{r})}\frac{\delta n(\boldsymbol{r})}{\delta \psi_i^*(\boldsymbol{r})} + \frac{\delta E_{ext}[n]}{\delta n(\boldsymbol{r})}\frac{\delta n(\boldsymbol{r})}{\delta \psi_i^*(\boldsymbol{r})} + \frac{\delta E_{xc}[n]}{\delta n(\boldsymbol{r})}\frac{\delta n(\boldsymbol{r})}{\delta \psi_i^*(\boldsymbol{r})}$$

242

To evaluate the first term on the right hand side of Equation 242, we note that we can write the Kinetic Energy (Equation 235) as:

$$T_s = -\frac{1}{2}\sum_{i=1}^{N} \int d^3r\, \psi_i^*(\boldsymbol{r}) \nabla^2 \psi_i(\boldsymbol{r})$$

243

Equation 243 is a linear functional of $\psi_i^*(\boldsymbol{r})$, therefore,

$$\frac{\delta T_s[n]}{\delta \psi_i^*(\boldsymbol{r})} = -\frac{1}{2}\nabla^2 \psi_i(\boldsymbol{r})$$

244

Similarly,

$$\frac{\delta n(\boldsymbol{r})}{\delta \psi_i^*(\boldsymbol{r})} = \psi_i(\boldsymbol{r})$$

245

and

$$\frac{\delta E_{ext}[n]}{\delta n(\boldsymbol{r})} = \frac{\delta[\int d^3r\, V_{ext}(\boldsymbol{r})\, n(\boldsymbol{r})]}{\delta n(\boldsymbol{r})} = V_{ext}(\boldsymbol{r})$$

246

Using these in Equation 241, we get the stationary points of Lagrangian thus:

$$\left[-\frac{1}{2}\nabla^2\psi_i(\boldsymbol{r}) + \frac{\delta E_{Hartree}[n]}{\delta n(\boldsymbol{r})} + V_{ext}(\boldsymbol{r}) + \frac{\delta E_{xc}[n]}{\delta n(\boldsymbol{r})} - \epsilon_i\right]\psi_i(\boldsymbol{r}) = 0 \tag{247}$$

Equations 247 are the well known Kohn-Sham Equations.

We can put the KS Equations in the familiar form of independent particle Schrodinger equations, thus,

$$H_{KS}(\boldsymbol{r})\,\psi_i(\boldsymbol{r}) = \epsilon_i\psi_i(\boldsymbol{r}) \tag{248}$$

with

$$H_{KS}(\boldsymbol{r}) = -\frac{1}{2}\nabla^2\psi_i(\boldsymbol{r}) + \frac{\delta E_{Hartree}[n]}{\delta n(\boldsymbol{r})} + V_{ext}(\boldsymbol{r}) + \frac{\delta E_{xc}[n]}{\delta n(\boldsymbol{r})} \tag{249}$$

Because the KS potential,

$$V_{KS}(\boldsymbol{r}) = \frac{\delta E_{Hartree}[n]}{\delta n(\boldsymbol{r})} + V_{ext}(\boldsymbol{r}) + \frac{\delta E_{xc}[n]}{\delta n(\boldsymbol{r})} \tag{250}$$

depends on the electron density $n(\boldsymbol{r})$, the Kohn-Sham Equations have to be solved self-consistently (in such a way that the resulting electron density is consistent with the KS potential).

Extracting Physical Observables

In this section, we try to determine whether we can make sense of the output of our DFT calculations (other than the total SCF energy). In particular, we like to decompose the total energy results into its various components (Kinetic, Coulombic, etc)

$$\left[-\frac{\hbar^2}{2m_e}\sum_i \nabla_i^2 - \sum_{i,I}\frac{Z_I e^2}{|r_i - R_I|} + \sum_{i\neq j}\frac{e^2}{|r_i - r_j|} - \frac{\hbar^2}{2M_I}\sum_I \nabla_I^2 + \frac{1}{2}\sum_{I\neq J}\frac{Z_I Z_J}{|R_I - R_J|}\right]\psi(r_i) = E_i\psi(r_i)$$

251

Output of Quantum Espresso

A sample output of Quantum Espresso SCF run (the main DFT calculation) is given below:

```
!    total energy              =   -2434.16877502 Ry
     Harris-Foulkes estimate   =   -2434.16924056 Ry
     estimated scf accuracy    <       0.00057787 Ry

     The total energy is the sum of the following terms:

     one-electron contribution =     328.27526527 Ry
     hartree contribution      =     231.77750778 Ry
     xc contribution           =   -1000.22065260 Ry
     ewald contribution        =   -1994.09563536 Ry
     smearing contrib. (-TS)   =       0.09473990 Ry

     convergence has been achieved in   7 iterations
```

One-Electron Contribution

The one electron contribution or band energy contains contributions from both kinetic and the external KS potential (the latter comes out of minimizing Equation 236 with respect to electron density). The calculation is done in k-space, so there is really no straightforward correspondence between this and a physical quantity.

However, the information about kinetic energy may be retrieved from electronic wave functions, which QE calculates and stores. This may be done using the post-processing program (pp.x) which actually calculates the electron localization function or kinetic energy density.

Hartree Contribution

This is the classical electron-electron interaction energy (Equation 232). This has a physical meaning.

Exchange Correlation Energy

The closest physical interpretation we can attach to the exchange correlation energy is Equation 238.

Summary

We have presented a brief summary of DFT theory for reference purposes. We then connect it to energy calculation within our particular implementation of DFT (Giannozzi, 2010).

Chapter 6 - SuperCell Configurational Considerations

Introduction

So far, we have calculated state energies *ab initio* via a random placement of hydrogen atoms within the palladium interstices. We have done this because the large number of possible configurations makes it impractical to interrogate them all. As the following elementary figure shows for a 2x2x2 supercell, the number of combinations is very large:

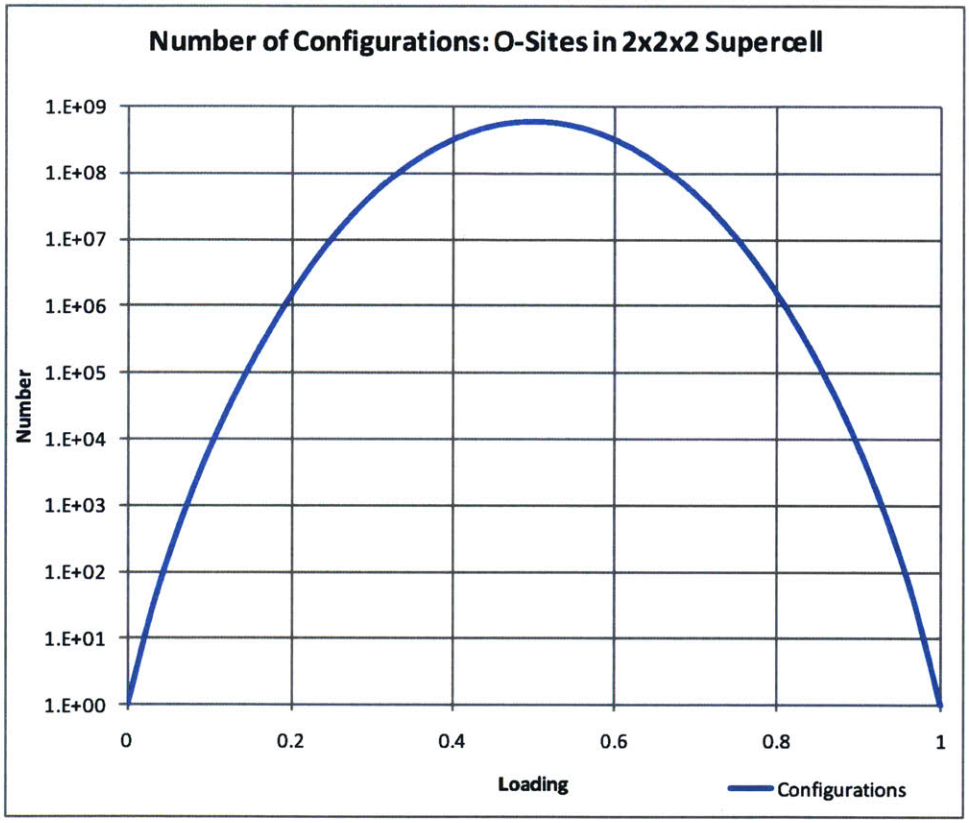

Figure 67: Number of different configurations for Loading a 2x2x2 super cell

Obviously some of these states are degenerate, nevertheless, lacking some intuition on the bonding states of H in Pd, we still have a very large number of computations to grapple with.

Current Understanding of PdH Bonding States

There is currently a general consensus about how H bonds with Pd atoms (Flanagan & Oates, 1991). The bonding occurs via a small charge transfer from around Pd to H. These electrons come from Pd's d-band (Chan & Louie, 1983), thus creating a new bonding state several eV below it.

It is also generally understood that the PdH interaction is short range and does not extend beyond nearest neighbors [ibid]. It takes just one electron to screen the proton, independent of the loading level of course. Therefore, it is plausible that our state energies should not be much affected by the configuration chosen, but should depend on loading.

Ab Initio Calculation

2 H Configuration.

With the above assumption about state energy dependence on configuration, we set out to validate the hypothesis. To do this with a 2x2x2 Pd Super Cell, we can start with a simple case of two H atoms as a 'stick model' exercise. For this simple case, we can identify the following configurations. All atomic coordinates are Cartesian {x, y, z} relative to the supercell lattice constant, a.

We then calculate the interaction energy as follows: We pick the first H atom at the center of the first FCC unit cell {0.25,0.25,0.25}, while the second is picked at a distance away as shown in the following table.

H1	H2	H-H Distance	Interaction Energy (eV/atom)
{0.25,0.25,0.25}	{0.75,0.25,0.25}	0.5 a	-0.42098
{0.25,0.25,0.25}	{0.75,0.75,0.25}	0.707 a	-0.42479
{0.25,0.25,0.25}	{0.75,0.75,0.75}	0.866 a	-0.41991

The results indicate that the lowest energy is achieved by placing both H atoms at the center of a unit cell vs. at the edge (Figure 68).

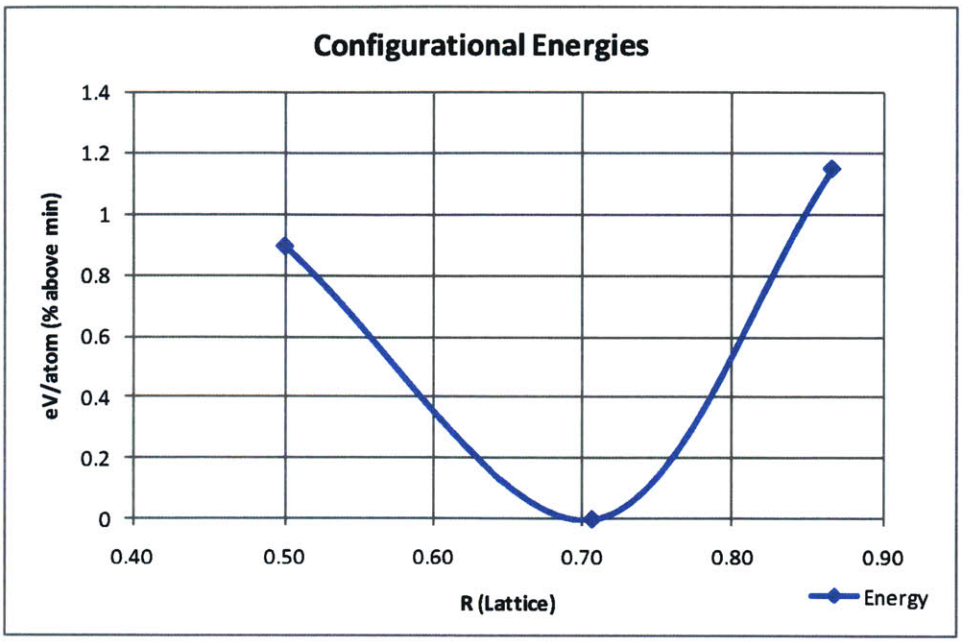

Figure 68: Energy as a percentage above the minimum for three configurations with two Hydrogen atoms.

The energy difference is about 1% per H atom, which is significant. The hypothesis of a distance-based energy, therefore, does not appear to hold.

We believe that energy is minimized by placing the Hydrogen atom in an electron density that is closer to the one in hydrogen gas. There is some support of this hypothesis from other authors, (Christensen, Stoltze, Jacobsen, & Norskov, 1990) for example, who found out that the electron density in the interstice was a crucial factor in determining the heat of solution. We also have some preliminary electron density data that appear to confirm this view, shown below. In each case, the density is taken along a line containing the two hydrogen atoms. The lowest energy configuration contains a potential energy hole with the lowest electron density:

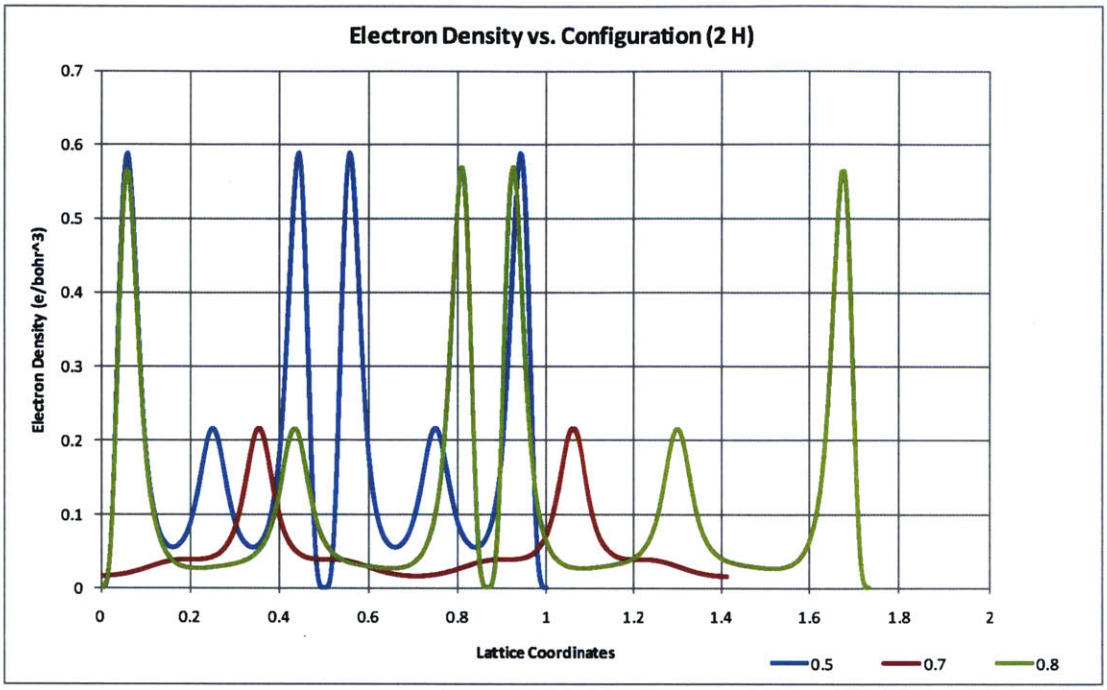

Figure 69: Electron density along the line of site of two H atoms in Pd O sites. See visual model below.

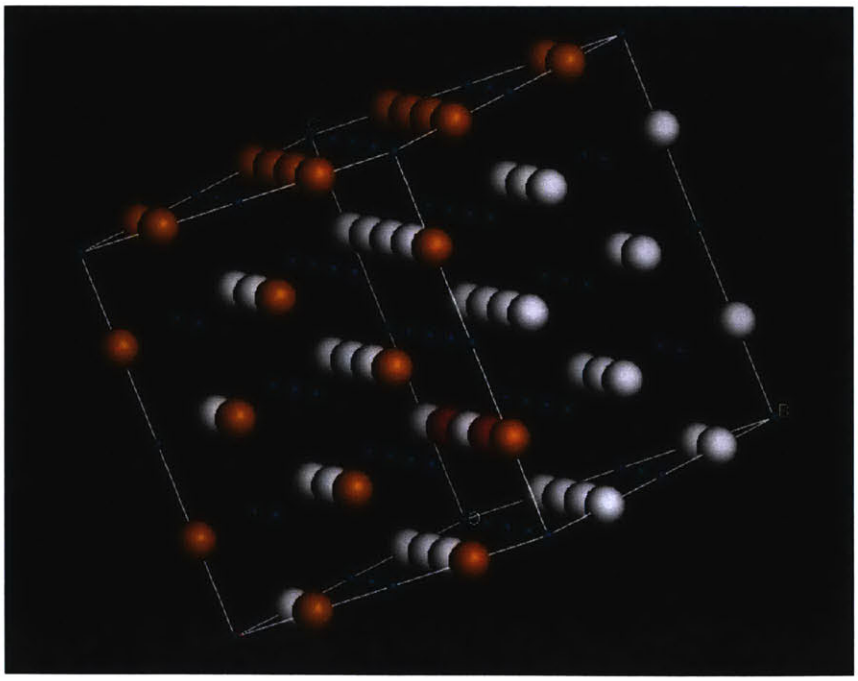

Figure 70: Lowest Energy configuration. Fully loaded Supercell shown. Pd atoms are in Blue, H atoms white and the 2 H configuration is shown in Red. Orange are H atoms that are not part of the supercell.

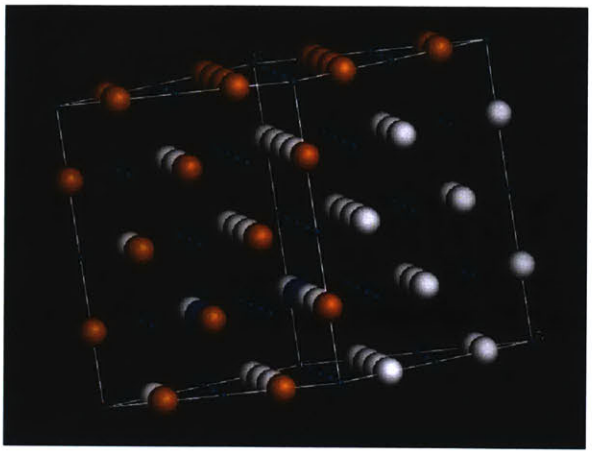

Figure 71: Example 2H Higher Energy Configurations (Blue)

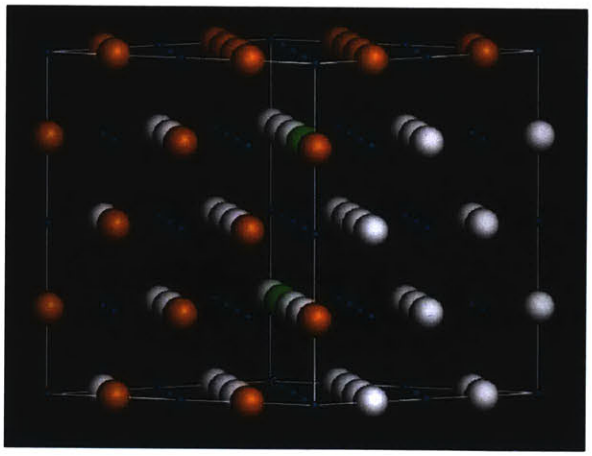

Figure 72: Example 2H Higher Energy Configurations (Green)

Summary

We have attempted to analyze configurational energy differences. We have found some differences, as should be expected. However, despite these results, it is unclear if this dependence holds in general – we may not generalize the model based on such a limited configurational testing.

Chapter 7 - Understanding Enthalpy and Entropy

Introduction

In this chapter, we switch gears and try to understand the enthalpy and entropy changes resulting from the loading a metal with hydrogen. Our aim is to gain some understanding of the model results by approaching the problem from a physical chemistry point of view here.

We start with basic thermodynamics by following the basic formulation presented by (Silbey, Alberty, & Bawendi, 2004), and writing the combined First and Second Laws of Thermodynamics as follows:

$$dU = TdS - PdV + \sum_{i=1}^{N} \mu_i dn_i \quad (252)$$

where U is the total internal energy, T is temperature, S is system entropy, P is pressure, and μ_i is the chemical potential of species i, of which there are n_i in number, and N is the total number of species.

Enthalpy, on the other hand, is defined by the system variables U, P and V according to

$$H = U + PV \quad (253)$$

A change in enthalpy is a measure of the energy change involved in a process. For example, at constant pressure, Equation 253 indicates that the enthalpy change will be equivalent to the heat absorbed by the system.

Formally, we may write differential change in enthalpy as, using Equation 253

$$dH = dU + PdV + VdP \quad (254)$$

Substituting for dU from Equation 252, we get:

$$dH = TdS + VdP + \sum_{i=1}^{N} \mu_i d\, n_i \tag{255}$$

We may use Legendre transforms on the state equation for enthalpy, Equation 253, to define a new thermodynamic potential, the Gibbs Free Energy, G. Thus, subtracting TS from Equation 253, we get:

$$G = U + PV - TS = H - TS \tag{256}$$

and

$$dG = dU + PdV + VdP - TdS - SdT \tag{257}$$

or, using Equation 252:

$$dG = VdP - SdT + \sum_{i=1}^{N} \mu_i d\, n_i \tag{258}$$

We understand Gibbs Free Energy as the useful, non-mechanical useful work that may be extracted from a closed system. At equilibrium, we expect it to attain a minimum with respect to state variables, T, P and μ.

Enthalpy-Pressure Connection

We like to connect pressure that we calculate from our model to enthalpy and entropy that are measured by experimentalists. In order to do this, we note that, from Equation 258 above,

$$V = \left(\frac{dG}{dP}\right)_{T,n} \tag{259}$$

where we have dropped the i subscript on n for brevity. The two sides of Equation 259 may be integrated thus

$$\int_{-G^0}^{G} dG' = -G^0 + G \tag{260}$$

and

$$\int_{P_0}^{P} VdP' = nRT * ln\frac{P}{P^0} \tag{261}$$

where $-G^0$ is standard Gibbs energy and P^0 is standard pressure, and we have assumed an ideal gas in the last step.

The result is

$$G = G^0 + nRT * ln\frac{P}{P^0} \tag{262}$$

Equation 262 provides a connection between Gibbs Free Energy and pressure. To connect enthalpy and Gibbs Free Energy, we note from Equation 258 above that

$$S = -\left(\frac{\partial G}{\partial T}\right)_{P,n} \tag{263}$$

Using this result in Equation 256, we get

$$G = H + T\left(\frac{\partial G}{\partial T}\right)_{P,n} \tag{264}$$

We can use a mathematical device to eliminate G from Equation 264 by noting that (Silbey, Alberty, & Bawendi, 2004)

$$\left(\frac{\partial\left(\frac{G}{T}\right)}{\partial T}\right)_{P,n} = \left(\frac{T\frac{\partial G}{\partial T} - G}{T^2}\right)_{P,n} = -\frac{G}{T^2} + \frac{1}{T}\left(\frac{\partial G}{\partial T}\right)_{P,n} \tag{265}$$

Using Equation 264 to eliminate G from Equation 265, we get

$$\left(\frac{\partial\left(\frac{G}{T}\right)}{\partial T}\right)_{P,n} = -\frac{1}{T^2}\left(H + T\left(\frac{\partial G}{\partial T}\right)_{P,n}\right) + \frac{1}{T}\left(\frac{\partial G}{\partial T}\right)_{P,n} \tag{266}$$

or

$$H = -T^2\left(\frac{\partial\left(\frac{G}{T}\right)}{\partial T}\right)_{P,n} \tag{267}$$

which is the Gibbs-Helmholtz equation. From it, we get the enthalpy change as

$$\Delta H = -T^2\left(\frac{\partial\left(\frac{\Delta G}{T}\right)}{\partial T}\right)_{P,n} \tag{268}$$

Connection to pressure is achieved via Equation 262, which we may rewrite, since Gibbs energy is relative, as

$$\Delta G = nRT * ln(P) \tag{269}$$

The final result is

$$\Delta H = -T^2\left(\frac{\partial\left(\frac{nRTln(P)}{T}\right)}{\partial T}\right)_n = -nRT^2\left(\frac{\partial(lnP)}{\partial T}\right)_n \tag{270}$$

Entropy Pressure Connection

We use Equations 256 & 270 to make the connection between pressure and entropy

$$-\Delta S = \frac{\Delta G - \Delta H}{T} = nR * l\,n(P) + nRT\left(\frac{\partial(lnP)}{\partial T}\right)_n \tag{271}$$

Fugacity

We used ideal gas model to derive the Gibbs Free Energy, Equation 262. For a real gas, G. N. Lewis recognized the convenience of using the same form by defining a fugacity f according to

$$G = G^0 + nRT * ln\frac{f}{P^0} \tag{272}$$

We have previously [Chapter 2] used fugacity models, e.g. (Tkacz & Litwiniuk, 2002), that we may use together with Equation 272, i.e.,

$$ln\, f = \frac{\{1.5 * A * P^{2/3} + 3 * B * P^{1/3} + (D + E * T) * ln(P) - 3 * C * P^{-1/3}\}}{R * T} \tag{273}$$

For real gases, therefore, overall results are then given by the following

$$\Delta H = -nRT^2 \left(\frac{\partial\, ln(f)}{\partial T}\right)_n \tag{274}$$

and

$$-\Delta S = nR * ln(f) + nRT \left(\frac{\partial\, ln(f)}{\partial T}\right)_n \tag{275}$$

Model Enthalpy Calculation: Differential Fugacity Formulation

In the single phase regions only, we can use Equations 274 & 275 to connect model fugacity calculations and experimental enthalpy data. In literature, for example (Flanagan & Oates, 1991), these two equations take the equivalent "molar" form, with the ½ factor used to go from hydrogen gas to the atom, thus:

$$\left(\frac{\partial\left(\ln p^{\frac{1}{2}}\right)}{\partial\left(\frac{1}{T}\right)}\right)_{\theta}=\frac{\Delta\bar{H}}{R} \tag{276}$$

and

$$T\left(\frac{\partial\left(\ln p^{\frac{1}{2}}\right)}{\partial T}\right)_{\theta}+\ln p^{\frac{1}{2}}=-\frac{\Delta\bar{S}}{R} \tag{277}$$

To proceed, we take $\varepsilon_h(\theta)$ as the total interaction energy of the configuration, and re-write the fugacity model, Chapter 2, as:

$$f(\theta,T)=A(T)*e^{\frac{B(\theta,T)}{\kappa_B T}} \tag{278}$$

where

$$A(T)=\kappa_B T\left(\frac{2\pi m\kappa_B T}{h^2}\right)^{\frac{3}{2}} \tag{279}$$

$$B(\theta,T)=2\kappa_B T\ ln\frac{\theta_o}{1-\theta_o}-2\kappa_B T\ ln(z)+2\theta\frac{\partial\varepsilon_h(\theta)}{\partial\theta}+2\varepsilon_h(\theta)+\kappa_B T ln\frac{e^{-\frac{\epsilon_{0v}}{2\kappa_B T}}}{1-e^{-\frac{\epsilon_{0v}}{\kappa_B T}}}+\kappa_B T ln\frac{8\pi^2 I\kappa_B T}{\sigma h^2}+\epsilon_D \tag{280}$$

or, using,

$$z = \left(2\,sinh\frac{\epsilon_{0v}}{2\kappa_B T}\right)^{-3} \tag{281}$$

we get to

$$B(\theta,T) = 2\kappa_B T\,ln\frac{\theta_o}{1-\theta_o} + 6\kappa_B T\,ln\left(2\,sinh\frac{\epsilon_{0v}}{2\kappa_B T}\right) + 2\theta\frac{\partial\varepsilon_h(\theta)}{\partial\theta} + 2\varepsilon_h(\theta) + \kappa_B T\,ln\frac{8\pi^2 I\kappa_B T}{\sigma h^2} + \epsilon_D \tag{282}$$

and $\varepsilon_h(\theta)$ is the total interaction energy of the configuration at a loading of θ as before.

♦

To calculate the relative enthalpy change, it is perhaps easiest to start with Equations 274 & 275 in their molar forms (later, we will actually use a 'per hydrogen atom' metric):

$$\Delta H = -\frac{RT^2}{2}\left(\frac{\partial\,ln(f)}{\partial T}\right)_n \tag{283}$$

and

$$-\Delta S = \frac{R}{2} * l\,n(f) + \frac{RT}{2}\left(\frac{d\,ln(f)}{dT}\right)_n \tag{284}$$

Then, simplifying Equation 283 first, we get, after noting that we may dispense with the following algebra:

$$\Delta H(\theta,T) = -\frac{RT^2}{2}\left(\frac{\partial\ln f(\theta,x)}{\partial T}\right)_\theta$$

$$= -\frac{RT^2}{2}\frac{1}{f(\theta,T)}\left(\frac{\partial f(\theta,T)}{\partial T}\right)_\theta$$

$$= -\frac{RT^2}{2}\frac{1}{f(\theta,T)}\left(\frac{\partial\left(A(T) * e^{\frac{B(\theta,T)}{\kappa_B T}}\right)}{\partial T}\right)_\theta$$

$$= -\frac{RT^2}{2}\frac{1}{f(\theta,T)}\left(A(T) * e^{\frac{B(\theta,T)}{\kappa_B T}}\left[\frac{\kappa_B T B'(\theta,T) - \kappa_B B(\theta,T)}{(\kappa_B T)^2}\right] + A'(T) * e^{\frac{B(\theta,T)}{\kappa_B T}}\right)_\theta$$

$$= -\frac{R}{2}\left(\left[\frac{TB'(\theta,T) - B(\theta,T)}{\kappa_B}\right] + T^2\frac{A'(T)}{A(T)}\right)_\theta$$

$$\boldsymbol{\Delta H(\theta,T) = -\frac{R}{2}\left(\left[\frac{TB'(\theta,T) - B(\theta,T)}{\kappa_B}\right] + T^2\frac{A'(T)}{A(T)}\right)_\theta \left(\frac{J}{Mol}\right)} \quad (285)$$

where

$$A'(T) = \frac{5}{2}\kappa_B\left(\frac{2\pi m\kappa_B T}{h^2}\right)^{\frac{3}{2}} \quad (286)$$

$$B(\theta,T) = 2\kappa_B T\, ln\frac{\theta_o}{1-\theta_o} + 6\kappa_B T\, ln\left(2\, sinh\frac{\epsilon_{0v}}{2\kappa_B T}\right) + 2\theta\frac{\partial\varepsilon_h(\theta)}{\partial\theta} + 2\varepsilon_h(\theta) + \kappa_B T\, ln\frac{8\pi^2 I\kappa_B T}{\sigma h^2} + \epsilon_D \quad (287)$$

$$B'(\theta,T) = 2\kappa_B ln\frac{\theta_o}{1-\theta_o} + 6\kappa_B T\frac{\partial}{\partial T}\left(ln\left(2\,sinh\frac{\epsilon_{0v}}{2\kappa_B T}\right)\right) + 6\kappa_B l\,n\left(2\,sinh\frac{\epsilon_{0v}}{2\kappa_B T}\right) + \kappa_B T\frac{\partial}{\partial T}\left(ln\frac{8\pi^2 I\kappa_B T}{\sigma h^2}\right)$$

$$+ \kappa_B ln\frac{8\pi^2 I\kappa_B T}{\sigma h^2}$$

$$= 2\kappa_B ln\frac{\theta_o}{1-\theta_o} + 6\kappa_B T\frac{1}{2\,sinh\frac{\epsilon_{0v}}{2\kappa_B T}}\frac{\partial}{\partial T}\left(2\,sinh\frac{\epsilon_{0v}}{2\kappa_B T}\right) + 6\kappa_B l\,n\left(2\,sinh\frac{\epsilon_{0v}}{2\kappa_B T}\right) + \kappa_B T\frac{\sigma h^2}{8\pi^2 I\kappa_B T}\frac{\partial}{\partial T}\left(\frac{8\pi^2 I\kappa_B T}{\sigma h^2}\right)$$

$$+ \kappa_B ln\frac{8\pi^2 I\kappa_B T}{\sigma h^2}$$

$$= 2\kappa_B ln\frac{\theta_o}{1-\theta_o} + 6\kappa_B T\frac{cosh\frac{\epsilon_{0v}}{2\kappa_B T}}{sinh\frac{\epsilon_{0v}}{2\kappa_B T}}\left(-\frac{\epsilon_{0v}}{2\kappa_B T^2}\right) + 6\kappa_B\,ln\left(2\,sinh\frac{\epsilon_{0v}}{2\kappa_B T}\right) + \kappa_B + \kappa_B ln\frac{8\pi^2 I\kappa_B T}{\sigma h^2}$$

$$= 2\kappa_B ln\frac{\theta_o}{1-\theta_o} - 3\frac{\epsilon_{0v}}{T}coth\frac{\epsilon_{0v}}{2\kappa_B T} + 6\kappa_B\,ln\left(2\,sinh\frac{\epsilon_{0v}}{2\kappa_B T}\right) + \kappa_B + \kappa_B ln\frac{8\pi^2 I\kappa_B T}{\sigma h^2}$$

$$\boldsymbol{B'(\theta,T) = 2\kappa_B ln\frac{\theta_o}{1-\theta_o} - 3\frac{\epsilon_{0v}}{T}coth\frac{\epsilon_{0v}}{2\kappa_B T} + 6\kappa_B\,ln\left(2\,sinh\frac{\epsilon_{0v}}{2\kappa_B T}\right) + \kappa_B + \kappa_B ln\frac{8\pi^2 I\kappa_B T}{\sigma h^2}}$$

288

The entropy change is given by

$$-\Delta S(\theta,T) = \frac{RT}{2}\left(\frac{\partial \ln f(\theta,T)}{\partial T}\right)_{\theta} + \frac{R}{2} * \ln f(\theta,T)$$

$$= \frac{R}{2}\left[\frac{T}{f(\theta,T)}\frac{\partial f(\theta,T)}{\partial T} + \ln f(\theta,T)\right]$$

$$= \frac{R}{2}\left[\frac{T}{f(\theta,T)}\left(\frac{\partial\left[A(T) * e^{\frac{B(\theta,T)}{\kappa_B T}}\right]}{\partial T}\right) + \ln f(\theta,T)\right]$$

$$= \frac{R}{2}\left[\frac{T}{f(\theta,T)}\left[A(T)e^{\frac{B(\theta,T)}{\kappa_B T}}\left(\frac{\kappa_B T * B'(\theta,T) - B(\theta,T) * \kappa_B}{(\kappa_B T)^2}\right) + e^{\frac{B(\theta,T)}{\kappa_B T}}A'(T)\right] + \ln f(\theta,T)\right]$$

$$= \frac{R}{2}\left[\left[\left(\frac{T * B'(\theta,T) - B(\theta,T)}{\kappa_B T}\right) + T\frac{A'(T)}{A(T)}\right] + \ln f(\theta,T)\right]$$

$$-\Delta S(\theta,T) = \frac{R}{2}\left[\left(\frac{T * B'(\theta,T) - B(\theta,T)}{\kappa_B T}\right) + T\frac{A'(T)}{A(T)} + \ln f(\theta,T)\right] \quad (289)$$

Alternatively, once the enthalpy change has been calculated, we can also use Equation 271 to calculate entropy change as follows:

$$-\Delta S = \frac{\Delta G - \Delta H}{T} \quad (290)$$

The results are shown below. To compare the model results to (Kuji, Oates, Bowerman, & Flanagan, 1983), we have made the results relative to those at zero loading.

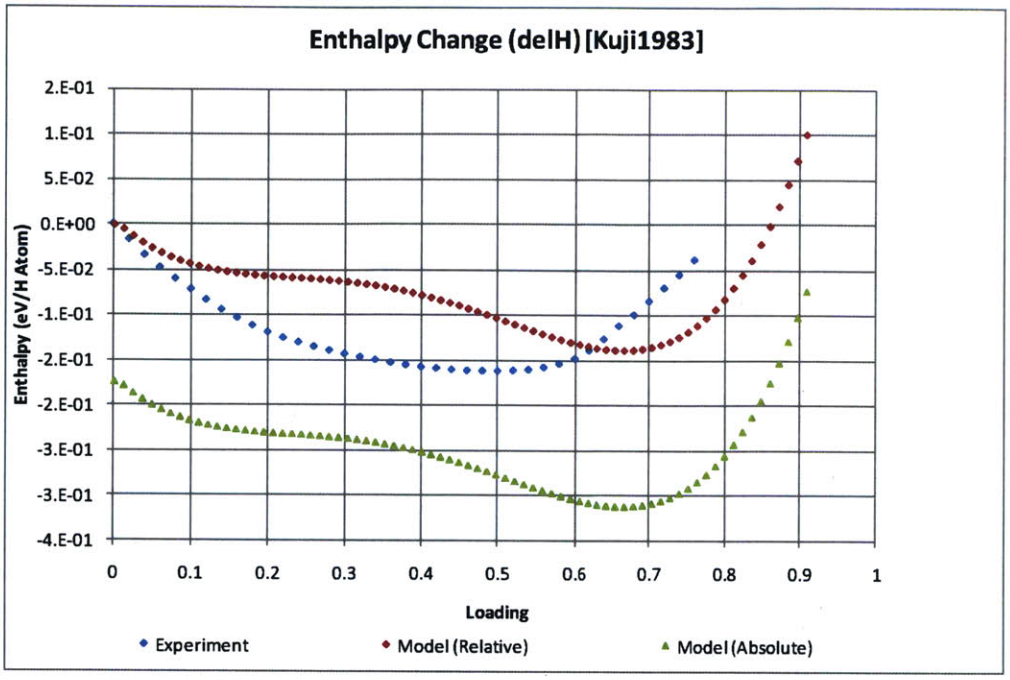

Figure 73: Enthalpy Change: Raw Model and Model relative to Zero Loading vs. Experiment

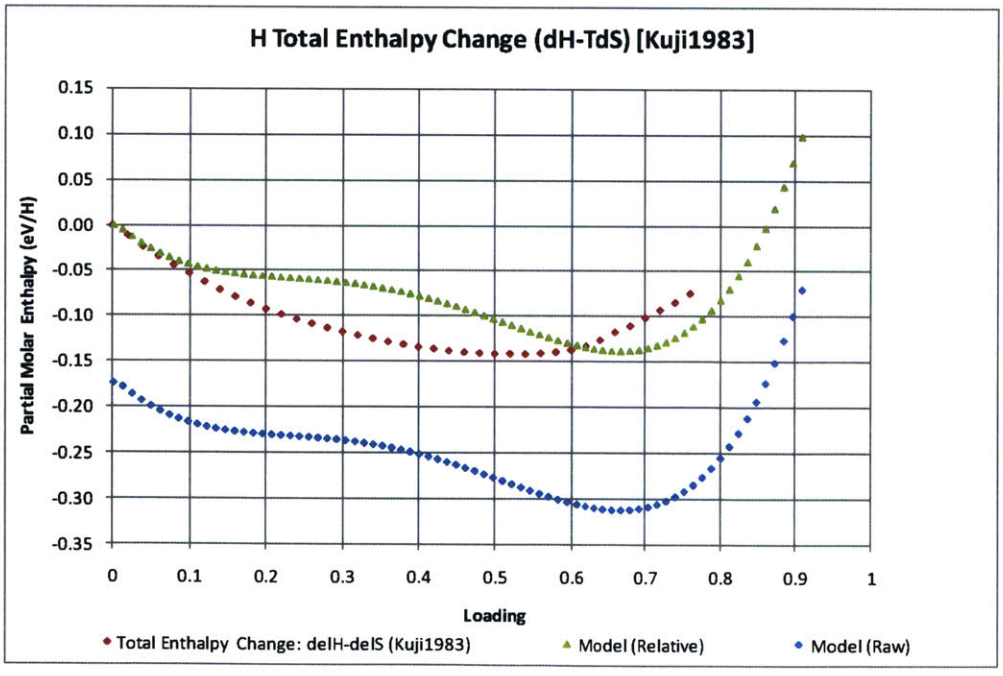

Figure 74: Total Enthalpy Change vs. Experiment

Excess Molar Enthalpy and Entropy

Excess Molar Enthalpy

To be able to accurately compare our results to those in literature, e.g. (Kuji, Oates, Bowerman, & Flanagan, 1983), we need to derive the so-called excess molar quantities. These are molar properties with the infinite dilution quantities subtracted out as explained below.

We begin with Equation 269, written for the hydrogen gas and with pressure replaced by fugacity. As is customary in physical chemistry literature, we have used an over bar to denote that we are dealing with a molar quantity, with the mole defined for hydrogen atoms:

$$\Delta\bar{G}_H = \frac{1}{2}RTlnf_{H_2} \tag{291}$$

As before, the relative enthalpy change is given by Equation 270:

$$\Delta\bar{H}_H = -T^2\left(\frac{\partial\left(\frac{\Delta\bar{G}_H}{T}\right)}{\partial T}\right)_{P,n} \tag{292}$$

However, Equation 292 is the total enthalpy change of dissolution of hydrogen in metal, not the excess enthalpy in the sense of (Kuji, Oates, Bowerman, & Flanagan, 1983). To get the excess enthalpy, we follow the definition of (Boureau, Kleppa, & Dantzer, 1976) by separating the Gibbs Energy changes as a sum of two terms:

$$\Delta\bar{G}_H = \bar{G}_H^{Ideal} + \Delta\bar{G}_H^{Excess} \tag{293}$$

where, assuming that only one type of site is occupied, we may write the ideal entropy term as

$$\bar{G}_H^{Ideal} = RTln\,\frac{\theta_o}{1-\theta_o} \tag{294}$$

Therefore, using Equations 278, 279 & 282, we may write $\Delta\bar{G}_H$ as

$$\Delta\bar{G}_H = \frac{1}{2}RT * ln\left(A(T) * e^{\frac{B(\theta,T)}{\kappa_B T}}\right)$$

$$= \frac{1}{2}RT\left[ln(A(T)) + \frac{B(\theta,T)}{\kappa_B T}\right]$$

$$= \frac{RT}{2}lnA(T) + \frac{1}{2}RT\left[2ln\frac{\theta_o}{1-\theta_o} + 6\,ln\left(2\,sinh\frac{\epsilon_{0v}}{2\kappa_B T}\right) + \frac{2\theta}{\kappa_B T}\frac{\partial\varepsilon_h(\theta)}{\partial\theta} + \frac{2}{\kappa_B T}\varepsilon_h(\theta) + ln\frac{8\pi^2 I\kappa_B T}{\sigma h^2} + \frac{\epsilon_D}{\kappa_B T}\right]$$

$$= \frac{RT}{2}lnA(T) + RTln\frac{\theta_o}{1-\theta_o} + 3RT\,ln\left(2\,sinh\frac{\epsilon_{0v}}{2\kappa_B T}\right) + \frac{R}{\kappa_B}\theta\frac{\partial\varepsilon_h(\theta)}{\partial\theta} + \frac{R}{\kappa_B}\varepsilon_h(\theta) + \frac{RT}{2}ln\frac{8\pi^2 I\kappa_B T}{\sigma h^2} + \frac{R}{2\kappa_B}\epsilon_D \quad (295)$$

Comparing Equations 293 & 295, we get the following expression for the excess Gibbs Energy in the context of our model:

$$\Delta\bar{G}_H^E = \frac{RT}{2}lnA(T) + 3RT\,ln\left(2\,sinh\frac{\epsilon_{0v}}{2\kappa_B T}\right) + \frac{R}{\kappa_B}\theta\frac{\partial\varepsilon_h(\theta)}{\partial\theta} + \frac{R}{\kappa_B}\varepsilon_h(\theta) + \frac{RT}{2}ln\frac{8\pi^2 I\kappa_B T}{\sigma h^2} + \frac{R}{2\kappa_B}\epsilon_D \quad (296)$$

Using Equation 292, we can get the excess molar enthalpy change as:

$$\Delta\bar{H}_H^E = -T^2\left(\frac{\partial\left(\frac{\Delta\bar{G}_H^E}{T}\right)}{\partial T}\right)_{P,n} \quad (297)$$

We simplify Equation 297 using Equation 295, noting once again that we may dispense with the following algebra. The numerator of Equation 297 is

$$\frac{\Delta\bar{G}_H^E}{T} \to \frac{R}{2} lnA(T) + 3R\, ln\left(2\, sinh\frac{\epsilon_{0v}}{2\kappa_B T}\right) + \frac{R}{\kappa_B T}\theta\frac{\partial\varepsilon_h(\theta)}{\partial\theta} + \frac{R}{\kappa_B T}\varepsilon_h(\theta) + \frac{R}{2} ln\frac{8\pi^2 I\kappa_B T}{\sigma h^2} + \frac{R}{2\kappa_B T}\epsilon_D \tag{298}$$

such that

$$\Delta\bar{H}_H^E$$

$$= -T^2\left(\frac{\partial\left(\frac{R}{2} lnA(T) + 3Rln\left(2\, sinh\frac{\epsilon_{0v}}{2\kappa_B T}\right) + \frac{R\theta}{\kappa_B T}\frac{\partial\varepsilon_h(\theta)}{\partial\theta} + \frac{R}{\kappa_B T}\varepsilon_h(\theta) + \frac{R}{2} ln\frac{8\pi^2 I\kappa_B T}{\sigma h^2} + \frac{R}{2\kappa_B T}\epsilon_D\right)}{\partial T}\right)_{P,n}$$

$$= -T^2\left(\frac{R}{2}\frac{A'(T)}{A(T)} + 3R\frac{2\cosh\left(\frac{\epsilon_{0v}}{2\kappa_B T}\right)}{2\sinh\frac{\epsilon_{0v}}{2\kappa_B T}}\left(-\frac{\epsilon_{0v}}{2\kappa_B T^2}\right) - \frac{R}{\kappa_B T^2}\theta\frac{\partial\varepsilon_h(\theta)}{\partial\theta} - \frac{R}{\kappa_B T^2}\varepsilon_h(\theta) + \frac{R}{2}\frac{\sigma h^2}{8\pi^2 I\kappa_B T}\frac{8\pi^2 I\kappa_B}{\sigma h^2} - \frac{R}{2\kappa_B T^2}\epsilon_D\right)$$

$$= -T^2\left(\frac{R}{2}\frac{A'(T)}{A(T)} - \frac{3R\epsilon_{0v}}{2\kappa_B T^2}coth\frac{\epsilon_{0v}}{2\kappa_B T} - \frac{R}{\kappa_B T^2}\theta\frac{\partial\varepsilon_h(\theta)}{\partial\theta} - \frac{R}{\kappa_B T^2}\varepsilon_h(\theta) + \frac{R}{2T} - \frac{R}{2\kappa_B T^2}\epsilon_D\right)$$

$$\Delta\bar{H}_H^E = -\frac{RT^2}{2}\frac{A'(T)}{A(T)} + \frac{3R\epsilon_{0v}}{2\kappa_B}coth\frac{\epsilon_{0v}}{2\kappa_B T} + \frac{R}{\kappa_B}\theta\frac{\partial\varepsilon_h(\theta)}{\partial\theta} + \frac{R}{\kappa_B}\varepsilon_h(\theta) - \frac{RT}{2} + \frac{R}{2\kappa_B}\epsilon_D \tag{299}$$

Lastly, to compare to (Kuji, Oates, Bowerman, & Flanagan, 1983) or (Sakamoto, Imoto, Takai, Yanaru, & Ohshima, 1996) data, we arrive at excess enthalpy term by subtracting out the value enthalpy change at infinite dilution, i.e.,

$$\bar{H}_H^E = \Delta\bar{H}_H^E - \Delta\bar{H}_H^0 \tag{300}$$

We get the infinite dilution enthalpy term, $\Delta\bar{H}_H^0$ from (Kuji, Oates, Bowerman, & Flanagan, 1983), presented here as a functional fit of temperature. The infinite dilution enthalpy increases with temperature as expected, with the dependence approximately linear.

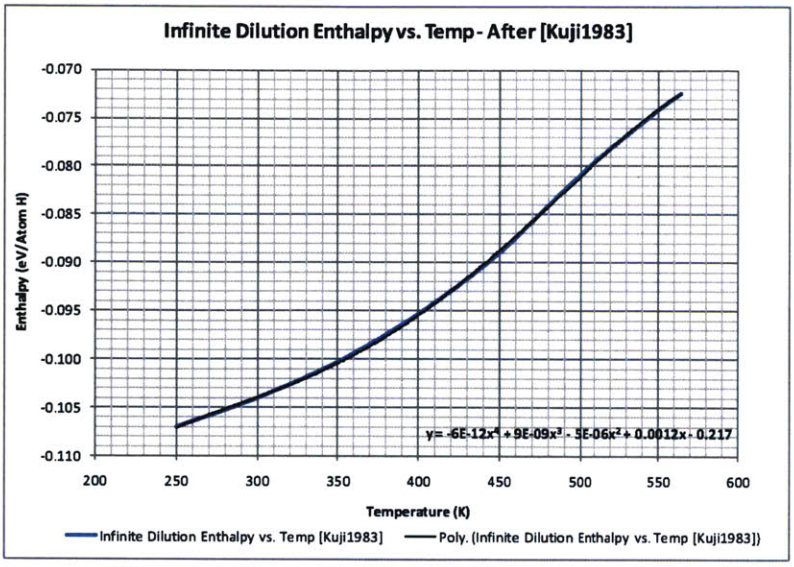

Figure 75: Change of Enthalpy at Infinite Dilution

The results are shown below compared to experiment:

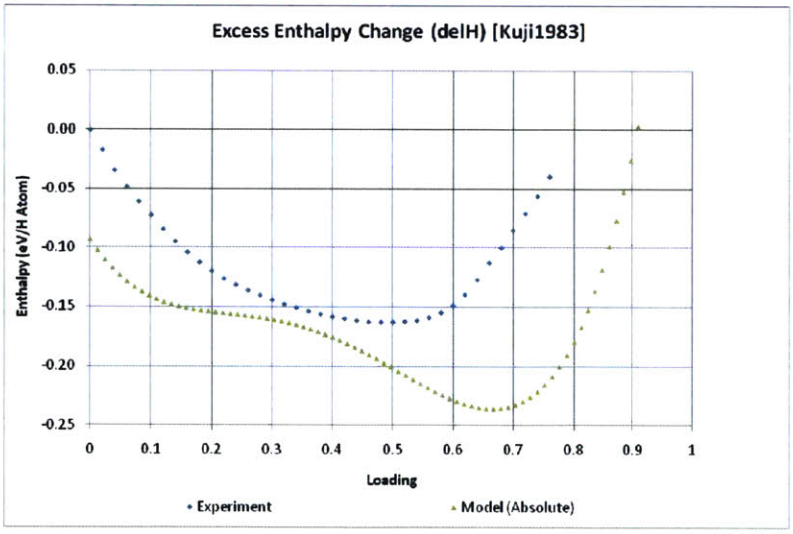

Figure 76: Excess Enthalpy Change - Model vs. Experiment.

Excess Molar Entropy

We can use Equations 263 & 296 to calculate the excess entropy in the sense of (Kuji, Oates, Bowerman, & Flanagan, 1983) and (Boureau & Kleppa, 1976):

$$-\Delta\bar{S}_H^E = \left(\frac{\partial \Delta \bar{G}_H^E}{\partial T}\right)_{P,n} =$$

$$\frac{\partial\left[\frac{RT}{2} lnA(T) + 3RT\, ln\left(2\, sinh\frac{\epsilon_{0v}}{2\kappa_B T}\right) + \frac{R}{\kappa_B}\theta\frac{\partial \varepsilon_h(\theta)}{\partial\theta} + \frac{R}{\kappa_B}\varepsilon_h(\theta) + \frac{RT}{2} ln\frac{8\pi^2 I\kappa_B T}{\sigma h^2} + \frac{R}{2\kappa_B}\epsilon_D\right]}{\partial T}$$

$$= \frac{RT}{2}\frac{A'(T)}{A(T)} + \frac{R}{2} lnA(T) + 3RT\, coth\frac{\epsilon_{0v}}{2\kappa_B T}\left(-\frac{\epsilon_{0v}}{2\kappa_B T^2}\right) + 3Rln\left(2\, sinh\frac{\epsilon_{0v}}{2\kappa_B T}\right) + \frac{RT}{2}\frac{\sigma h^2}{8\pi^2 I\kappa_B T}\frac{8\pi^2 I\kappa_B}{\sigma h^2}$$

$$+\frac{R}{2} ln\frac{8\pi^2 I\kappa_B T}{\sigma h^2}$$

$$-\Delta\bar{S}_H^E = \frac{RT}{2}\frac{A'(T)}{A(T)} + \frac{R}{2} lnA(T) - \frac{3R\epsilon_{0v}}{2\kappa_B T} coth\frac{\epsilon_{0v}}{2\kappa_B T} + 3Rln\left(2\, sinh\frac{\epsilon_{0v}}{2\kappa_B T}\right) + \frac{R}{2} + \frac{R}{2} ln\frac{8\pi^2 I\kappa_B T}{\sigma h^2} \quad (301)$$

Alternatively, we can use Equation 290 to define the excess molar entropy as

$$\Delta\bar{S}_H^E = \frac{\Delta\bar{H}_H^E - \Delta\bar{G}_H^E}{T} \quad (302)$$

Finally, just as in the case for enthalpy, the Excess Entropy excludes ideal and infinite dilution terms (Sakamoto, Imoto, Takai, Yanaru, & Ohshima, 1996):

$$\bar{S}_H^E = \Delta\bar{S}_H^E - \Delta\bar{S}_H^0 \quad (303)$$

Infinite dilution entropy data is from (Kuji, Oates, Bowerman, & Flanagan, 1983) – see Figure 77 below:

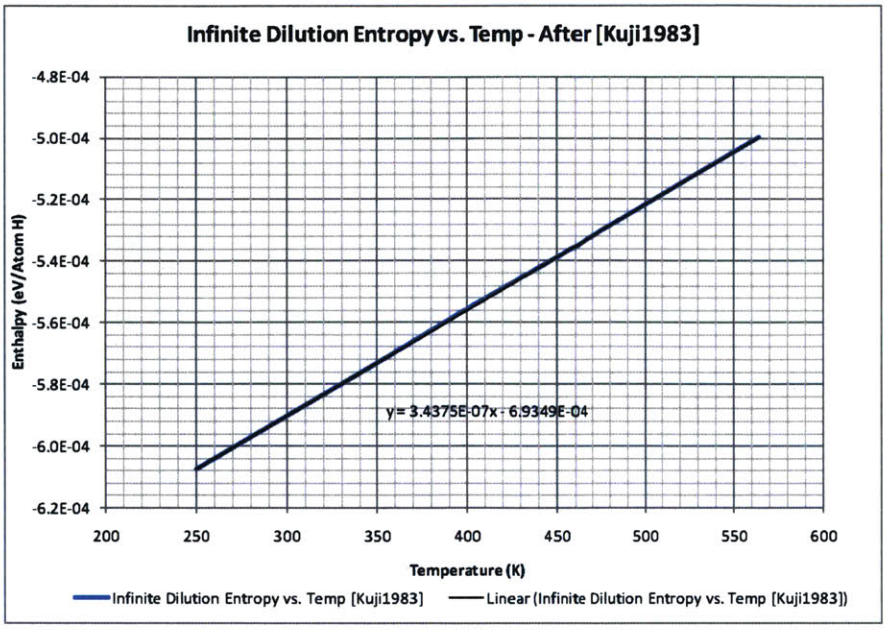

Figure 77: Infinite Dilution Entropy - after (Kuji, Oates, Bowerman, & Flanagan, 1983)

The results are shown in the following figure, followed by an attempt at an interpretation of the results.

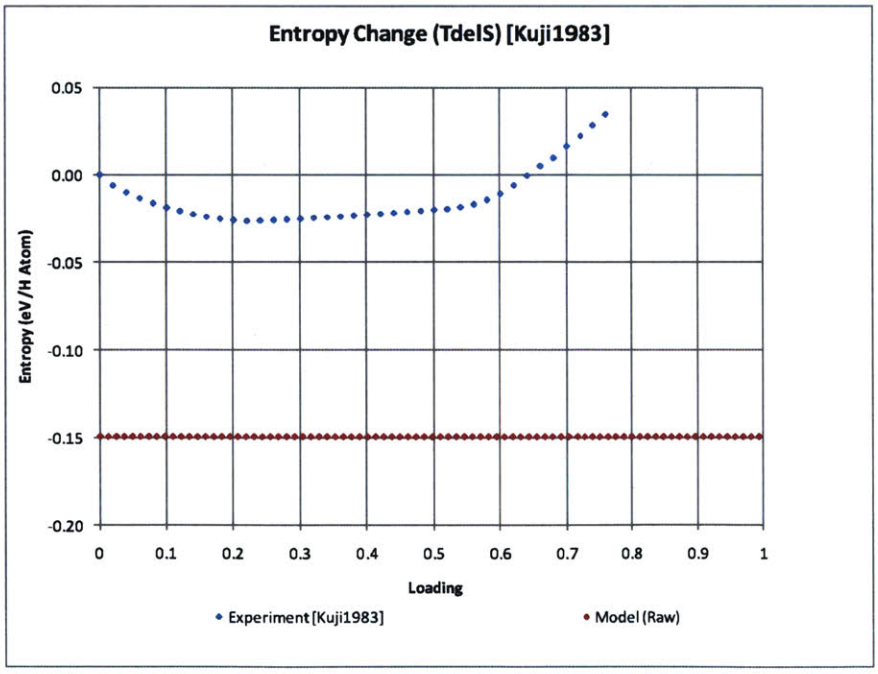

Figure 78: Entropy Change (T*dS): Experiment vs. Model

We also added some higher loading results from (Sakamoto, Imoto, Takai, Yanaru, & Ohshima, 1996) that show some leveling off in the beta phase (loading of 0.68-0.85). The results are shown below compared to model.

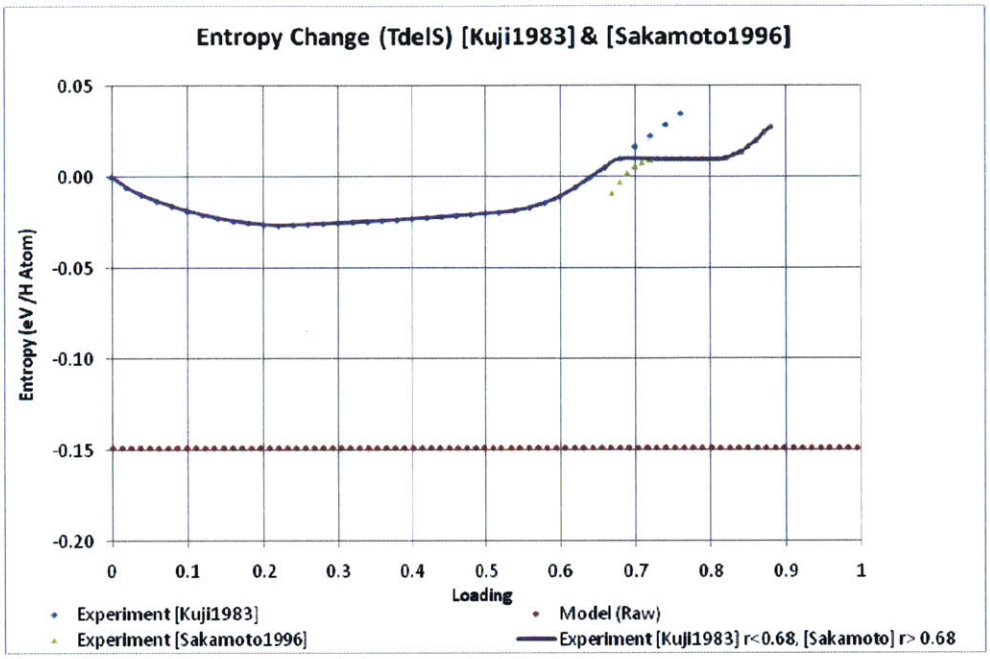

Figure 79: Excess Molar Entropy*T at room temperature. We show different experimental data, (Kuji, Oates, Bowerman, & Flanagan, 1983) for r < 0.68 and (Sakamoto, Imoto, Takai, Yanaru, & Ohshima, 1996) for r> 0.68 (purple solid line). Model result is shown in red.

Correction to Model Molar Entropy

From the discussion in Chapter 2, it is apparent that the calculated enthalpy term for dissolved hydrogen in metal, will contain electronic and configurational entropy terms, but not acoustical, option and image interaction terms. These need to be added as correction terms. We attempt to capture this correction term here following the treatment of (Kuji, Oates, Bowerman, & Flanagan, 1983).

For dissolved hydrogen, we identify the following excess entropy correction terms (relative to zero loading):

$$\Delta S_{corr} = \Delta S_{opt} + \Delta S_{ac} + \Delta S_{el} + \Delta S_{im} + \Delta S_{nc}$$

304

for optical, acoustic, electronic, image interaction, and non-ideal configurational entropy, respectively.

We ignore magnetic and translational contributions since we expect these to be small (Kuji, Oates, Bowerman, & Flanagan, 1983). Next, we attempt to estimate each term as in [ibid]:

ΔS_{opt} is estimated to increase from 4.15E-05*T to 6.15E-05*T eV per H atom as the loading θ increases from $\theta = 0$ to $\theta = 1$. (Rush, 1982) in (Kuji, Oates, Bowerman, & Flanagan, 1983)

ΔS_{ac} is estimated to be zero ($\Delta S_{ac} \sim 0$) [ibid]

ΔS_{elec} may be estimated to rise from zero at zero loading to about $\Delta S_{el} = 4.15\text{E} - 05 * \text{T}$ eV per H atom (Oates & Flanagan, 1971) in (Kuji, Oates, Bowerman, & Flanagan, 1983).

ΔS_{im} may be estimated to be $\Delta S_{im} = -3.01\text{E} - 05 * \theta * \text{T}$ eV per H atom (Alefeld, 1972).

Of course ΔS_{nc} is already included in our model. From these results, we estimate the total entropy correction to be

$$\Delta S_{corr} = 7.26 * 10^{-5} * T \left(\frac{eV}{Atom}\right)$$

305

The corrected model entropy is shown below:

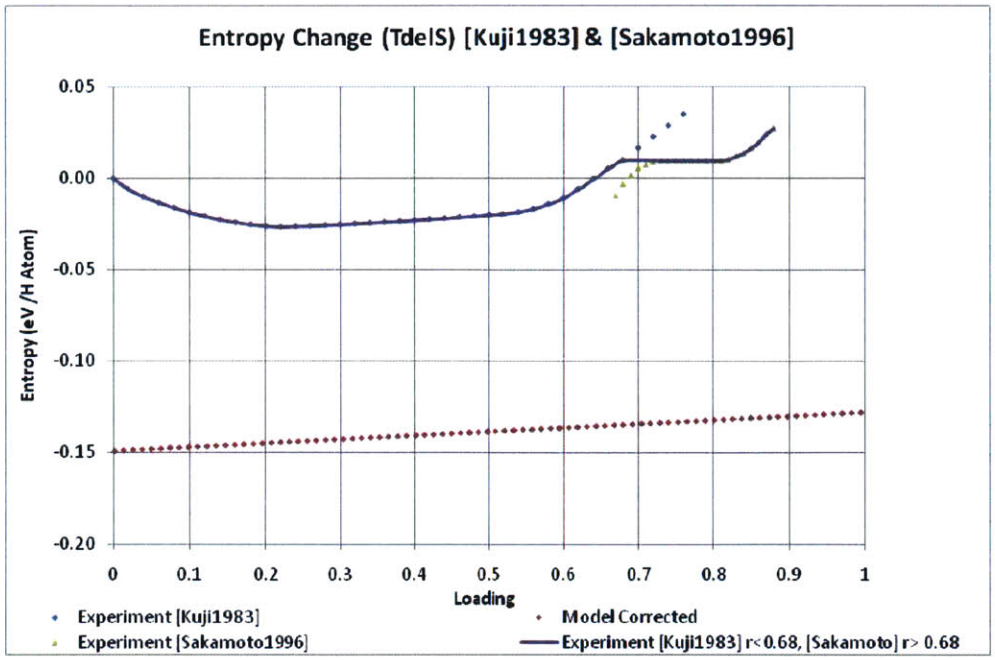

Figure 80: Same as Figure 79 but showing the results of our model entropy calculation after a simple correction based on experiment (Blue solid line). Details of correction above, based on [Kuji1983].

Can We Understand Entropy Using Our Model?

In this section, we will attempt to understand entropy in the context of our model. In other words, once we calculate the entropy according to Equation 301, what meaning can we attach to it?

To answer this, we start with the fundamental Boltzman relationship between entropy and the number of accessible microstates:

$$S = \kappa_B * log\, \Omega \tag{306}$$

In Equation 306, Ω is the number of equally accessible microstates. A simple count of the O-sites yields

$$\Omega = \frac{N!}{n!(N-n)!} \tag{307}$$

where n is the number of hydrogen atoms, distributed among N available O-sites. This is obviously pure configurational entropy.

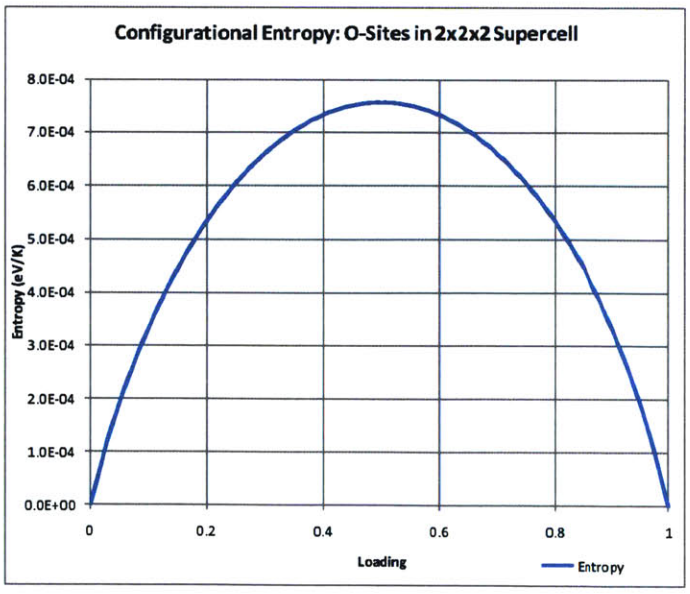

Figure 81: Configurational Entropy (H in Pd 2x2x2 Cell)

The interpretation of Figure 81 is straightforward: configurational entropy increases with loading until a peak at the half way point – where the system is at its most disordered. It thereafter decreases until, at a loading of unity, there obtains a perfect PdH lattice with zero configurational entropy. However, this so called ideal entropy is rather un-interesting and we subtract it as indicated in Equations 293 & 294 above.

Accessible Excess Microstates

To understand what the excess entropy means, we can write Equation 306 in terms of excess entropy, i.e.

$$\Delta \bar{S}_H^E = \kappa_B \, ln \, \Omega^E \tag{308}$$

where

$$\Omega^E = \frac{\Omega^{final}}{\Omega^{initial}} \tag{309}$$

$\Omega^{initial}$ is the initial number of states while Ω^{final} is the final number of states as the hydrogen moves from gas phase into palladium bulk. We interpret Equation 308 as quantifying the change in the number of accessible microstates during the absorption process. The ratio

$$\frac{\Omega^{final}}{\Omega^{initial}} = e^{\frac{\Delta S}{\kappa_B}} \tag{310}$$

therefore, is the fractional increase (or decrease if less than 1) of the excess microstates available for the H-atom to go into during the absorption process.

We plot Equation 310 as a function of loading for the model and experimental data in Figure 82 below.

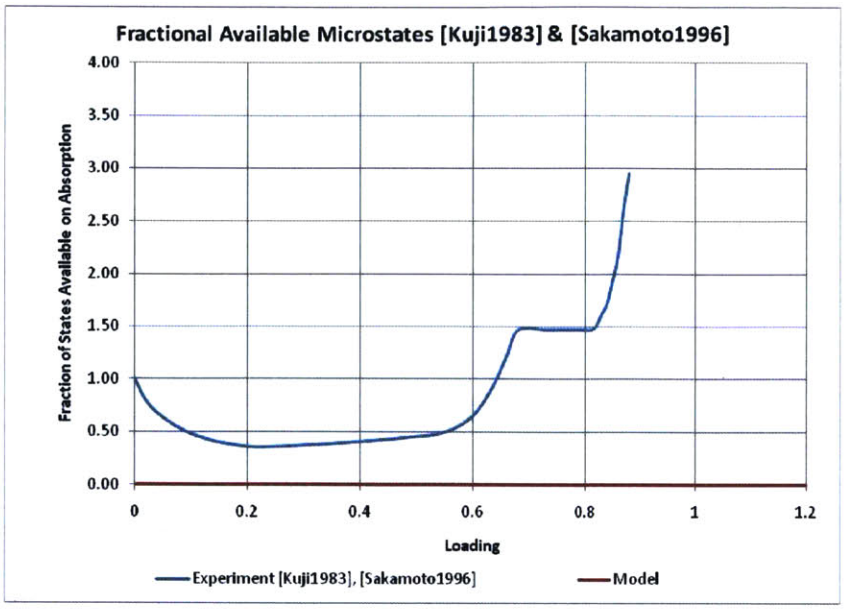

Figure 82: Fraction of Available Microstates, model vs. experiment. Experiment from (Kuji, Oates, Bowerman, & Flanagan, 1983) r <0.68 and (Sakamoto, Imoto, Takai, Yanaru, & Ohshima, 1996) (r>0.68)

We also provide below the results based on (Kuji, Oates, Bowerman, & Flanagan, 1983)'s results in the loading range

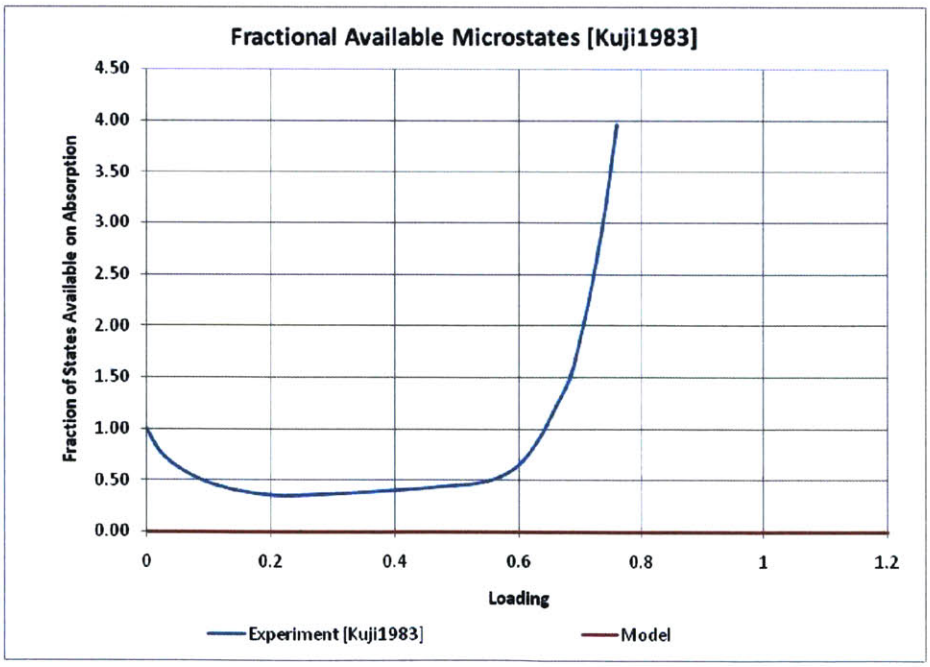

Figure 83: Same as Figure 82 but showing the results based on (Kuji, Oates, Bowerman, & Flanagan, 1983) only.

Figure 82 and Figure 83 show that the model has not correctly predicted the reduction in the microstates. This is perhaps not surprising in view of Figure 76 and Equation 302, and – the errors in model excess enthalpy results errors in excess entropy, and the resulting excess entropy (Figure 80) is simply not good enough to model available microstates.

Interpretation of Fractional Accessible Excess Microstates Result

According to the results of Figure 82, the absorption process leads to the loss of about half the number of accessible microstates in the miscibility gap. In the beta phase, the number of microstates approximately doubles from its initial value. There also appears to be a leveling off based on experimental data from (Sakamoto, Imoto, Takai, Yanaru, & Ohshima, 1996) in the loading range 0.7-0.82 beyond which the number of states again increases rapidly.

The results based on the (Kuji, Oates, Bowerman, & Flanagan, 1983) data alone shows similar loss of half the microstates in the miscibility gap. In the beta phase however, the increase in available states is about 4x. A central question is whether we can understand these results.

As a first attempt at a model, we hypothesize that, in the miscibility gap, the loss of available microstates is due to the hydrogen forming clusters, while in the beta phase, the electronic states of the electron in protium play a crucial role in the increase in the number of available microstates. Let's see if we can validate or otherwise disprove these hypotheses.

Mixed Phase "Clumping" Model

In the miscibility gap, the loading is non-uniform and clustered or "clumpy". The hydrogen may then be thought of as loading the metal bulk in clusters. One way to model this is to use a clustered statistical formulation as described below.

Previously, we considered a purely random statistical placement of hydrogen within the metal lattice. This is the model captured by Equations 38 Chapter 2,

$$Z_H(\tau,\mu) = \sum_n \sum_{ASN} e^{\frac{n\mu-\varepsilon_h}{\tau}} z^n$$

311

and using the Bragg-Williams approximation,

$$Z_H(\tau, n) \cong \frac{N!}{n!\,(N-n)!} e^{\frac{-n\varepsilon_h}{\tau}} z^n$$

312

In Equation 312, n is the number of H atoms, randomly distributed among N available O-sites, and we shall consider octahedral occupations only for now, such that

$$0 < n < N$$

313

and the implied summation is over all integer values of n. The distribution is then purely random in n.

To model a PdH cluster or "clumping" characteristic of the miscibility gap, we may consider loading the hydrogen in pairs, triplets, quadruplets, etc. To do this, we choose an integer clustering factor, γ, such that

$$\gamma = \frac{n}{k}$$

314

for some integers k. k is then the sequence

$$k = 0,1,2,\ldots,\frac{n}{\gamma},\ldots,\frac{N}{\gamma}$$

315

For example, if the clustering is in pairs, $\gamma = 2$; for loading in clusters of 3, $\gamma = 3$, and so on. In general, for $\gamma - tuple$ clustering, Equation 311 becomes

$$Z_H(\tau, \mu) = \sum_{k=0}^{\frac{N}{\gamma}} \sum_{ASN} e^{\frac{k\gamma\mu - \varepsilon_h}{\tau}} z^{k\gamma}$$

316

and

$$\frac{1}{\gamma}\frac{1}{\partial k} = \frac{1}{\partial n}$$

317

Equation 316 becomes

$$Z_H(\tau, k) \cong \left(\frac{\frac{N}{\gamma}!}{k!\left(\frac{N}{\gamma} - k\right)!} \right) e^{\frac{-k\gamma\varepsilon_h}{\tau}} z^{k\gamma}$$

318

where the first term in brackets is the number of ways of choosing k sites at a time. Obviously, in this formulation, N must be chosen in such a way that $\frac{N}{\gamma}$ is an integer according to Equation 315. Additionally, in Equation 318, there are no additional entropy terms related to the tuple because we choose the entire tuple and it has a known entropy, i.e.,

$$\binom{\gamma}{\gamma} = 1$$

319

Paralleling earlier treatment in Chapter 2, we derive the chemical potential for the dissolved hydrogen in the miscibility gap as:

$$\mu_H = -\tau\frac{\partial}{\partial n}\left\{ ln\frac{\frac{N}{\gamma}!}{k!\left(\frac{N}{\gamma} - k\right)!} + ln\, z^{k\gamma} - \frac{k\gamma}{\tau}\varepsilon_h \right\} = -\frac{\tau}{\gamma}\frac{\partial}{\partial k}\left\{ ln\frac{\frac{N}{\gamma}!}{k!\left(\frac{N}{\gamma} - k\right)!} + ln\, z^{k\gamma} - \frac{k\gamma}{\tau}\varepsilon_h \right\}$$

$$= -\frac{\tau}{\gamma}\frac{\partial}{\partial k}\{T_1 + T_2 + T_3\}$$

320

We use the Stirling approximation as before,

$$ln(x!) \cong \frac{1}{2} ln(\sqrt{2\pi}) + \left(x + \frac{1}{2}\right) ln(x) - x$$

321

to write (algebra may be dispensed with)

$$T_1 = ln \frac{\frac{N}{\gamma}!}{k! \left(\frac{N}{\gamma} - k\right)!}$$

$$= ln \frac{N}{\gamma}! - ln\, k\,! - ln(N-k)\,!$$

$$\cong \left[ln(\sqrt{2\pi}) + \left(\frac{N}{\gamma} + \frac{1}{2}\right) ln\left(\frac{N}{\gamma}\right) - \frac{N}{\gamma}\right] - \left[ln(\sqrt{2\pi}) + \left(k + \frac{1}{2}\right) ln\, k - k\right]$$

$$- \left[ln(\sqrt{2\pi}) + \left(\frac{N}{\gamma} - k + \frac{1}{2}\right) ln\left(\frac{N}{\gamma} - k\right) - \frac{N}{\gamma} + k\right]$$

322

Collecting only terms dependent on k, we get the gradient term as

$$\frac{\partial}{\partial k} T_1 = -\frac{\partial}{\partial k}\left\{\left(k + \frac{1}{2}\right) ln\, k - k + \left(\frac{N}{\gamma} - k + \frac{1}{2}\right) ln\left(\frac{N}{\gamma} - k\right) + k\right\}$$

$$= -\frac{\partial}{\partial k}\left\{\left(k + \frac{1}{2}\right) ln\, k + \left(\frac{N}{\gamma} - k + \frac{1}{2}\right) ln\left(\frac{N}{\gamma} - k\right)\right\}$$

$$= -\left\{\left(k + \frac{1}{2}\right)\frac{1}{k} + ln\, k - \left(\frac{N}{\gamma} - k + \frac{1}{2}\right)\frac{1}{\frac{N}{\gamma} - k} - ln\left(\frac{N}{\gamma} - k\right)\right\}$$

$$= -\left\{1 + \frac{1}{2k} + ln\, k - 1 - \frac{1}{2}\frac{1}{\frac{N}{\gamma} - k} - ln\left(\frac{N}{\gamma} - k\right)\right\} = -\left\{\frac{1}{2k} + ln\frac{\gamma k}{N - \gamma k} - \frac{1}{2}\frac{\gamma}{N - \gamma k}\right\}$$

323

The other terms are

$$\frac{\partial}{\partial k}T_2 = \frac{\partial}{\partial k} ln\, z^{k\gamma} = \frac{\partial}{\partial k}(k\gamma\, ln\, z) = \gamma\, ln\, z$$

324

and

$$\frac{\partial}{\partial k}T_3 = -\frac{\partial}{\partial k}\left(\frac{\gamma}{\tau}k\varepsilon_h\right) = -\frac{\gamma}{\tau}\frac{\partial}{\partial k}(k\varepsilon_h(n)) = -\frac{\gamma}{\tau}\left(k\frac{\partial}{\partial k}[\varepsilon_h(n)] + \varepsilon_h(n)\right) = -\frac{\gamma}{\tau}\left(k\varepsilon_h'(n)\frac{\partial n}{\partial k} + \varepsilon_h(n)\right)$$

$$= -\frac{\gamma}{\tau}(k\gamma\varepsilon_h'(n) + \varepsilon_h(n))$$

325

In Equation 325 $\varepsilon_h'(n)$ denotes a derivative with respect to the "n-space" argument. This is important because our model calculates $\varepsilon_h(n)$ in n-space – but because there is a simple scaling between n and k, the result is particularly simple, as shown.

Using hydrogen to metal atomic ratio,

$$\theta = \frac{n}{N} = \frac{k\gamma}{N}$$

326

we rewrite Equation 323 as

$$\frac{\partial}{\partial k}T_1 = -\left\{\frac{\gamma}{2N\theta} - \frac{1}{2N}\frac{\gamma}{1-\theta} + ln\frac{\theta}{1-\theta}\right\} \cong -ln\frac{\theta}{1-\theta}$$

327

In Equation 327, we think we are justified in making the last approximation because, for N very large, the first two terms will always be much smaller than the last, even in the low loading limit, $\theta \to 0$, because N quickly overwhelms the former.

The rest of the terms are, Equation 324, as before,

$$\frac{\partial}{\partial k}T_2 = \gamma\, ln\, z$$

328

and Equation 325:

$$\frac{\partial}{\partial k}T_3 = -\frac{\gamma}{\tau}\left(k\gamma\varepsilon_h'(n) + \varepsilon_h(n)\right) = -\frac{1}{\tau}\left(\theta\varepsilon_h'(\theta) + \varepsilon_h(\theta)\right) \quad 329$$

The chemical potential valid for the mixed phase is, therefore, from Equation 320,

$$\mu_H = \frac{\tau}{\gamma}ln\frac{\theta}{1-\theta} - \tau\, ln\, z + \theta\frac{\partial}{\partial\theta}\varepsilon_h(\theta) + \varepsilon_h(\theta) \quad valid\ for\ 0.02 < \theta < 0.6 \quad 330$$

which obviously matches the results of Equation 50, Chapter 2 in the case of $\gamma = 1$, i.e. random arrangement without clustering $(1 - tuple)$.

♦

We need to use the results of Equation 330 in Equation 295 to get the Gibbs Energy. Note that $(\tau \equiv k_B T)$. Additionally, k, the clustering factor is not to be confused with Boltzmann constant, k_B. Thus,

$$\Delta\bar{G}_H = \frac{1}{2}RT * ln\left(A(T) * e^{\frac{B(\theta,T)}{k_B T}}\right)$$

$$= \frac{1}{2}RT\left[ln(A(T)) + \frac{B(\theta,T)}{k_B T}\right]$$

$$= \frac{RT}{2}lnA(T) + \frac{1}{2}RT\left[\frac{2}{\gamma}ln\frac{\theta}{1-\theta} + 6\, ln\left(2\, sinh\frac{\epsilon_{0v}}{2k_B T}\right) + \frac{2\theta}{k_B T}\frac{\partial\varepsilon_h(\theta)}{\partial\theta} + \frac{2}{k_B T}\varepsilon_h(\theta) + ln\frac{8\pi^2 I k_B T}{\sigma h^2} + \frac{\epsilon_D}{k_B T}\right]$$

$$= \frac{RT}{2}lnA(T) + \frac{RT}{\gamma}ln\frac{\theta}{1-\theta} + 3RT\, ln\left(2\, sinh\frac{\epsilon_{0v}}{2k_B T}\right) + \frac{R}{k_B}\theta\frac{\partial\varepsilon_h(\theta)}{\partial\theta} + \frac{R}{k_B}\varepsilon_h(\theta) + \frac{RT}{2}ln\frac{8\pi^2 I k_B T}{\sigma h^2} + \frac{R}{2k_B}\epsilon_D \quad 331$$

The excess Gibbs Energy is defined as before: Equations 293 & 294

$$\Delta\bar{G}_H^{Excess} = \Delta\bar{G}_H - \bar{G}_H^{Ideal} \tag{332}$$

$$\bar{G}_H^{Ideal} = RT * ln\frac{\theta}{1-\theta} \tag{333}$$

or

$$\Delta\bar{G}_H^{E,Clump} = \frac{RT}{2}lnA(T) + \frac{RT}{\gamma}ln\frac{\theta}{1-\theta} + 3RT\,ln\left(2\,sinh\frac{\epsilon_{0v}}{2k_BT}\right) + \frac{R}{k_B}\theta\frac{\partial\varepsilon_h(\theta)}{\partial\theta} + \frac{R}{k_B}\varepsilon_h(\theta) + \frac{RT}{2}ln\frac{8\pi^2 Ik_BT}{\sigma h^2} + \frac{R}{2k_B}\epsilon_D - RTln\frac{\theta}{1-\theta} \tag{334}$$

Following previous derivation, Equations 297-300, we may use our new excess Gibbs Energy model, Equation 334, to write the excess enthalpy as:

$$\Delta\bar{H}_H^E = -T^2\left(\frac{\partial\left(\frac{\Delta\bar{G}_H^{E,Clump}}{T}\right)}{\partial T}\right)_{P,n} \tag{335}$$

$$\frac{\Delta\bar{G}_H^{E,Clump}}{T} \to \frac{R}{2}lnA(T) + \frac{R}{\gamma}ln\frac{\theta}{1-\theta} + 3R\,ln\left(2\,sinh\frac{\epsilon_{0v}}{2k_BT}\right) + \frac{R}{k_BT}\theta\frac{\partial\varepsilon_h(\theta)}{\partial\theta} + \frac{R}{k_BT}\varepsilon_h(\theta) + \frac{R}{2}ln\frac{8\pi^2 Ik_BT}{\sigma h^2} + \frac{R}{2k_BT}\epsilon_D - Rln\frac{\theta}{1-\theta} \tag{336}$$

and

$$\Delta H_H^{E,Clump} = -T^2\left(\frac{\partial\left(\frac{R}{2}lnA(T)+\frac{R}{\gamma}ln\frac{\theta}{1-\theta}+3R\,ln\left(2\sinh\frac{\epsilon_{0v}}{2k_BT}\right)+\frac{R\theta}{k_BT}\frac{\partial\varepsilon_h(\theta)}{\partial\theta}+\frac{R}{k_BT}\varepsilon_h(\theta)+\frac{R}{2}ln\frac{8\pi^2Ik_BT}{\sigma h^2}+\frac{R}{2k_BT}\epsilon_D-Rln\frac{\theta}{1-\theta}\right)}{\partial T}\right)_{P,n}$$

$$= -T^2\left(\frac{R}{2}\frac{A'(T)}{A(T)}-\frac{3R\epsilon_{0v}}{2\gamma\kappa_BT^2}\coth\frac{\epsilon_{0v}}{2\kappa_BT}-\frac{R}{\kappa_BT^2}\theta\frac{\partial\varepsilon_h(\theta)}{\partial\theta}-\frac{R}{\kappa_BT^2}\varepsilon_h(\theta)+\frac{R}{2T}-\frac{R}{2\kappa_BT^2}\epsilon_D\right)$$

$$\Delta\bar{H}_H^{E,Clump} = -\frac{RT^2}{2}\frac{A'(T)}{A(T)}+\frac{3R\epsilon_{0v}}{2\kappa_B}coth\frac{\epsilon_{0v}}{2\kappa_BT}+\frac{R}{\kappa_B}\theta\frac{\partial\varepsilon_h(\theta)}{\partial\theta}+\frac{R}{\kappa_B}\varepsilon_h(\theta)-\frac{RT}{2}+\frac{R}{2\kappa_B}\epsilon_D \quad (337)$$

$$\bar{H}_H^{E,Clump} = \Delta\bar{H}_H^{E,Clump} - \Delta\bar{H}_H^0 \quad (338)$$

Finally, we get the Excess Entropy from Equations 302 & 303, which, due to the dependence of the excess Gibbs Energy on the clumping factor, k, may show the effect we are trying to model:

$$\Delta\bar{S}_H^{E,Clump} = \frac{\Delta\bar{H}_H^{E,Clump} - \Delta\bar{G}_H^{E,Clump}}{T} \quad (Miscibility\ Gap) \quad (339)$$

$$\bar{S}_H^{E,Clump} = \Delta\bar{S}_H^{E,Clump} - \Delta\bar{S}_H^0 \quad (340)$$

The results are shown below.

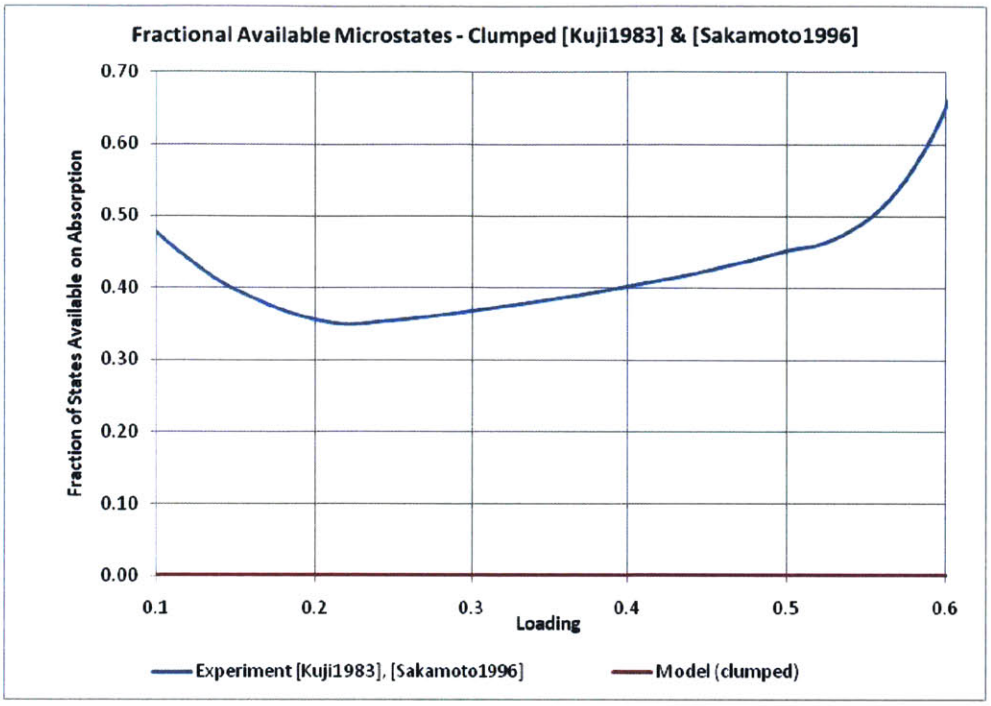

Figure 84: Fractional Microstates in the miscibility gap within the clumped Model

Obviously, the results are not much different from those presented earlier, and the reasons already given for the deviation of the un-clumped model apply equally here. Qualitatively, however, we see in the "clumped" model that the decrease in available sites is ALWAYS LARGER than would be expected from a random arrangement, which validates our overall hypothesis. However, the decrease is not anywhere close to expectation since our model has a large constant correction. Also, beyond a loading of about 1/3, the clumped model actually exhibits a smaller decrease in the available microstates. We may explain this on physical grounds, namely that as the loading increases, the effect of clumping decreases.

A plot is shown below:

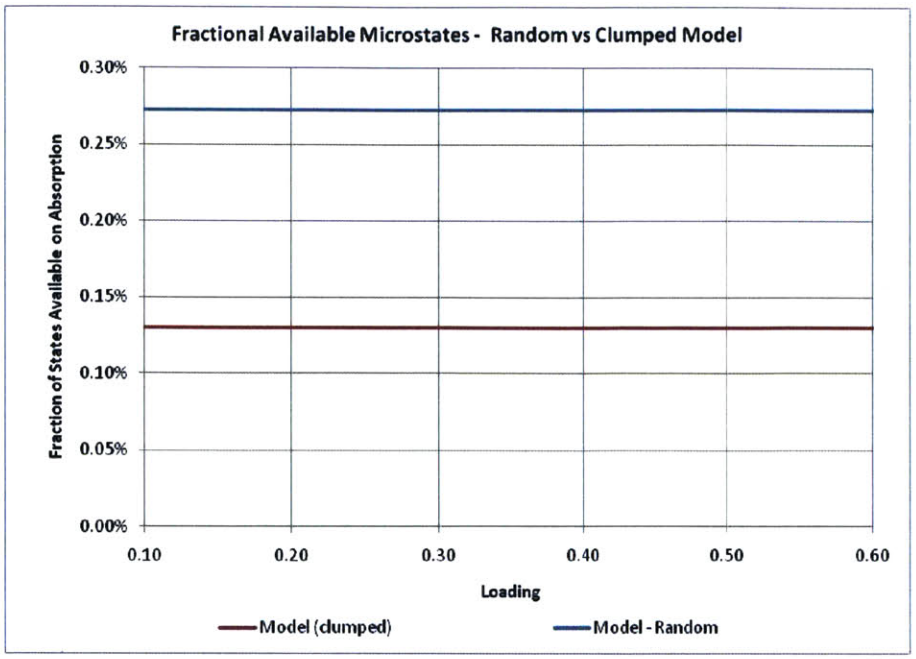

Figure 85: Clumped vs. Random Loading (clumped in 3-tuples example shown)

We may perhaps see the clumping model more clearly if we do some correction to eliminate DFT errors. We attempt such a model below

Mixed Phase "Clumping" Model – Corrected Gibbs Energy

We would like to find a systematic way to correct the entropy results. At first, we may be tempted to reprise our methodology of Chapter 2. But such a path would be misguided since entropy is a measure of the number of available states, such that we cannot simply "correct" entropy. To make progress, we may try correcting Gibbs Energy, since that is directly tied to our model calculations.

We may start from Equations 297 & 300, rewritten below to emphasize temperature dependence:

$$\Delta\bar{H}_H^E(T) = -T^2\left(\frac{\partial\left(\frac{\Delta\bar{G}_H^E(T)}{T}\right)}{\partial T}\right)_{P,n} \qquad 341$$

$$\bar{H}_H^E(T) = \Delta\bar{H}_H^E(T) - \Delta\bar{H}_H^0(T) \tag{342}$$

Substituting Equation 342 into Equation 341 and integrating with respect to T,

$$-\int\left(\frac{\bar{H}_H^E(T) + \Delta\bar{H}_H^0(T)}{T^2}\right)dT = \int\left(\frac{\partial\left(\frac{\Delta\bar{G}_H^E(T)}{T}\right)}{\partial T}\right)dT \tag{343}$$

The left hand side may be accessible from experiment, and the right hand is derived from the fundamental theorem of calculus. The results are

$$\Delta\bar{G}_H^E(T) = -\frac{1}{T}\int\left(\frac{\bar{H}_H^E(T) + \Delta\bar{H}_H^0(T)}{T^2}\right)dT \tag{344}$$

Unfortunately, we could not find experimental data from which to evaluate the right hand side of Equation 344. However, the left hand side of Equation 344 is readily accessible since Gibbs Energy per mole is nothing more than chemical potential, such that we may write

$$\Delta\bar{G}_H^E(\theta, T) = \Delta\mu_H^E(\theta, T) \tag{345}$$

The excess chemical potential $\mu_H^E(\theta)$ is accessible from (Kuji, Oates, Bowerman, & Flanagan, 1983) and is defined by

$$\mu_H^E(\theta) = \Delta\mu_H^E(\theta) - \Delta\mu_H^0 \tag{346}$$

and $\Delta\bar{G}_H^E(T)$ is available directly from our model. Combining Equations 345 & 346 trivially, we get

$$\Delta\bar{G}_H^E(T) - \Delta\mu_H^0 = \mu_H^E(\theta)$$

347

We write Equation 347 this way so we can easily compare experiment and model – the right hand side of available directly from (Kuji, Oates, Bowerman, & Flanagan, 1983), while $\Delta\bar{G}_H^E(T)$ is directly from our model, and $\Delta\mu_H^0$ is also available from [ibid].

In the figure below, we plot the two sides of Equation 347. The experimental data is at several temperatures based on experimental/model after [ibid]. We also show the experimental data side by side. Lastly, we compare these with our model results. The model already has an explicit temperature dependence.

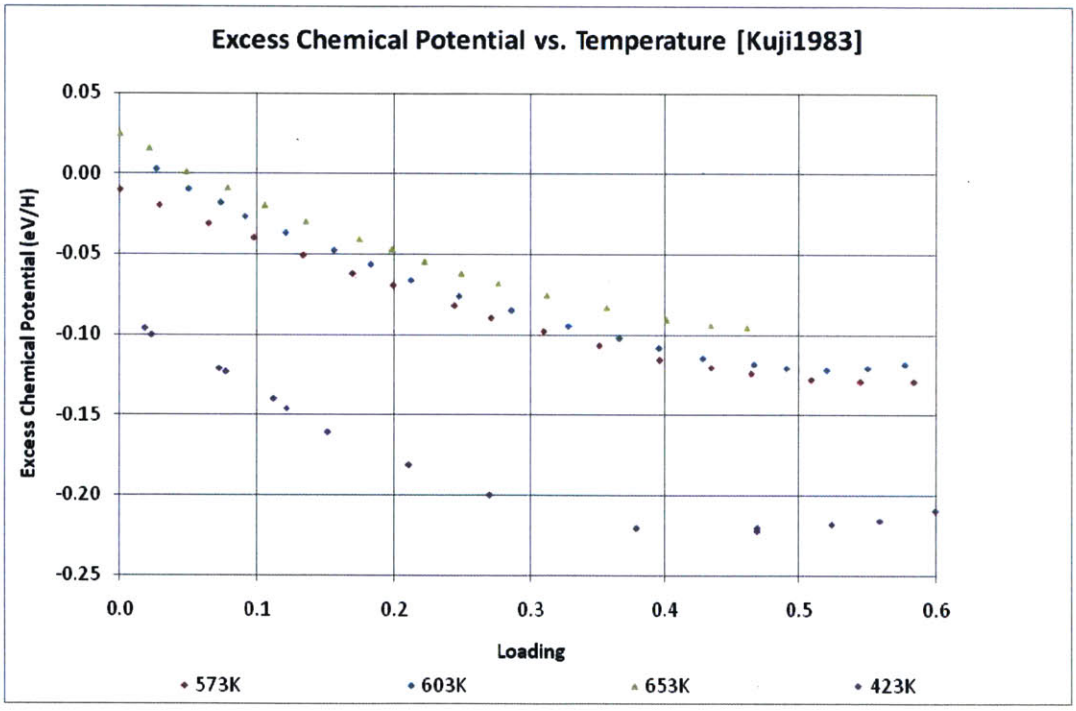

Figure 86: Excess Chemical Potential vs. Temperature, after (Kuji, Oates, Bowerman, & Flanagan, 1983)

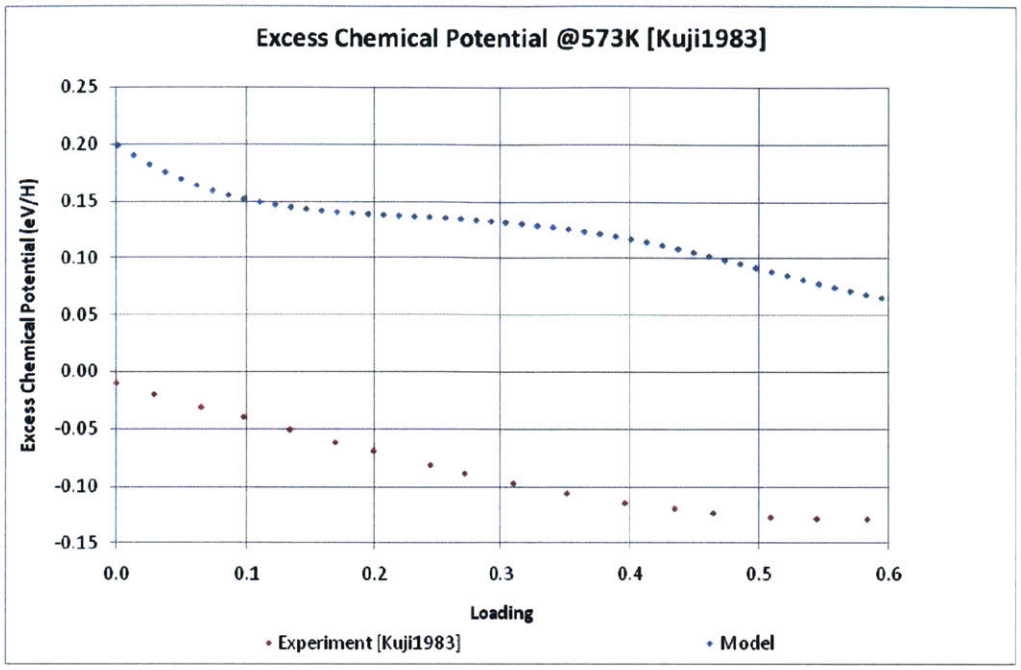

Figure 87: Excess Chemical Potential at 573K: Experiment vs. Model

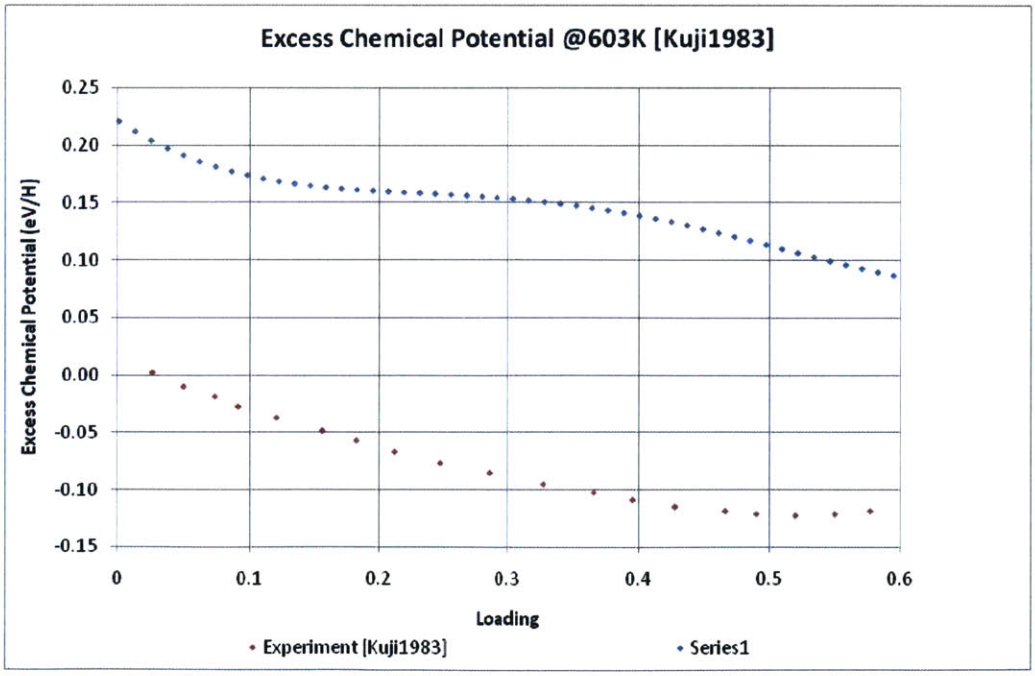

Figure 88: Excess Chemical Potential at 603K: Experiment vs. Model

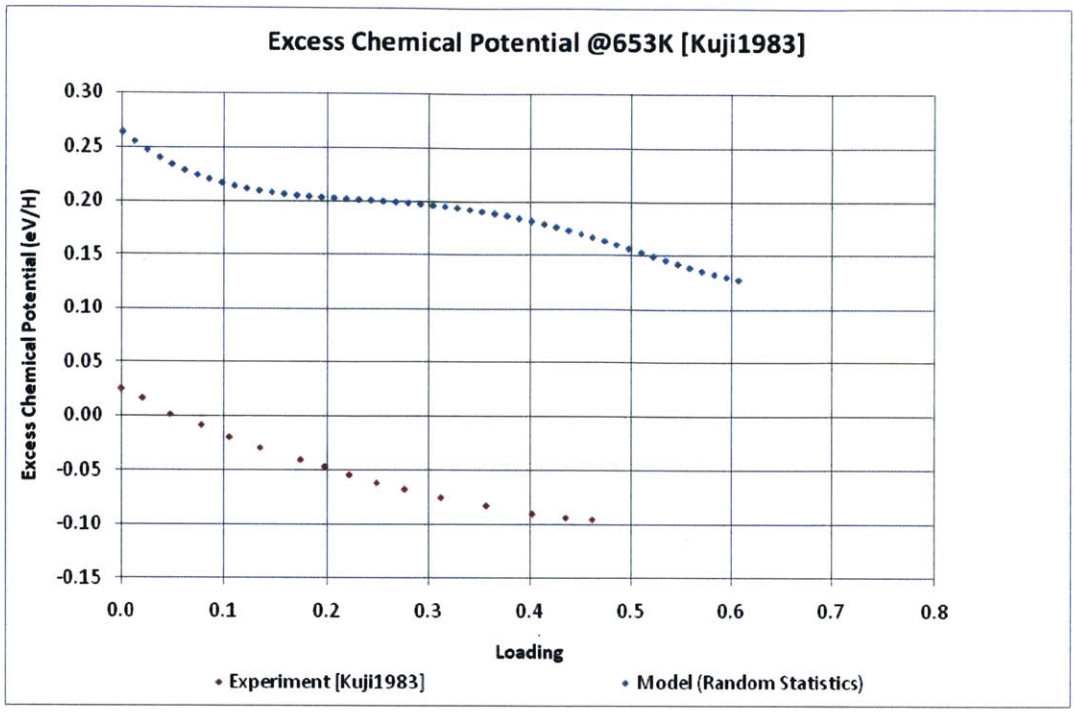

Figure 89: Excess Chemical Potential at 653K: Experiment vs. Model

One trend we see in the above results is that the temperature dependence is slight, both in the model and in the experimental data.

The excess chemical potential at infinite dilution (polynomial fit to (Kuji, Oates, Bowerman, & Flanagan, 1983) experiment) is also shown below)

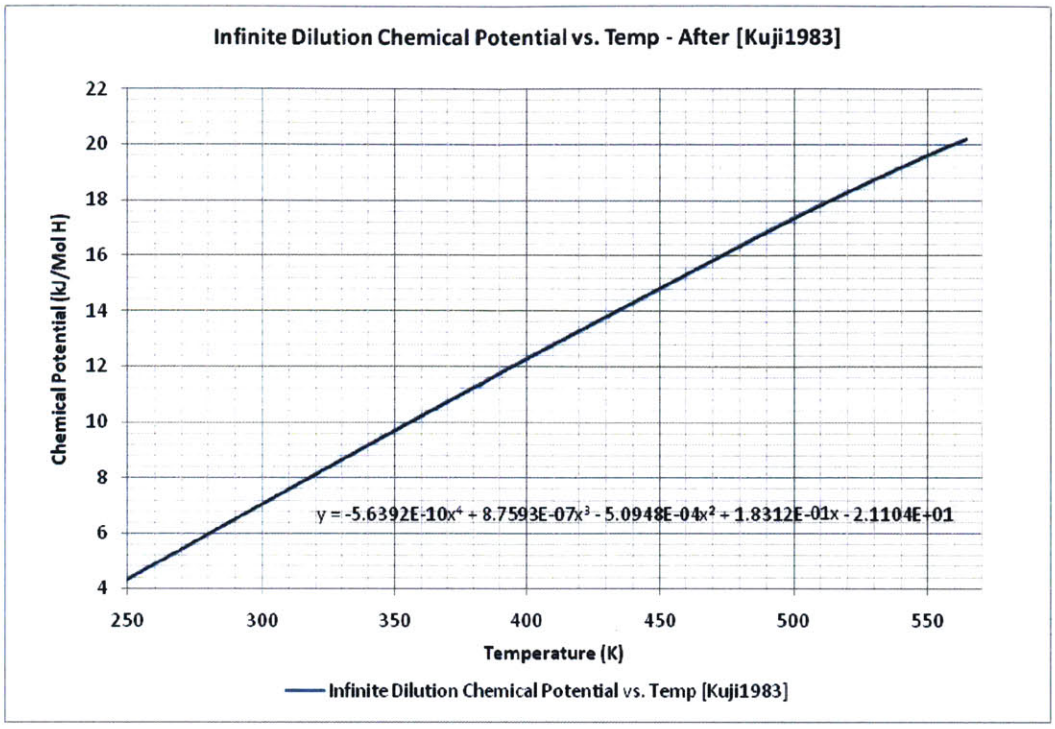

Figure 90: Excess Chemical Potential – Experiment

From Figure 87, Figure 88 and Figure 89, we may attempt various degrees of correction, from a constant to linear to quadratic. The results are shown below, for various temperatures, followed by regression graphs:

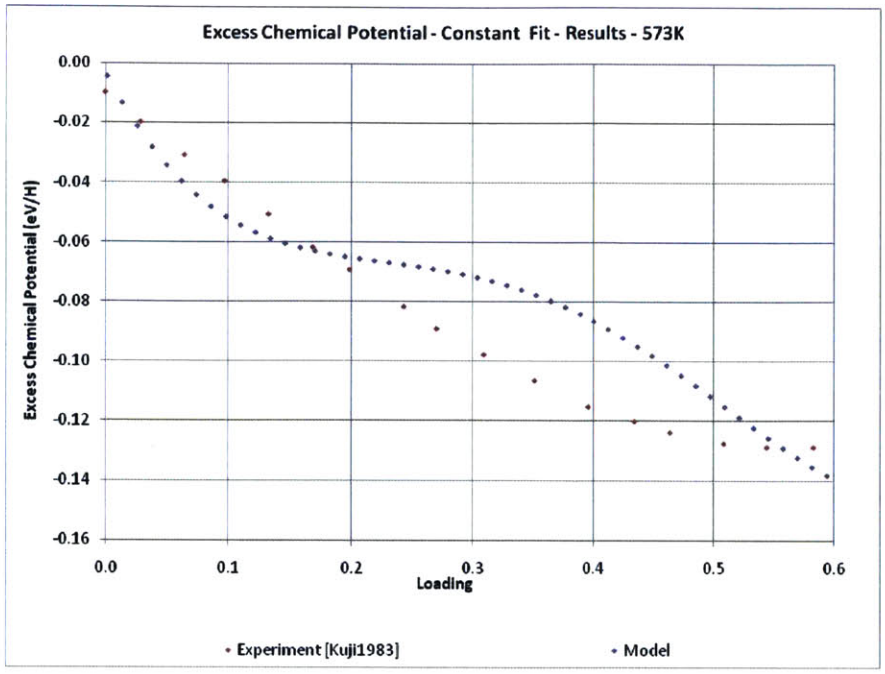

Figure 91: Regression Fit of Model to Experimental Chemical Potential (Constant Fit)

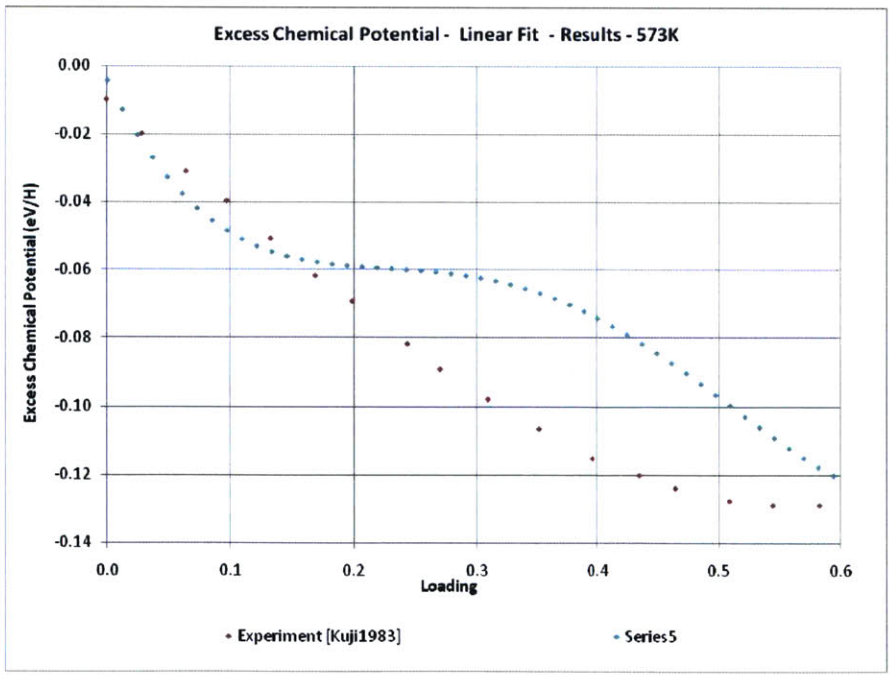

Figure 92: Regression Fit of Model to Experimental Chemical Potential (Linear Fit)

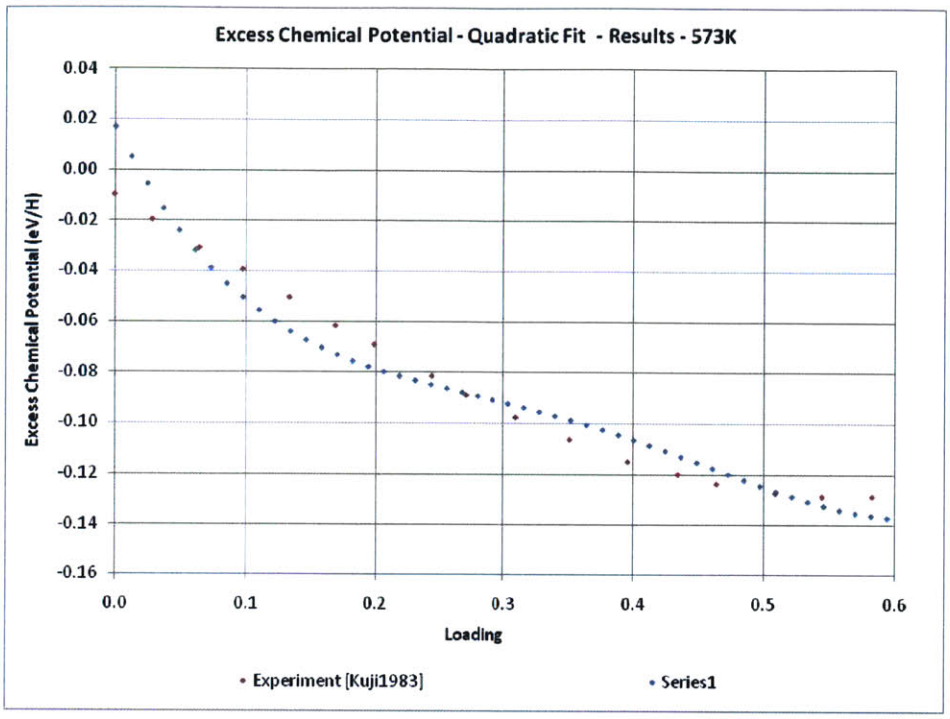

Figure 93: Regression Fit of Model to Experimental Chemical Potential (Quadratic Fit)

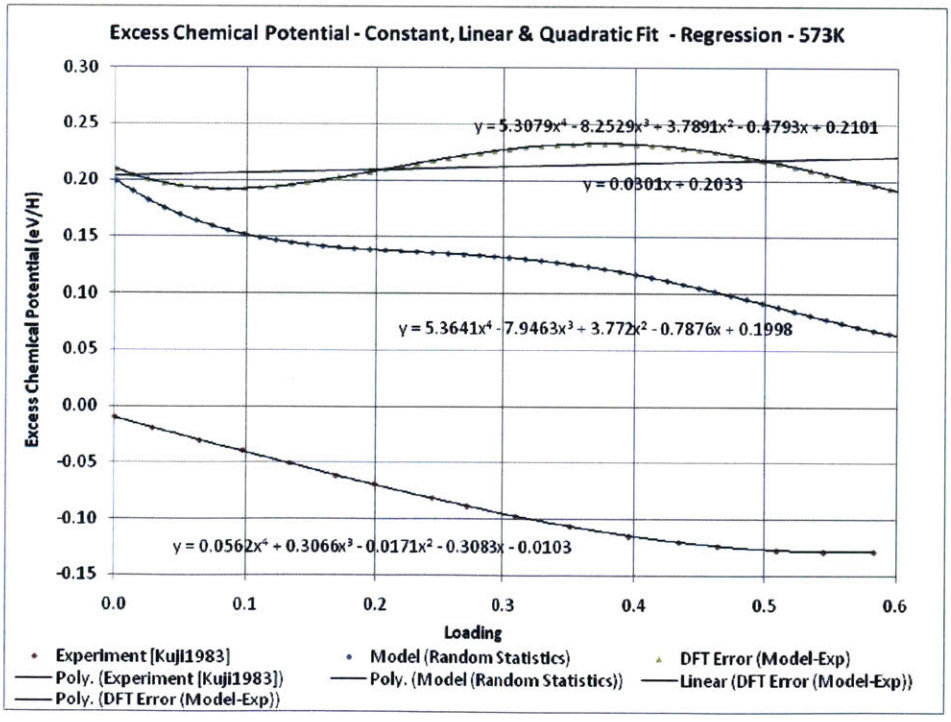

Figure 94: Regression Details (T=573)

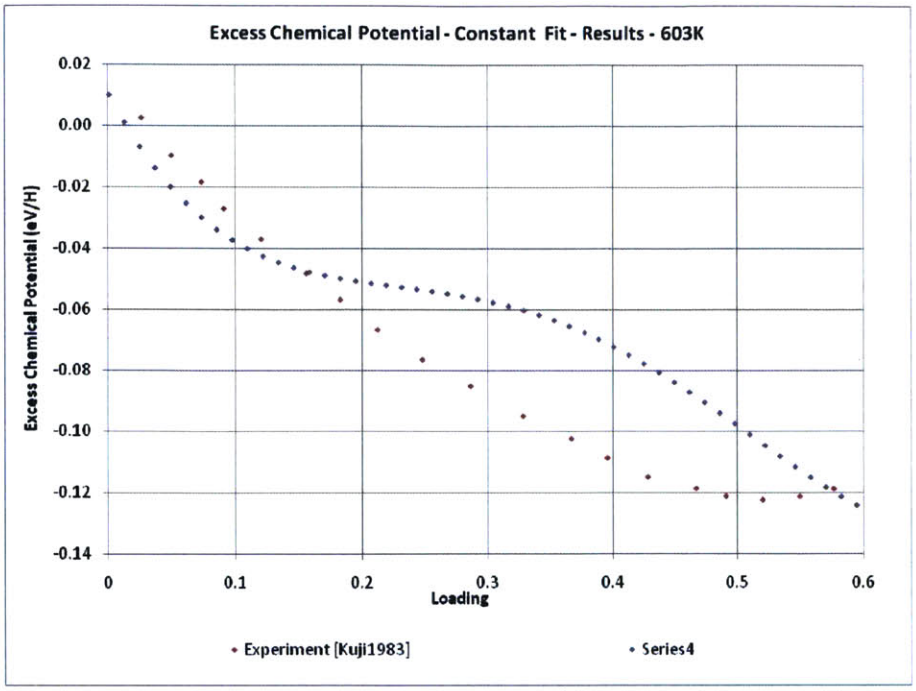

Figure 95: Regression Fit of Model to Experimental Chemical Potential (Constant Fit)

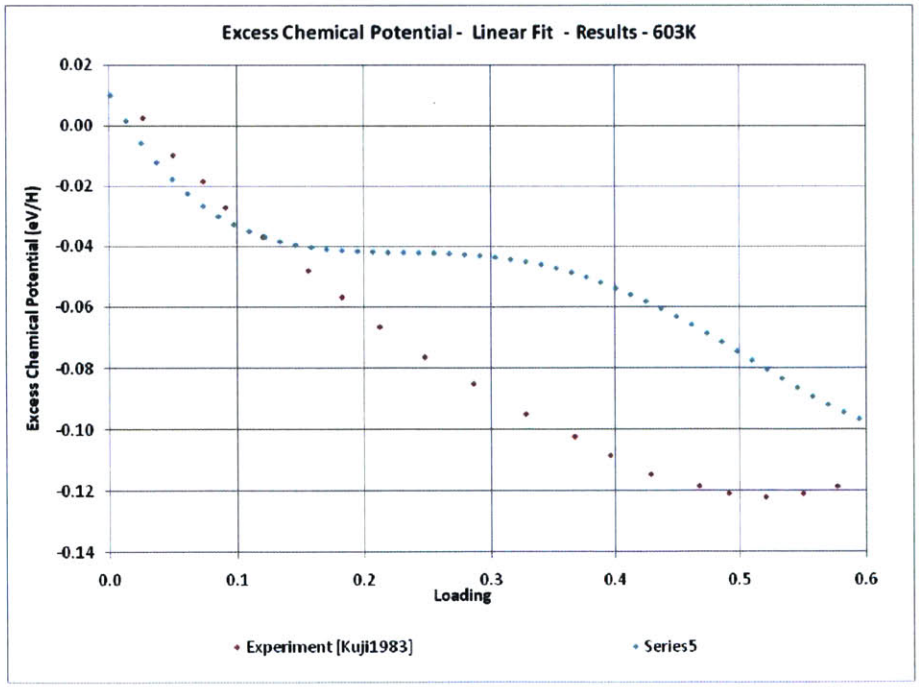

Figure 96: Regression Fit of Model to Experimental Chemical Potential (Linear Fit)

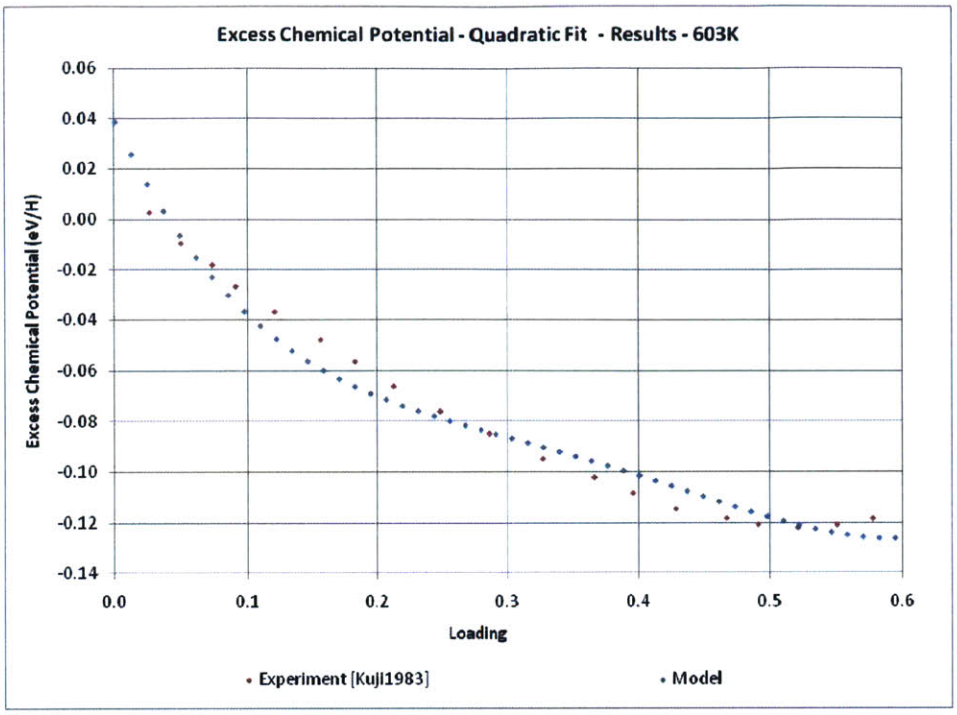

Figure 97: Regression Fit of Model to Experimental Chemical Potential (Quadratic Fit)

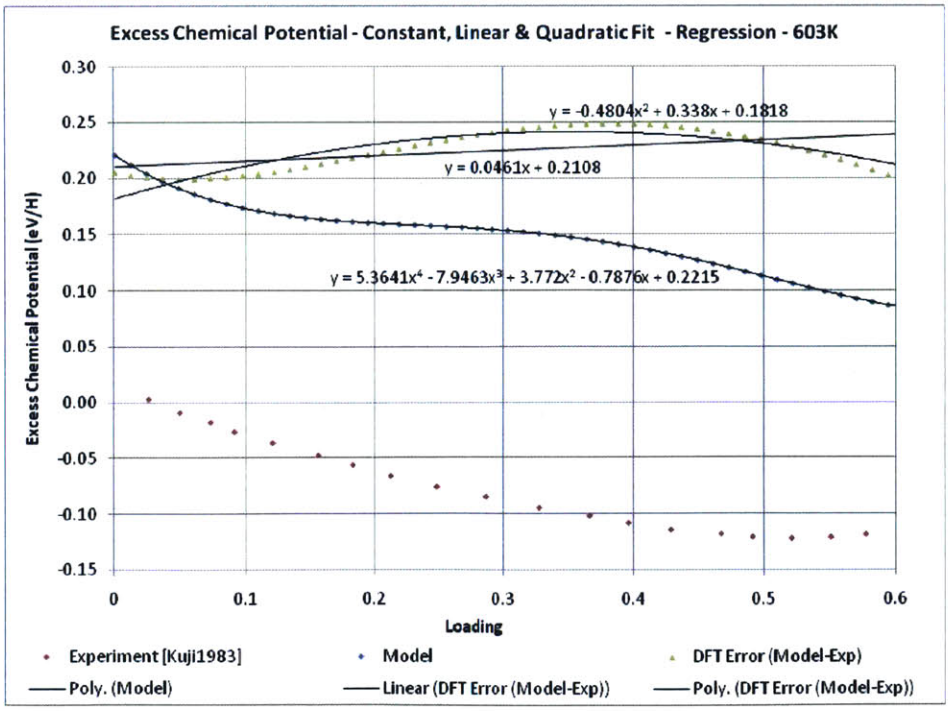

Figure 98: Regression Details (T=603)

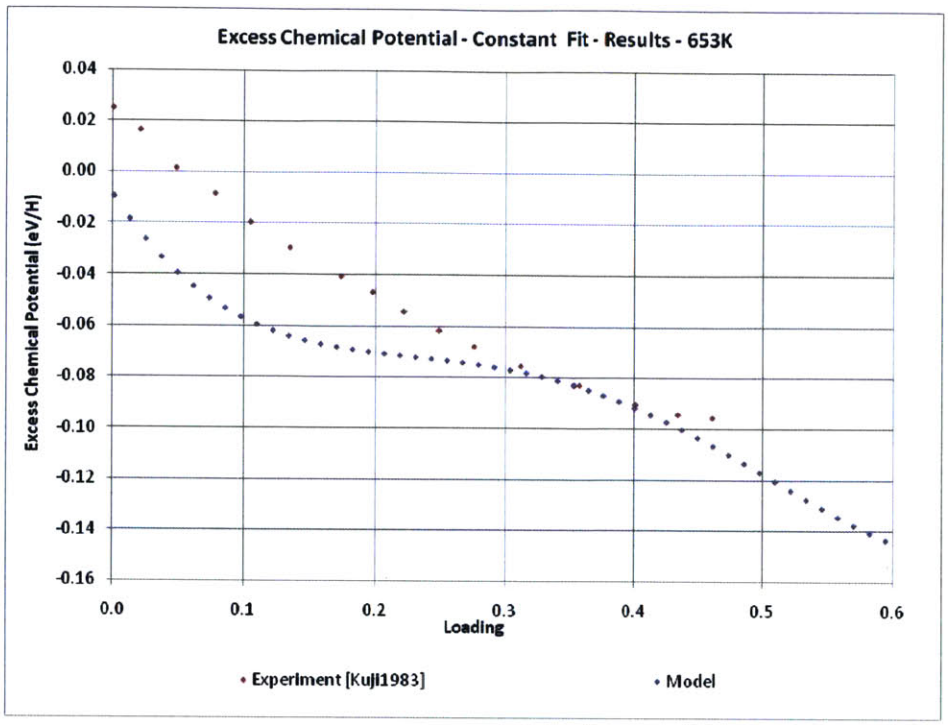

Figure 99: Regression Fit of Model to Experimental Chemical Potential (Constant Fit)

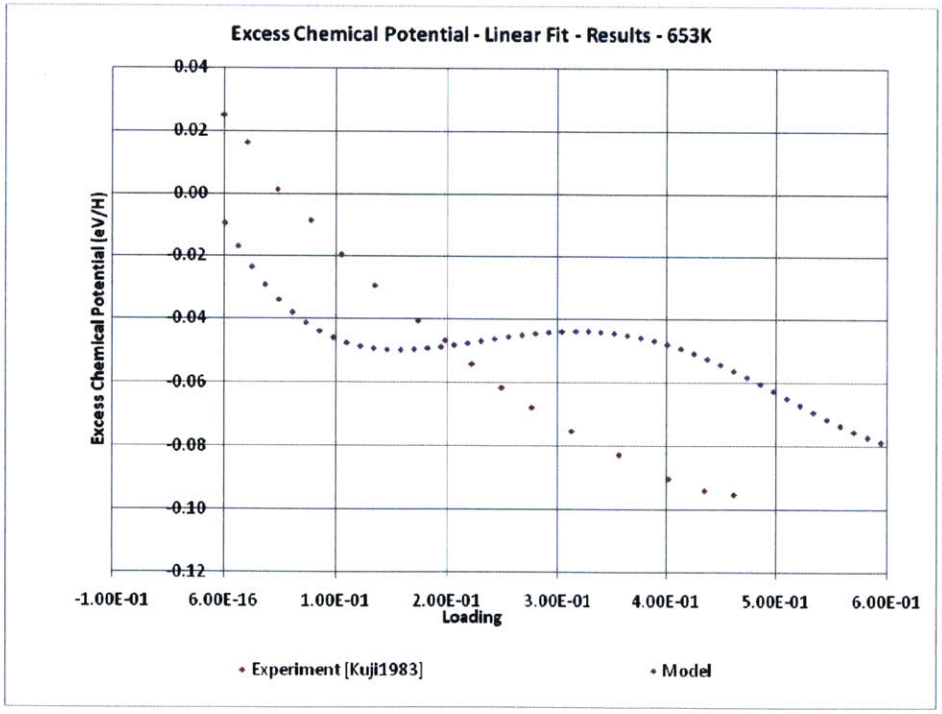

Figure 100: Regression Fit of Model to Experimental Chemical Potential (Linear Fit)

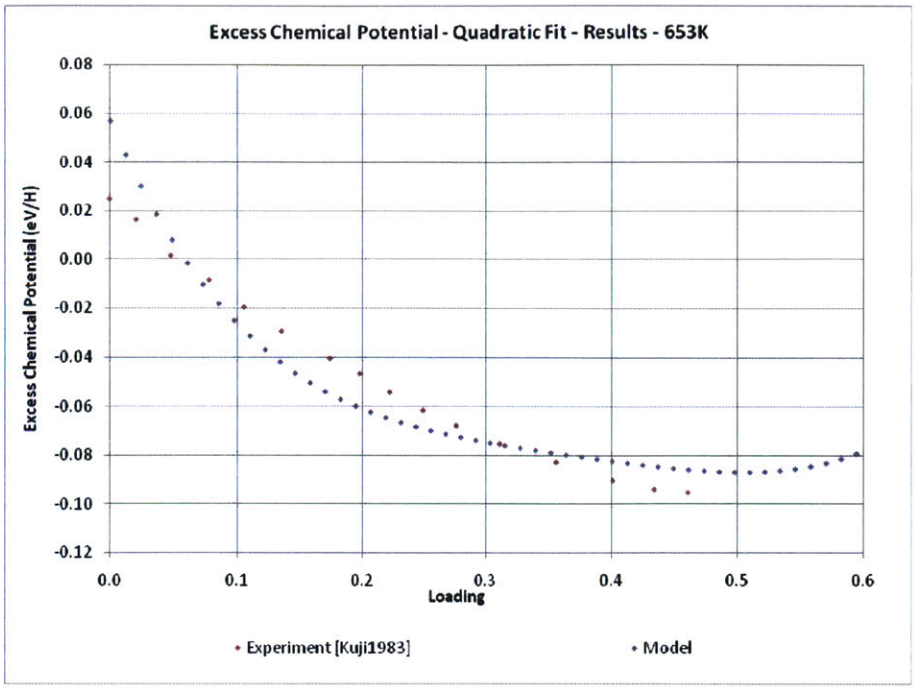

Figure 101: Regression Fit of Model to Experimental Chemical Potential (Quadratic Fit)

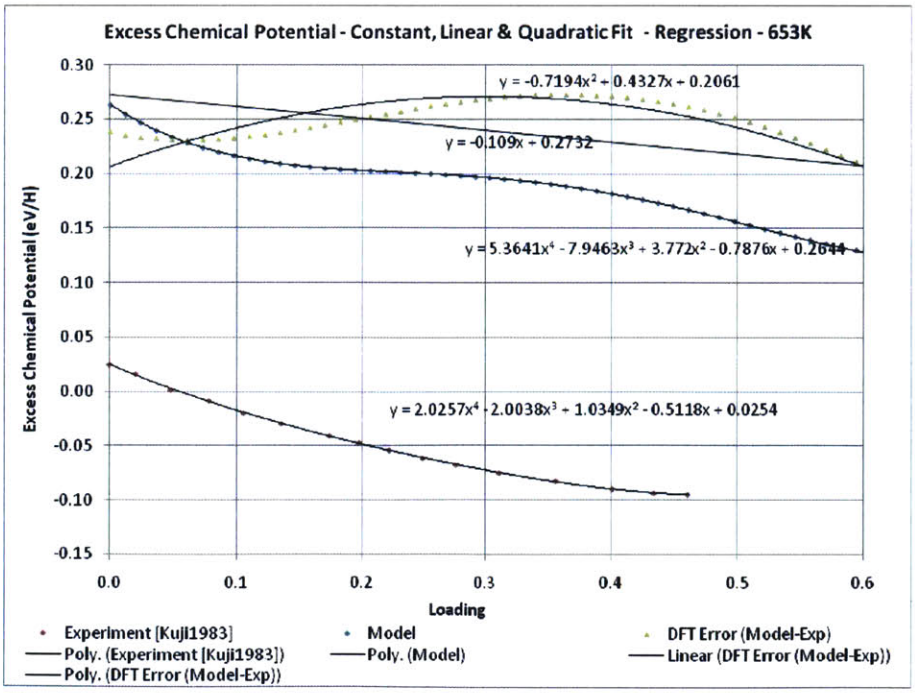

Figure 102: Regression Details (T=653)

What Does This All Mean?

We may write, with view of Equation 291 for enthalpy and Equation 301 for the entropy, and noting the temperature dependence as "small", the correction to the Gibbs energy as a Taylor expansion around some temperature, T_0,

$$\Delta\bar{G}_H^{E,Error}(\theta,T) = \Delta g(\theta,T_0) + \frac{\partial}{\partial T}\left(\Delta g(\theta,T_0)\right)(T-T_0) + \frac{1}{2}\frac{\partial^2}{\partial T^2}\left(\Delta g(\theta,T_0)\right)(T-T_0)^2 + \cdots \quad 348$$

where $g(\theta,T)$ is a θ and T-dependent corrective term. The excess entropy is then derived from the corrected Gibbs Energy, $\Delta\bar{G}_H^{E,Corr}(\theta,T)$, thus,

$$-\Delta\bar{S}_H^{E,Corr} = \left(\frac{\partial\Delta\bar{G}_H^{E,Corr}}{\partial T}\right)_{P,n} = \left(\Delta\bar{G}_H^{E}(T)\right)' + \left(\Delta\bar{G}_H^{E,Error}(\theta,T)\right)' \quad 349$$

The corrected excess enthalpy is also derived from Equation 291

$$-\frac{\Delta\bar{H}_H^E}{T^2} = \left(\frac{\partial\left(\frac{\Delta\bar{G}_H^E}{T}\right)}{\partial T}\right)_{P,n} = \left(\frac{\Delta\bar{G}_H^E}{T}\right)' + \left(\frac{\Delta\bar{G}_H^{E,Error}(\theta,T)}{\mathrm{T}}\right)' \quad 350$$

We obviously need a model for $\Delta g(\theta,T)$. One thing we know is that Δg is connected via Equation 349 for Entropy and Equation 350 for enthalpy, such that any model of $\Delta g(\theta,T)$ must be consistent between these two equations.

We also know that Equation 348 allows us to make connection to experiment. Starting from this perspective, we may get an approximate model for $\Delta g(T)$ (Kuji, Oates, Bowerman, & Flanagan, 1983). Perhaps the only difficulty may be calculating the temperature derivatives in Equation 348. To make things simpler, we concentrate first on one particular arbitrary value of loading, namely, $\theta = 0$, before generalizing. Using results from Figure 91 through Figure 102, we have for $\theta = 0$, in a least squares quadratic fit sense:

Temperature (K)	$g(0,T)$
423	0.1686
573	0.1815
603	0.1818
653	0.2061

Approximately, therefore,

$$g(0,T) = 1.1797 * 10^{-6}T^2 - 1.1130 * 10^{-3}T + 4.285 * 10^{-1} \quad 351$$

Equation 348 then becomes, substituting Equation 351 to get a concrete example,

$$\Delta\bar{G}_H^{E,Error}(0,T) = \Delta g(0,T_0) + \frac{\partial}{\partial T}\left(\Delta g(0,T)\right)\Big|_{T=T_0}(T-T_0) + \frac{1}{2}\frac{\partial^2}{\partial T^2}\left(\Delta g(\theta,T)\right)\Big|_{T=T_0}(T-T_0)^2 + \cdots$$

$$= (1.1797 * 10^{-6}T^2 - 1.1130 * 10^{-3}T + 4.285 * 10^{-1})|_{T=T_0} + (2 * 1.1797 * 10^{-6}T - 1.1130 * 10^{-3})|_{T=T_0}(T-T_0) + \frac{1}{2}(2 * 1.1797 * 10^{-6})\Big|_{T=T_0}(T-T_0)^2 \quad 352$$

Around $T = T_0 = 573K$ therefore, Equation 352 becomes

$$\Delta\bar{G}_H^{E,Error}(0,T) = 1.780807 * 10^{-1} + 2.389362 * 10^{-4}(T-573) + 6.759681 * 10^{-4}(T-T_0)^2 \quad 353$$

Then, with view of Equation 349,

$$\left(\Delta\bar{G}_H^{E,Error}(0,T)\right)' = 2.389362 * 10^{-4} + 2 * 6.759681 * 10^{-4}(T-573) \quad 354$$

Beta Phase

We shall begin by considering the issue of electronic contribution to entropy that is already estimated by (Kuji, Oates, Bowerman, & Flanagan, 1983), based on the prior work of (Oates & Flanagan, 1971). According to [ibid], the change in the heat capacity of Pd upon the addition of hydrogen is shown to contribute to the excess entropy [ibid]. Based on this, (Kuji, Oates, Bowerman, & Flanagan, 1983) estimated this contribution to increase only slightly in the alpha and mixed phases, then increase more substantially up to a value of $\Delta S_{el} = 4.15\text{E} - 05 *$ T $eV\ per\ H\ atom$ at unity loading.

We take a slightly different approach by phenomenologically including the electronic partition function in our grand partition function, Equation **54** Chapter 2:

$$Z_H(\tau,\mu) = \sum_{n_o}\sum_{n_t}\sum_{ASN} e^{\frac{(n_o+n_t)\mu-\varepsilon_h}{\tau}} z^{(n_o+n_t)} z_e^{(n_o+n_t)}$$

355

where $z_e^{(n_o+n_t)}$ is the electronic partition function for the dissolved protium, and the other terms have already been defined. The electronic partition function may be written as

$$z_e = \sum_{j,e} g_j e^{-\frac{\varepsilon_{j,e}}{\kappa_B T}}$$

356

where g_j is the degeneracy of state j with energy ε_j and the summation is carried out over all electronic states. Because the electronic energies are usually large and well separated, the terms of Equation **356** all drop off except the first one:

$$z_e = \sum_{j,e} g_j e^{-\frac{\varepsilon_{j,e}}{\kappa_B T}} = g_0 + g_1 e^{-\frac{\varepsilon_{1,e}}{\kappa_B T}} + g_2 e^{-\frac{\varepsilon_{2,e}}{\kappa_B T}} + \cdots \cong g_0$$

357

The ground state is a doublet, such that the degeneracy for the electron is 2. The grand partition function for the dissolved hydrogen, Equation 355, then becomes

$$Z_H(\tau,\mu) = \sum_{n_o}\sum_{n_t}\sum_{ASN} e^{\frac{(n_o+n_t)\mu-\varepsilon_h}{\tau}} z^{(n_o+n_t)} g_0^{(n_o+n_t)}$$

358

Following our results from Chapter 2, we calculate the chemical potential as

$$\mu_o(\tau,n_o,n_t) = -\tau\frac{\partial \ln Z_H(\tau,n_o,n_t)}{\partial n_o}$$

359

$$\mu_t(\tau,n_o,n_t) = -\tau\frac{\partial \ln Z_H(\tau,n_o,n_t)}{\partial n_t}$$

360

whereby

$$\mu_o(\tau,n_o,n_t) = \mu_t(\tau,n_o,n_t)$$

361

and we use the Bragg-Williams Approximation:

$$Z_H(\tau,n_o,n_t) \cong \frac{N_o!}{n_o!\,(N_o-n_o)!}\frac{N_t!}{n_t!\,(N_t-n_t)!} e^{-\frac{(n_o+n_t)\varepsilon_h(n_o,n_t)}{\tau}} z^{(n_o+n_t)} g_0^{(n_o+n_t)}$$

362

Using prior analysis, we can write down the chemical potential terms by inspection, thus:

$$\mu_o(\tau,\theta_o,\theta_t) = \tau\, ln\frac{\theta_o}{1-\theta_o} - \tau\, ln(z) - \tau\, l\,n(g_0) + (\theta_o + 2\theta_t)\frac{\partial\varepsilon_h(\theta_o,\theta_t)}{\partial\theta_o} + \varepsilon_h(\theta_o,\theta_t)$$

363

$$\mu_t(\tau,\theta_o,\theta_t) = \tau\, ln\frac{\theta_t}{1-\theta_t} - \tau\ ln(z) - \tau\, l\,n(g_0) + (\theta_t + \frac{1}{2}\theta_o)\frac{\partial\varepsilon_h(\theta_o,\theta_t)}{\partial\theta_t} + \varepsilon_h(\theta_o,\theta_t)$$

364

Using earlier results once again, the fugacity is calculated by matching the chemical potential at the Pd-H boundary:

$$\mu_H(absorbed) = \frac{1}{2}\mu_{H_2}(gas)$$

365

Therefore:

$$f(\theta) = A(\tau)e^{\frac{B(\theta)}{\tau}}$$

366

where now, respectively,

$$A(\tau) = \tau\left(\frac{2\pi m\tau}{h^2}\right)^{\frac{3}{2}}$$

367

$$B(\theta,T) = 2\tau ln\frac{\theta_o}{1-\theta_o} - 2\tau\, ln\, z - 2\tau\, ln\, g_0 + 2\theta\frac{\partial\varepsilon_h(\theta)}{\partial\theta} + 2\varepsilon_h(\theta) + \tau\, ln\frac{e^{-\frac{\epsilon_{0V}}{2\tau}}}{1-e^{-\frac{\epsilon_{0V}}{\tau}}} + \tau ln\frac{8\pi^2 I\tau}{\sigma h^2} + \epsilon_D$$

368

To get the corrected enthalpy, we calculate the Gibbs free energy as in Equation 295, but now using $B(\theta,T)$ from above, Equation 368:

$$\Delta\bar{G}_H = \frac{1}{2}RT * ln\left(A(T) * e^{\frac{B(\theta,T)}{\kappa_B T}}\right)$$

$$= \frac{1}{2}RT\left[ln(A(T)) + \frac{B(\theta,T)}{\kappa_B T}\right]$$

$$= \frac{RT}{2}lnA(T) + \frac{1}{2}RT\left[2ln\frac{\theta_o}{1-\theta_o} + 6\,ln\left(2\,sinh\frac{\epsilon_{0v}}{2\kappa_B T}\right) - 2\,ln\,g_0 + \frac{2\theta}{\kappa_B T}\frac{\partial\varepsilon_h(\theta)}{\partial\theta} + \frac{2}{\kappa_B T}\varepsilon_h(\theta)\right.$$

$$\left. + ln\frac{8\pi^2 I\kappa_B T}{\sigma h^2} + \frac{\epsilon_D}{\kappa_B T}\right]$$

$$= \frac{RT}{2}lnA(T) + RT\,ln\frac{\theta_o}{1-\theta_o} + 3RT\,ln\left(2\,sinh\frac{\epsilon_{0v}}{2\kappa_B T}\right) - RT\,ln\,g_0 + \frac{R}{\kappa_B}\theta\frac{\partial\varepsilon_h(\theta)}{\partial\theta} + \frac{R}{\kappa_B}\varepsilon_h(\theta)$$

$$+ \frac{RT}{2}ln\frac{8\pi^2 I\kappa_B T}{\sigma h^2} + \frac{R}{2\kappa_B}\epsilon_D$$

369

The excess Gibbs Free Energy (Equation 296), then becomes

$$\Delta\bar{G}_H^{E,e} = \frac{RT}{2}lnA(T) + 3RT\,ln\left(2\,sinh\frac{\epsilon_{0v}}{2\kappa_B T}\right) - RT\,ln\,g_0 + \frac{R}{\kappa_B}\theta\frac{\partial\varepsilon_h(\theta)}{\partial\theta} + \frac{R}{\kappa_B}\varepsilon_h(\theta) + \frac{RT}{2}ln\frac{8\pi^2 I\kappa_B T}{\sigma h^2}$$

$$+ \frac{R}{2\kappa_B}\epsilon_D$$

370

and Equation 298 is:

$$\frac{\Delta\bar{G}_H^{E,e}}{T} \rightarrow \frac{R}{2}lnA(T) + 3R\,ln\left(2\,sinh\frac{\epsilon_{0v}}{2\kappa_B T}\right) - R\,ln\,g_0 + \frac{R}{\kappa_B T}\theta\frac{\partial\varepsilon_h(\theta)}{\partial\theta} + \frac{R}{\kappa_B T}\varepsilon_h(\theta) + \frac{R}{2}ln\frac{8\pi^2 I\kappa_B T}{\sigma h^2}$$

$$+ \frac{R}{2\kappa_B T}\epsilon_D$$

371

such that, similar to Equation 299,

$$\Delta\bar{H}_H^E = -T^2\frac{\partial}{\partial T}\left(\frac{R}{2}lnA(T) + 3R\,ln\left(2\,sinh\frac{\epsilon_{0v}}{2\kappa_B T}\right) - R\,ln\,g_0 + \frac{R\theta}{\kappa_B T}\frac{\partial\varepsilon_h(\theta)}{\partial\theta} + \frac{R}{\kappa_B T}\varepsilon_h(\theta) + \frac{R}{2}ln\frac{8\pi^2 I\kappa_B T}{\sigma h^2} + \frac{R}{2\kappa_B T}\epsilon_D\right)_{P,n}$$

$$\Delta\bar{H}_H^E = -\frac{RT^2}{2}\frac{A'(T)}{A(T)} + \frac{3R\epsilon_{0v}}{2\kappa_B}coth\frac{\epsilon_{0v}}{2\kappa_B T} + \frac{R}{\kappa_B}\theta\frac{\partial\varepsilon_h(\theta)}{\partial\theta} + \frac{R}{\kappa_B}\varepsilon_h(\theta) - \frac{RT}{2} + \frac{R}{2\kappa_B}\epsilon_D \quad (372)$$

Finally, as in Equation 300,

$$\bar{H}_H^E = \Delta\bar{H}_H^E - \Delta\bar{H}_H^0 \quad (373)$$

It is therefore abundantly clear that there is at best a high order electronic correction to excess enthalpy.

The relative molar entropy is given by Equation 302, except that excess Gibbs Energy is now given by Equation 370:

$$\Delta\bar{S}_H^E = \frac{\Delta\bar{H}_H^E - \Delta\bar{G}_H^{E,e}}{T} \quad (valid\ in\ Beta\ Phase) \quad (374)$$

Lastly, excess entropy is

$$\bar{S}_H^E = \Delta\bar{S}_H^E - \Delta\bar{S}_H^0 \quad (375)$$

The results are shown below, where once again, no discernible difference from the model without electronic correction.

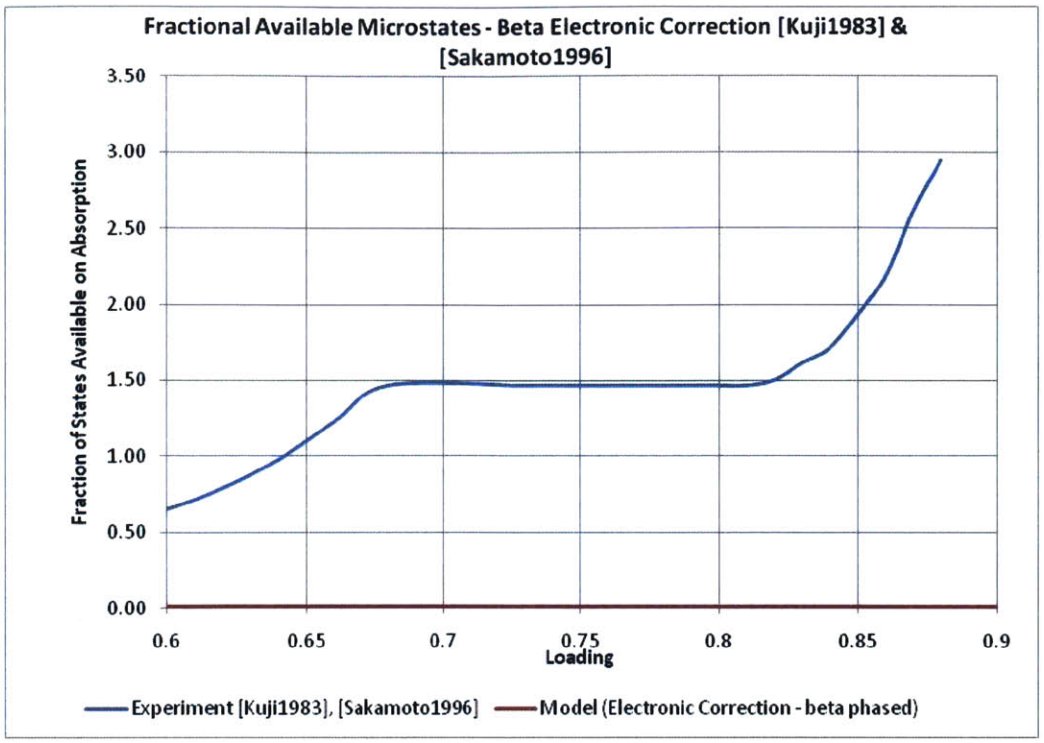

Figure 103: Beta Phase Fractional Microstates with Electronic Correction

Thinking About SHO Approximation to the Vibrational States of Hydrogen in Pd

So far, we have only considered the ground state for the dissolved hydrogen. The partition function was thus described using a harmonic oscillator approximation, Equation 53 of Chapter 2:

$$z = \left(\sum_{n=0}^{\infty} e^{-\frac{\epsilon_{0v}\left(n+\frac{1}{2}\right)}{\tau}}\right)^3 = \left(e^{-\frac{\epsilon_{0v}}{2\tau}}\sum_{n=0}^{\infty} e^{-\frac{\epsilon_{0v}n}{\tau}}\right)^3 = \left(\frac{e^{-\frac{\epsilon_{0v}}{2\tau}}}{1-e^{-\frac{\epsilon_{0v}}{\tau}}}\right)^3 = \left(2sinh\frac{\epsilon_{0v}}{2\tau}\right)^{-3} \quad 376$$

where ϵ_{0v} is the ground state vibrational quantum, and we have included all three normal modes. In reality, however, we know that there will be excited states.

Now, it is well known that within the lattice, the partition function of hydrogen is actually anharmonic, see for example (Wallace, 1992) . In this section, we will correct the pure harmonic treatment to include the first excited state from experiment. The goal is to find out how much difference it makes to our results.

We will take the first excited state to be at an energy of ϵ_{1v}. As a first approximation, we can simply include the two quanta at ϵ_{0v} and ϵ_{1v} in the partition function, thus:

$$z \approx \left(e^{-\frac{\epsilon_{0v}}{2\tau}} + e^{-\frac{\epsilon_{1v}}{\tau}}\right)^3 \quad 377$$

In Equation 377, we ignore all the higher order states.

Using this result, and following (Powell, 1976), we write the partition function of the H in Pd as

$$Z_H(\tau,\mu) = \sum_n \sum_{ASN} e^{\frac{n\mu-\varepsilon_h}{\tau}} z^n \quad 378$$

Even before we make any calculations, we can anticipate the results of this approach to our model. Because the excited vibrational quantum level is about twice that of the ground state, 138 meV vs. 68.5 meV, (Rush, Rowe, & Richter, 1984), we do expect only a slight correct in the model results.

Following results from Chapter 2, we can write down the chemical potential for H in Pd from Equation 40 as follows:

$$\mu_H \equiv \frac{\partial F}{\partial n} = -\tau \frac{\partial \ln Z_H}{\partial n} \tag{379}$$

or

$$\mu_o(\tau, \theta_o, \theta_t) = \tau \ln \frac{\theta_o}{1-\theta_o} - \tau \ln(z) + (\theta_o + 2\theta_t) \frac{\partial \varepsilon_h(\theta_o, \theta_t)}{\partial \theta_o} + \varepsilon_h(\theta_o, \theta_t) \tag{380}$$

$$\mu_t(\tau, \theta_o, \theta_t) = \tau \ln \frac{\theta_t}{1-\theta_t} - \tau \ln(z) + \left(\theta_t + \frac{1}{2}\theta_o\right) \frac{\partial \varepsilon_h(\theta_o, \theta_t)}{\partial \theta_t} + \varepsilon_h(\theta_o, \theta_t) \tag{381}$$

As before, we calculate fugacity as (Chapter 2)

$$f(\theta) = A e^{\frac{B(\theta)}{\tau}} \tag{382}$$

where

$$A = \tau \left(\frac{2\pi m \tau}{h^2}\right)^{\frac{3}{2}} \tag{383}$$

$$B(\theta) = 2\tau \ln \frac{\theta_o}{1-\theta_o} - 2\tau \ln(z) + 2\theta \frac{\partial \varepsilon_h(\theta)}{\partial \theta} + 2\varepsilon_h(\theta_o, \theta_t) + \tau \ln \frac{e^{-\frac{\epsilon_{0v}}{2\tau}}}{1 - e^{-\frac{\epsilon_{0v}}{\tau}}} + \tau \ln \frac{8\pi^2 I \tau}{\sigma h^2} + \epsilon_D \tag{384}$$

The results are shown below, where we compare them with those from pure SHO approximation.

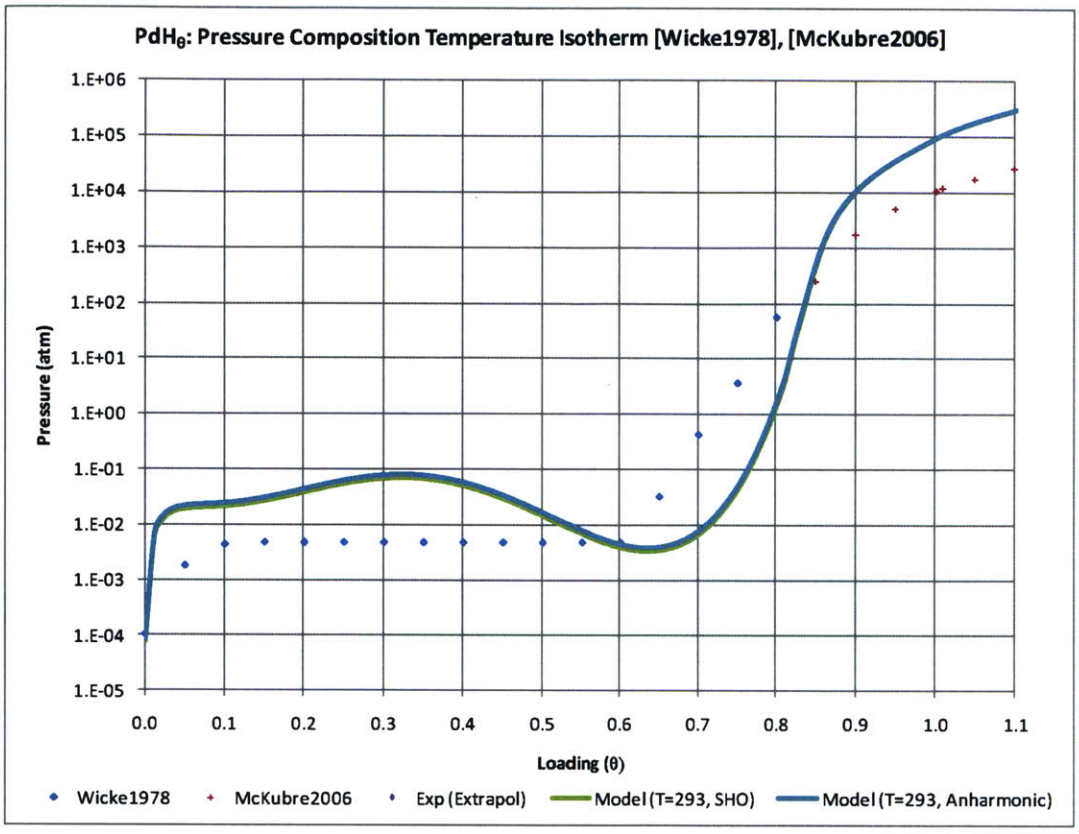

Figure 104: For the partition function of hydrogen in Pd, a comparison of SHO approximation with an anharmonic approximation using two first excited states.

Summary

In this Chapter, we have connected our analysis to molar quantities (enthalpy and entropy) in a fundamental way, beginning with first and second laws of thermodynamics. A simple, initial correction mechanism is also attempted – see later chapters for a fuller analysis of the corrections.

Chapter 8 -Understanding DFT Energy Shift

Introduction

In this chapter, we would like to gain some intuition into the DFT energy calculations. In particular we would like to quantify the order of differences between the DFT results and experiment.

Second, we would like to gain some understanding whether there is consistency when the same set of parameters is used to calculate different configurations energies (say in H-H binding energy vs. Pd-H binding energy).

Lastly, we like to use any insight gained to correct derived quantities like enthalpy and entropy.

We begin with analysis of the energy differences between DFT and experiment in potential energy curves.

Potential Energy Curves: Pd-H and H-H. Model vs. Experiment

A good starting point is the potential energy curve for Pd-H and H-H. We show the curves below, noting that even though the works cited are not experimental, (Kolos & Wolniewicz, 1964) for H-H, and (Balasubramanian, Feng, & Liao, 1987) for Pd-H, their agreement with experiment (Herzberg, 1970) for H-H, and (Lagerquist, Neuhaus, & Scullman, 1964) for PdH, is well established.

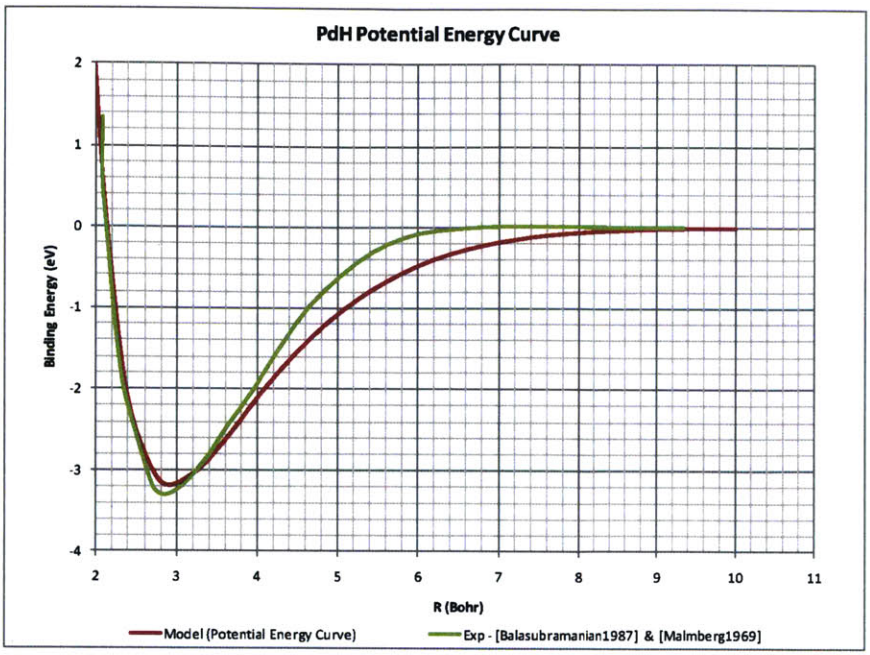

Figure 105: Potential Energy Curve, PdH: Model vs. Experiment

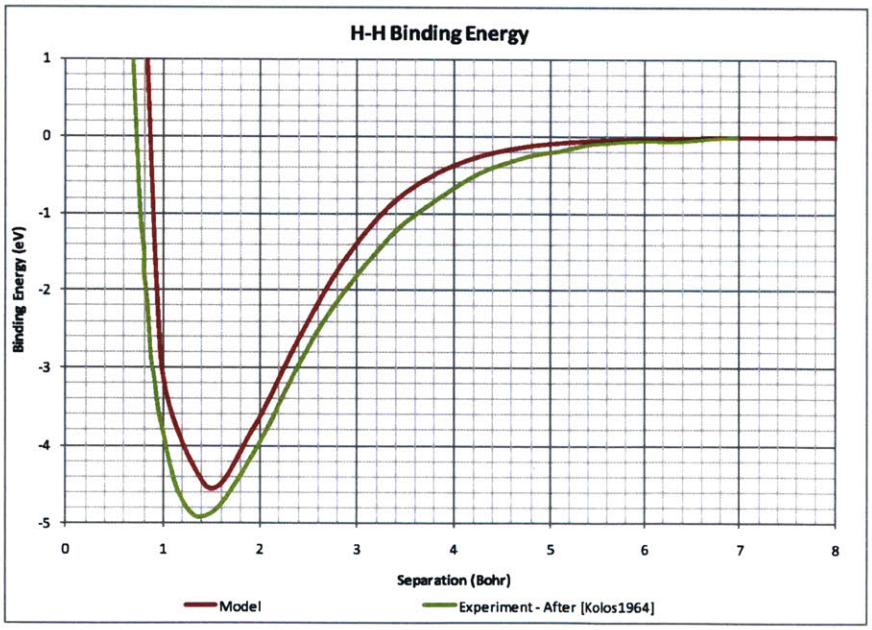

Figure 106: Potential Energy Curve, H-H: Model vs. Experiment.

In the case of H-H, the difference between model and experiment is 310 meV while that for Pd-H is 110 meV:

$$\Delta E_{H-H} = E_{Model} - E_{Exp} = 310\ meV \tag{385}$$

$$\Delta E_{Pd-H} = E_{Model} - E_{Exp} = 110\ meV \tag{386}$$

These values are taken at the minima of the potential energy curve. In fact, the experimental value of the dissociation energy for H-H is 4.49 eV (Herzberg, 1970) in (Silbey, Alberty, & Bawendi, 2004) – (Kolos & Wolniewicz, 1964) curve on which Figure 106 is based is theoretical, not experimental, i.e. our model results are closer to experiment, and

$$\Delta E_{H-H} = E_{Model} - E_{Exp} = 54.7\ meV \tag{387}$$

The initial results are comforting because in each case, model results are above those of experiment. The model results were arrived at using the same DFT framework, such that we may attribute the difference between Equations 385 and 386 to experimental uncertainties in the two experimental values.

Excess Enthalpy Comparison to Model

Energy Offset Comparison

To make a comparison of our model to experiment, we may compare our model enthalpy calculation to experimental data:

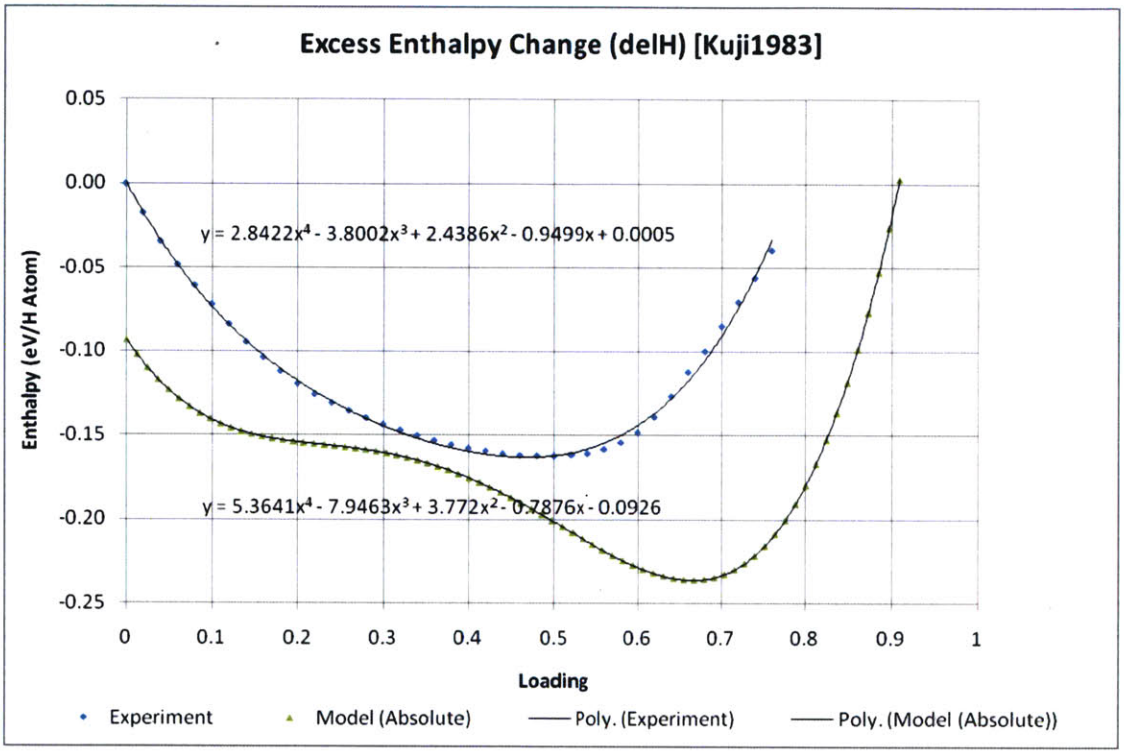

Figure 107: Excess Enthalpy: Model vs. Experiment (Kuji, Oates, Bowerman, & Flanagan, 1983)

If we ignore loading dependence for now, we see from Figure 107 that the difference between experiment and model is approximately

$$\Delta E_{H_H^E} = \overline{H}^E_{H\,Model} - \overline{H}^E_{H\,Exp} = 93.4\ meV\ (infinite\ dilution) \tag{388}$$

In the sense of Equation 388, the results are indeed of the same order of magnitude as Equations 385 and 386, which shows that our model calculations in three contexts are consistent with one another.

Constant Regression Fit to Experiment

Given the favorable energy comparisons in the previous section, we may attempt to correct our DFT results using the constant off-set suggested by Equation 388. The result is shown in Figure 108 below.

The results indicate a reasonable fit in the single phase regions, especially the alpha phase. This is perhaps not surprising since in these two phases, the excess enthalpy is approximately linear, so a linear correction is expected to yield good agreement with experiment. In the mixed phase region, the match is relatively poor. Note that in absolute terms, the largest error occurs approximately in the middle of the miscibility gap, and is a modest 80 meV per H atom.

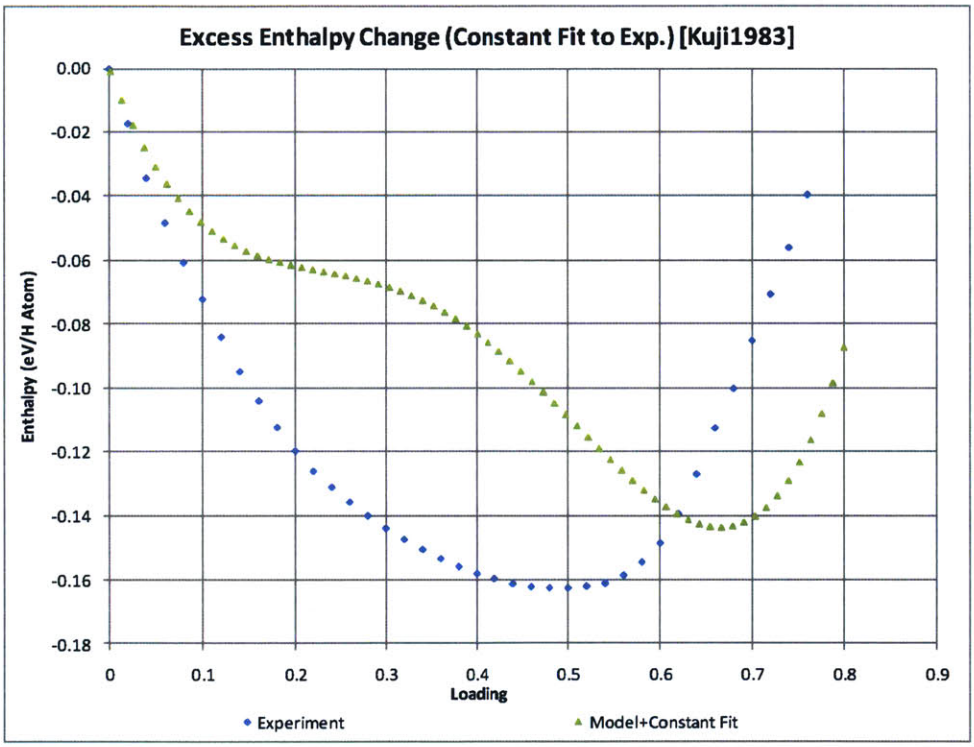

Figure 108: The result of a Constant fit to Model to Experimental Excess Enthalpy Data.

Linear vs. Quadratic Regression Fit to Experiment

It is also plausible that the dependence of the DFT error on loading is not constant, and that Equation 388 is simply the lowest order correction of a more generalized dependence:

$$\Delta E_{DFT} = \varepsilon(\theta) = \sum_k \varepsilon_k \theta^k \tag{389}$$

We stress that, except for $k = 0$ for which we have a foundational argument, we take Equation 389 for $k > 0$ as pure conjecture at this point. Nonetheless, the idea is that the difference in energy calculations between DFT and experiment may be expressed in terms of a Taylor series in loading, with the weights chosen in a least squares sense to match experiment. A particular choice of the weights for a linear fit leads to

$$\varepsilon_0 = 0.0926, \quad \varepsilon_1 = 0.0229 \tag{390}$$

and, for a quadratic regression

$$\varepsilon_0 = 0.1104, \quad \varepsilon_1 = -0.5756, \quad \varepsilon_2 = 0.8805 \tag{391}$$

as shown below (Figure 109). The final results are shown in Figure 110.

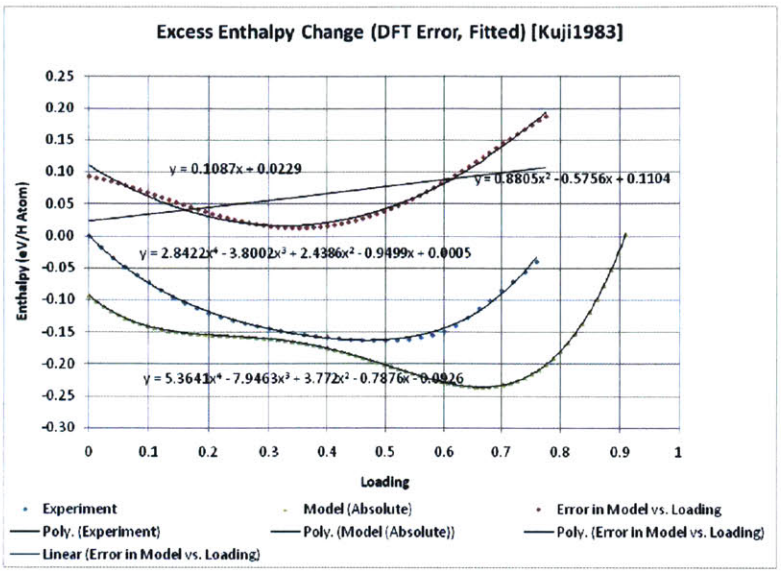

Figure 109: Polynomial Fit of DFT error vs. Loading

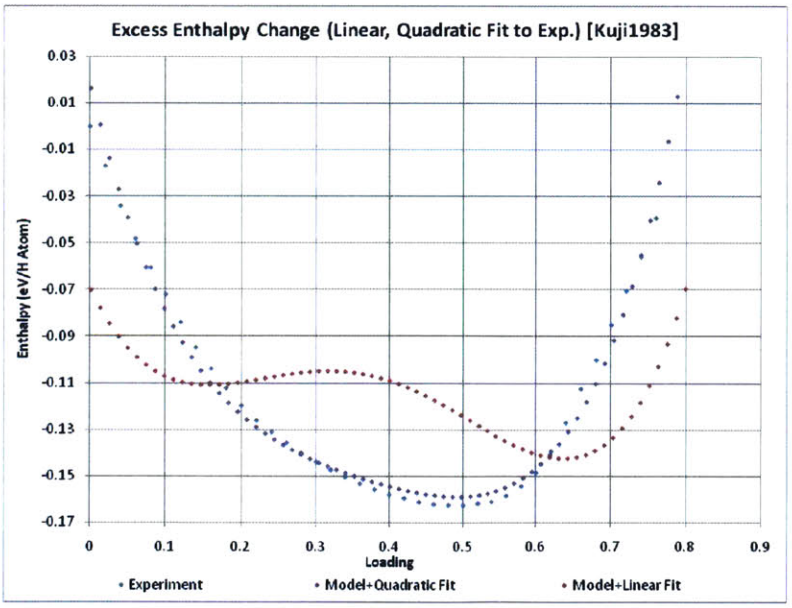

Figure 110: Excess Enthalpy: Linear Fit (red) and Quadratic Fit (purple) to Experiment

Summary

The primary aim of this chapter is to characterize the magnitude of DFT. We find it to be about 100 for the class of problems considered.

Chapter 9 - A New Model of Interstitial Hydrogen in Palladium

Introduction

In the last few chapters, we have attempted to build a progressively more complete description of the physics of hydrogen absorption in Pd bulk. Starting with a relatively simple statistical description of octahedral-only occupation, in Chapter 2 we added tetrahedral occupation and a simple O-to-T excitation model. We proceeded to model the absorption process by using DFT to calculate state energies and using these in the statistical model to derive thermodynamic quantities like chemical potential, enthalpy and entropy.

We also improved the results by adding energy corrections that we could not calculate within the DFT model. These included zero point and thermal excitation energies, DFT corrections and others, as described in Chapter 2. From there we were able to reasonably accurately predict experimental pressure isotherms with only constant corrections to DFT state energies.

In Chapter 3, we tried to come up with a model to account for the miscibility gap, and thereby modeled fairly accurately, the phase change during the absorption process. We found that applying the Rule of Equal Areas was a reasonable description of the clumping that occurs in the miscibility gap.

In Chapters 4, 5 & 6 were foundational chapters, designed to validate the DFT framework in simple, well understood systems.

In Chapters 7 & 8, we used our basic model to understand fundamental thermodynamic quantities of enthalpy and entropy changes in the absorption process. In particular, we were interested in modeling excess enthalpy and excess entropy and based on those results, we were able to gain some understanding of the accessible microstates associated with the absorption of hydrogen into metal lattice. As a result we made some model modifications to account for clumping in the miscibility gap, and also attempted to understand the electronic contribution to entropy from a first principles view.

The question at hand, therefore, is whether we can put together a model that encompasses all of the above model elements. Since we now have a good understanding of the different components of the physics of the problem, the hope is that we can include any corrections *a priori* in the model formulation, instead of after-the-fact like we have been doing. For example, instead of starting our model with an approximate statistical model, deriving the Gibbs energy from it, and using experiment to determine the amount of correction, we would like to include the correction terms explicitly in the statistical mechanical formulation.

Based on our understanding of the accessible microstates reduction, we also would like to further explore our clumped model in the miscibility gap, except that, instead of choosing a clumping

factor, we will instead make it a function of the model temperature. As a result, we hope to phenomenologically determine enthalpies that were heretofore obscured by the miscibility gap.

We attempt a model below.

An Improved Statistical Model

The model we attempt to build has the following components:

(1) Octahedral and tetrahedral site occupations are modeled as in Chapter 2.

(2) Interaction energy corrections are added phenomenologically to the model, not as *a posteriori* experimental fit.

(3) We include hydrogen clustering or "clumping" as a third occupation type, by defining a "Clumped Occupation".

(4) We make the clumping occupation temperature dependent.

(5) We include electronic contributions to the partition function, in singlets for the clumped configuration, and doublets for the octahedral or tetrahedral occupations.

(6) We will need to model clumping, by making clumping factor a parameter in the model.

With view to these considerations, and Equation 38 of Chapter 2, therefore, we can write the partition function of the improved model as

$$Z_H(\tau,\mu) = \sum_{n_c}\sum_{n_t}\sum_{n_{nc}}\sum_{ASN} e^{\frac{(n_o+n_t+n_c)\mu-\varepsilon_h(n_o,n_t,n_c)}{\tau}} z_o^{n_{nc}} z_t^{n_t} z_c^{n_c} z_{e,o}^{n_o} z_{e,t}^{n_t} z_{e,c}^{n_c} \qquad 392$$

In Equation **392**,

n_{nc} is the number of hydrogen atoms distributed among N_{nc} available non-clumped sites (see below),

n_t is the number of hydrogen atoms distributed among N_t available tetrahedral sites,

n_c is the corresponding number of particles in "clumped" sites. A clumped site is a cluster of sites containing a total of γ hydrogen atoms. We assume only octahedral sites are clumped (see below),

γ is the clumping factor or tuple in the sense of Chapter 7,

$\varepsilon_h(n_{nc}, n_t, n_c)$ is the total interaction energy of the configuration having $n = n_{nc} + n_t + n_c$ hydrogen atoms, distributed among a total available interstitials sites $N = N_{nc} + N_t + N_c$,

N_o is the total number of octahedral sites, such that $N_o = N_{nc} + N_c$,

z_o is the hydrogen partition function when in an octahedral non-clumped site,

z_t is the hydrogen partition function when in an tetrahedral site,

z_c is the hydrogen partition function when in an octahedral "clumped" site,

$z_{e,o}$ is the electronic partition function for an octahedral site, which is a doublet, (degeneracy=2)

$z_{e,t}$ is the electronic partition function for an tetrahedral site, which is a also doublet, (degeneracy=2)

$z_{e,c}$ is the electronic partition function for an clumped site, which is a singlet (degeneracy=1), and

"ASN" means all configurations containing (n_{nc}, n_t, n_c) hydrogen atoms.

H Particle Count

To make some sense of Equation **392**, we need to make sure our particle count comes out correctly for the total number of hydrogen atoms at any particular configuration.

First, the total number of interstitial sites available is given by

$$N = N_{nc} + N_c + N_t \tag{393}$$

In other words, we are initially treating clumped configurations as a type of site, on the same footing as octahedral and tetrahedral interstitials.

One way to perform the count is to take the view that only sites of type octahedral will be clustered. This is certainly justified in light of our O-to-T excitation models in Chapter 2, and from experiment.

With this assumption, we may perform the count in Equation 392 as:

$$Z_H(\tau,\mu) = \sum_{n_{nc}=0}^{N_o} \sum_{n_c=0}^{N_o-n_{nc}} \sum_{n_t=0}^{N_t} \sum_{ASN} e^{\frac{(n_{nc}+n_t+n_c)\mu-\varepsilon_h(n_{nc},n_t,n_c)}{\tau}} z_o^{n_{nc}} z_t^{n_t} z_c^{n_c} z_{e,o}^{n_{nc}} z_{e,t}^{n_t} z_{e,c}^{n_c} \tag{394}$$

In Equation 394, we note that our count of the clumped sites is coupled with that of the non-clumped octahedral sites, making the partition function non-separable. The counts have been adjusted to make the summations over n_{nc} and n_c consistent with the total number of octahedral sites at any given loading level, such that, as above,

$$N_o = N_{nc} + N_c \tag{395}$$

Additionally, because of its coupled nature, Equation 394 is sufficiently foundational for what follows that a simple example may be in order to clarify the coupled nature of the summation. And because the tetrahedral sites summation has no coupling by assumption, we leave it out of the example, such that the summation we want to clarify is

$$Z'_H(\tau,\mu) = \sum_{n_{nc}=0}^{N_o} \sum_{n_c=0}^{N_o-n_{nc}} \sum_{ASN} (\cdots) \tag{396}$$

Note that we have left the configurational summation, "ASN", intact since it captures the statistical formalism at the core of our model.

An Example

Suppose that

$$N = 10 \tag{397}$$

Then, if we further suppose that, based on a self consistent determination (see below), the available octahedral and tetrahedral sites are apportioned as

$$N_o = N_{nc} + N_c = 9 \tag{398}$$

$$N_t = 1 \tag{399}$$

then, we may visualize the octahedral sites being loaded as follows, using Equations 396 & 398:

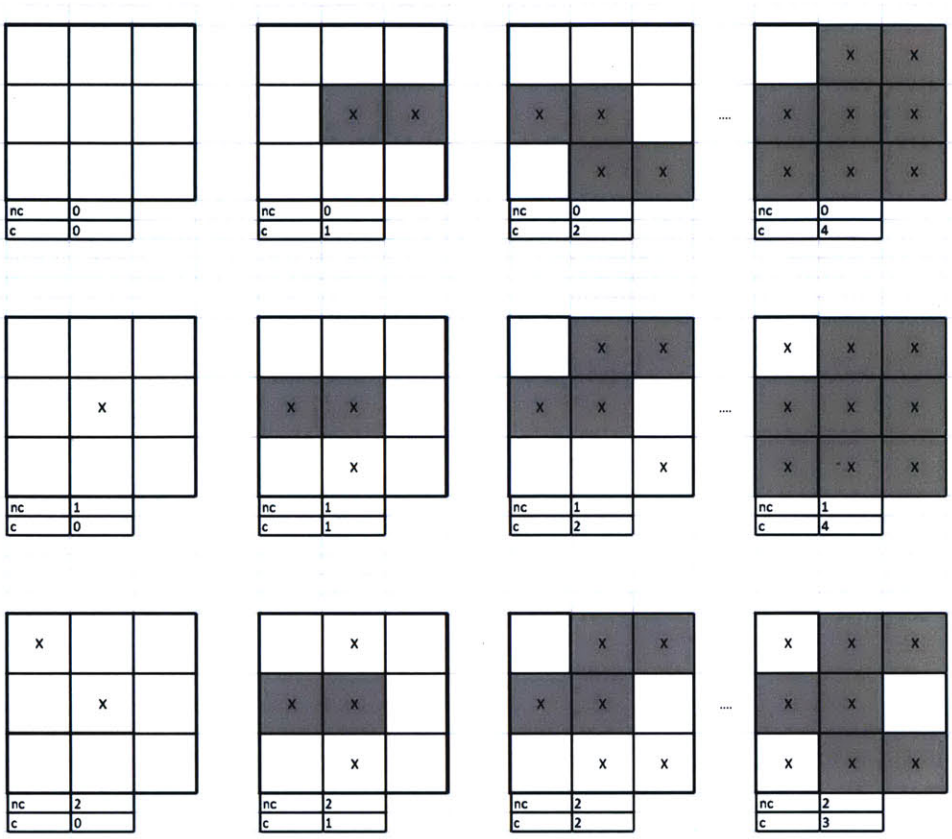

Figure 111: Example of coupled loading of clumped vs. non-clumped O-sites. c=clumped sites, nc=non-clumped and grey sites are clumped. Clumping factor=2 is shown. "ASN" means all arrangements having the same number of hydrogen atoms, preserving the clumps.

Another way to proceed is to perform a brute force count of the number of states suggested by Equation 396, and compare the results to the non-clumped case.

$$N_{States}(n) = \frac{N_o!}{n_{nc}!\,(N_o - n_{nc})!}\frac{(N_o - n_{nc})!}{n_c!\,(N_o - n_{nc} - n_c)!}\frac{N_t!}{n_t!\,(N_t - n_t)!} \quad 400$$

and its non-clumped approximation

$$N'_{States}(n) = \frac{N_o!}{n_o!\,(N_o - n_o)!}\frac{N_t!}{n_t!\,(N_t - n_t)!} \quad 401$$

The results below are shown for a particular value of $k = \frac{n_c}{\gamma} = 4$ since Equation 400 introduces a large number of configurations compared to Equation 401. In Equations 400 and 401, at each loading, we pick the configurations with the largest number of microstates, since that is the most likely configuration (Christensen, Stoltze, Jacobsen, & Norskov, 1990).

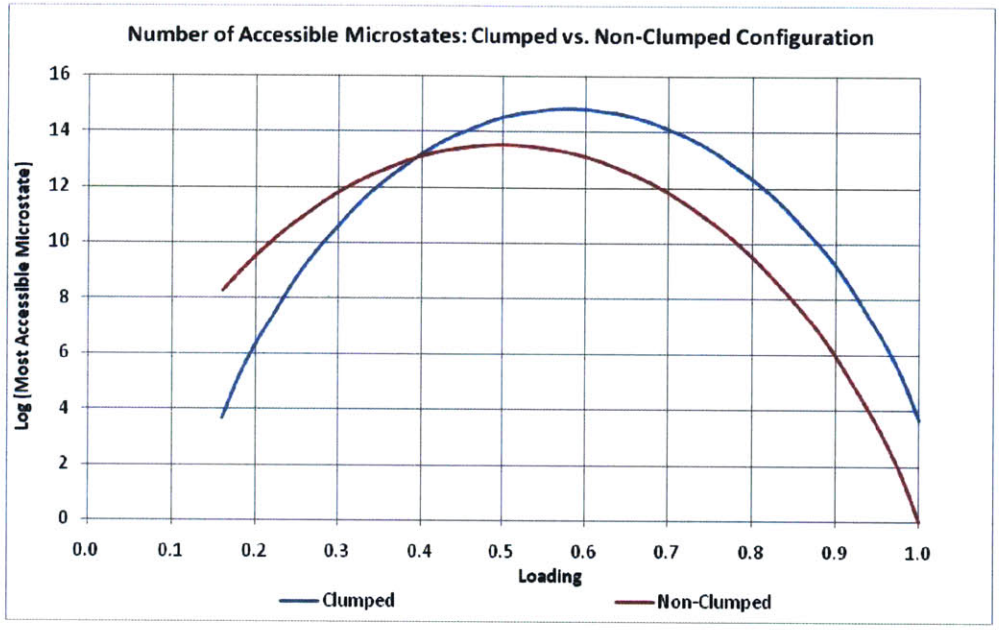

Figure 112: Number of microstates for a clumped vs. non-clumped configuration, as a function of loading

Equation 394 suggests that we need to do the summation of the clumped sites in another "integer space", say k, via a simple change of variables as in Chapter 7. This avoids any over-counting of the clumped states since Equation 396 assumes all integer values of the clumped states counter, n_c. Suppose:

$$k = \frac{n_c}{\gamma} \tag{402}$$

for some integer k. The result is that Equation 394 becomes,

$$Z_H(\tau,\mu) = \sum_{n_{nc}=0}^{N_o} \sum_{k=0}^{\frac{N_o-n_{nc}}{\gamma}} \sum_{n_t=0}^{N_t} \sum_{ASN} e^{\frac{(n_{nc}+n_t+k\gamma)\mu-\varepsilon_h(n_{nc},n_t,k\gamma)}{\tau}} Z_o^{n_{nc}} Z_t^{n_t} Z_c^{k\gamma} Z_{e,o}^{n_{nc}} Z_{e,t}^{n_t} Z_{e,c}^{k\gamma} \tag{403}$$

In Equation 403, the relative fractions of clumped versus non-clumped occupations is left to be determined consistently with the free parameters – see below. Equation 403 also makes it clear that

$$n = n_{nc} + n_t + k\gamma \tag{404}$$

Protium Particle Partition Function

For the protium partition functions of the non-clumped octahedral and tetrahedral sites, we use the harmonic approximation as before, (Chapter 2), including the zero point contribution,

$$z_o = z_t = \left(\sum_{n=0}^{\infty} e^{-\frac{\epsilon_{0v}\left(n+\frac{1}{2}\right)}{\tau}}\right)^3 = \left(e^{-\frac{\epsilon_{0v}}{2\tau}}\sum_{n=0}^{\infty} e^{-\frac{\epsilon_{0v}n}{\tau}}\right)^3 = \left(\frac{e^{-\frac{\epsilon_{0v}}{2\tau}}}{1-e^{-\frac{\epsilon_{0v}}{\tau}}}\right)^3 = \left(2sinh\frac{\epsilon_{0v}}{2\tau}\right)^{-3} \tag{405}$$

Clumped Binding Energy Contribution

In the clumped configuration, we propose that clustering has the effect of lowering the overall configurational energy. We may therefore define a binding energy that represents the difference between the completely random configuration and the clumped case, keeping in mind that each bulk configuration is referenced against the free gas. This energy is NOT accessible from our DFT model, so we have to make it a free parameter that is a function of loading.

We depict this binding energy conceptually below, where the "clumped" configuration binding energy is defined to depend on overall loading as follows:

$$E^c_{Bind}(n) = \Delta\varepsilon_{Clump}(n) - \Delta\varepsilon_{Rand}(n) \tag{406}$$

and we note that Figure 113 below is simply a conjecture at this point.

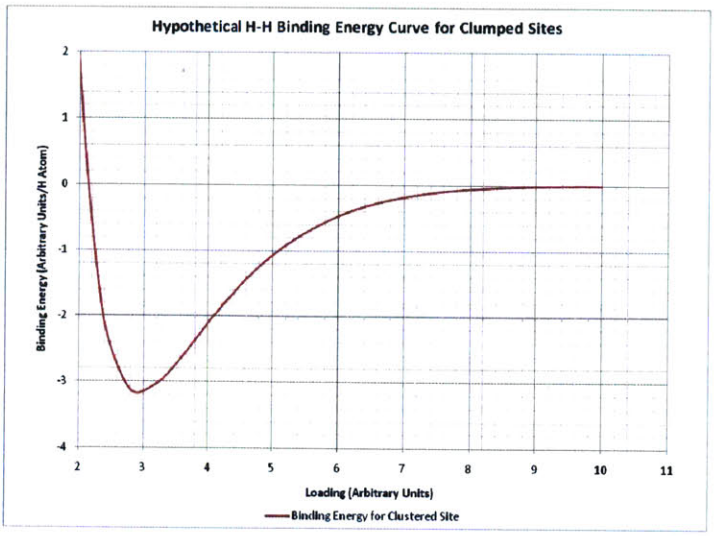

Figure 113: Depiction of Conjectured H-H Binding for Clumped Configuration

We may factor in this binding energy difference in the clumped configuration by adding an energy factor to the single particle partition function

$$z_c(n) = \left(\sum_{n=0}^{\infty} e^{-\frac{\epsilon_{0v}\left(n+\frac{1}{2}\right)}{\tau}}\right)^3 e^{-\frac{E_B^c(n)}{\tau}} \tag{407}$$

Because there are no excited states in clumped configuration, we take only the ground state in the SHO contribution to Equation 407. The SHO contribution is then, for all 3 modes,

$$z(n) = \left(\sum_{n=0}^{0} e^{-\frac{\epsilon_{0v}\left(n+\frac{1}{2}\right)}{\tau}}\right)^3 = \left(e^{-\frac{\epsilon_{0v}}{2\tau}}\right)^3 \tag{408}$$

Equation 407, the clumped partition function, is then

$$z_c(n) = e^{-\left(\frac{3\epsilon_{0v}}{2\tau} + \frac{E_B^c(n)}{\tau}\right)} \tag{409}$$

Electronic Contribution to the Partition Function

The electronic contribution to the partition function was previously derived in Chapter 7, Equation 357:

$$z_{e,o} = \sum_{j,e} g_j^o e^{-\frac{\varepsilon_{j,e,o}}{\kappa_B T}} \approx g_0^o \tag{410}$$

$$z_{e,t} = \sum_{j,e} g_j^t e^{-\frac{\varepsilon_{j,e,t}}{\kappa_B T}} \approx g_0^t \tag{411}$$

where the octahedral and tetrahedral electron contributions are taken to be a doublet, i.e.,

$$g_0^o = g_0^t = 2 \tag{412}$$

For the clumped case, the electronic configuration is a singlet, or,

$$z_{e,c} = \sum_{j,e} g_j^c e^{-\frac{\varepsilon_{j,e,c}}{\kappa_B T}} \approx g_0^c = 1 \tag{413}$$

Model "Free" Parameters

We have previously added DFT energy corrections to the model *a posteriori*. We now add these corrections phenomenologically to the model, thus:

$$\varepsilon_h(\theta) \rightarrow \varepsilon_h(\theta) + \varepsilon_\delta^0 + \varepsilon_\delta^1\theta + \varepsilon_\delta^2\theta^2 + \mathcal{O}(\theta^3) \tag{414}$$

This gives us three free parameters.

The other three parameters may be chosen to be the binding energy of the clumped configuration, $E_B^c(n)$, which we may chose to depend on the overall loading, thus:

$$E_B^c(\theta) \rightarrow \varepsilon_c^0 + \varepsilon_c^1\theta + \varepsilon_c^2\theta^2 + \mathcal{O}(\theta^3) \tag{415}$$

where θ is the overall bulk loading, and ε_c^i are constants to be determined based on experimental fit.

Overall Model

From the foregoing, we get the overall model as below

$$\sum_{n_{nc}=0}^{N_o} \sum_{k=0}^{\frac{N_o-n_{nc}}{\gamma}} \sum_{n_t=0}^{N_t} \sum_{ASN} e^{\frac{(n_{nc}+n_t+k\gamma)\mu-\varepsilon_h(n_{nc},n_t,k\gamma)}{\tau}} z_o^{n_{nc}} z_t^{n_t} z_c^{k\gamma} z_{e,o}^{n_{nc}} z_{e,t}^{n_t} z_{e,c}^{k\gamma} \tag{416}$$

We may simplify Equation 416 using Equations **409**-413, with,

$$z_{o,t} \equiv z_o = z_t = \left(2sinh\frac{\epsilon_{0v}}{2\tau}\right)^{-3} \tag{417}$$

and

$$g_{o,t} \equiv z_{e,o} = z_{e,t} = g_0^o = g_0^t = 2 \tag{418}$$

such that

$$Z_H(\tau,\mu) = \sum_{n_{nc}=0}^{N_o} \sum_{k=0}^{\frac{N_o-n_{nc}}{\gamma}} \sum_{n_t=0}^{N_t} \sum_{ASN} e^{\frac{(n_{nc}+n_t+k\gamma)\mu-\varepsilon_h(n_{nc},n_t,k\gamma)}{\tau}} z_{o,t}^{\,n_{nc}+n_t} z_c^{\,k\gamma} g_{o,t}^{\,n_{nc}+n_t} \tag{419}$$

For the moment, we will assume that we can use Bragg-Williams approximation, where such an approximation would be consistent with the earlier, simpler models. We write Equation 419 as

$$Z_H(\tau,\mu) \cong \frac{N_o!}{n_{nc}!\,(N_o-n_{nc})!} \frac{\left(\frac{N_o-n_{nc}}{\gamma}\right)!}{k!\left(\frac{N_o-n_{nc}}{\gamma}-k\right)!} \frac{N_t!}{n_t!\,(N_t-n_t)!} e^{\frac{(n_{nc}+n_t+k\gamma)\varepsilon_h(n_{nc},n_t,k\gamma)}{\tau}} z_{o,t}^{\,n_{nc}+n_t} g_{o,t}^{\,n_{nc}+n_t} z_c^{\,k\gamma} \tag{420}$$

Paralleling earlier analysis, we make the argument that each site, regardless of its type, has the same chemical potential. If that were not true, then particles would be expected to build up in sites with lower chemical potential, something that does not happen physically. Therefore,

$$\mu_c(\tau,n_c,n_{nc},n_t) = \mu_{nc}(\tau,n_c,n_{nc},n_t) = \mu_t(\tau,n_c,n_{nc},n_t) \tag{421}$$

for clumped octahedral, non-clumped octahedral and tetrahedral site chemical potentials, respectively.

Clumped Chemical Potential

These chemical potential terms are

$$\mu_c(\tau,n) = -\tau\frac{\partial}{\partial n_c}\Bigg\{ln\frac{N_o!}{n_{nc}!\,(N_o-n_{nc})!} + ln\frac{\left(\frac{N_o-n_{nc}}{\gamma}\right)!}{k!\left(\frac{N_o-n_{nc}-k\gamma}{\gamma}\right)!} + ln\frac{N_t!}{n_t!\,(N_t-n_t)!}$$

$$-\frac{(n_{nc}+n_t+k\gamma)\varepsilon_h(n_{nc},n_t,k\gamma)}{\tau} + (n_{nc}+n_t)ln(z_{o,t}) + (n_{nc}+n_t)ln(g_{o,t})$$

$$+k\gamma\,ln(z_c)\Bigg\} = -\tau\frac{\partial}{\partial n_c}\{T_1+T_2+T_3+T_4+T_5+T_6+T_7\}$$

422

and similarly for μ_{nc} and μ_t.

In previous chapters, we have simplified Equation 422 using the Stirling approximation. We will do so again here:

$$ln(x!) \cong \frac{1}{2}ln(2\pi) + \left(x+\frac{1}{2}\right)ln(x) - x$$

423

The results are, after some algebra,

$$T_1 = ln\frac{N_o!}{n_{nc}!\,(N_o-n_{nc})!} = ln\,N_o! - ln\,n_{nc}! - ln(N_o-n_{nc})!$$

$$\cong \left[\frac{1}{2}ln(2\pi) + \left(N_o+\frac{1}{2}\right)ln\,N_o - N_o\right] - \left[\frac{1}{2}ln(2\pi) + \left(n_{nc}+\frac{1}{2}\right)ln(n_{nc}) - n_{nc}\right]$$

$$-\left[\frac{1}{2}ln(2\pi) + \left(N_o-n_{nc}+\frac{1}{2}\right)ln(N_o-n_{nc}) - N_o + n_{nc}\right]$$

424

and

$$\frac{\partial}{\partial n_c} T_1 = \frac{1}{\gamma}\frac{\partial}{\partial k} T_1 = 0$$

425

Similarly, the other terms and their partial derivatives are

$$T_2 = ln\frac{\left(\frac{N_o - n_{nc}}{\gamma}\right)!}{k!\left(\frac{N_o - n_{nc} - k\gamma}{\gamma}\right)!} = ln\frac{N_o - n_{nc}}{\gamma}! - ln\,k! - ln\frac{N_o - n_{nc} - k\gamma}{\gamma}!$$

$$\cong \left[\frac{1}{2}ln(2\pi) + \left(\frac{N_o - n_{nc}}{\gamma} + \frac{1}{2}\right)ln\frac{N_o - n_{nc}}{\gamma} - \frac{N_o - n_{nc}}{\gamma}\right] - \left[\frac{1}{2}ln(2\pi) + \left(k + \frac{1}{2}\right)ln\,k - k\right]$$

$$- \left[\frac{1}{2}ln(2\pi) + \left(\frac{N_o - n_{nc} - k\gamma}{\gamma} + \frac{1}{2}\right)ln\frac{N_o - n_{nc} - k\gamma}{\gamma} - \frac{N_o - n_{nc} - k\gamma}{\gamma}\right]$$

426

$$\frac{\partial}{\partial n_c} T_2 = \frac{1}{\gamma}\frac{\partial}{\partial k} T_2 = \frac{1}{\gamma}\left\{-\left[\left(k + \frac{1}{2}\right)\frac{1}{k} + ln\,k - 1\right]\right.$$

$$\left. - \left[-\left(\frac{N_o - n_{nc} - k\gamma}{\gamma} + \frac{1}{2}\right)\frac{\gamma}{N_o - n_{nc} - k\gamma} - ln\frac{N_o - n_{nc} - k\gamma}{\gamma} + 1\right]\right\}$$

$$= \frac{1}{\gamma}\left\{-\left[\frac{1}{2k} + ln\,k\right] + \left[\frac{1}{2}\frac{\gamma}{N_o - n_{nc} - k\gamma} + ln\frac{N_o - n_{nc} - k\gamma}{\gamma}\right]\right\}$$

427

$$T_3 = ln\left(\frac{N_t!}{n_t!\,(N_t - n_t)!}\right) = lnN_t! - ln\,n_t! - ln(N_t - n_t)!!$$

$$\cong ln(2\pi) + \left(N_t + \frac{1}{2}\right)ln(N_t) - (N_t) - \left[ln(2\pi) + \left(n_t + \frac{1}{2}\right)ln\;n_t - n_t\right]$$

$$- \left[ln(2\pi) + \left(N_t - n_t + \frac{1}{2}\right)ln(N_t - n_t) - (N_t - n_t)\right]$$

428

$$\frac{\partial}{\partial n_c} T_3 = 0$$

429

$$T_4 = -\frac{(n_{nc} + n_t + k\gamma)\varepsilon_h(n_{nc}, n_t, k\gamma)}{\tau} \tag{430}$$

$$\frac{\partial}{\partial n_c} T_4 = \frac{1}{\gamma}\frac{\partial}{\partial k} T_4 = -\frac{1}{\gamma\tau}\left((n_{nc} + n_t + k\gamma)\frac{\partial}{\partial k}\varepsilon_h(n_{nc}, n_t, k\gamma) + \gamma\varepsilon_h(n_{nc}, n_t, k\gamma)\right) \tag{431}$$

$$T_5 = (n_{nc} + n_t) ln(z_{o,t}) \tag{432}$$

$$\frac{\partial}{\partial n_c} T_5 = 0 \tag{433}$$

$$T_6 = (n_{nc} + n_t) ln(g_{o,t}) \tag{434}$$

$$\frac{\partial}{\partial n_c} T_6 = 0 \tag{435}$$

$$T_7 = k\gamma\, ln(z_c) = k\gamma\, ln\left(e^{-\left(\frac{3\epsilon_{0v}}{2\tau} + \frac{E_B^c(n)}{\tau}\right)}\right) = -\frac{k\gamma}{\tau}\left(\frac{3}{2}\epsilon_{0v} + E_B^c(n)\right) \tag{436}$$

$$\frac{\partial}{\partial n_c} T_7 = \frac{1}{\gamma}\frac{\partial}{\partial k} T_7 = -\frac{1}{\tau}\left(k\frac{\partial}{\partial k}E_B^c(n) + \frac{3}{2}\epsilon_{0v} + E_B^c(n)\right) \tag{437}$$

Collecting the terms

$$-\frac{\mu_c(\tau,n)}{\tau}=\frac{\partial}{\partial n_c}\{T_1+T_2+T_3+T_4+T_5+T_6+T_7\}$$

$$=\frac{1}{\gamma}\left\{-\left[\frac{1}{2k}+ln\,k\right]+\left[\frac{1}{2}\frac{\gamma}{N_o-n_{nc}-k\gamma}+ln\frac{N_o-n_{nc}-k\gamma}{\gamma}\right]\right\}$$

$$-\frac{1}{\gamma\tau}\left((n_{nc}+n_t+k\gamma)\frac{\partial}{\partial k}\varepsilon_h(n_{nc},n_t,k\gamma)+\gamma\varepsilon_h(n_{nc},n_t,k\gamma)\right)$$

$$-\frac{1}{\tau}\left(k\frac{\partial}{\partial k}E_B^c(n)+\frac{3}{2}\epsilon_{0v}+E_B^c(n)\right)$$

438

We first approximate Equation 438 by dropping terms that are considered "small" - N_o^{-1}, n_o^{-1}, etc, in line with prior chapters. Thus,

$$-\frac{\mu_c(\tau,n)}{\tau}\cong-\frac{1}{\gamma}l\,n(k)+\frac{1}{\gamma}ln\frac{N_o-n_{nc}-k\gamma}{\gamma}$$

$$-\frac{1}{\gamma\tau}\left((n_{nc}+n_t+k\gamma)\frac{\partial}{\partial k}\varepsilon_h(n_{nc},n_t,k\gamma)+\gamma\varepsilon_h(n_{nc},n_t,k\gamma)\right)$$

$$-\frac{1}{\tau}\left(k\frac{\partial}{\partial k}E_B^c(n)+\frac{3}{2}\epsilon_{0v}+E_B^c(n)\right)$$

439

or

$$\mu_c(\tau,n)\cong\frac{\tau}{\gamma}l\,n(k)-\frac{\tau}{\gamma}ln\frac{N_o-n_{nc}-k\gamma}{\gamma}+\frac{1}{\gamma}\left((n_{nc}+n_t+k\gamma)\frac{\partial}{\partial k}\varepsilon_h(n_{nc},n_t,k\gamma)+\gamma\varepsilon_h(n_{nc},n_t,k\gamma)\right)$$

$$+\left(k\frac{\partial}{\partial k}E_B^c(n)+\frac{3}{2}\epsilon_{0v}+E_B^c(n)\right)$$

$$=\frac{\tau}{\gamma}l\,n\frac{k\gamma}{N_o-n_{nc}-k\gamma}+\frac{1}{\gamma}\left((n_{nc}+n_t+k\gamma)\frac{\partial}{\partial k}\varepsilon_h(n_{nc},n_t,k\gamma)+\gamma\varepsilon_h(n_{nc},n_t,k\gamma)\right)$$

$$+\left(k\frac{\partial}{\partial k}E_B^c(n)+\frac{3}{2}\epsilon_{0v}+E_B^c(n)\right)$$

440

If we define the fractional "clumped" loading and fractional non-clumped loading as, respectively,

$$\theta_c = \frac{k\gamma}{N} = \frac{n_c}{N} \tag{441}$$

$$\theta_{nc} = \frac{n_{nc}}{N} \tag{442}$$

Additionally, we define the following fractional loading terms,

$$\theta_t = \frac{n_t}{N} \tag{443}$$

$$\Theta_o = \frac{N_o}{N} \tag{444}$$

$$\Theta_t = \frac{N_t}{N} \tag{445}$$

$$\theta = \frac{n}{N} \tag{446}$$

then Equation 440 may be written as, after making the change from $k\gamma \rightarrow n_c$, $n_{nc} + n_t + k\gamma \rightarrow n$, etc.,

$$\mu_c(\tau,\theta) = \frac{\tau}{\gamma} ln \frac{\theta_c}{\Theta_o - \theta_{nc} - \theta_c} + \frac{1}{\gamma}\left((n_{nc} + n_t + k\gamma)\gamma \frac{\partial}{\partial n_c}\varepsilon_h(n) + \gamma\varepsilon_h(n_{nc}, n_t, k\gamma)\right)$$

$$+\left(k\gamma \frac{\partial}{\partial n_c} E_B^c(n) + \frac{3}{2}\epsilon_{0v} + E_B^c(n)\right)$$

$$= \frac{\tau}{\gamma} ln \frac{\theta_c}{\Theta_o - \theta_{nc} - \theta_c} + \left((n_{nc} + n_t + n_c)\frac{\partial}{\partial n}\varepsilon_h(n)\frac{\partial n}{\partial n_c} + \varepsilon_h(n_{nc}, n_t, n_c)\right)$$

$$+\left(n_c \frac{\partial}{\partial n} E_B^c(n)\frac{\partial n}{\partial n_c} + \frac{3}{2}\epsilon_{0v} + E_B^c(n)\right)$$

$$= \frac{\tau}{\gamma} ln \frac{\theta_c}{\Theta_o - \theta_{nc} - \theta_c} + \left(\theta \frac{\partial}{\partial \theta}\varepsilon_h(\theta) + \varepsilon_h(\theta)\right) + \left(\theta_c \frac{\partial}{\partial \theta} E_B^c(\theta) + \frac{3}{2}\epsilon_{0v} + E_B^c(\theta)\right)$$

447

The final result is quite simple:

$$\boldsymbol{\mu_c(\tau,\theta) = \frac{\tau}{\gamma} ln \frac{\theta_c}{\Theta_o - \theta_o} + \theta \frac{\partial}{\partial \theta}\varepsilon_h(\theta) + \varepsilon_h(\theta) + \theta_c \frac{\partial}{\partial \theta} E_B^c(\theta) + \frac{3}{2}\epsilon_{0v} + E_B^c(\theta)}$$

448

where we have used $\boldsymbol{\theta_o = \theta_{nc} + \theta_c}$.

Equation 448 is certainly of the right form based on earlier results from Chapter 2, with entropic terms, energy terms and energy slope terms.

Non-Clumped Chemical Potential

For the non clumped sites, we proceed similarly,

$$\frac{\partial}{\partial n_{nc}}T_1 = -\left[\left(n_{nc}+\frac{1}{2}\right)\frac{1}{n_{nc}} + ln(n_{nc}) - 1\right] - \left[-\left(N_o - n_{nc}+\frac{1}{2}\right)\frac{1}{N_o - n_{nc}} - ln(N_o - n_{nc}) + 1\right]$$

$$= -\left[\frac{1}{2n_{nc}} + ln(n_{nc})\right] + \left[\frac{1}{2}\frac{1}{N_o - n_{nc}} + ln(N_o - n_{nc})\right]$$

449

$$\frac{\partial}{\partial n_{nc}}T_2 = \frac{1}{\gamma}\left[-\left(\frac{N_o - n_{nc}}{\gamma}+\frac{1}{2}\right)\frac{\gamma}{N_o - n_{nc}} - ln\frac{N_o - n_{nc}}{\gamma} + 1\right]$$

$$-\frac{1}{\gamma}\left[-\left(\frac{N_o - n_{nc} - k\gamma}{\gamma}+\frac{1}{2}\right)\frac{\gamma}{N_o - n_{nc} - k\gamma} - ln\frac{N_o - n_{nc} - k\gamma}{\gamma} + 1\right]$$

$$= -\frac{1}{\gamma}\left[\frac{1}{2}\frac{\gamma}{N_o - n_{nc}} + ln\frac{N_o - n_{nc}}{\gamma}\right] + \frac{1}{\gamma}\left[\frac{1}{2}\frac{\gamma}{N_o - n_{nc} - k\gamma} + ln\frac{N_o - n_{nc} - k\gamma}{\gamma}\right]$$

450

$$\frac{\partial}{\partial n_{nc}}T_3 = 0$$

451

$$\frac{\partial}{\partial n_{nc}}T_4 = -\frac{1}{\tau}\left\{(n_{nc} + n_t + k\gamma)\frac{\partial}{\partial n_{nc}}\varepsilon_h(n) + \varepsilon_h(n)\right\} = -\frac{1}{\tau}\left[n\frac{\partial}{\partial n_{nc}}\varepsilon_h(n) + \varepsilon_h(n)\right]$$

452

$$\frac{\partial}{\partial n_{nc}}T_5 = ln(z_{o,t})$$

453

$$\frac{\partial}{\partial n_{nc}}T_6 = ln(g_{o,t})$$

454

$$\frac{\partial}{\partial n_{nc}} T_7 = -\frac{n_c}{\tau} \frac{\partial}{\partial n_{nc}} E_B^c(n)$$

455

The result, after dropping "small" terms, is

$$-\frac{\mu_{nc}(\tau, n)}{\tau} = \frac{\partial}{\partial n_c}\{T_1 + T_2 + T_3 + T_4 + T_5 + T_6 + T_7\}$$

$$\cong -ln(n_{nc}) + ln(N_o - n_{nc}) - \frac{1}{\gamma} ln \frac{N_o - n_{nc}}{\gamma} + \frac{1}{\gamma} ln \frac{N_o - n_{nc} - k\gamma}{\gamma}$$

$$-\frac{1}{\tau}\left[n \frac{\partial}{\partial n_{nc}} \varepsilon_h(n) + \varepsilon_h(n)\right] + ln(z_{o,t}) + ln(g_{o,t}) - \frac{n_c}{\tau} \frac{\partial}{\partial n_{nc}} E_B^c(n)$$

$$= -ln \frac{n_{nc}}{N_o - n_{nc}} - \frac{1}{\gamma} ln \frac{N_o - n_{nc}}{N_o - n_{nc} - k\gamma} - \frac{1}{\tau}\left[n \frac{\partial}{\partial n_{nc}} \varepsilon_h(n) + \varepsilon_h(n)\right] + ln(z_{o,t}) + ln(g_{o,t})$$

$$-\frac{n_c}{\tau} \frac{\partial}{\partial n_{nc}} E_B^c(n)$$

456

or

$$\mu_{nc}(\tau, n) \cong \tau\, ln \frac{n_{nc}}{N_o - n_{nc}} + \frac{\tau}{\gamma} ln \frac{N_o - n_{nc}}{N_o - n_{nc} - k\gamma} + \left[n \frac{\partial}{\partial n_{nc}} \varepsilon_h(n) + \varepsilon_h(n)\right] - \tau ln(z_{o,t}) - \tau ln(g_{o,t})$$

$$+ n_c \frac{\partial}{\partial n_{nc}} E_B^c(n)$$

457

In terms of fractional parameters,

$$\boldsymbol{\mu_{nc}(\tau, \theta) = \tau\, ln \frac{\theta_{nc}}{\theta_o - \theta_{nc}} + \frac{\tau}{\gamma} ln \frac{\theta_o - \theta_{nc}}{\theta_o - \theta_o} + \theta \frac{\partial}{\partial \theta} \varepsilon_h(\theta) + \varepsilon_h(\theta) - \tau\, lnz_{o,t} - \tau\, lng_{o,t} + \theta_c \frac{\partial}{\partial \theta} E_B^c(\theta)}$$

458

Tetrahedral Chemical Potential

Lastly,

$$\frac{\partial}{\partial n_t} T_1 = \frac{\partial}{\partial n_t} T_2 = 0 \tag{459}$$

$$\frac{\partial}{\partial n_t} T_3 = \left\{ -\left[\left(n_t + \frac{1}{2} \right) \frac{1}{n_t} + ln\ n_t - 1 \right] - \left[-\left(N_t - n_t + \frac{1}{2} \right) \frac{1}{N_t - n_t} - ln(N_t - n_t) + 1 \right] \right\}$$

$$= \left\{ -\left[\frac{1}{2n_t} + ln\ n_t \right] + \left[\frac{1}{2} \frac{1}{N_t - n_t} + ln(N_t - n_t) \right] \right\} \tag{460}$$

$$\frac{\partial}{\partial n_t} T_4 = -\frac{1}{\tau} \left\{ n \frac{\partial}{\partial n_t} \varepsilon_h(n) + \varepsilon_h(n) \right\} \tag{461}$$

$$\frac{\partial}{\partial n_t} T_5 = ln(z_{o,t}) \tag{462}$$

$$\frac{\partial}{\partial n_t} T_6 = ln(g_{o,t}) \tag{463}$$

$$\frac{\partial}{\partial n_t} T_7 = -\frac{n_c}{\tau} \frac{\partial}{\partial n_t} E_B^c(n) \tag{464}$$

The result is,

$$-\frac{\mu_t(\tau,n)}{\tau} \cong -\ln\, n_t + \ln(N_t - n_t) - \frac{1}{\tau}\left(n\frac{\partial}{\partial n_t}\varepsilon_h(n) + \varepsilon_h(n)\right) + \ln(z_{o,t}) + \ln(g_{o,t}) - \frac{n_c}{\tau}\frac{\partial}{\partial n_t}E_B^c(n)$$

465

or, including a summary of earlier results,

$$\boldsymbol{\mu_t(\tau,\theta) = \tau\, ln\frac{\theta_t}{\theta_t - \theta_t} + \theta\frac{\partial}{\partial\theta}\varepsilon_h(\theta) + \varepsilon_h(\theta) - \tau\, lnz_{o,t} - \tau\, lng_{o,t} + \theta_c\frac{\partial}{\partial\theta}E_B^c(\theta)}$$

466

$$\boldsymbol{\mu_{nc}(\tau,\theta) = \tau\, ln\frac{\theta_{nc}}{\theta_o - \theta_{nc}} + \frac{\tau}{\gamma}ln\frac{\theta_o - \theta_{nc}}{\theta_o - \theta_o} + \theta\frac{\partial}{\partial\theta}\varepsilon_h(\theta) + \varepsilon_h(\theta) - \tau\, lnz_{o,t} - \tau\, lng_{o,t} + \theta_c\frac{\partial}{\partial\theta}E_B^c(\theta)}$$

467

$$\boldsymbol{\mu_c(\tau,\theta) = \frac{\tau}{\gamma}ln\frac{\theta_c}{\theta_o - \theta_o} + \theta\frac{\partial}{\partial\theta}\varepsilon_h(\theta) + \varepsilon_h(\theta) + \theta_c\frac{\partial}{\partial\theta}E_B^c(\theta) + \frac{3}{2}\epsilon_{0v} + E_B^c(\theta)}$$

468

Constraints on Binding Energy Parameter: "Orondo Isotherm"

We may use Equations 466 and 467 to get a simple O-to-T excitation model as before – the prior results apply, as can be seen from here, noting that the binding energy and all the non-entropic terms cancel out.

Equating Equation 467 and 468, however, places a constraint on the binding energy, thus

$$\tau\, ln\frac{\theta_{nc}}{\Theta_o-\theta_{nc}}+\frac{\tau}{\gamma}ln\frac{\Theta_o-\theta_{nc}}{\Theta_o-\theta_o}-\frac{\tau}{\gamma}ln\frac{\theta_c}{\Theta_o-\theta_o}=\tau\, ln(z_{o,t})+\tau\, ln(g_{o,t})+\frac{3}{2}\epsilon_{0v}+E_B^c(\theta) \tag{469}$$

We may uncover a clumping isotherm form from Equation 469 if we start by rewriting it as

$$\frac{\theta_c^{\frac{1}{\gamma}}}{\theta_{nc}(\Theta_o-\theta_{nc})^{\frac{1-\gamma}{\gamma}}}=e^{-\left[ln(z_{o,t})+ln(g_{o,t})+\frac{1}{\tau}\left(\frac{3}{2}\epsilon_{0v}+E_B^c(\theta)\right)\right]} \tag{470}$$

We then write Equation 470 as

$$\frac{\theta_c}{\theta_{nc}{}^{\gamma}(\Theta_o-\theta_{nc})^{1-\gamma}}=\left(\frac{1}{z_{o,t}g_{o,t}}e^{-\frac{E_B^c(\theta)+\frac{3}{2}\epsilon_{0v}}{\kappa_B T}}\right)^{\gamma} \tag{471}$$

from which we arrive at the isotherm form

$$\frac{\theta_c}{\theta_{nc}{}^{\gamma}(\Theta_o-\theta_{nc})^{1-\gamma}}=\left(\frac{z_c^{n_c}}{z_o^{n_{nc}}}\frac{z_{e,c}^{n_c}}{z_{e,o}^{n_{nc}}}\right)^{\gamma} \tag{472}$$

From above, Equation 409,

$$z_c^{n_c}(n) = e^{-\left(\frac{3\epsilon_{0V}}{2\tau} + \frac{E_B^c(n)}{\tau}\right)} \tag{473}$$

and, from Equation 405,

$$z_o^{n_{nc}} = \left(\frac{e^{\frac{\epsilon_{0V}}{2\tau}}}{1 - e^{-\frac{\epsilon_{0V}}{\tau}}}\right)^3 \tag{474}$$

Additionally, from Equation 413, and Equations 411 and 412, respectively,

$$z_{e,c}^{n_c} = \sum_{j,e} g_j^c e^{-\frac{\varepsilon_{j,e,c}}{K_B T}} \approx g_0^c = 1 \tag{475}$$

$$z_{e,o}^{n_{nc}} = \sum_{j,e} g_j^t e^{-\frac{\varepsilon_{j,e,t}}{K_B T}} \approx g_0^t \tag{476}$$

$$g_0^o = g_0^t = 2 \tag{477}$$

such that Equation 471 becomes

$$\frac{\theta_c}{{\theta_{nc}}^{\gamma}(\Theta_o - \theta_{nc})^{1-\gamma}} = \left(\frac{e^{-\left(\frac{3\epsilon_{0V}}{2\tau} + \frac{E_B^c(n)}{\tau}\right)}}{\left(\frac{e^{\frac{\epsilon_{0V}}{2\tau}}}{1 - e^{-\frac{\epsilon_{0V}}{\tau}}}\right)^3 \frac{1}{2}}\right)^{\gamma} \tag{478}$$

Simplifying

$$\frac{\theta_c}{\theta_{nc}{}^{\gamma}(\Theta_o - \theta_{nc})^{1-\gamma}} = \left(\frac{e^{-\frac{3\epsilon_{0V}}{2\tau}}}{\left(\frac{e^{-\frac{\epsilon_{0V}}{2\tau}}}{1-e^{-\frac{\epsilon_{0V}}{\tau}}}\right)^3} \frac{1}{2} e^{-\frac{E_B^c(n)}{\tau}} \right)^{\gamma}$$

479

Finally,

$$\frac{\boldsymbol{\theta_c}}{\boldsymbol{\theta_{nc}{}^{\gamma}(\Theta_o - \theta_{nc})^{1-\gamma}}} = \frac{\mathbf{1}}{\mathbf{2^{\gamma}}} \left(\mathbf{1} - e^{-\frac{\epsilon_{0V}}{\kappa_B T}}\right)^{3\gamma} e^{-\gamma \frac{E_B^c(n)}{\kappa_B T}}$$

480

To find the range of values that θ_c may assume in Equation 480, we require that the denominator never vanishes. To this end, $(\Theta_o - \theta_{nc})^{1-\gamma}$ is always positive, so the requirement of $\theta_{nc} \neq 0$ is such that, based on physical considerations, $\theta_{nc} > 0$, or

$$\theta_c < \theta_o$$

481

Equation 480 is an isotherm that determines the fractional clumping for a given binding energy. We call it the "Orondo Isotherm" since, to our knowledge, and despite its simplicity, this is the first time anyone has ever derived it.

Continuity Condition, Full Model

The full model continuity condition, using Equation 467 or 468, with Equation 480,

$$\frac{\tau}{\gamma} ln \frac{\theta_c}{\theta_o - \theta_o} + \theta \frac{\partial}{\partial \theta} \varepsilon_h(\theta) + \varepsilon_h(\theta) + \theta_c \frac{\partial}{\partial \theta} E_B^c(\theta) + \frac{3}{2} \epsilon_{0v} + E_B^c(\theta)$$

$$= -\frac{\tau}{2} \left[ln \left[\left(\frac{2\pi m \tau}{h^2} \right)^{\frac{3}{2}} \frac{\tau}{f} \right] + ln \frac{e^{\frac{\epsilon_{0v}}{2\tau}}}{1 - e^{-\frac{\epsilon_{0v}}{\tau}}} + ln \frac{8\pi^2 I \tau}{\sigma h^2} + \frac{\epsilon_D}{\tau} \right] \quad 482$$

or

$$f(\tau, \theta) = A(\tau) e^{\frac{B(\tau,\theta)}{\tau}} \quad 483$$

with

$$A(\tau) = \tau \left(\frac{2\pi m \tau}{h^2} \right)^{\frac{3}{2}} \quad 484$$

and

$$B(\tau, \theta) = \left[2 \left(\frac{\tau}{\gamma} ln \frac{\theta_c}{\theta_o - \theta_o} + \theta \frac{\partial}{\partial \theta} \varepsilon_h(\theta) + \varepsilon_h(\theta) + \theta_c \frac{\partial}{\partial \theta} E_B^c(\theta) + \frac{3}{2} \epsilon_{0v} + E_B^c(\theta) \right) + \tau ln \frac{e^{\frac{\epsilon_{0v}}{2\tau}}}{1 - e^{-\frac{\epsilon_{0v}}{\tau}}} \right.$$

$$\left. + \tau ln \frac{8\pi^2 I \tau}{\sigma h^2} + \epsilon_D \right] \quad 485$$

Simplifying Equation 485, using

$$\frac{e^{-\frac{\epsilon_{0v}}{2\tau}}}{1-e^{-\frac{\epsilon_{0v}}{\tau}}} = \left(2sinh\frac{\epsilon_{0v}}{2\tau}\right)^{-1}$$

486

we get

$$B(\theta,T) = \left[\frac{2\kappa_B T}{\gamma} ln\frac{\theta_c}{\Theta_o-\theta_o} + 2\left(\theta\frac{\partial}{\partial\theta}\varepsilon_h(\theta)+\varepsilon_h(\theta)\right) + 2\left(\theta_c\frac{\partial}{\partial\theta}E_B^c(\theta)+E_B^c(\theta)\right) + 3\epsilon_{0v}\right.$$
$$\left. - \kappa_B T\, ln\left(2sinh\frac{\epsilon_{0v}}{2\kappa_B T}\right) + \kappa_B T\, ln\frac{8\pi^2 I\kappa_B T}{\sigma h^2} + \epsilon_D\right]$$

487

Substituting for model parameters, Equations 414 & 415, we get

$$B(\theta,T) = \left[\frac{2\kappa_B T}{\gamma} ln\frac{\theta_c}{\Theta_o-\theta_o} + 2\left(\theta\frac{\partial}{\partial\theta}[\varepsilon_h(\theta)+\varepsilon_\delta^0+\varepsilon_\delta^1\theta+\varepsilon_\delta^2\theta^2] + [\varepsilon_h(\theta)+\varepsilon_\delta^0+\varepsilon_\delta^1\theta+\varepsilon_\delta^2\theta^2]\right)\right.$$
$$+ 2\left(\theta_c\frac{\partial}{\partial\theta}[\varepsilon_c^0+\varepsilon_c^1\theta+\varepsilon_c^2\theta^2] + [\varepsilon_c^0+\varepsilon_c^1\theta+\varepsilon_c^2\theta^2]\right) + 3\epsilon_{0v} - \kappa_B T\, ln\left(2sinh\frac{\epsilon_{0v}}{2\kappa_B T}\right)$$
$$\left. + \kappa_B T\, ln\frac{8\pi^2 I\kappa_B T}{\sigma h^2} + \epsilon_D\right]$$
$$= \frac{2\kappa_B T}{\gamma} ln\frac{\theta_c}{\Theta_o-\theta_o} + 2\left(\theta\frac{\partial}{\partial\theta}\varepsilon_h(\theta)+\varepsilon_h(\theta)+\varepsilon_\delta^0+2\varepsilon_\delta^1\theta+3\varepsilon_\delta^2\theta^2\right)$$
$$+ 2[\varepsilon_c^0+\varepsilon_c^1(\theta_c+\theta)+\varepsilon_c^2(2\theta_c\theta+\theta^2)] + 3\epsilon_{0v} - \kappa_B T ln\left(2sinh\frac{\epsilon_{0v}}{2\kappa_B T}\right) + \kappa_B T ln\frac{8\pi^2 I\kappa_B T}{\sigma h^2}$$
$$+ \epsilon_D$$

488

Excess Molar Enthalpy

We derive the excess molar quantities as before, Chapter 7. Thus the excess Gibbs Energy is defined by

$$\Delta\bar{G}_H = \frac{1}{2}RTln\,(f_{H_2}) \tag{489}$$

$$\Delta\bar{G}_H = \bar{G}_H^{Ideal} + \Delta\bar{G}_H^{Excess} \tag{490}$$

where we use previous definition of the ideal Gibbs energy in the non-clumped model

$$\bar{G}_H^{Ideal} = RTln\frac{\theta}{1-\theta} \tag{491}$$

The excess enthalpy change is then

$$\Delta\bar{H}_H^E = -T^2\left(\frac{\partial\left(\frac{\Delta\bar{G}_H^E}{T}\right)}{\partial T}\right)_{P,n} \tag{492}$$

Using Equations 483, 484, 488 & 489, we get

$$\Delta\bar{G}_H(\theta,T) = \frac{1}{2}RT\,ln\left(A(T) * e^{\frac{B(\theta,T)}{\kappa_B T}}\right) = \frac{1}{2}RT\left[lnA(T) + \frac{B(\theta,T)}{\kappa_B T}\right]$$

$$\begin{aligned}\Delta\bar{G}_H(\theta,T) = {} & \frac{RT}{2}lnA(T) + \frac{RT}{\gamma}ln\frac{\theta_c}{\Theta_o-\theta_o} + \frac{R}{\kappa_B}\left(\theta\frac{\partial}{\partial\theta}\varepsilon_h(\theta) + \varepsilon_h(\theta) + \varepsilon_\delta^0 + 2\varepsilon_\delta^1\theta + 3\varepsilon_\delta^2\theta^2\right) \\ & + \frac{R}{\kappa_B}[\varepsilon_c^0 + \varepsilon_c^1(\theta_c+\theta) + \varepsilon_c^2(2\theta_c\theta+\theta^2)] + \frac{3R}{2\kappa_B}\epsilon_{0v} - \frac{RT}{2}ln\left(2sinh\,\frac{\epsilon_{0v}}{2\kappa_B T}\right) \\ & + \frac{RT}{2}ln\frac{8\pi^2 I\kappa_B T}{\sigma h^2} + \frac{1}{2}\frac{R}{\kappa_B}\epsilon_D\end{aligned}$$

493

and therefore, the excess molar Gibbs Energy is

$$\begin{aligned}\Delta\bar{G}_H^E(\theta,T) = {} & \frac{RT}{2}lnA(T) + \frac{RT}{\gamma}ln\frac{\theta_c}{\Theta_o-\theta_o} + \frac{R}{\kappa_B}\left(\theta\frac{\partial}{\partial\theta}\varepsilon_h(\theta) + \varepsilon_h(\theta) + \varepsilon_\delta^0 + 2\varepsilon_\delta^1\theta + 3\varepsilon_\delta^2\theta^2\right) \\ & + \frac{R}{\kappa_B}[\varepsilon_c^0 + \varepsilon_c^1(\theta_c+\theta) + \varepsilon_c^2(2\theta_c\theta+\theta^2)] + \frac{3R}{2\kappa_B}\epsilon_{0v} - \frac{RT}{2}ln\left(2sinh\,\frac{\epsilon_{0v}}{2\kappa_B T}\right) \\ & + \frac{RT}{2}ln\frac{8\pi^2 I\kappa_B T}{\sigma h^2} + \frac{1}{2}\frac{R}{\kappa_B}\epsilon_D - RTln\frac{\theta}{1-\theta}\end{aligned}$$

494

and

$$\begin{aligned}\frac{\Delta\bar{G}_H^E(\theta,T)}{T} \rightarrow {} & \frac{R}{2}lnA(T) + \frac{R}{\gamma}ln\frac{\theta_c}{\Theta_o-\theta_o} + \frac{R}{\kappa_B T}\left(\theta\frac{\partial}{\partial\theta}\varepsilon_h(\theta) + \varepsilon_h(\theta) + \varepsilon_\delta^0 + 2\varepsilon_\delta^1\theta + 3\varepsilon_\delta^2\theta^2\right) \\ & + \frac{R}{\kappa_B T}[\varepsilon_c^0 + \varepsilon_c^1(\theta_c+\theta) + \varepsilon_c^2(2\theta_c\theta+\theta^2)] + \frac{3R}{2\kappa_B T}\epsilon_{0v} - \frac{R}{2}ln\left(2sinh\,\frac{\epsilon_{0v}}{2\kappa_B T}\right) \\ & + \frac{R}{2}ln\frac{8\pi^2 I\kappa_B T}{\sigma h^2} + \frac{1}{2}\frac{R}{\kappa_B T}\epsilon_D - Rln\frac{\theta}{1-\theta}\end{aligned}$$

495

such that

$$\Delta\bar{H}_H^E(\theta,T) = -T^2\left(\frac{\partial\left(\frac{\Delta\bar{G}_H^E}{T}\right)}{\partial T}\right)_{P,n}$$

$$= -T^2\left(\frac{R}{2}\frac{A'(T)}{A(T)} - \frac{R}{\kappa_B T^2}\left(\theta\frac{\partial}{\partial\theta}\varepsilon_h(\theta) + \varepsilon_h(\theta) + \varepsilon_\delta^0 + 2\varepsilon_\delta^1\theta + 3\varepsilon_\delta^2\theta^2\right)\right.$$

$$- \frac{R}{\kappa_B T^2}[\varepsilon_c^0 + \varepsilon_c^1(\theta_c + \theta) + \varepsilon_c^2(2\theta_c\theta + \theta^2)] - \frac{3R}{2\kappa_B T^2}\epsilon_{0v} + \frac{R}{4}\frac{\epsilon_{0v}}{\kappa_B T^2}\coth\frac{\epsilon_{0v}}{2\kappa_B T} + \frac{R}{2T}$$

$$\left. - \frac{R}{2\kappa_B T^2}\epsilon_D\right)$$

496

or

$$\Delta\bar{H}_H^E(\boldsymbol{\theta},\boldsymbol{T}) = -\frac{\boldsymbol{RT^2}}{\boldsymbol{2}}\frac{\boldsymbol{A'(T)}}{\boldsymbol{A(T)}} + \frac{\boldsymbol{R}}{\boldsymbol{\kappa_B}}\left(\boldsymbol{\theta}\frac{\boldsymbol{\partial}}{\boldsymbol{\partial\theta}}\boldsymbol{\varepsilon_h(\theta)} + \boldsymbol{\varepsilon_h(\theta)} + \boldsymbol{\varepsilon_\delta^0} + \boldsymbol{2\varepsilon_\delta^1\theta} + \boldsymbol{3\varepsilon_\delta^2\theta^2}\right)$$

$$+ \frac{\boldsymbol{R}}{\boldsymbol{\kappa_B}}[\boldsymbol{\varepsilon_c^0} + \boldsymbol{\varepsilon_c^1}(\boldsymbol{\theta_c} + \boldsymbol{\theta}) + \boldsymbol{\varepsilon_c^2}(\boldsymbol{2\theta_c\theta} + \boldsymbol{\theta^2})] + \frac{\boldsymbol{3R}}{\boldsymbol{2\kappa_B}}\boldsymbol{\epsilon_{0v}} - \frac{\boldsymbol{R}}{\boldsymbol{4}}\frac{\boldsymbol{\epsilon_{0v}}}{\boldsymbol{\kappa_B}}\boldsymbol{\coth}\frac{\boldsymbol{\epsilon_{0v}}}{\boldsymbol{2\kappa_B T}} - \frac{\boldsymbol{RT}}{\boldsymbol{2}} + \frac{\boldsymbol{R}}{\boldsymbol{2\kappa_B}}\boldsymbol{\epsilon_D}$$

497

Finally,

$$\bar{H}_H^E = \Delta\bar{H}_H^E - \Delta\bar{H}_H^0$$

498

which completes the excess enthalpy model. Equations 497 and 300 need to be solved for the unknown parameters ε_δ^0, ε_δ^1, ε_δ^2, ε_c^0, ε_c^1 and ε_c^2.

Excess Molar Entropy

The excess molar entropy is

$$-\Delta\bar{S}_H = \left(\frac{\partial \Delta\bar{G}_H(\theta,T)}{\partial T}\right)_{P,n}$$

$$= \frac{RT}{2}\frac{A'(T)}{A(T)} + \frac{R}{2}lnA(T) + \frac{R}{\gamma}ln\frac{\theta_c}{\Theta_o - \theta_o} + \frac{1}{4}\frac{R\epsilon_{0v}}{\kappa_B T}coth\frac{\epsilon_{0v}}{2\kappa_B T} - \frac{R}{2}ln\left(2\,sinh\frac{\epsilon_{0v}}{2\kappa_B T}\right) + \frac{R}{2}$$

$$+ \frac{R}{2}ln\frac{8\pi^2 I\kappa_B T}{\sigma h^2}$$

$$-\Delta\bar{S}_H = \frac{RT}{2}\frac{A'(T)}{A(T)} + \frac{R}{2}lnA(T) + \frac{R}{\gamma}ln\frac{\theta_c}{\Theta_o - \theta_o} + \frac{1}{4}\frac{R\epsilon_{0v}}{\kappa_B T}coth\frac{\epsilon_{0v}}{2\kappa_B T} - \frac{R}{2}ln\left(2\,sinh\frac{\epsilon_{0v}}{2\kappa_B T}\right) + \frac{R}{2}$$

$$+ \frac{R}{2}ln\frac{8\pi^2 I\kappa_B T}{\sigma h^2} \qquad 499$$

and

$$\Delta\bar{S}_H^E = -\frac{RT}{2}\frac{A'(T)}{A(T)} - \frac{R}{2}lnA(T) - \frac{R}{\gamma}ln\frac{\theta_c}{\Theta_o - \theta_o} - \frac{1}{4}\frac{R\epsilon_{0v}}{\kappa_B T}coth\frac{\epsilon_{0v}}{2\kappa_B T} + \frac{R}{2}ln\left(2\,sinh\frac{\epsilon_{0v}}{2\kappa_B T}\right) - \frac{R}{2}$$

$$- \frac{R}{2}ln\frac{8\pi^2 I\kappa_B T}{\sigma h^2} + Rln\frac{\theta}{1-\theta} \qquad 500$$

Finally,

$$\bar{S}_H^E = \Delta\bar{S}_H^E - \Delta\bar{S}_H^0 \qquad 501$$

From Equation 500, we see that our parameters only enter into the determination of entropy indirectly, i.e. via the determination of relative clumped vs. non-clumped states according to the "Orondo Isotherm", Equation 480.

Summary of Model Equations of State

Here we summarize all the equations of the model

(1) From the O-to-T Excitation Model, we determine the relative O vs. T occupation (Chapter 2)

$$e^{-\frac{\Delta\varepsilon_{O-T}(\theta)}{\kappa_B T}} = \frac{\theta_t(1-\theta_o)}{\theta_o(1-\theta_t)}$$

502

(2) From the "Orondo Isotherm", Equation 480, we determine the relative clumped occupations, with the "free" binding energy parameters $\varepsilon_c^0, \varepsilon_c^1, \varepsilon_c^2$ (Equation 415):

$$\frac{\theta_c}{\theta_{nc}{}^{\gamma}(\Theta_o - \theta_{nc})^{1-\gamma}} = \frac{1}{2^{\gamma}}\left(1 - e^{-\frac{\epsilon_{0v}}{\kappa_B T}}\right)^{3\gamma} e^{-\gamma\frac{E_B^c(n)}{\kappa_B T}}$$

503

(3) From the continuity condition, we determine bulk fugacity and hence the excess molar quantities, Equations 497 & 500, with state energy "free" parameters $\varepsilon_\delta^0, \varepsilon_\delta^1, \varepsilon_\delta^2, \varepsilon_c^0, \varepsilon_c^1, \varepsilon_c^2$ (Equations 414 and 415):

$$\bar{H}_H^E(\theta,T) = -\frac{RT^2}{2}\frac{A'(T)}{A(T)} + \frac{R}{\kappa_B}\left(\theta\frac{\partial}{\partial\theta}\varepsilon_h(\theta) + \varepsilon_h(\theta) + \varepsilon_\delta^0 + 2\varepsilon_\delta^1\theta + 3\varepsilon_\delta^2\theta^2\right)$$
$$+\frac{R}{\kappa_B}[\varepsilon_c^0 + \varepsilon_c^1(\theta_c+\theta) + \varepsilon_c^2(2\theta_c\theta+\theta^2)] + \frac{3R\epsilon_{0v}}{2\kappa_B} - \frac{R\epsilon_{0v}}{4\kappa_B}coth\frac{\epsilon_{0v}}{2\kappa_B T} - \frac{RT}{2} + \frac{R\epsilon_D}{2\kappa_B} - \Delta\bar{H}_H^0$$

504

$$\bar{S}_H^E(\theta,T) = -\frac{RT}{2}\frac{A'(T)}{A(T)} - \frac{R}{2}lnA(T) - \frac{R}{\gamma}ln\frac{\theta_c}{\Theta_o-\theta_o} - \frac{1}{4}\frac{R\epsilon_{0v}}{\kappa_B T}coth\frac{\epsilon_{0v}}{2\kappa_B T} + \frac{R}{2}ln\left(2\,sinh\frac{\epsilon_{0v}}{2\kappa_B T}\right) - \frac{R}{2}$$
$$-\frac{R}{2}ln\frac{8\pi^2 I\kappa_B T}{\sigma h^2} + Rln\frac{\theta}{1-\theta} - \Delta\bar{S}_H^0$$

505

(4) The solutions of Equations 502-505 must be consistent with experiment.

This completes the model.

Special Case Solutions: Clumping Factor $\gamma = 2$

To get further intuition into the nature of solutions of Equations 502-505 above, and hence the value of the free parameters, we can make the following approximation, valid for the O-to-T model in the miscibility gap. (Note that this section is not strictly necessary since Equations 502-505 may be solved readily using a numerical approach for any value of γ. Nonetheless, to get some intuition regarding the solutions, a simple analytical exposition is helpful) .

We start by approximating

$$\theta_o \approx \theta \tag{506}$$

$$\theta_o \approx 1 \tag{507}$$

and write the isotherm, enthalpy and entropy, Equations 503, 504 and 505, respectively, as (Equation 502 remains as is, obviously)

$$\frac{\theta_c(1-\theta_{nc})}{{\theta_{nc}}^2} = \frac{1}{4}\left(1 - e^{-\frac{\epsilon_{0v}}{\kappa_B T}}\right)^6 e^{-2\frac{E_B^c(n)}{\kappa_B T}} \tag{508}$$

$$\bar{H}_H^E(\theta,T) = -\frac{RT^2}{2}\frac{A'(T)}{A(T)} + \frac{R}{\kappa_B}\left(\theta\frac{\partial}{\partial\theta}\varepsilon_h(\theta) + \varepsilon_h(\theta) + \varepsilon_\delta^0 + 2\varepsilon_\delta^1\theta + 3\varepsilon_\delta^2\theta^2\right)$$
$$+\frac{R}{\kappa_B}[\varepsilon_c^0 + \varepsilon_c^1(\theta_c+\theta) + \varepsilon_c^2(2\theta_c\theta+\theta^2)] + \frac{3R\epsilon_{0v}}{2\kappa_B} + \frac{R\epsilon_{0v}}{4\kappa_B}coth\frac{\epsilon_{0v}}{2\kappa_B T} - \frac{RT}{2} + \frac{R\epsilon_D}{2\kappa_B} - \Delta\bar{H}_H^0 \tag{509}$$

$$\bar{S}_H^E(\theta,T) = -\frac{RT}{2}\frac{A'(T)}{A(T)} - \frac{R}{2}lnA(T) - \frac{R}{2}ln\frac{\theta_c}{1-\theta} - \frac{1}{4}\frac{R\epsilon_{0v}}{\kappa_B T}coth\frac{\epsilon_{0v}}{2\kappa_B T} + \frac{R}{2}ln\left(2\,sinh\frac{\epsilon_{0v}}{2\kappa_B T}\right) - \frac{R}{2}$$
$$-\frac{R}{2}ln\frac{8\pi^2 I\kappa_B T}{\sigma h^2} + Rln\frac{\theta}{1-\theta} - \Delta\bar{S}_H^0 \tag{510}$$

Because of the θ_c term, we have to similarly expand the "Orondo Isotherm" in terms of loading. With $\gamma = 2$ and the above approximations, we have

$$\frac{\theta_c(1-\theta_{nc})}{{\theta_{nc}}^2} = \frac{1}{4}\left(1 - e^{-\frac{\epsilon_{0V}}{\kappa_B T}}\right)^6 e^{-2\frac{2(\varepsilon_c^0 + \theta\varepsilon_c^1 + \theta^2\varepsilon_c^2)}{\kappa_B T}}$$

511

such that Equations 509 and 510 need to be solved consistently with the isotherm. For this special case, the isotherm is a quadratic. The solutions are

$$\theta_c(\theta) = \frac{-1 - (2\beta(\theta) - 1)\theta \pm \sqrt{[1 + (2\beta(\theta) - 1)\theta]^2 + 4[1 - \beta(\theta)]\beta(\theta)\theta^2}}{2(1 - \beta(\theta))}$$

$$= \frac{-1 - (2\beta(\theta) - 1)\theta \pm \sqrt{1 + 4\beta(\theta) - 2\theta + \theta^2}}{2(1 - \beta(\theta))}$$

512

where

$$\beta(\theta) = \frac{1}{4}\left(1 - e^{-\frac{\epsilon_{0V}}{\kappa_B T}}\right)^6 e^{-\frac{2(\varepsilon_c^0 + \theta\varepsilon_c^1 + \theta^2\varepsilon_c^2)}{\kappa_B T}}$$

513

From Equations 512 and 513, it is clear that only certain solutions are possible. Thus, because

$$\beta(\theta) > 0, \qquad all\ \theta$$

514

it follows that, depending on the value of the discriminant in Equation 512, the possible solutions for clumped fractional loading are the following:

$$\theta_c(\theta) = \begin{cases} \dfrac{-1-(2\beta(\theta)-1)\theta}{2[1-\beta(\theta)]} & \Delta = 0 \\ \dfrac{-1-(2\beta(\theta)-1)\theta+\sqrt{1+4\beta(\theta)-2\theta+\theta^2}}{2[1-\beta(\theta)]} & \Delta > 0 \\ \dfrac{-1-(2\beta(\theta)-1)\theta-\sqrt{1+4\beta(\theta)-2\theta+\theta^2}}{2[1-\beta(\theta)]} & \Delta > 0 \end{cases} \quad 515$$

Equations 515 may be used to eliminate non-physical solutions in a computational framework.

♦

Assuming Equation 512 is analytic, we can expand it as a Taylor Series in loading, with a view that solutions must obey one of Equations 515. We write the result symbolically below since it is too complicated for a simple analytical expression.

$$\theta_c(\theta) = C_0 + C_1\theta + C_2\theta^2 + \cdots \quad 516$$

where

$$C_i \rightarrow C_i(T, \varepsilon_c^0, \varepsilon_c^1, \varepsilon_c^2) \quad 517$$

and C_i may be determined using a symbolic mathematical software like Matlab.

Substituting Equation 516 in Equation 509, we have for enthalpy,

$$\bar{H}_H^{E,M}(\theta,T) \cong -\frac{RT^2}{2}\frac{A'(T)}{A(T)} + \frac{R}{\kappa_B}\left(\theta\frac{\partial}{\partial\theta}\varepsilon_h(\theta) + \varepsilon_h(\theta) + \varepsilon_\delta^0 + 2\varepsilon_\delta^1\theta + 3\varepsilon_\delta^2\theta^2\right)$$

$$+\frac{R}{\kappa_B}[\varepsilon_c^0 + \varepsilon_c^1(C_0 + C_1\theta + C_2\,\theta^2 + \theta) + \varepsilon_c^2(2[C_0 + C_1\theta + C_2\,\theta^2]\theta + \theta^2)] + \frac{3R\epsilon_{0v}}{2\kappa_B}$$

$$+\frac{R\epsilon_{0v}}{4\kappa_B}\coth\frac{\epsilon_{0v}}{2\kappa_B T} - \frac{RT}{2} + \frac{R\epsilon_D}{2\kappa_B} - \Delta\bar{H}_H^0(\theta)$$

$$\bar{H}_H^{E,M}(\theta,T) = (\bar{H}_0^{E,M} - \Delta\bar{H}_0^0) + (\bar{H}_1^{E,M} - \Delta\bar{H}_1^0)\theta + (\bar{H}_2^{E,M} - \Delta\bar{H}_2^0)\theta^2 + \cdots$$

518

Similarly substituting Equation 516 into Equation 510 yields for entropy, which we write in the form

$$\frac{\bar{S}_H^E(\theta,T)}{R} = \frac{\bar{S}_0}{R} - \frac{\Delta\bar{S}_H^0(\theta,T)}{R} - \frac{1}{2}ln\left[\frac{C_0 + C_1\theta + C_2\theta^2}{1-\theta}\right] + ln\left(\frac{\theta}{1-\theta}\right)$$

$$= \frac{\bar{S}_0(T)}{R} - \frac{\Delta\bar{S}_H^0(\theta,T)}{R} - ln\left[\left(\frac{\theta}{1-\theta}\right)\left(\frac{1-\theta}{C_0 + C_1\theta + C_2\theta^2}\right)^{\frac{1}{2}}\right]$$

519

or

$$exp\left(\frac{\bar{S}_H^E(\theta,T) - \bar{S}_0(T)}{R}\right) = -exp\left(-\frac{\Delta\bar{S}_H^0(\theta,T)}{R}\right)\left[\left(\frac{\theta}{1-\theta}\right)\left(\frac{1-\theta}{C_0 + C_1\theta + C_2\theta^2}\right)^{\frac{1}{2}}\right]$$

520

where $\bar{S}_0(T)$ is a constant independent of loading in the overall model approximation:

$$\bar{S}_0(T) = -\frac{RT}{2}\frac{A'(T)}{A(T)} - \frac{R}{2}lnA(T) - \frac{1}{4}\frac{R\epsilon_{0v}}{\kappa_B T}coth\frac{\epsilon_{0v}}{2\kappa_B T} + \frac{R}{2}ln\left(2\,sinh\frac{\epsilon_{0v}}{2\kappa_B T}\right) - \frac{R}{2} - \frac{R}{2}ln\frac{8\pi^2 I\kappa_B T}{\sigma h^2}$$

521

The infinite dilution entropy term is known from experiment as a function of loading, so we may write it as

$$exp\left(-\frac{\Delta\bar{S}_H^0(\theta,T)}{R}\right) = \Delta\bar{S}_0^0(T) + \Delta\bar{S}_1^0(T)\theta + \Delta\bar{S}_2^0(T)\theta^2 + \cdots$$

522

Equation 520 then becomes

$$exp\left(\frac{\bar{S}_H^E - \bar{S}_0}{R}\right) = -(\Delta\bar{S}_0^0(T) + \Delta\bar{S}_1^0(T)\theta + \Delta\bar{S}_2^0(T)\theta^2)\left[\left(\frac{\theta}{1-\theta}\right)\left(\frac{1-\theta}{C_0 + C_1\theta + C_2\theta^2}\right)^{\frac{1}{2}}\right]$$

$$= \bar{S}_0^{E,M} + \bar{S}_1^{E,M}\theta + S_2^{E,M}\theta^2 + \cdots$$

523

Expansion Terms

The enthalpy constant coefficient terms are readily derivable from Equation 518, but we use symbolic expressions below

$$\bar{H}_0^{E,M} = \left(\bar{H}_0^{E,M} - \Delta\bar{H}_0^0\right)$$

524

$$\bar{H}_1^{E,M} = \left(\bar{H}_1^{E,M} - \Delta\bar{H}_1^0\right)$$

525

$$\bar{H}_2^{E,M} = \left(\bar{H}_2^{E,M} - \Delta\bar{H}_2^0\right)$$

526

We note that the "Orondo Isotherm" couples the clumping parameters. Nonetheless, Equations 524-526 provide constraints on $\{\varepsilon_c^0, \varepsilon_c^1, \varepsilon_c^2\}$ and $\{\varepsilon_\delta^0, \varepsilon_\delta^1, \varepsilon_\delta^2\}$.

♦

The entropy constant coefficient terms may also be derived in closed form using a symbolic mathematical tool like Matlab, thus, using a Taylor series approximation

$$\sum_{n=0}^{\infty} \frac{f^n(a)}{n!}(\theta - a)^n \tag{527}$$

where we choose $a = 0.25$ near the mid-point of the miscibility gap. We choose $a = 0.25$ instead of the closer value of $a = 0.3$ for simplicity in the Taylor expansion terms.

We then have the following symbolic expression for the expansion, from Equation 523:

$$\bar{S}_0^{E,M} = -\frac{7\left(\Delta\bar{S}_0^0 + \frac{\Delta\bar{S}_1^0}{4} + \frac{\Delta\bar{S}_2^0}{16}\right)}{16\left(\frac{C_0}{4} + \frac{C_1}{16} + \frac{C_2}{64} - \frac{1}{16}\right)} \tag{528}$$

$$\bar{S}_1^{E,M} = -\left[\frac{7\left(\Delta\bar{S}_1^0 + \frac{\Delta\bar{S}_2^0}{2}\right)}{16\left(\frac{C_0}{4} + \frac{C_1}{16} + \frac{C_2}{64} - \frac{1}{16}\right)} - \left(\frac{5}{2\left(\frac{C_0}{4} + \frac{C_1}{16} + \frac{C_2}{64} - \frac{1}{16}\right)} + \frac{7\left(C_0 + \frac{C_1}{2} + \frac{3C_2}{16} - \frac{1}{2}\right)}{16\left(\frac{C_0}{4} + \frac{C_1}{16} + \frac{C_2}{64} - \frac{1}{16}\right)^2}\right)\left(\Delta\bar{S}_0^0 + \frac{\Delta\bar{S}_1^0}{4} + \frac{\Delta\bar{S}_2^0}{16}\right)\right] \tag{529}$$

$$\bar{S}_2^{E,M} = \cdots (long\ expression) \tag{530}$$

Obviously, the idea is to compare Equations 524-530 to experimental data in a least squares sense, i.e., from experimental data we have

$$\bar{H}_H^{E,E}(\theta, T) \cong \bar{H}_0^{E,E} + \bar{H}_1^{E,E}\theta + \bar{H}_2^{E,E}\theta^2 + \cdots \tag{531}$$

and

$$exp\left(\frac{\bar{S}_H^{E,E} - \bar{S}_0}{R}\right) \cong \bar{S}_0^{E,E} + \bar{S}_1^{E,E}\theta + \bar{S}_2^{E,E}\theta^2 + \cdots$$

532

where $\bar{H}_i^{E,E}$ and $\bar{S}_i^{E,E}$ are all known.

Zeroth Order Approximation

The zeroth's order approximation, using Equations 524-526 and 531, leads to the following, with a view to Equations 518, reproduced next, and Equation 531 above:

$$\bar{H}_H^{E,M}(\theta,T) = \left(\bar{H}_0^{E,M} - \Delta\bar{H}_0^0\right) + \left(\bar{H}_1^{E,M} - \Delta\bar{H}_1^0\right)\theta + \left(\bar{H}_2^{E,M} - \Delta\bar{H}_2^0\right)\theta^2 + \cdots$$

533

$$\bar{H}_0^{E,E} = \left(\bar{H}_0^{E,M} - \Delta\bar{H}_0^0\right)$$

534

such that

$$\bar{H}_0^{E,E} = -\frac{RT^2}{2}\frac{A'(T)}{A(T)} + \frac{R}{\kappa_B}\left(\varepsilon_h^0 + \varepsilon_\delta^0\right) + \frac{5R}{4}\frac{\epsilon_{0v}}{\kappa_B}\coth\left(\frac{\epsilon_{0v}}{2\kappa_B T}\right) + \frac{R}{\kappa_B}\varepsilon_c^1 C_0 - \frac{RT}{2} + \frac{R}{2\kappa_B}\epsilon_D$$

535

$$\varepsilon_\delta^1 = \varepsilon_\delta^2 = 0$$

536

and

$$\varepsilon_c^1 = \varepsilon_c^2 = 0$$

537

Equation 535 simplifies to

$$\varepsilon_\delta^0 = -\varepsilon_h^0 + \frac{\kappa_B}{R}\bar{H}_0^{E,E} + \frac{\kappa_B T^2}{2}\frac{A'(T)}{A(T)} - \frac{5}{4}\epsilon_{0v}\coth\left(\frac{\epsilon_{0v}}{2\kappa_B T}\right) + \frac{\kappa_B T}{2} - \frac{1}{2}\epsilon_D \tag{538}$$

which is simple enough, but not expected to yield much of a correction other than a simple energy shift.

Similarly, for entropy, we compare Equations 520, 528 & 532 to arrive at

$$\bar{S}_0^{E,E} = -\frac{7\left(\Delta\bar{S}_0^0 + \frac{\Delta\bar{S}_1^0}{4} + \frac{\Delta\bar{S}_2^0}{16}\right)}{16\left(\frac{C_0}{4} + \frac{C_1}{16} + \frac{C_2}{64} - \frac{1}{16}\right)}\Bigg|_{\varepsilon_c^1=0,\varepsilon_c^2=0} = -\frac{7\left(\Delta\bar{S}_0^0 + \frac{\Delta\bar{S}_1^0}{4} + \frac{\Delta\bar{S}_2^0}{16}\right)}{16\left(\frac{C_0(\varepsilon_c^0)}{4} + \frac{C_1(\varepsilon_c^0)}{16} + \frac{C_2(\varepsilon_c^0)}{64} - \frac{1}{16}\right)} \tag{539}$$

whereby Equation 539 is evaluated for the single unknown ε_c^0 by setting $\varepsilon_c^1 = 0, \varepsilon_c^2 = 0$, denoted above by making the constants only a function of the single zeroth order parameter:

$$C_i(\varepsilon_c^0, \varepsilon_c^1, \varepsilon_c^2) \rightarrow C_i(\varepsilon_c^0) \tag{540}$$

i.e. by solving for $\theta_c(\theta)$ using Equation 512, while setting Equation 513 to

$$\beta(\theta)_{Zero\ Order} = \frac{1}{4}\left(1 - e^{-\frac{\epsilon_{0v}}{\kappa_B T}}\right)^6 e^{\frac{2\varepsilon_c^0}{\kappa_B T}} \tag{541}$$

First Order Approximation

Similarly, a first order approximation leads to, for enthalpy,

$$\bar{H}_0^{E,E} = \left(\bar{H}_0^{E,M} - \Delta\bar{H}_0^0\right) \tag{542}$$

$$\bar{H}_1^{E,E} = \left(\bar{H}_1^{E,M} - \Delta\bar{H}_1^0\right) \tag{543}$$

or

$$\bar{H}_0^{E,E} = -\frac{RT^2}{2}\frac{A'(T)}{A(T)} + \frac{R}{\kappa_B}\left(\varepsilon_h^0 + \varepsilon_\delta^0\right) + \frac{5R}{4}\frac{\epsilon_{0v}}{\kappa_B}\coth\left(\frac{\epsilon_{0v}}{2\kappa_B T}\right) + \frac{R}{\kappa_B}\varepsilon_c^1 C_0(\varepsilon_c^0, \varepsilon_c^1) - \frac{RT}{2} + \frac{R}{2\kappa_B}\epsilon_D \tag{544}$$

$$\bar{H}_1^{E,E} = \frac{2R}{\kappa_B}\left(\varepsilon_h^1 + \varepsilon_\delta^1\right) + \frac{R}{\kappa_B}\left[\varepsilon_c^1 C_1(\varepsilon_c^0, \varepsilon_c^1) + 2\varepsilon_c^2 C_0(\varepsilon_c^0, \varepsilon_c^1)\right] \tag{545}$$

$$\varepsilon_c^2 = \varepsilon_\delta^2 = 0 \tag{546}$$

Equation 544 simplifies to

$$\varepsilon_\delta^0 + \varepsilon_c^1 C_0(\varepsilon_c^0, \varepsilon_c^1) = -\varepsilon_h^0 + \frac{\kappa_B}{R}\bar{H}_0^{E,E} + \frac{\kappa_B T^2}{2}\frac{A'(T)}{A(T)} - \frac{5}{4}\epsilon_{0v}\coth\left(\frac{\epsilon_{0v}}{2\kappa_B T}\right) + \frac{\kappa_B T}{2} - \frac{1}{2}\epsilon_D \tag{547}$$

while Equation 545 becomes

$$2\varepsilon_\delta^1 + \varepsilon_c^1 C_1(\varepsilon_c^0, \varepsilon_c^1) + 2\varepsilon_c^2 C_0(\varepsilon_c^0, \varepsilon_c^1) = -2\varepsilon_h^1 + \frac{\kappa_B}{R}\bar{H}_1^{E,E} \tag{548}$$

For entropy, we have Equations 523 and 532 (repeated below for convenience)

$$exp\left(\frac{\bar{S}_H^E - \bar{S}_0}{R}\right) = (\Delta\bar{S}_0^0 + \Delta\bar{S}_1^0\theta + \Delta\bar{S}_2^0\theta^2)\left(\frac{1-2\theta-\theta^2}{-C_0\theta + (1-C_1)\theta^2 - C_2\theta^3}\right) = \bar{S}_0^{E,M} + \bar{S}_1^{E,M}\theta + S_2^{E,M}\theta^2 + \cdots$$

549

$$exp\left(\frac{\bar{S}_H^{E,E} - \bar{S}_0}{R}\right) \cong \bar{S}_0^{E,E} + \bar{S}_1^{E,E}\theta + \bar{S}_2^{E,E}\theta^2 + \cdots$$

550

from which, using Equations 528 & 529, we get by matching terms

$$\bar{S}_0^{E,E} = -\frac{7\left(\Delta\bar{S}_0^0 + \frac{\Delta\bar{S}_1^0}{4} + \frac{\Delta\bar{S}_2^0}{16}\right)}{16\left(\frac{C_0}{4} + \frac{C_1}{16} + \frac{C_2}{64} - \frac{1}{16}\right)}$$

551

$$\bar{S}_1^{E,E} = -\left[\frac{7\left(\Delta\bar{S}_1^0 + \frac{\Delta\bar{S}_2^0}{2}\right)}{16\left(\frac{C_0}{4} + \frac{C_1}{16} + \frac{C_2}{64} - \frac{1}{16}\right)} - \left(\frac{5}{2\left(\frac{C_0}{4} + \frac{C_1}{16} + \frac{C_2}{64} - \frac{1}{16}\right)} + \frac{7\left(C_0 + \frac{C_1}{2} + \frac{3C_2}{16} - \frac{1}{2}\right)}{16\left(\frac{C_0}{4} + \frac{C_1}{16} + \frac{C_2}{64} - \frac{1}{16}\right)^2}\right)\left(\Delta\bar{S}_0^0 + \frac{\Delta\bar{S}_1^0}{4} + \frac{\Delta\bar{S}_2^0}{16}\right)\right]$$

552

and $C_i \to C_i(\varepsilon_c^0, \varepsilon_c^1)$ are implied.

Equations 547, 548, 551, 552 form a system of four equations in the four unknowns, $\{\varepsilon_\delta^0, \varepsilon_\delta^1, \varepsilon_c^0, \varepsilon_c^1\}$.

Results

Clumped vs. non-clumped occupation – this depends critically on the shape of the binding energy curve, see below, which shows a decrease with loading.

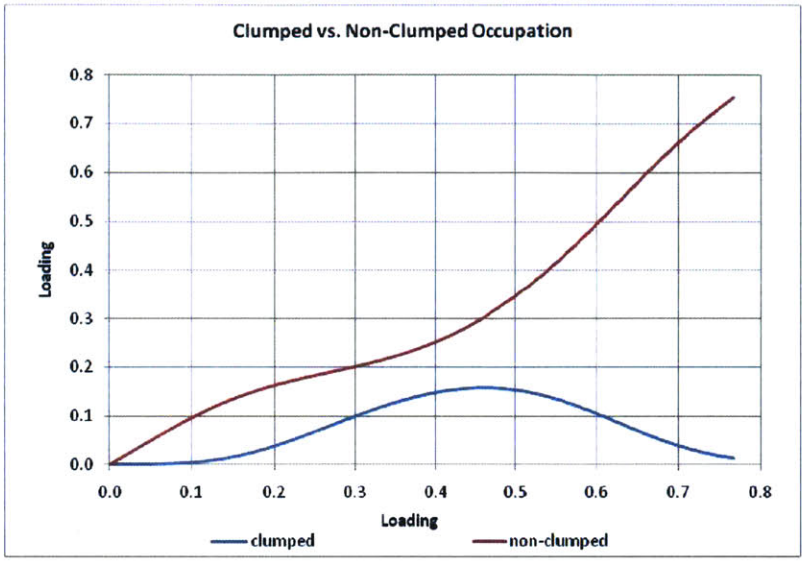

Figure 114: Clumped and non-Clumped Occupation vs. Loading

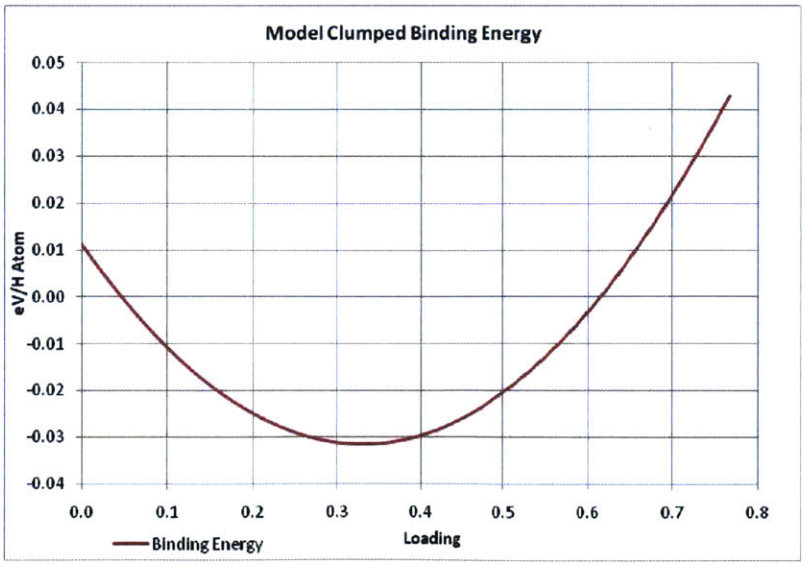

Figure 115: Binding Energy vs. Loading

We also show fractional occupation as a function of loading:

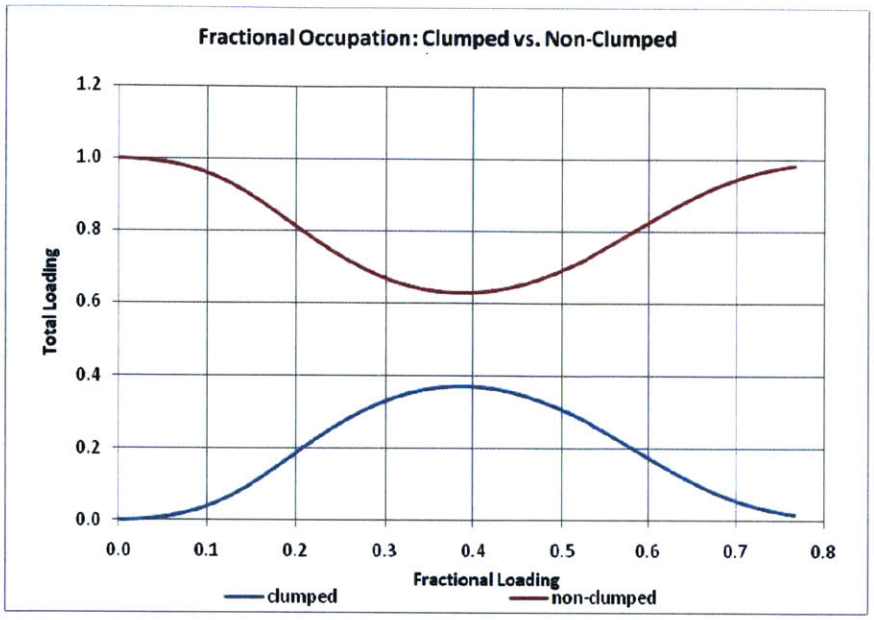

Figure 116: Fractional clumped and non-clumped populations

Next, we show available fractional microstates

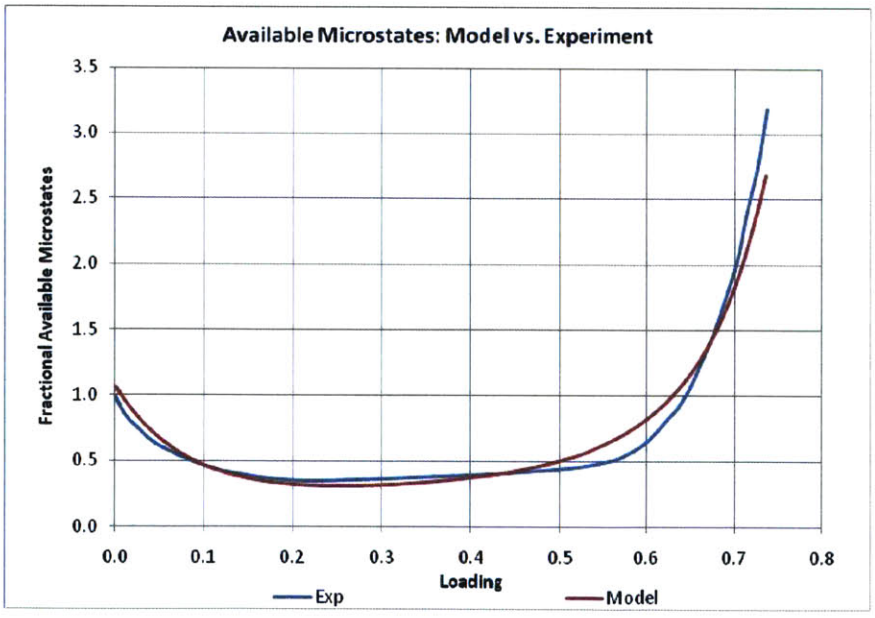

Figure 117: Available Microstates upon absorption

Finally, we show model molar entropy and enthalpy compared to experiment.

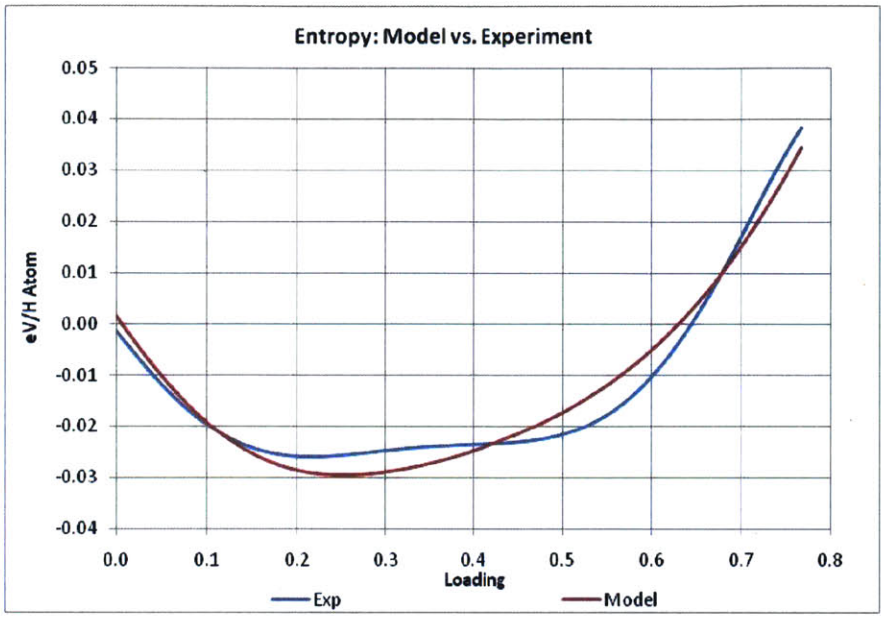

Figure 118: Enthalpy vs. Experiment. Experiment is from (Kuji, Oates, Bowerman, & Flanagan, 1983)

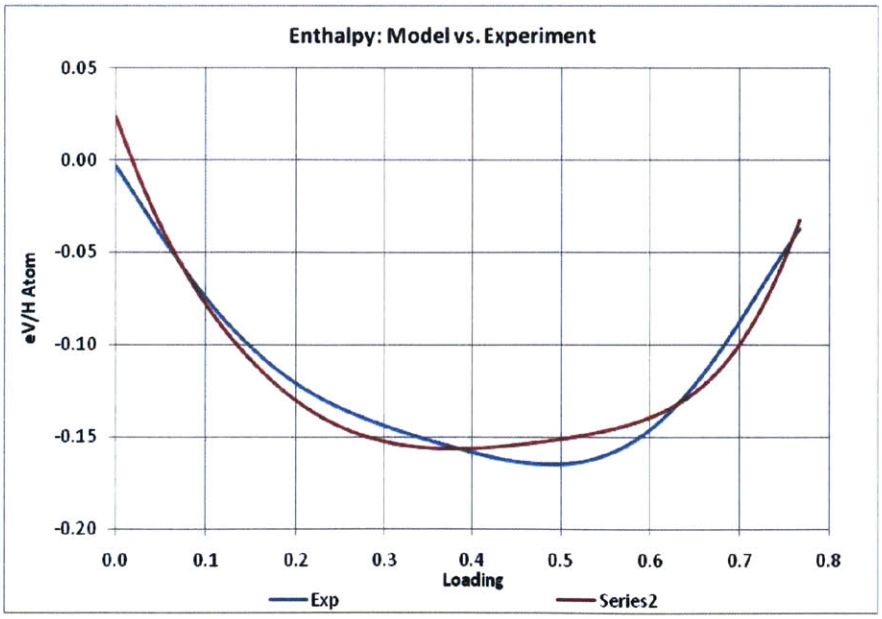

Figure 119: Model Entropy vs. Experiment. Experimentis from (Kuji, Oates, Bowerman, & Flanagan, 1983)

Summary & Discussion

The molar quantities show that our model indeed provides an excellent description of the problem. In fact the match is incredibly good. Of note is that our clumping model provides exactly the expected behavior, namely, the clumped population is highest in the miscibility gap and drops to near zero in the beta phase.

Additionally, the degree of binding is highest in the miscibility gap where the clumps form, and is lower in the single phase regions, just as would be expected (note that the binding is defined as in Equation 407).

In the next Chapter, we try to compete this model by including exclusions around the clumps.

Chapter 10 – Interstitial Hydrogen Clumped Model with Nearest Neighbors Exclusion

Introduction

In this Chapter, we will investigate a variation of the prior clumped model in Chapter 9 that excludes nearest neighbors. This effort is motivated by the realization that we may improve on the prior model by restricting the clumps to form in isolation, a restriction that was not placed on the prior model.

Nearest Neighbor Exclusion

Formulation

We propose that clumping will form singlets, consistent with last chapter's model, only if they are isolated. This means we need a slight correction to Equation 394 of Chapter 9. To do so, we may find it most convenient to proceed as follows, thus

$$Z_H(\tau,\mu) = \sum_{n_{nc}=0}^{N_o} \sum_{k=0}^{\frac{N_o-n_{nc}}{\alpha+\gamma}} \sum_{n_t=0}^{N_t} \sum_{ASN} e^{\frac{(n_{nc}+n_t+k\gamma)\mu-\varepsilon_h(n_{nc},n_t,k\gamma)}{\tau}} Z_o^{n_{nc}} Z_t^{n_t} Z_c^{k\gamma} Z_{e,o}^{n_{nc}} Z_{e,t}^{n_t} Z_{e,c}^{k\gamma} \quad (553)$$

where α is the number of "exclusion sites" surrounding a clump. Equation 553 is obviously an approximation, but it is designed to explicitly reproduce the physical result that, at high loading, we do not expect clumps to form and thereby exclude them statistically. It is also designed to create a physical picture whereby clumps form via an annihilation of surrounding interstitials. We use the following pictorial depiction (Figure 120) to appreciate that Equation 553 has the right form.

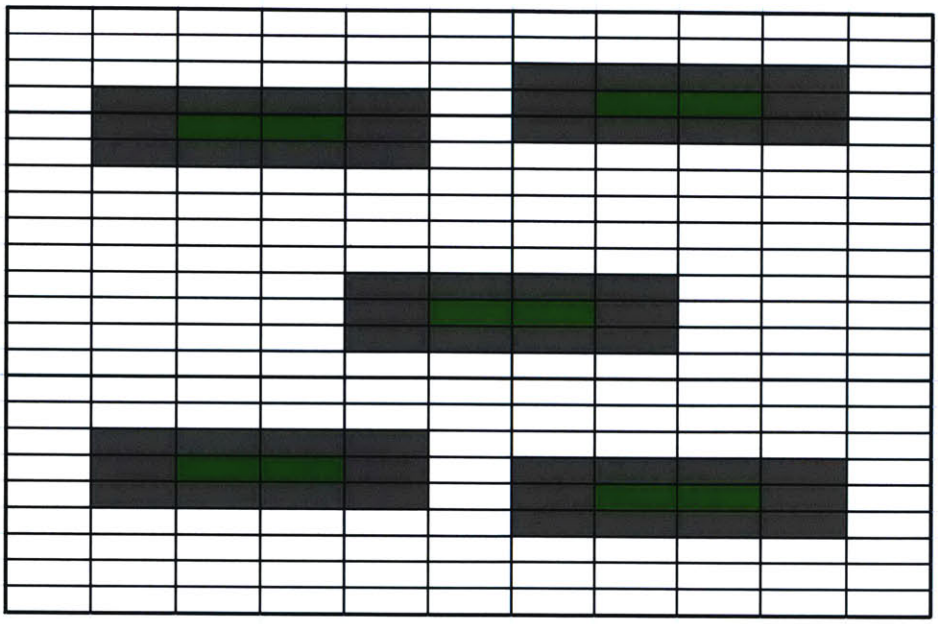

Figure 120: Pictorial depiction of the model. Clumped sites are shown in green and nearest neighbors in grey.

We proceed as before, thus,

$$Z_H(\tau,\mu) \cong \frac{N_o!}{n_{nc}!\,(N_o-n_{nc})!}\frac{\left(\frac{N_o-n_{nc}}{\alpha+\gamma}\right)!}{k!\left(\frac{N_o-n_{nc}}{\alpha+\gamma}-k\right)!}\frac{N_t!}{n_t!\,(N_t-n_t)!}e^{\frac{(n_{nc}+n_t+k\gamma)\varepsilon_h(n_{nc},n_t,k\gamma)}{\tau}}{z_{o,t}}^{n_{nc}+n_t}{g_{o,t}}^{n_{nc}+n_t}z_c^{k\gamma} \quad (554)$$

and

$$\mu_c(\tau,n_c,n_{nc},n_t)=\mu_{nc}(\tau,n_c,n_{nc},n_t)=\mu_t(\tau,n_c,n_{nc},n_t) \quad (555)$$

Clumped Species Chemical Potential

The clumped species chemical potential terms are

$$\mu_c(\tau,n) = -\tau\frac{\partial}{\partial n_c}\left\{ ln\frac{N_o!}{n_{nc}!\,(N_o-n_{nc})!} + ln\frac{\left(\frac{N_o-n_{nc}}{\alpha+\gamma}\right)!}{k!\left(\frac{N_o-n_{nc}}{\alpha+\gamma}-k\right)!} + ln\left(\frac{N_t!}{n_t!\,(N_t-n_t)!}\right)\right.$$

$$\left. -\frac{(n_{nc}+n_t+k\gamma)\varepsilon_h(n_{nc},n_t,k\gamma)}{\tau} + (n_{nc}+n_t)ln(z_{o,t}) + (n_{nc}+n_t)ln(g_{o,t}) + k\gamma\, ln(z_c)\right\}$$

$$= -\tau\frac{\partial}{\partial n_c}\{T_1+T_2+T_3+T_4+T_5+T_6+T_7\}$$

556

and similarly for μ_{nc} and μ_t. Using the Stirling approximation,

$$ln(x!) \cong \frac{1}{2}ln(2\pi) + \left(x+\frac{1}{2}\right)ln(x) - x$$

557

the results are, including some of the algebra,

$$T_1 = ln\frac{N_o!}{n_{nc}!\,(N_o-n_{nc})!} = ln\,N_o! - ln\,n_{nc}! - ln(N_o-n_{nc})!$$

$$\cong \left[\frac{1}{2}ln(2\pi) + \left(N_o+\frac{1}{2}\right)ln\,N_o - N_o\right] - \left[\frac{1}{2}ln(2\pi) + \left(n_{nc}+\frac{1}{2}\right)ln\,n_{nc} - n_{nc}\right]$$

$$- \left[\frac{1}{2}ln(2\pi) + \left(N_o-n_{nc}+\frac{1}{2}\right)ln(N_o-n_{nc}) - (N_o-n_{nc})\right]$$

558

such that

$$\frac{\partial}{\partial n_c}T_1 = 0$$

559

and

$$T_2 = ln\frac{\left(\frac{N_o - n_{nc}}{\alpha+\gamma}\right)!}{k!\left(\frac{N_o - n_{nc}}{\alpha+\gamma} - k\right)!} = ln\frac{N_o - n_{nc}}{\alpha+\gamma}! - ln\,k! - ln\left(\frac{N_o - n_{nc}}{\alpha+\gamma} - k\right)!$$

$$\cong \left[\frac{1}{2}ln(2\pi) + \left(\frac{N_o - n_{nc}}{\alpha+\gamma} + \frac{1}{2}\right)ln\frac{N_o - n_{nc}}{\alpha+\gamma} - \frac{N_o - n_{nc}}{\alpha+\gamma}\right] - \left[\frac{1}{2}ln(2\pi) + \left(k + \frac{1}{2}\right)ln\,k - k\right]$$

$$- \left[\frac{1}{2}ln(2\pi) + \left(\frac{N_o - n_{nc} - k(\alpha+\gamma)}{\alpha+\gamma} + \frac{1}{2}\right)ln\frac{N_o - n_{nc} - k(\alpha+\gamma)}{\alpha+\gamma}\right.$$

$$\left. - \frac{N_o - n_{nc} - k(\alpha+\gamma)}{\alpha+\gamma}\right]$$

560

with

$$\frac{\partial}{\partial n_c}T_2 = \frac{1}{\gamma}\frac{\partial}{\partial k}T_2 = -\frac{1}{\gamma}\left[\left(k + \frac{1}{2}\right)\frac{1}{k} + ln\,k - 1\right]$$

$$-\frac{1}{\gamma}\left[\left(\frac{N_o - n_{nc} - k(\alpha+\gamma)}{\alpha+\gamma} + \frac{1}{2}\right)\frac{\alpha+\gamma}{N_o - n_{nc} - k(\alpha+\gamma)}(-1)\right.$$

$$\left. + ln\frac{N_o - n_{nc} - k(\alpha+\gamma)}{\alpha+\gamma}(-1) - 1\right)$$

$$\approx -\frac{1}{\gamma}\left\{ln\,k - ln\frac{N_o - n_{nc} - k(\alpha+\gamma)}{\alpha+\gamma}\right\}$$

$$= -\frac{1}{\gamma}ln\frac{k(\alpha+\gamma)}{N_o - n_{nc} - k(\alpha+\gamma)}$$

561

The other terms are unchanged from Chapter 9. The results are repeated here for ease of readability, thus,

$$\frac{\partial}{\partial n_c} T_3 = 0$$

562

$$\frac{\partial}{\partial n_c} T_4 = \frac{1}{\gamma}\frac{\partial}{\partial k} T_4 = -\frac{1}{\gamma\tau}\left((n_{nc} + n_t + k\gamma)\frac{\partial}{\partial k}\varepsilon_h(n_{nc}, n_t, k\gamma) + \gamma\varepsilon_h(n_{nc}, n_t, k\gamma)\right)$$

563

$$\frac{\partial}{\partial n_c} T_5 = \frac{\partial}{\partial n_c} T_6 = 0$$

564

$$\frac{\partial}{\partial n_c} T_7 = \frac{1}{\gamma}\frac{\partial}{\partial k} T_7 = -\frac{1}{\tau}\left(k\frac{\partial}{\partial k} E_B^c(n) + \frac{3}{2}\epsilon_{0v} + E_B^c(n)\right)$$

565

Collecting the terms

$$\begin{aligned} -\frac{\mu_c(\tau, n)}{\tau} &= \frac{\partial}{\partial n_c}\{T_1 + T_2 + T_3 + T_4 + T_5 + T_6 + T_7\} \\ &= -\frac{1}{\gamma} ln\frac{k(\alpha+\gamma)}{N_o - n_{nc} - k(\alpha+\gamma)} - \frac{1}{\gamma\tau}\left((n_{nc} + n_t + k\gamma)\frac{\partial}{\partial k}\varepsilon_h(n_{nc}, n_t, k\gamma) + \gamma\varepsilon_h(n)\right) \\ &\quad -\frac{1}{\tau}\left(k\frac{\partial}{\partial k} E_B^c(n) + \frac{3}{2}\epsilon_{0v} + E_B^c(n)\right) \end{aligned}$$

566

or

$$\begin{aligned} \mu_c(\tau, n) &= \frac{1}{\gamma}\tau\, ln\frac{k(\alpha+\gamma)}{N_o - n_{nc} - k(\alpha+\gamma)} + \frac{1}{\gamma}\left((n_{nc} + n_t + k\gamma)\frac{\partial}{\partial k}\varepsilon_h(n) + \gamma\varepsilon_h(n_{nc}, n_t, k\gamma)\right) \\ &\quad + \left(k\frac{\partial}{\partial k} E_B^c(n) + \frac{3}{2}\epsilon_{0v} + E_B^c(n)\right) \end{aligned}$$

567

As before, we may write Equation 567 in terms of the fractional loading parameters of Chapter 9. Additionally, we may define

$$\theta_\alpha = \frac{k\alpha}{N} = \frac{\alpha}{\gamma}\theta_c \tag{568}$$

where Equation 568 is a simple result of the definition of an exclusion around a clump. The result is

$$\begin{aligned}\mu_c(\tau,\theta) = &\frac{1}{\gamma}\tau\, ln\frac{\theta_\alpha + \theta_c}{\Theta_o - \theta_{nc} - \theta_\alpha - \theta_c} + \left((n_{nc} + n_t + n_c)\frac{\partial}{\partial n}\varepsilon_h(n)\frac{\partial n}{\partial n_c} + \varepsilon_h(n_{nc}, n_t, n_c)\right) \\ &+ \left(n_c\frac{\partial}{\partial n}E_B^c(n)\frac{\partial n}{\partial n_c} + \frac{3}{2}\epsilon_{0v} + E_B^c(n)\right) \\ &= \tau\frac{1}{\gamma}ln\frac{\varphi\theta_c}{\Theta_o - \theta_{nc} - \varphi\theta_c} + \theta\frac{\partial}{\partial\theta}\varepsilon_h(\theta) + \varepsilon_h(\theta) + \theta_c\frac{\partial}{\partial\theta}E_B^c(\theta) + \frac{3}{2}\epsilon_{0v} + E_B^c(\theta)\end{aligned} \tag{569}$$

where

$$\varphi = \frac{\alpha + \gamma}{\gamma} \tag{570}$$

The final expression is again fairly simple

$$\boldsymbol{\mu_c(\tau,\theta) = \tau\frac{1}{\gamma}ln\frac{\varphi\theta_c}{\Theta_o - \theta_{nc} - \varphi\theta_c} + \theta\frac{\partial}{\partial\theta}\varepsilon_h(\theta) + \varepsilon_h(\theta) + \theta_c\frac{\partial}{\partial\theta}E_B^c(\theta) + \frac{3}{2}\epsilon_{0v} + E_B^c(\theta)} \tag{571}$$

Equation 571 reduces to Equation 448 of Chapter 9 when there are no exclusions around the clumps, i.e., $\alpha = 0$ or $\varphi = 1$.

Non-Clumped Species Chemical Potential

For the non clumped and tetrahedral sites, the results are, similar to those from Chapter 9,

$$\frac{\partial}{\partial n_{nc}}T_1 = -\left[\left(n_{nc}+\frac{1}{2}\right)\frac{1}{n_{nc}} + ln\, n_{nc} - 1\right] - \left[-\left(N_o - n_{nc}+\frac{1}{2}\right)\frac{1}{N_o - n_{nc}} - ln(N_o - n_{nc}) + 1\right]$$

$$\approx -ln\, n_{nc} + ln(N_o - n_{nc}) = -ln\frac{n_{nc}}{N_o - n_{nc}}$$

572

$$\frac{\partial}{\partial n_{nc}}T_2 = \left[\left(\frac{N_o - n_{nc}}{\alpha+\gamma}+\frac{1}{2}\right)\frac{\alpha+\gamma}{N_o - n_{nc}}\left(-\frac{1}{\alpha+\gamma}\right) + ln\frac{N_o - n_{nc}}{\alpha+\gamma}\left(-\frac{1}{\alpha+\gamma}\right) - \left(-\frac{1}{\alpha+\gamma}\right)\right]$$

$$-\left[\left(\frac{N_o - n_{nc} - k(\alpha+\gamma)}{\alpha+\gamma}+\frac{1}{2}\right)\frac{\alpha+\gamma}{N_o - n_{nc} - k(\alpha+\gamma)}\left(-\frac{1}{\alpha+\gamma}\right)\right.$$

$$\left. + ln\frac{N_o - n_{nc} - k(\alpha+\gamma)}{\alpha+\gamma}\left(-\frac{1}{\alpha+\gamma}\right) - \left(-\frac{1}{\alpha+\gamma}\right)\right]$$

$$\approx -\frac{1}{\alpha+\gamma}\left[ln\frac{N_o - n_{nc}}{\alpha+\gamma} - ln\frac{N_o - n_{nc} - k(\alpha+\gamma)}{\alpha+\gamma}\right] = -\frac{1}{\alpha+\gamma}ln\frac{N_o - n_{nc}}{N_o - n_{nc} - k(\alpha+\gamma)}$$

573

$$\frac{\partial}{\partial n_{nc}}T_3 = 0$$

574

$$\frac{\partial}{\partial n_{nc}}T_4 = -\frac{1}{\tau}\left\{(n_{nc} + n_t + k\gamma)\frac{\partial}{\partial n_{nc}}\varepsilon_h(n) + \varepsilon_h(n)\right\} = -\frac{1}{\tau}\left[n\frac{\partial}{\partial n_{nc}}\varepsilon_h(n) + \varepsilon_h(n)\right]$$

575

$$\frac{\partial}{\partial n_{nc}}T_5 = ln(z_{o,t})$$

576

$$\frac{\partial}{\partial n_{nc}}T_6 = ln(g_{o,t})$$

577

$$\frac{\partial}{\partial n_{nc}} T_7 = -\frac{n_c}{\tau} \frac{\partial}{\partial n_{nc}} E_B^c(n) \tag{578}$$

Therefore

$$-\frac{\mu_{nc}(\tau, n)}{\tau} = -ln\frac{n_{nc}}{N_o - n_{nc}} - \frac{1}{\alpha + \gamma} ln\frac{N_o - n_{nc}}{N_o - n_{nc} - k(\alpha + \gamma)} - \frac{1}{\tau}\left[n\frac{\partial}{\partial n_{nc}}\varepsilon_h(n) + \varepsilon_h(n)\right] + ln(z_{o,t}) + ln(g_{o,t}) - \frac{n_c}{\tau}\frac{\partial}{\partial n_{nc}} E_B^c(n) \tag{579}$$

Simplifying,

$$\mu_{nc}(\tau, n) = \tau\, ln\frac{n_{nc}}{N_o - n_{nc}} + \frac{\tau}{\alpha + \gamma} ln\frac{N_o - n_{nc}}{N_o - n_{nc} - k(\alpha + \gamma)} + \left[n\frac{\partial}{\partial n_{nc}}\varepsilon_h(n) + \varepsilon_h(n)\right] - \tau\, ln(z_{o,t}) - \tau\, ln(g_{o,t}) + n_c\frac{\partial}{\partial n_{nc}} E_B^c(n) \tag{580}$$

or, by way of summary, including prior results,

$$\boldsymbol{\mu_t(\tau, \theta) = \tau\, ln\frac{\theta_t}{\theta_t - \theta_t} + \theta\frac{\partial}{\partial \theta}\varepsilon_h(\theta) + \varepsilon_h(\theta) - \tau\, ln(z_{o,t}) - \tau\, ln(g_{o,t}) + \theta_c\frac{\partial}{\partial \theta} E_B^c(\theta)} \tag{581}$$

$$\boldsymbol{\mu_{nc}(\tau, \theta) = \tau\, ln\frac{\theta_{nc}}{\theta_o - \theta_{nc}} + \frac{\tau}{\alpha + \gamma} ln\frac{\theta_o - \theta_{nc}}{\theta_o - \theta_{nc} - \varphi\theta_c} + \theta\frac{\partial}{\partial \theta}\varepsilon_h(\theta) + \varepsilon_h(\theta) - \tau ln z_{o,t} - \tau ln g_{o,t} + \theta_c\frac{\partial}{\partial \theta} E_B^c(\theta)} \tag{582}$$

$$\mu_c(\tau,\theta) = \tau\frac{1}{\gamma}ln\frac{\varphi\theta_c}{\Theta_o-\theta_{nc}-\varphi\theta_c} + \theta\frac{\partial}{\partial\theta}\varepsilon_h(\theta) + \varepsilon_h(\theta) + \theta_c\frac{\partial}{\partial\theta}E_B^c(\theta) + \frac{3}{2}\epsilon_{0v} + E_B^c(\theta) \quad 583$$

Note that Equation 582 reduces to Equation 467 when there are no exclusions.

Constraints on Binding Energy Parameter: "Orondo Isotherm"

The "Orondo Isotherm", via Equations 582 and 583, becomes

$$\tau\, ln\frac{\theta_{nc}}{\Theta_o-\theta_{nc}} + \frac{\tau}{\alpha+\gamma}ln\frac{\Theta_o-\theta_{nc}}{\Theta_o-\theta_{nc}-\varphi\theta_c} - \frac{\tau}{\gamma}ln\frac{\varphi\theta_c}{\Theta_o-\theta_{nc}-\varphi\theta_c} = E_B^c(\theta) + \tau\, ln\, z_{o,t} + \tau\, lng_{o,t} + \frac{3}{2}\epsilon_{0v} \quad 584$$

Simplifying,

$$\gamma\varphi\, ln\frac{\theta_{nc}}{\Theta_o-\theta_{nc}} + ln\frac{\Theta_o-\theta_{nc}}{\Theta_o-\theta_{nc}-\varphi\theta_c} - \varphi\, ln\frac{\varphi\theta_c}{\Theta_o-\theta_{nc}-\varphi\theta_c} = \gamma\varphi\left(ln\, z_{o,t} + lng_{o,t} + \frac{1}{\tau}\left[\frac{3}{2}\epsilon_{0v} + E_B^c(\theta)\right]\right) \quad 585$$

Equation 585, in its clumping isotherm form may be written as

$$ln\left[\frac{\left(\frac{\theta_{nc}}{\Theta_o-\theta_{nc}}\right)^{\gamma\varphi}\left(\frac{\Theta_o-\theta_{nc}}{\Theta_o-\theta_{nc}-\varphi\theta_c}\right)}{\left(\frac{\varphi\theta_c}{\Theta_o-\theta_{nc}-\varphi\theta_c}\right)^{\varphi}}\right] = \gamma\varphi\left(ln\, z_{o,t} + lng_{o,t} + \frac{1}{\tau}\left[\frac{3}{2}\epsilon_{0v} + E_B^c(\theta)\right]\right) \quad 586$$

We write Equation 586 as follows, where we have retained some of the algebra,

$$\frac{\left(\frac{\varphi\theta_c}{\Theta_o-\theta_{nc}-\varphi\theta_c}\right)^{\varphi}}{\left(\frac{\theta_{nc}}{\Theta_o-\theta_{nc}}\right)^{\gamma\varphi}\left(\frac{\Theta_o-\theta_{nc}}{\Theta_o-\theta_{nc}-\varphi\theta_c}\right)}=e^{-\gamma\varphi\left(ln\,z_{o,t}+ln g_{o,t}+\frac{1}{\tau}\left[\frac{3}{2}\epsilon_{ov}+E_B^c(\theta)\right]\right)}$$

$$\rightarrow\frac{(\Theta_o-\theta_{nc})^{\gamma\varphi}(\varphi\theta_c)^{\varphi}(\Theta_o-\theta_{nc}-\varphi\theta_c)}{\theta_{nc}{}^{\gamma\varphi}(\Theta_o-\theta_{nc}-\varphi\theta_c)^{\varphi}(\Theta_o-\theta_{nc})}=\left(\frac{1}{z_{o,t}g_{o,t}}\right)^{\gamma\varphi}e^{-\frac{\gamma\varphi}{\tau}\left(E_B^c(\theta)+\frac{3}{2}\epsilon_{ov}\right)}$$

$$\rightarrow\frac{\theta_c{}^{\varphi}(\Theta_o-\theta_{nc})^{\gamma\varphi-1}}{\theta_{nc}{}^{\gamma\varphi}(\Theta_o-\theta_{nc}-\varphi\theta_c)^{\varphi-1}}=\frac{1}{\varphi^{\varphi}}\left(\frac{1}{z_{o,t}g_{o,t}}\right)^{\gamma\varphi}e^{-\frac{\gamma\varphi}{\tau}\left(E_B^c(\theta)+\frac{3}{2}\epsilon_{ov}\right)}$$

587

or in isotherm form

$$\frac{\theta_c{}^{\varphi}(\Theta_o-\theta_{nc})^{\gamma\varphi-1}}{\theta_{nc}{}^{\gamma\varphi}(\Theta_o-\theta_{nc}-\varphi\theta_c)^{\varphi-1}}=\frac{1}{\varphi^{\varphi}}\left(\frac{z_c^{n_c}}{z_o^{n_{nc}}}\frac{z_{e,c}^{n_c}}{z_{e,o}^{n_{nc}}}\right)^{\gamma\varphi}$$

588

where the individual terms are described in Chapter 9, such that Equation 587 becomes the "Orondo Isotherm" with nearest neighbor exclusion:

$$\frac{\theta_c{}^{\varphi}(\Theta_o-\theta_{nc})^{\gamma\varphi-1}}{\theta_{nc}{}^{\gamma\varphi}(\Theta_o-\theta_{nc}-\varphi\theta_c)^{\varphi-1}}=\frac{1}{\varphi^{\varphi}}\left[\frac{1}{2}\left(1-e^{-\frac{\epsilon_{ov}}{\kappa_B T}}\right)^3 e^{\frac{E_B^c(n)}{\kappa_B T}}\right]^{\gamma\varphi}$$

589

By setting $\varphi = 1$, Equation 589 reduces to Equation 480, Chapter 9 as expected.

Continuity Condition, Full Model With Exclusion

The full model continuity condition, is unchanged from Chapter 9, i.e. using Equation 582 or 583, and Equation 589,

$$\frac{\tau}{\gamma} ln \frac{\varphi\theta_c}{\Theta_o - \theta_{nc} - \varphi\theta_c} + \theta \frac{\partial}{\partial\theta}\varepsilon_h(\theta) + \varepsilon_h(\theta) + \theta_c \frac{\partial}{\partial\theta} E_B^c(\theta) + \frac{3}{2}\epsilon_{0v} + E_B^c(\theta)$$

$$= -\frac{\tau}{2}\left[ln\left[\left(\frac{2\pi m\tau}{h^2}\right)^{\frac{3}{2}} \frac{\tau}{f}\right] + ln \frac{e^{-\frac{\epsilon_{0v}}{2\tau}}}{1 - e^{-\frac{\epsilon_{0v}}{\tau}}} + ln \frac{8\pi^2 I\tau}{\sigma h^2} + \frac{\epsilon_D}{\tau}\right] \quad 590$$

or

$$f(\tau, \theta) = A(\tau) e^{\frac{B(\tau,\theta)}{\tau}} \quad 591$$

with $A(\tau)$ already defined, and $B(\theta, T)$ is now

$$B(\theta, T) =$$

$$\left[2\left(\frac{\kappa_B T}{\gamma} ln \frac{\varphi\theta_c}{\Theta_o - \theta_{nc} - \varphi\theta_c} + \theta \frac{\partial}{\partial\theta}\varepsilon_h(\theta) + \varepsilon_h(\theta) + \theta_c \frac{\partial}{\partial\theta} E_B^c(\theta) + \frac{3}{2}\epsilon_{0v} + E_B^c(\theta)\right) + \kappa_B T\, ln \frac{e^{-\frac{\epsilon_{0v}}{2\kappa_B T}}}{1 - e^{-\frac{\epsilon_{0v}}{\kappa_B T}}}\right.$$

$$\left. + \kappa_B T\, ln \frac{8\pi^2 I\kappa_B T}{\sigma h^2} + \epsilon_D\right]$$

$$= \left[\frac{2\kappa_B T}{\gamma} ln \frac{\varphi\theta_c}{\Theta_o - \theta_{nc} - \varphi\theta_c} + 2\left(\theta \frac{\partial}{\partial\theta}\varepsilon_h(\theta) + \varepsilon_h(\theta)\right) + 2\left(\theta_c \frac{\partial}{\partial\theta} E_B^c(\theta) + E_B^c(\theta)\right) + 3\epsilon_{0v}\right.$$

$$\left. - \kappa_B T\, ln\left(2\, sinh \frac{\epsilon_{0v}}{2\kappa_B T}\right) + \kappa_B T\, ln \frac{8\pi^2 I\kappa_B T}{\sigma h^2} + \epsilon_D\right] \quad 592$$

Substituting for modeled $\varepsilon_h(\theta)$ and $E_B^c(\theta)$,

$$B(\theta,T) = \frac{2\kappa_B T}{\gamma} ln \frac{\varphi\theta_c}{\theta_o - \theta_{nc} - \varphi\theta_c} + 2\left(\theta \frac{\partial}{\partial\theta}[\varepsilon_h(\theta) + \varepsilon_\delta^0 + \varepsilon_\delta^1\theta + \varepsilon_\delta^2\theta^2] + [\varepsilon_h(\theta) + \varepsilon_\delta^0 + \varepsilon_\delta^1\theta + \varepsilon_\delta^2\theta^2]\right)$$
$$+ 2\left(\theta_c \frac{\partial}{\partial\theta}[\varepsilon_c^0 + \varepsilon_c^1\theta + \varepsilon_c^2\theta^2] + [\varepsilon_c^0 + \varepsilon_c^1\theta + \varepsilon_c^2\theta^2]\right) + 3\epsilon_{0v} - \kappa_B T\, ln\left(2\, sinh \frac{\epsilon_{0v}}{2\kappa_B T}\right)$$
$$+ \kappa_B T\, ln \frac{8\pi^2 I \kappa_B T}{\sigma h^2} + \epsilon_D$$

593

or

$$B(\theta,T) = \frac{2\kappa_B T}{\gamma} ln \frac{\varphi\theta_c}{\theta_o - \theta_{nc} - \varphi\theta_c} + 2\left[\theta \frac{\partial}{\partial\theta}\varepsilon_h(\theta) + \varepsilon_h(\theta) + \varepsilon_\delta^0 + 2\varepsilon_\delta^1\theta + 3\varepsilon_\delta^2\theta^2\right]$$
$$+ 2[\varepsilon_c^0 + \varepsilon_c^1(\theta_c + \theta) + \varepsilon_c^2(2\theta_c\theta + \theta^2)] + 3\epsilon_{0v} - \kappa_B T ln\left(2\, sinh \frac{\epsilon_{0v}}{2\kappa_B T}\right) + \kappa_B T ln \frac{8\pi^2 I \kappa_B T}{\sigma h^2}$$
$$+ \epsilon_D$$

594

Excess Molar Enthalpy With Nearest Neighbor Exclusion

We derive the excess molar quantities as before, Chapter 7. Thus, the excess enthalpy change is then

$$\Delta\bar{H}_H^E = -T^2\left(\frac{\partial\left(\frac{\Delta\bar{G}_H^E}{T}\right)}{\partial T}\right)_{P,n} \tag{595}$$

and

$$\Delta\bar{G}_H = \frac{1}{2}RT * ln\,(f_{H_2}) \tag{596}$$

$$\Delta\bar{G}_H = \bar{G}_H^{Ideal} + \Delta\bar{G}_H^{Excess} \tag{597}$$

$$\bar{G}_H^{Ideal} = RTln\frac{\theta}{1-\theta} \tag{598}$$

$$\Delta\bar{G}_H(\theta,T) = \frac{1}{2}RT\,ln\left(A(T) * e^{\frac{B(\theta,T)}{\kappa_B T}}\right) = \frac{1}{2}RT\left[lnA(T) + \frac{B(\theta,T)}{\kappa_B T}\right]$$

$$\Delta\bar{G}_H(\boldsymbol{\theta},T) = \frac{RT}{2}lnA(T) + \frac{RT}{\gamma}ln\frac{\varphi\theta_c}{\theta_o - \theta_{nc} - \varphi\theta_c} + \frac{R}{\kappa_B}\left[\theta\frac{\partial}{\partial\theta}\varepsilon_h(\theta) + \varepsilon_h(\theta) + \varepsilon_\delta^0 + 2\varepsilon_\delta^1\theta + 3\varepsilon_\delta^2\theta^2\right]$$
$$+\frac{R}{\kappa_B}[\varepsilon_c^0 + \varepsilon_c^1(\theta_c+\theta) + \varepsilon_c^2(2\theta_c\theta + \theta^2)] + \frac{3R}{2\kappa_B}\epsilon_{0v} - \frac{RT}{2}ln\left(2\,sinh\frac{\epsilon_{0v}}{2\kappa_B T}\right)$$
$$+\frac{RT}{2}ln\frac{8\pi^2 I\kappa_B T}{\sigma h^2} + \frac{R}{2\kappa_B}\epsilon_D \tag{599}$$

$$\Delta\bar{G}_H^E(\theta,T) = \frac{RT}{2} lnA(T) + \frac{RT}{\gamma} ln\frac{\varphi\theta_c}{\theta_o - \theta_{nc} - \varphi\theta_c} + \frac{R}{\kappa_B}\left[\theta\frac{\partial}{\partial\theta}\varepsilon_h(\theta) + \varepsilon_h(\theta) + \varepsilon_\delta^0 + 2\varepsilon_\delta^1\theta + 3\varepsilon_\delta^2\theta^2\right]$$
$$+ \frac{R}{\kappa_B}[\varepsilon_c^0 + \varepsilon_c^1(\theta_c + \theta) + \varepsilon_c^2(2\theta_c\theta + \theta^2)] + \frac{3R}{2\kappa_B}\epsilon_{0v} - \frac{RT}{2} ln\left(2\,sinh\frac{\epsilon_{0v}}{2\kappa_B T}\right)$$
$$+ \frac{RT}{2} ln\frac{8\pi^2 I\kappa_B T}{\sigma h^2} + \frac{R}{2\kappa_B}\epsilon_D - RT ln\frac{\theta}{1-\theta}$$

600

$$\frac{\Delta\bar{G}_H^E(\theta,T)}{T} \rightarrow \frac{R}{2} lnA(T) + \frac{R}{\gamma} ln\frac{\varphi\theta_c}{\theta_o - \theta_{nc} - \varphi\theta_c} + \frac{R}{\kappa_B T}\left[\theta\frac{\partial}{\partial\theta}\varepsilon_h(\theta) + \varepsilon_h(\theta) + \varepsilon_\delta^0 + 2\varepsilon_\delta^1\theta + 3\varepsilon_\delta^2\theta^2\right]$$
$$+ \frac{R}{\kappa_B T}[\varepsilon_c^0 + \varepsilon_c^1(\theta_c + \theta) + \varepsilon_c^2(2\theta_c\theta + \theta^2)] + \frac{3R}{2\kappa_B T}\epsilon_{0v} - \frac{R}{2} ln\left(2\,sinh\frac{\epsilon_{0v}}{2\kappa_B T}\right)$$
$$+ \frac{R}{2} ln\frac{8\pi^2 I\kappa_B T}{\sigma h^2} + \frac{R}{2\kappa_B T}\epsilon_D - R ln\frac{\theta}{1-\theta}$$

601

$$\Delta\bar{H}_H^E(\theta,T) = -T^2\left(\frac{\partial\left(\frac{\Delta\bar{G}_H^E}{T}\right)}{\partial T}\right)_{P,n}$$

$$= -T^2\left(\frac{R}{2}\frac{A'(T)}{A(T)} - \frac{R}{\kappa_B T^2}\left(\theta\frac{\partial}{\partial\theta}\varepsilon_h(\theta) + \varepsilon_h(\theta) + \varepsilon_\delta^0 + 2\varepsilon_\delta^1\theta + 3\varepsilon_\delta^2\theta^2\right)\right.$$
$$- \frac{R}{\kappa_B T^2}[\varepsilon_c^0 + \varepsilon_c^1(\theta_c + \theta) + \varepsilon_c^2(2\theta_c\theta + \theta^2)] - \frac{3R}{2\kappa_B T^2}\epsilon_{0v} + \frac{R}{4}\frac{\epsilon_{0v}}{\kappa_B T^2}\coth\left(\frac{\epsilon_{0v}}{2\kappa_B T}\right) + \frac{R}{2T}$$
$$\left. - \frac{R}{2\kappa_B T^2}\epsilon_D\right)$$

602

$$\bar{H}_H^E(\theta,T) = -\frac{RT^2}{2}\frac{A'(T)}{A(T)} + \frac{R}{\kappa_B}\left(\theta\frac{\partial}{\partial\theta}\varepsilon_h(\theta) + \varepsilon_h(\theta) + \varepsilon_\delta^0 + 2\varepsilon_\delta^1\theta + 3\varepsilon_\delta^2\theta^2\right)$$
$$+ \frac{R}{\kappa_B}[\varepsilon_c^0 + \varepsilon_c^1(\theta_c + \theta) + \varepsilon_c^2(2\theta_c\theta + \theta^2)] + \frac{3R}{2\kappa_B}\epsilon_{0v} - \frac{R}{4}\frac{\epsilon_{0v}}{\kappa_B}coth\frac{\epsilon_{0v}}{2\kappa_B T} - \frac{RT}{2} + \frac{R}{2\kappa_B}\epsilon_D$$
$$- \Delta\bar{H}_H^0(T)$$

603

Excess Molar Entropy With Nearest Neighbor Exclusion

The excess molar entropy is

$$-\Delta\bar{S}_H(\theta,T) = \left(\frac{\partial\Delta\bar{G}_H(\theta,T)}{\partial T}\right)_{P,n}$$

$$= \frac{RT}{2}\frac{A'(T)}{A(T)} + \frac{R}{2}lnA(T) + \frac{R}{\gamma}ln\frac{\varphi\theta_c}{\Theta_o - \theta_{nc} - \varphi\theta_c} + \frac{R\epsilon_{0v}}{4\kappa_B T}coth\frac{\epsilon_{0v}}{2\kappa_B T} - \frac{R}{2}ln\left(2\,sinh\frac{\epsilon_{0v}}{2\kappa_B T}\right)$$

$$+\frac{R}{2} + \frac{R}{2}ln\frac{8\pi^2 I\kappa_B T}{\sigma h^2}$$

604

$$\bar{S}_H^E(\theta,T) = -\frac{RT}{2}\frac{A'(T)}{A(T)} - \frac{R}{2}lnA(T) - \frac{R}{\gamma}ln\frac{\varphi\theta_c}{\Theta_o - \theta_{nc} - \varphi\theta_c} - \frac{R\epsilon_{0v}}{4\kappa_B T}coth\frac{\epsilon_{0v}}{2\kappa_B T} + \frac{R}{2}ln\left(2\,sinh\frac{\epsilon_{0v}}{2\kappa_B T}\right)$$

$$-\frac{R}{2} - \frac{R}{2}ln\frac{8\pi^2 I\kappa_B T}{\sigma h^2} + Rln\frac{\theta}{1-\theta} - \Delta\bar{S}_H^0(T)$$

605

Octahedral Occupation Approximation

To get closer to a computable model (one we can use in Matlab for example), and determine the free parameters, we can make the following approximations, valid for the O-to-T model in the miscibility gap:

$$\theta_o \approx \theta$$

606

$$\theta_o \approx 1$$

607

and write the enthalpy and entropy, respectively, as

$$\bar{H}_H^E(\theta,T) = -\frac{RT^2}{2}\frac{A'(T)}{A(T)} + \frac{R}{\kappa_B}\left(\theta\frac{\partial}{\partial\theta}\varepsilon_h(\theta) + \varepsilon_h(\theta) + \varepsilon_\delta^0 + 2\varepsilon_\delta^1\theta + 3\varepsilon_\delta^2\theta^2\right)$$
$$+\frac{R}{\kappa_B}[\varepsilon_c^0 + \varepsilon_c^1(\theta_c+\theta) + \varepsilon_c^2(2\theta_c\theta+\theta^2)] + \frac{3R}{2\kappa_B}\epsilon_{0v} - \frac{R}{4}\frac{\epsilon_{0v}}{\kappa_B}coth\frac{\epsilon_{0v}}{2\kappa_B T} - \frac{RT}{2} + \frac{R}{2\kappa_B}\epsilon_D$$
$$-\Delta\bar{H}_H^0(T)$$

608

$$\bar{S}_H^E(\theta,T) = -\frac{RT}{2}\frac{A'(T)}{A(T)} - \frac{R}{2}lnA(T) - \frac{R}{\gamma}ln\frac{\varphi\theta_c}{\Theta_o - \theta_{nc} - \varphi\theta_c} - \frac{R\epsilon_{0v}}{4\kappa_B T}coth\frac{\epsilon_{0v}}{2\kappa_B T} + \frac{R}{2}ln\left(2\,sinh\frac{\epsilon_{0v}}{2\kappa_B T}\right) - \frac{R}{2}$$
$$-\frac{R}{2}ln\frac{8\pi^2 I\kappa_B T}{\sigma h^2} + Rln\,\frac{\theta}{1-\theta} - \Delta\bar{S}_H^0(T)$$

609

The "Orondo Isotherm" is then given by (after a slight rewrite),

$$\varphi^{\frac{1}{\gamma}}\frac{\theta_c^{\frac{1}{\gamma}}(1-\theta_{nc})^{\frac{\gamma\varphi-1}{\gamma\varphi}}}{\theta_{nc}(1-\theta_{nc}-\varphi\theta_c)^{\frac{\varphi-1}{\gamma\varphi}}} = \frac{1}{2}\left(1-e^{-\frac{\epsilon_{0v}}{\kappa_B T}}\right)^3 e^{\frac{E_B^c(n)}{\kappa_B T}}$$

610

such that Equations 608 and 609 need to be solved consistently with the "Orondo Isotherm", Equation 610 which, in this case, does not have as simple a form as before. Nonetheless, solutions to the isotherm in this case exist in the regime where the denominator does not vanish, which is equivalent to

$$1-\theta_{nc}-\varphi\theta_c > 0$$

611

or

$$\theta_c < \frac{\gamma}{\alpha}(1-\theta)$$

612

Results

We start by presenting clumped vs. non-clumped occupation – and corresponding binding energy. In all instances, we show a comparison between NN=0.5 and NN=1.0.

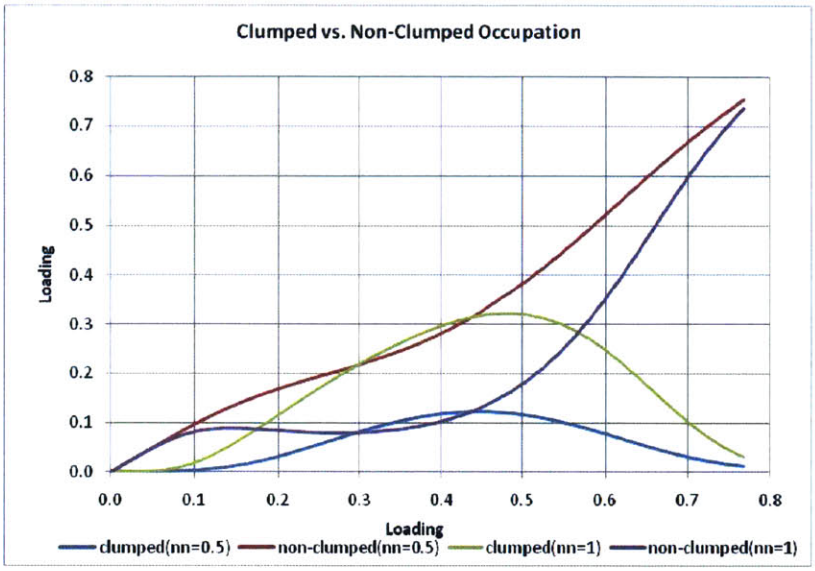

Figure 121: Clumped vs. non-clumped populations

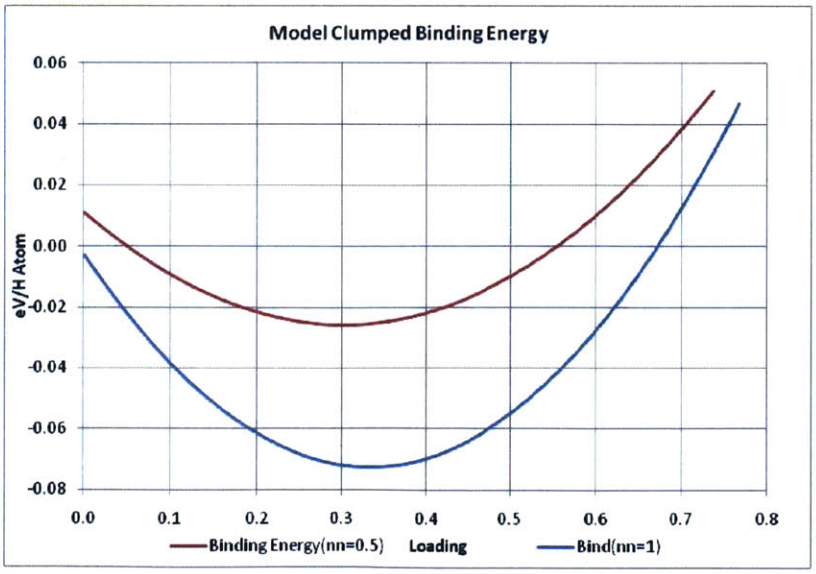

Figure 122: Binding Energy Model

We also show fractional occupation as a function of loading:

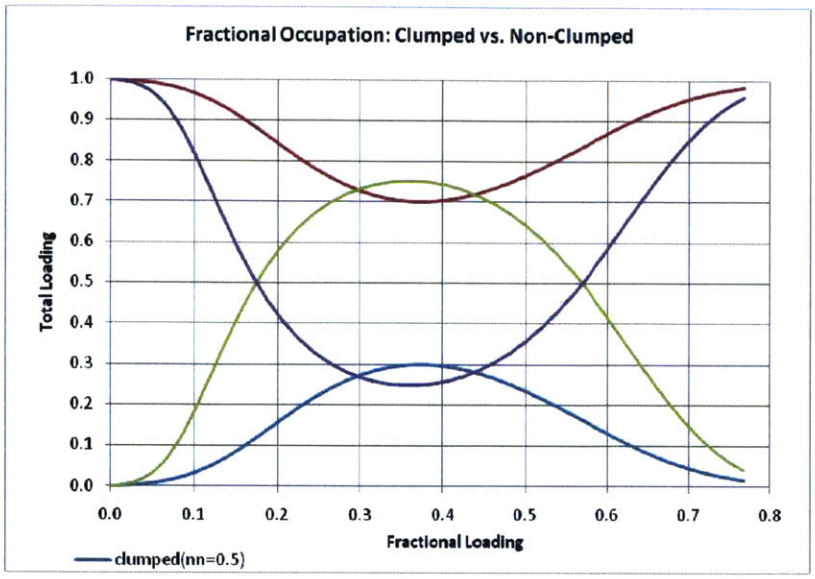

Figure 123: Clumped and non-clumped Fractional Occupation

Next, we show available fractional microstates

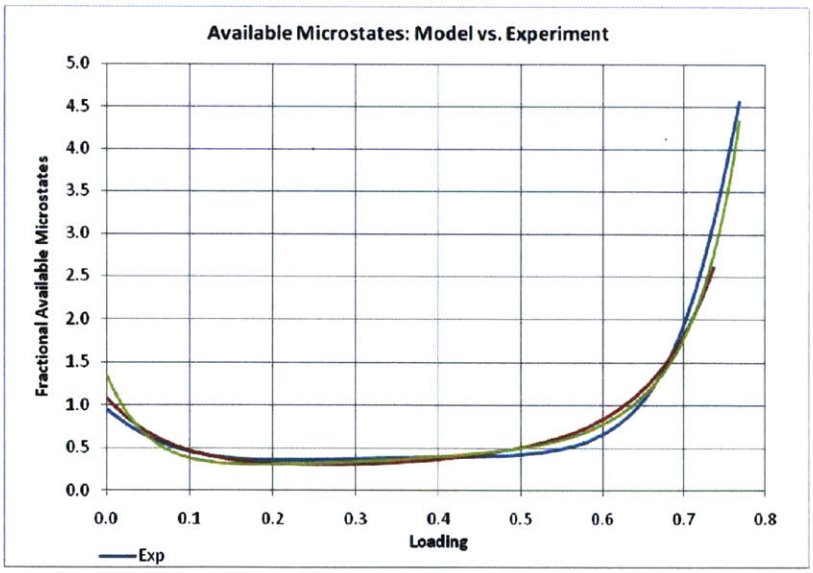

Figure 124: Available Excess Microstates

Finally, we show model molar entropy and enthalpy compared to experiment.

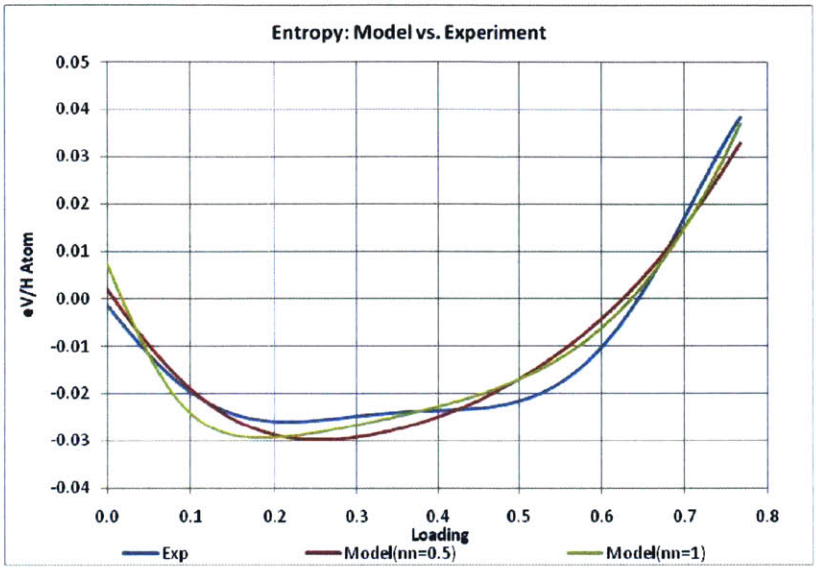

Figure 125: Entropy: Model vs. Experiment

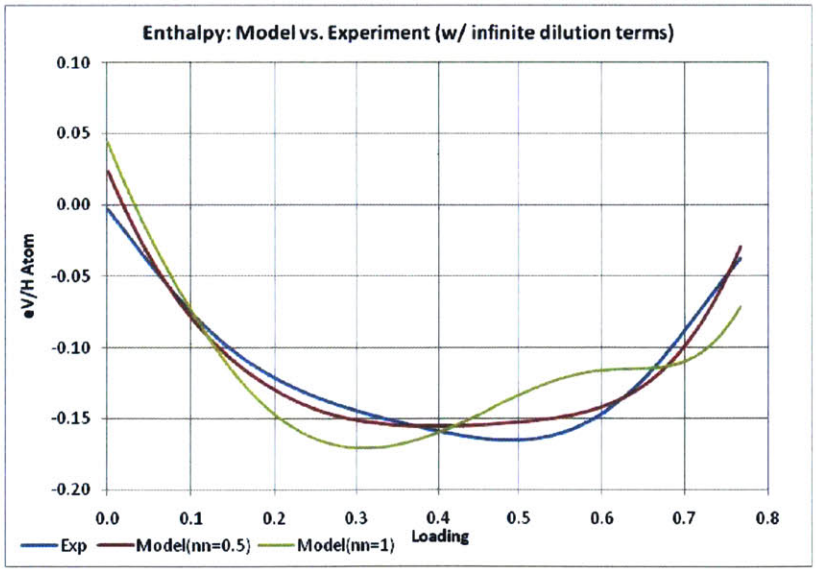

Figure 126: Enthalpy vs. Experiment

Discussion

As in the clumped case, we see that the clumped population is highest in the middle of the miscibility gap, as would be expected from physical considerations. We also see a reasonable match with experimental entropy but the enthalpy match deteriorates with more severe exclusion.

We also see that NN exclusion creates a tighter binding in the hydrogen quasi-molecules, which is perhaps not a real effect but rather an artifact.

It is also seen that a very small exclusion (NN=0.5) provides a closer match, and the match gets worse as the exclusion increases. We must therefore conclude that a clumped exclusion model does not accurately capture the physics of the problem.

An Improved Electronic Model

In this section, we take a second look at the electronic contributions to the thermodynamic quantities. As before, we begin with an examination of the partition function.

Taking a Second Look at the Electronic Partition Function

Equation 357, Chapter 7, contains the following approximation for the electronic contribution to the partition function:

$$z_e = \sum_{j,e} g_j e^{-\frac{\varepsilon_{j,e}}{\kappa_B T}} = g_0 + g_1 e^{-\frac{\varepsilon_{1,e}}{\kappa_B T}} + g_2 e^{-\frac{\varepsilon_{2,e}}{\kappa_B T}} + \cdots \cong g_0 \qquad 613$$

In Equation 613, g_j is the degeneracy of state j with energy ε_j and the summation is carried out over all electronic energies. We previously justified the approximation based on the electronic energies being large and well separated, such that subsequent terms decrease very rapidly. We would like to investigate if these higher order electronic terms make any significant contributions to thermodynamic terms, especially entropy in the high loading regime.

To proceed, we will propose that the clumped electronic contribution is given as before in Equation 413, Chapter 9, i.e.:

$$z_{e,c} = \sum_{j,e} g_j^c e^{-\frac{\varepsilon_{j,e,c}}{\kappa_B T}} \approx g_0^c = 1 \qquad 614$$

In other words, these clumped electrons will localize in the clump since they are needed in the very formation of the clump electronic states.

The non-clumped electrons, however, are free to move around the metal bulk and form electronic energy bands. It is the entropy from these bands that we propose may be responsible for the high entropy seen in experiment. To model them, we assume that these electrons have a loading dependent band energy, i.e.

$$\epsilon \rightarrow \varepsilon_\sigma(n, \kappa, T)$$

615

where n denotes the number of electrons (or loading), κ denotes their band, and σ is a spin index. We may further assume that band energy depends only weakly on temperature, such that, to a zeroth order approximation, we may have

$$\varepsilon_\sigma(n, \kappa, T) \approx \varepsilon_\sigma(n, \kappa)$$

616

If we assume some electronic chemical potential (Fermi) level $\mu_F(n, T)$, which will depend on temperature in general, we may express Equation 613 in its exact form as (Hagelstein, Senturia, & Orlando, 2004)

$$z_{e,o}(n) = \sum_\kappa \sum_\sigma g_\kappa^\sigma e^{-\frac{\varepsilon_\sigma(n,\kappa) - \mu_F(n,T)}{\kappa_B T}}$$

617

In Equation 617, g_κ^σ is the degeneracy of the κ^{th} band with spin σ, and we have assumed that the electronic chemical potential depends on loading in general.

With these approximations, Equation 553 yields the new model partition function

$$Z_H(\tau, \mu) = \sum_{n_{nc}=0}^{N_o} \sum_{k=0}^{\frac{N_o - n_{nc}}{\alpha+\gamma}} \sum_{n_t=0}^{N_t} \sum_{ASN} e^{\frac{(n_{nc}+n_t+k\gamma)\mu - \varepsilon_h(n)}{\kappa_B T}} z_o^{n_{nc}} z_t^{n_t} z_c^{k\gamma} \left(\sum_\kappa \sum_\sigma g_\kappa^\sigma e^{-\frac{\varepsilon_\sigma(n,\kappa) - \mu_F(n,T)}{\kappa_B T}} \right) z_{e,t}^{n_t} z_{e,c}^{k\gamma}$$

618

Equation 618 is a mere substitution for now. We can proceed by moving the electronic partition function out, since it is independent of the statistical configuration details in our model. Thus,

$$Z_H(\tau,\mu) = \sum_{\kappa}\sum_{\sigma}\left(\sum_{n_{nc}=0}^{N_o}\sum_{k=0}^{\frac{N_o-n_{nc}}{\alpha+\gamma}}\sum_{n_t=0}^{N_t}\sum_{ASN} e^{\frac{(n_{nc}+n_t+k\gamma)\mu-\varepsilon_h(n)}{\kappa_B T}} z_o^{n_{nc}} z_t^{n_t} z_c^{k\gamma} z_{e,t}^{n_t} z_{e,c}^{k\gamma}\right) g_\kappa^\sigma e^{-\frac{\varepsilon_\sigma(n,\kappa)-\mu_F(n,T)}{\kappa_B T}} \quad 619$$

The terms in brackets contain configurational entropy that we already evaluated in Equation 554 above. Using those prior results, we have

$$Z_H(\tau,\mu) \cong \sum_{\kappa}\sum_{\sigma}\left(\frac{N_o!}{n_{nc}!\,(N_o-n_{nc})!}\frac{\left(\frac{N_o-n_{nc}}{\alpha+\gamma}\right)!}{k!\left(\frac{N_o-n_{nc}}{\alpha+\gamma}-k\right)!}\frac{N_t!}{n_t!\,(N_t-n_t)!} e^{-\frac{n\varepsilon_h(n)}{\kappa_B T}} z_{o,t}^{\,n_{nc}+n_t} g_{o,t}^{\,n_t} z_c^{k\gamma}\right) g_\kappa^\sigma e^{-\frac{\varepsilon_\sigma(n,\kappa)-\mu_F(n,T)}{\kappa_B T}} \quad 620$$

Clumped vs. Non-Clumped Chemical Potentials

Clumped Species

Equations 555 & 556 hold as before, assuming we can exchange the summation and the partial derivative:

$$\mu_c(\tau,n) = \mu_{nc}(\tau,n) = \mu_t(\tau,n) \quad 621$$

$$\mu_c(\tau,n) = -\tau\frac{\partial}{\partial n_c} ln\, Z_H(\tau,\mu) \quad 622$$

However, now we also have the following constraint on charge neutrality

$$n_{nc} = \int g_\kappa^\sigma(\varepsilon)\frac{1}{1+exp\left(-\frac{\varepsilon_\sigma(n_{nc},\kappa)-\mu_F(n_{nc},T)}{\kappa_B T}\right)}d\varepsilon \quad 623$$

Equation 623 is understood to apply within the Brillouin Zone and may be evaluated numerically and self consistently, or obtained from literature.

We write

$$ln\, Z_H(\tau,\mu)$$

$$\cong ln\left(\frac{N_o!}{n_{nc}!\,(N_o-n_{nc})!}\frac{\left(\frac{N_o-n_{nc}}{\alpha+\gamma}\right)!}{k!\left(\frac{N_o-n_{nc}}{\alpha+\gamma}-k\right)!}\frac{N_t!}{n_t!\,(N_t-n_t)!}\,e^{\frac{n\varepsilon_h(n)}{\kappa_B T}}{z_{o,t}}^{n_{nc}+n_t}{g_{o,t}}^{n_t}z_c^{k\gamma}\sum_{\kappa}\sum_{\sigma}g_\kappa^\sigma e^{\frac{\varepsilon_\sigma(n,\kappa)-\mu_F(n,T)}{\kappa_B T}}\right)$$

$$= ln\frac{N_o!}{n_{nc}!\,(N_o-n_{nc})!}+ln\frac{\left(\frac{N_o-n_{nc}}{\alpha+\gamma}\right)!}{k!\left(\frac{N_o-n_{nc}}{\alpha+\gamma}-k\right)!}+ln\frac{N_t!}{n_t!\,(N_t-n_t)!}-\frac{n\varepsilon_h(n)}{\kappa_B T}+(n_{nc}+n_t)lnz_{o,t}+n_t lng_{o,t}$$

$$+k\gamma\, ln(z_c)+ln\left(\sum_{\kappa}\sum_{\sigma}g_\kappa^\sigma e^{\frac{\varepsilon_\sigma(n,\kappa)-\mu_F(n,T)}{\kappa_B T}}\right)=\{T_1+T_2+T_3+T_4+T_5+T_6+T_7+T_8\}$$

624

from which we can evaluate the effect of electronic contributions to entropy. We proceed similar to above, thus

$$\frac{\partial}{\partial n_c}T_1=\frac{\partial}{\partial n_c}T_3=\frac{\partial}{\partial n_c}T_5=\frac{\partial}{\partial n_c}T_6=0$$

625

$$\frac{\partial}{\partial n_c}T_2=-\frac{1}{\gamma}ln\frac{k(\alpha+\gamma)}{N_o-n_{nc}-k(\alpha+\gamma)}$$

626

$$\frac{\partial}{\partial n_c}T_4=-\frac{1}{\gamma\tau}\left(n\frac{\partial}{\partial k}\varepsilon_h(n)+\gamma\varepsilon_h(n)\right)$$

627

$$\frac{\partial}{\partial n_c}T_7 = -\frac{1}{\tau}\left(k\frac{\partial}{\partial k}E_B^c(n) + \frac{3}{2}\epsilon_{0v} + E_B^c(n)\right) \tag{628}$$

The T_8 term is a little bit complicated, at least initially. We start by writing

$$\frac{\partial}{\partial n_c}T_8 = \frac{\partial}{\partial n_c}ln\left(\sum_\kappa\sum_\sigma g_\kappa^\sigma e^{-\frac{\varepsilon_\sigma(n,\kappa)-\mu_F(n,T)}{\kappa_B T}}\right) = \frac{\frac{\partial}{\partial n_c}\sum_\kappa\sum_\sigma g_\kappa^\sigma e^{-\frac{\varepsilon_\sigma(n,\kappa)-\mu_F(n,T)}{\kappa_B T}}}{\sum_\kappa\sum_\sigma g_\kappa^\sigma e^{-\frac{\varepsilon_\sigma(n,\kappa)-\mu_F(n,T)}{\kappa_B T}}} \tag{629}$$

By taking the partial derivative inside the summation, we have

$$\frac{\partial}{\partial n_c}T_8 = \frac{\sum_\kappa\sum_\sigma\frac{\partial}{\partial n_c}g_\kappa^\sigma e^{-\frac{\varepsilon_\sigma(n,\kappa)-\mu_F(n,T)}{\kappa_B T}}}{\sum_\kappa\sum_\sigma g_\kappa^\sigma e^{-\frac{\varepsilon_\sigma(n,\kappa)-\mu_F(n,T)}{\kappa_B T}}} = \frac{\sum_\kappa\sum_\sigma g_\kappa^\sigma e^{-\frac{\varepsilon_\sigma(n,\kappa)-\mu_F(n,T)}{\kappa_B T}}\left(-\frac{\partial}{\partial n_c}\frac{\varepsilon_\sigma(n,\kappa)-\mu_F(n,T)}{\kappa_B T}\right)}{\sum_\kappa\sum_\sigma g_\kappa^\sigma e^{-\frac{\varepsilon_\sigma(n,\kappa)-\mu_F(n,T)}{\kappa_B T}}} \tag{630}$$

Equation 630 may be re-written as

$$\frac{\partial}{\partial n_c}T_8 = -\frac{1}{\kappa_B T}\frac{\sum_\kappa\sum_\sigma g_\kappa^\sigma e^{-\frac{\varepsilon_\sigma(n,\kappa)-\mu_F(n,T)}{\kappa_B T}}\frac{\partial}{\partial n_c}(\varepsilon_\sigma(n,\kappa)-\mu_F(n,T))}{\sum_\kappa\sum_\sigma g_\kappa^\sigma e^{-\frac{\varepsilon_\sigma(n,\kappa)-\mu_F(n,T)}{\kappa_B T}}} \tag{631}$$

which looks like a thermal average of the gradient of the band energy relative to the Fermi level. For compactness, we write Equation 631 as

$$\frac{\partial}{\partial n_c}T_8 = -\frac{1}{\kappa_B T}\langle\frac{\partial}{\partial n_c}(\varepsilon_\sigma(n,\kappa)-\mu_F(n,T))\rangle_T = -\frac{1}{\kappa_B T}\left[\langle\frac{\partial}{\partial n_c}\varepsilon_\sigma(n,\kappa)\rangle_T - \langle\frac{\partial}{\partial n_c}\mu_F(n,T)\rangle_T\right] \tag{632}$$

which reveals a chemical potential dependence on the slope of the Band energy and (negative) slope of the electronic Fermi level.

The first term is

$$\langle \frac{\partial}{\partial n_c} \varepsilon_\sigma(n,\kappa) \rangle_T = \frac{\sum_\kappa \sum_\sigma g_\kappa^\sigma e^{-\frac{\varepsilon_\sigma(n,\kappa)-\mu_F(n,T)}{\kappa_B T}} \frac{\partial}{\partial n_c} \varepsilon_\sigma(n,\kappa)}{\sum_\kappa \sum_\sigma g_\kappa^\sigma e^{-\frac{\varepsilon_\sigma(n,\kappa)-\mu_F(n,T)}{\kappa_B T}}} \quad 633$$

The second chemical potential term is particularly simple because:

$$\langle \frac{\partial}{\partial n_c} \mu_F(n,T) \rangle_T = \frac{\sum_\kappa \sum_\sigma g_\kappa^\sigma e^{-\frac{\varepsilon_\sigma(n,\kappa)-\mu_F(n,T)}{\kappa_B T}} \frac{\partial}{\partial n_c} \mu_F(n,T)}{\sum_\kappa \sum_\sigma g_\kappa^\sigma e^{-\frac{\varepsilon_\sigma(n,\kappa)-\mu_F(n,T)}{\kappa_B T}}} = \frac{\partial}{\partial n_c} \mu_F(n,T) \quad 634$$

The resulting chemical potential, similar to Equation 571, is

$$\mu_c(\tau,n) = \frac{\tau}{\gamma} ln \frac{k(\alpha+\gamma)}{N_o - n_{nc} - k(\alpha+\gamma)} + \frac{1}{\gamma}\left(n \frac{\partial}{\partial k} \varepsilon_h(n) + \gamma \varepsilon_h(n)\right) + \left(k \frac{\partial}{\partial k} E_B^c(n) + \frac{3}{2}\epsilon_{0v} + E_B^c(n)\right) + \langle \frac{\partial}{\partial n_c} \varepsilon_\sigma(n,\kappa) \rangle_T - \frac{\partial}{\partial n_c} \mu_F(n,T) \quad 635$$

which shows that electronic correction terms in this approximation will be small, on the order of $\frac{1}{N}$. We therefore drop them in the following expression of the chemical potential to be consistent with earlier approximations.

$$\mu_c(\tau,\theta) = \tau \frac{1}{\gamma} ln \frac{\varphi\theta_c}{\Theta_o - \theta_{nc} - \varphi\theta_c} + \theta \frac{\partial}{\partial\theta} \varepsilon_h(\theta) + \varepsilon_h(\theta) + \theta_c \frac{\partial}{\partial\theta} E_B^c(\theta) + \frac{3}{2}\epsilon_{0v} + E_B^c(\theta) \quad 636$$

Non-Clumped Species

For the non-clumped species, we have

$$\frac{\partial}{\partial n_{nc}} T_1 = -ln \frac{n_{nc}}{N_o - n_{nc}} \tag{637}$$

$$\frac{\partial}{\partial n_{nc}} T_2 = -\frac{1}{\alpha + \gamma} ln \frac{N_o - n_{nc}}{N_o - n_{nc} - k(\alpha + \gamma)} \tag{638}$$

$$\frac{\partial}{\partial n_{nc}} T_3 = 0 \tag{639}$$

$$\frac{\partial}{\partial n_{nc}} T_4 = -\frac{1}{\tau} \left[n \frac{\partial}{\partial n_{nc}} \varepsilon_h(n) + \varepsilon_h(n) \right] \tag{640}$$

$$\frac{\partial}{\partial n_{nc}} T_5 = ln(z_{o,t}) \tag{641}$$

$$\frac{\partial}{\partial n_{nc}} T_6 = 0 \tag{642}$$

$$\frac{\partial}{\partial n_{nc}} T_7 = -\frac{n_c}{\tau} \frac{\partial}{\partial n_{nc}} E_B^c(n) \tag{643}$$

T_8 once again requires a lit bit more work:

$$\frac{\partial}{\partial n_{nc}} T_8 = \frac{\partial}{\partial n_{nc}} ln\left(\sum_{\kappa}\sum_{\sigma} g_{\kappa}^{\sigma} e^{-\frac{\varepsilon_{\sigma}(n,\kappa)-\mu_F(n,T)}{\kappa_B T}}\right) = \frac{\frac{\partial}{\partial n_{nc}}\sum_{\kappa}\sum_{\sigma} g_{\kappa}^{\sigma} e^{-\frac{\varepsilon_{\sigma}(n,\kappa)-\mu_F(n,T)}{\kappa_B T}}}{\sum_{\kappa}\sum_{\sigma} g_{\kappa}^{\sigma} e^{-\frac{\varepsilon_{\sigma}(n,\kappa)-\mu_F(n,T)}{\kappa_B T}}}$$

644

However, as in the prior section, we can at once determine that this term is also negligibly small, such that

$$\mu_{nc}(\tau,n) = \tau\, ln\frac{n_{nc}}{N_o - n_{nc}} + \frac{\tau}{\alpha+\gamma} ln\frac{N_o - n_{nc}}{N_o - n_{nc} - k(\alpha+\gamma)} + \left[n\frac{\partial}{\partial n_{nc}}\varepsilon_h(n) + \varepsilon_h(n)\right] - \tau\, ln(z_{o,t}) + n_c\frac{\partial}{\partial n_{nc}} E_B^c(n)$$

645

and therefore our results are the same as before.

An Estimate

Even though the analysis of the prior section indicates that the electronic correction to band energy is negligible, it would be interesting to estimate this entropy term, $\frac{R}{\kappa_B}\frac{\partial}{\partial T}\frac{\partial}{\partial \theta}\boldsymbol{\mu_F(\theta,T)}$. To do so, we will assume that the chemical potential dependence on temperature and loading is separable, i.e.,

$$\mu_F(\theta,T) = \mu_{F,\theta}(\theta)\mu_{F,T}(T)$$

646

We estimate these below.

Chemical Potential Dependence on Temperature

There is an approximation for chemical potential temperature dependence based on the linearization of the number of states around the Fermi level. The result, stated here without proof (Hagelstein, Senturia, & Orlando, 2004), is

$$\mu_F(T) = \mu_F(0) - \frac{\pi^2}{6}(\kappa_B T)^2 \left[\frac{1}{g(\varepsilon)}\frac{dg(\varepsilon)}{d\varepsilon}\right]_{\mu_F(0)} + o(T^4) \tag{647}$$

To Equation 647, we add the fourth order term, which we derive following the same arguments in [ibid]. The result is

$$\mu_F(T) = \mu_F(0) - \frac{\pi^2}{6}(\kappa_B T)^2 \left[\frac{1}{g(\varepsilon)}\frac{dg(\varepsilon)}{d\varepsilon}\right]_{\mu_F(0)} - \frac{1}{3}(\kappa_B T)^4 I(x) \left[\frac{1}{g(\varepsilon)}\frac{d^2 g(\varepsilon)}{d\varepsilon^2}\right]_{\mu_F(0)} + o(T^6) \tag{648}$$

where $I(x)$ is the definite integral

$$I(x) = \int_{-\infty}^{\infty} x'^4 \, sech^2(x') dx' \tag{649}$$

which we evaluate numerically to:

$$I(x) = 5.682196976983474 \tag{650}$$

We can take the zero-temperature value to coincide with the zero loading value from DFT (see below)

$$\mu_F(0) = 13.2213 \; eV \tag{651}$$

In Equation 647, $\mu_F(0)$ is the electronic Fermi level at $T = 0$ such that the equation describes an approximate evolution of the Fermi level with temperature. We can estimate the second term using (Mueller, Freeman, Dimmock, & Furdyna, 1970):

$$g(\mu_F(0)) = 2.281\ states\ per\ eV\ atom \pm 0.171 \tag{652}$$

and

$$\left[\frac{dg(\varepsilon)}{d\varepsilon}\right]_{\mu_F(0)} = -12.3\ states\ per\ eV^2\ atom \pm 1.62 \tag{653}$$

$$\left[\frac{d^2g(\varepsilon)}{d\varepsilon^2}\right]_{\mu_F(0)} = 84\ states\ per\ eV^3\ atom \pm 65.0 \tag{654}$$

We plot Equation 647 below.

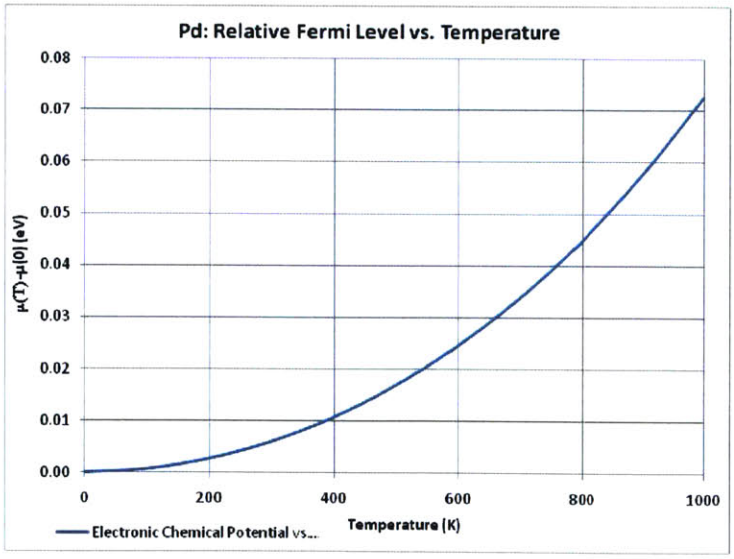

Figure 127: Relative Fermi Level vs Temperature

From Equation 647, we get

$$\frac{\partial}{\partial T}\mu_F(T) = -\frac{\pi^2}{3}{\kappa_B}^2 T\left[\frac{1}{g(\varepsilon)}\frac{dg(\varepsilon)}{d\varepsilon}\right]_{\mu_F(0)} - \frac{4}{3}{\kappa_B}^4 T^3 I(x)\left[\frac{1}{g(\varepsilon)}\frac{d^2g(\varepsilon)}{d\varepsilon^2}\right]_{\mu_F(0)} + \sigma(T^5) \quad 655$$

or using Equations 652-654, we get the following models

$$\mu_F(T) = 7.7807E-08T^2 - 6.0993E-06T + 1.3222E01 + \sigma(T^5)\ eV^{\frac{1}{2}} \quad 656$$

and

$$\frac{\partial}{\partial T}\mu_F(T) = 2.7290E-14T^3 + 5.2940E-23T^2 + 1.3173E-07T + 1.4745E-17 + \sigma(T^5)\ eV/K \quad 657$$

Fermi Energy vs. Loading

While there are several references, e.g. (Klein & Pickett, 1984), we have used the results of our DFT results for $\mu_{F,\theta}(\theta)$. The results are shown below, i.e.

$$\mu_{F,\theta}(\theta) = -0.0665*\theta^4 - 0.561*\theta^3 + 1.7866*\theta^2 - 1.5232*\theta + 13.223\ eV^{\frac{1}{2}} \quad 658$$

and

$$\frac{\partial}{\partial \theta}\mu_F(\theta) = -0.266164*\theta^3 - 1.683042*\theta^2 + 3.573148*\theta - 1.5232\ eV/atom \quad 659$$

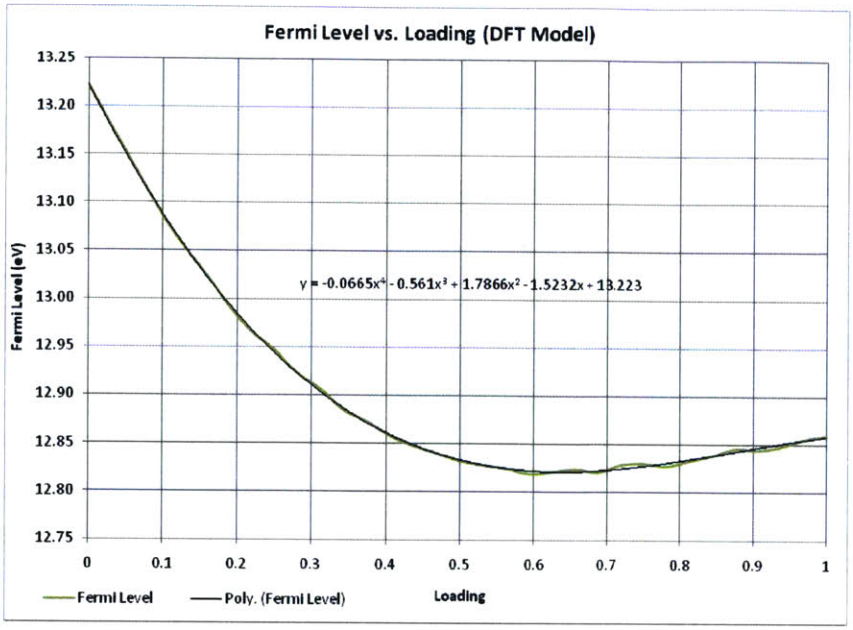

Figure 128: Fermi Energy vs. Loading (Model DFT)

By comparison, (Klein & Pickett, 1984), which has only a few data points, finds the Fermi level as follows,

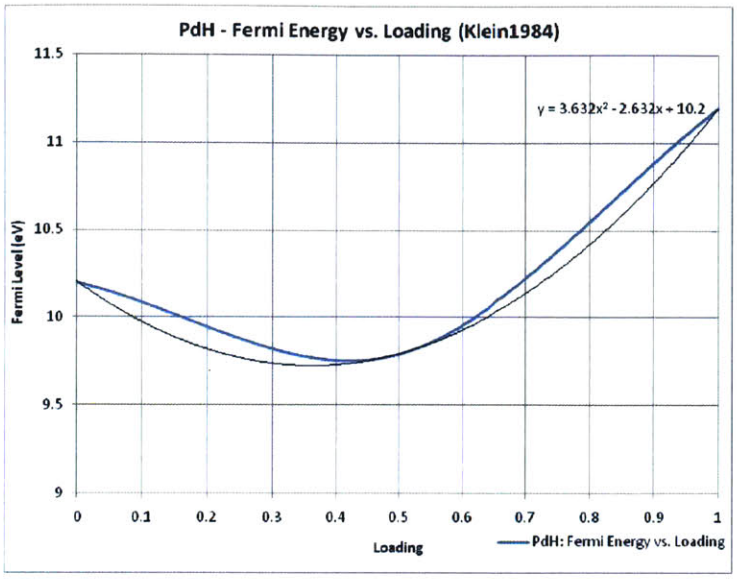

Figure 129: Fermi Level vs. Loading ((Klein & Pickett, 1984) Model)

Total correction

The total term is shown below:

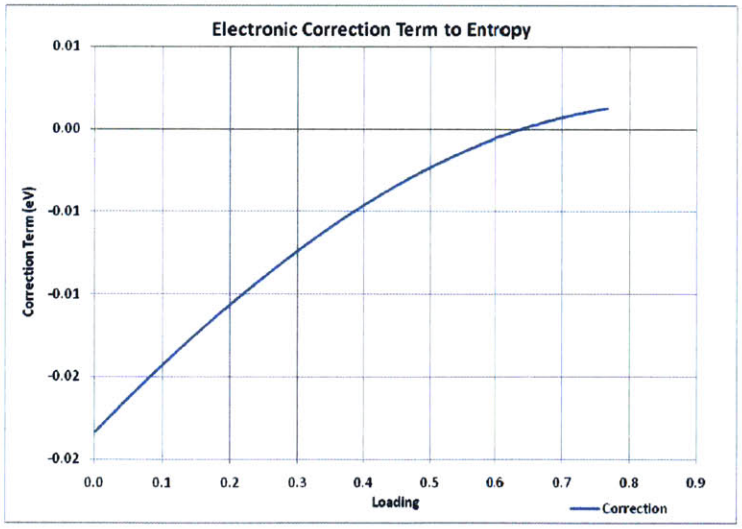

Figure 130: Total Electronic Correction to Entropy

A Second Look at the Electronic Contribution to Enthalpy/Entropy

Introduction

So far in our analysis above, we have modeled the electronic contribution to enthalpy and entropy via the grand partition function, for example, Equation 619, rewritten here for convenience.

$$Z_H(\tau,\mu)=\sum_{\kappa}\sum_{\sigma}\left(\sum_{n_{nc}=0}^{N_o}\sum_{k=0}^{\frac{N_o-n_{nc}}{\alpha+\gamma}}\sum_{n_t=0}^{N_t}\sum_{ASN}e^{\frac{(n_{nc}+n_t+k\gamma)\mu-\varepsilon_h(n)}{\kappa_B T}}z_o^{n_{nc}}z_t^{n_t}z_c^{k\gamma}z_{e,t}^{n_t}z_{e,c}^{k\gamma}\right)g_\kappa^\sigma e^{-\frac{\varepsilon_\sigma(n,\kappa)-\mu_F(n,T)}{\kappa_B T}} \tag{660}$$

However, all the subsequent analysis was denominated upon the chemical potential of hydrogen's proton, even though we know that the absorption includes the proton and an electron, see, for example, (Oates, 1982). It therefore means, except for empirical corrections in Chapter 2 based on the work of (Kuji, Oates, Bowerman, & Flanagan, 1983), we have not accounted for the electronic chemical potential in a first principles manner. We seek a resolution below.

♦

It is known that electronic contribution to entropy comes in the form of a change in electronic specific heat as hydrogen is absorbed, see for example, (Wuttig, 1974), (Oates & Flanagan, 1981). The resultant change in entropy is given by [ibid]

$$\Delta\bar{S}_H^E(\theta,T)=\int_0^T\left(\frac{\partial}{\partial\theta}\Upsilon(T)\right)dT \tag{661}$$

In Equation 661, $\Upsilon(T)$ is the electronic specific heat coefficient of the metal.

Empirical Correction to Clumped Results with No NN Exclusion

Given that the exclusion model does not appear to capture the physics of the problem (see above results), we drop it momentarily and revert back to the model with no nearest neighbor exclusions (Chapter 9) in the following analysis.

Separating Electronic Contribution

One way to deal with the electronic contribution is to separate protonic vs. electronic chemical potentials since the two are absorbed almost independently [see, for example, (Oates & Stoneham, 1983)]. We acknowledge as in [ibid] that the two contributions are likely to be coupled in interesting ways. Nonetheless, to a first order approximation, as in (Fowler, 1936), etc, we may write the total contributions as a simple sum, i.e.

$$\bar{\mu}_H^E(\theta,T) = \bar{\mu}_{H^+}^E(\theta,T) + \bar{\mu}_F^E(\theta,T) \tag{662}$$

Protonic contributions, $\bar{\mu}_{H^+}^E(\theta,T)$, have already been modeled above via a continuity with gas phase value. We therefore concentrate on the electronic component below.

Basic Formulation

To model electronic contributions, we go back to basic principles for a metallic crystal. While this is a basic result and well documented in literature – see for example (Eriksson, Wills, & Wallace, 1992) or (Wallace, 1992) – we provide a full treatment below, complete with derivation from first principles for reference purposes, and consistent with our overall investigation philosophy.

The grand partition function that applies to fermions is

$$Z_E(\tau,\mu) = \sum_n \sum_l e^{\frac{n\mu - \varepsilon_l(n)}{\tau}} \tag{663}$$

where $\varepsilon_l(n)$ is the electronic energy for a given number of particles n, and μ is the electronic chemical potential (Fermi Level), which may depend on temperature. Due to the Pauli Exclusion Principle, only a single particle can occupy an *orbital* [in the sense of (Kittel, Thermal Physics, 1980)], such that Equation 663 becomes,

$$Z_E(\tau,\mu) = \sum_n \left(1 + e^{\frac{\mu-\varepsilon_l(n)}{\tau}}\right) \tag{664}$$

Concentrating first on the single particle partition function (the term in brackets in Equation 664), we let

$$x(\tau) = \frac{\mu - \varepsilon_l(n)}{\tau} \tag{665}$$

such that

$$z_E(x) = 1 + e^x \tag{666}$$

Still considering just the single particle, the electronic entropy is given by (in units of κ_B per atom)

$$s_E(\tau,x) = \frac{\partial}{\partial\tau}(\tau\, log\, z_E(\tau,\mu))_\mu \tag{667}$$

Simplifying, we get

$$s_E(x) = \tau\frac{1}{1+e^x}e^x\frac{\partial x}{\partial\tau} + log(1+e^x) \tag{668}$$

With (remember μ is kept constant)

$$\left(\frac{\partial x}{\partial \tau}\right)_{\mu} = -\frac{\mu - \varepsilon_l(n)}{\tau^2} = -\frac{x}{\tau} \tag{669}$$

we have

$$s_E(x) = \tau \frac{e^x}{1+e^x}\left(-\frac{x}{\tau}\right) + log(1+e^x) = -\frac{xe^x}{1+e^x} + log(1+e^x) \tag{670}$$

We now introduce the Fermi-Dirac distribution function

$$f_{FD}(x) = \frac{1}{e^{-x}+1} \tag{671}$$

If we also notice that

$$1 - f_{FD} = \frac{1}{1+e^x} = \frac{1}{z_E} \tag{672}$$

then we can rewrite Equation 670 as

$$s_E(x) = -xf_{FD} - log(1 - f_{FD}) \tag{673}$$

Furthermore, we notice that

$$\frac{f_{FD}}{1-f_{FD}} = e^{x}$$

674

which, together with the identity

$$x = log(e^{x})$$

675

lead us to

$$s_E(x) = -f_{FD} log\left(\frac{f_{FD}}{1-f_{FD}}\right) - log(1-f_{FD})$$

676

or

$$s_E(x) = -[f_{FD} log f_{FD} + (1-f_{FD}) log(1-f_{FD})]$$

677

Reintroducing the full problem – Equation 664 – we have

$$S_E(x) = -\sum_n [f_{FD} log f_{FD} + (1-f_{FD}) log(1-f_{FD})]$$

678

which may be turned into an integral via the introduction of a density of states function $g(\varepsilon)$. The final, well known, result is

$$S_E(x) = -\int g(\varepsilon) d\varepsilon \left(f_{FD} log f_{FD} + (1-f_{FD}) log(1-f_{FD})\right)$$

679

where, explicitly,

$$f_{FD}(x) = f_{FD}(\varepsilon, \mu) = \frac{1}{e^{(\varepsilon-\mu)/\tau} + 1} \tag{680}$$

Typically, we also require that the chemical potential $\mu(T)$ be determined in such a way that the number of valence electrons comes out correctly (Eriksson, Wills, & Wallace, 1992)

$$n_v = \int g(\varepsilon) f_{FD}(\varepsilon) d\varepsilon \tag{681}$$

Computational Details

To get to a computational model, we need to determine the following quantities as functions of loading:

Quantity	Description	Units
$g(\theta)$	Density of States	States/eV
$\varepsilon(\theta)$	Electron (Band) Energy	eV/atom
$\mu_F(\theta)$	Fermi Level	eV

The above quantities are accessible *ab initio*, meaning that we may dispense with Equation 681.

Density of States (DOS)

The density of states (DOS) may be calculated using a two step calculation; a first SCF to get a converged ground state electronic charge density followed by a much finer NSCF calculation to get the actual DOS. The density of states is assumed to depend on loading, such that

$$g(\varepsilon) \rightarrow g_\theta(\varepsilon)$$

682

Below, we plot DOS for several loading levels (derived from a 4-Pd unit primitive cell). We note that the zero loading results compare well to (Eriksson, Wills, & Wallace, 1992):

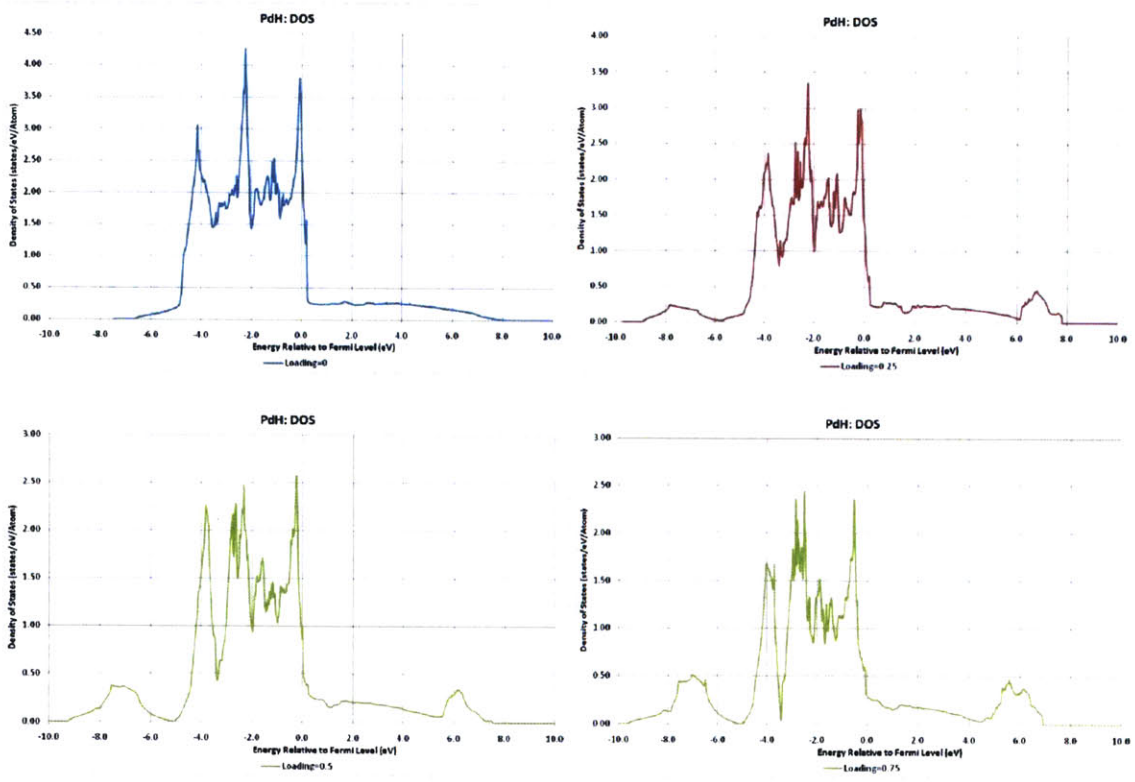

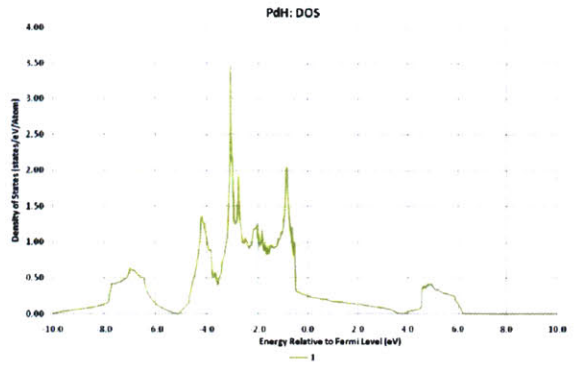

Figure 131: PdH Density of States vs. Loading (First Principles Calculations)

Fermi Level

The Fermi Level is also directly available *ab initio* as a function of loading. It is referenced against that at zero loading, so we may write

$$\Delta\mu_F(\theta) = -0.896\theta^3 + 2.6296\theta^2 - 1.9234\theta + 0.0032\ eV \quad (683)$$

The result is shown below:

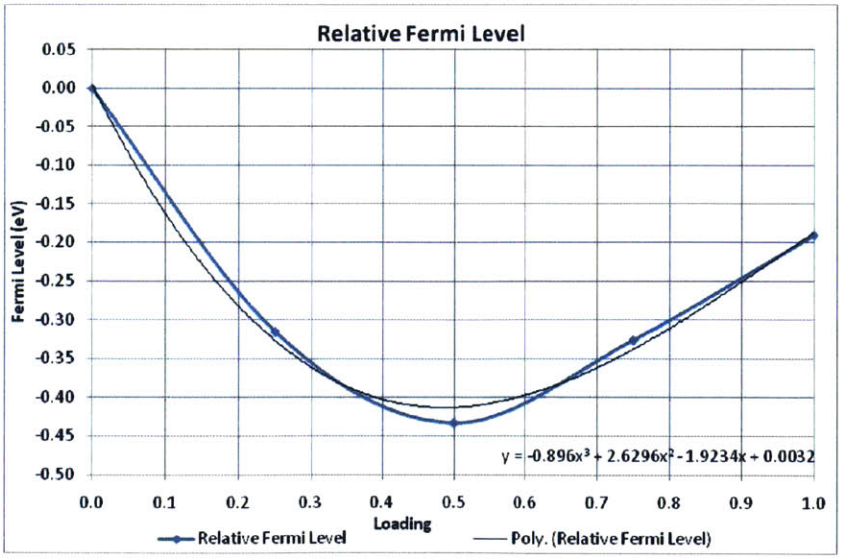

Figure 132: Fermi Level vs. Loading (First Principles Calculation)

Band Energy

The band energy is directly accessible *ab initio* as a function of loading. The band energies are also referenced against zero loading, i.e.

$$\Delta\varepsilon(\theta) = 17.382\theta^4 - 55.161\theta^3 + 66.683\theta^2 - 26.781\theta + 0.0427\, eV/atom \quad (684)$$

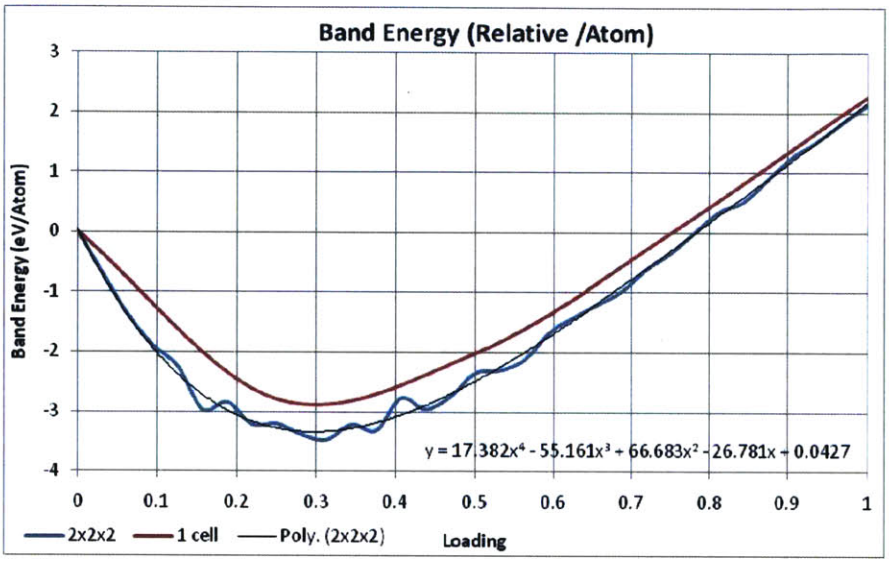

Figure 133: Band energy per atom (relative to zero level at loading). We show two results from two cell sizes.

Temperature Dependence: Fermi Dirac Distribution

As a first order approximation, we can assume that the temperature dependence of Equation 679 only enters via the Fermi Dirac distribution, and that the Fermi Level and band energies are temperature independent.

We therefore have

$$\Delta f_{FD}(\theta) = \Delta f_{FD}(\varepsilon(\theta), \mu(\theta)) = \frac{1}{e^{\frac{(\Delta\varepsilon(\theta) - \Delta\mu(\theta))}{\tau}} + 1} \quad (685)$$

Equation 685 is not of the usual form, $f_{FD}(\varepsilon)$, but rather its loading dependent version. An example is shown below for T=298.

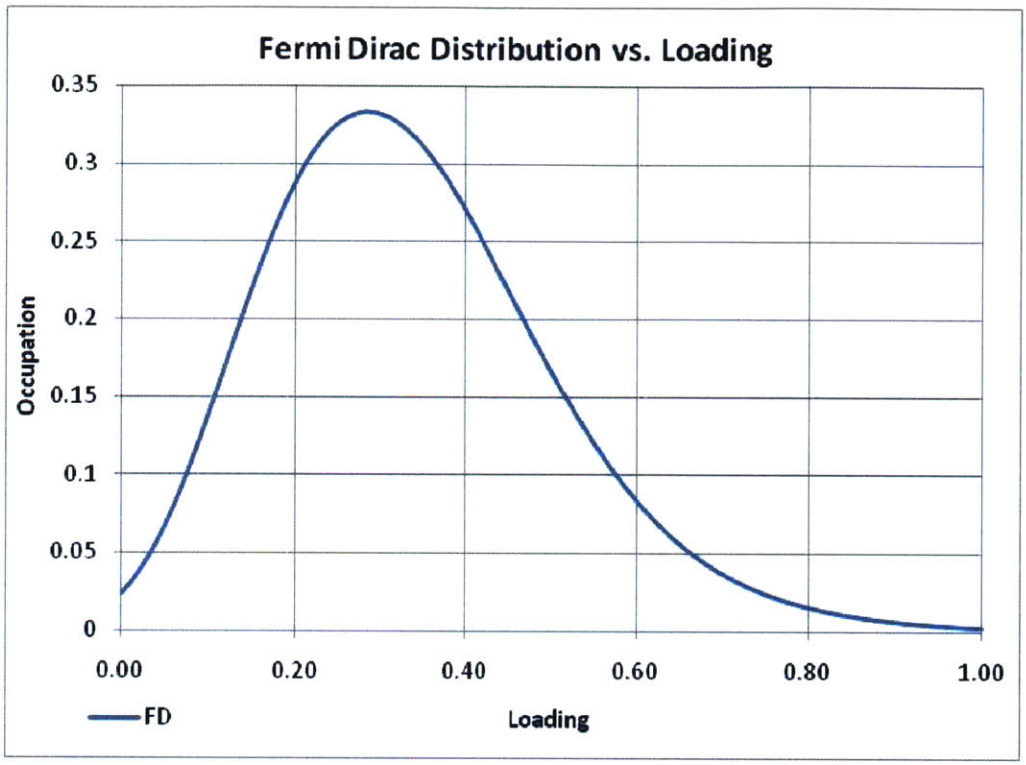

Figure 134: Model Fermi Dirac in "Loading" Space (Equation 685)

All that remains is to evaluate Equation 679 at each loading level for which we have the density of states data. In view of Equations 683 & 684, we rewrite the equation as

$$[\Delta S_E(\varepsilon)]_\theta = -\left[\int g(\varepsilon)d\varepsilon\left(f_{FD}\log f_{FD} + (1-f_{FD})\log(1-f_{FD})\right)\right]_\theta \quad 686$$

Results

The results are shown below. Note that the electronic entropy decreases with loading, consistent with other results (Oates & Flanagan, 1981). Additionally, the order of magnitude, in comparison with configurational entropy results above, at an order or magnitude lower, is also consistent with literature (Wallace, 1992)

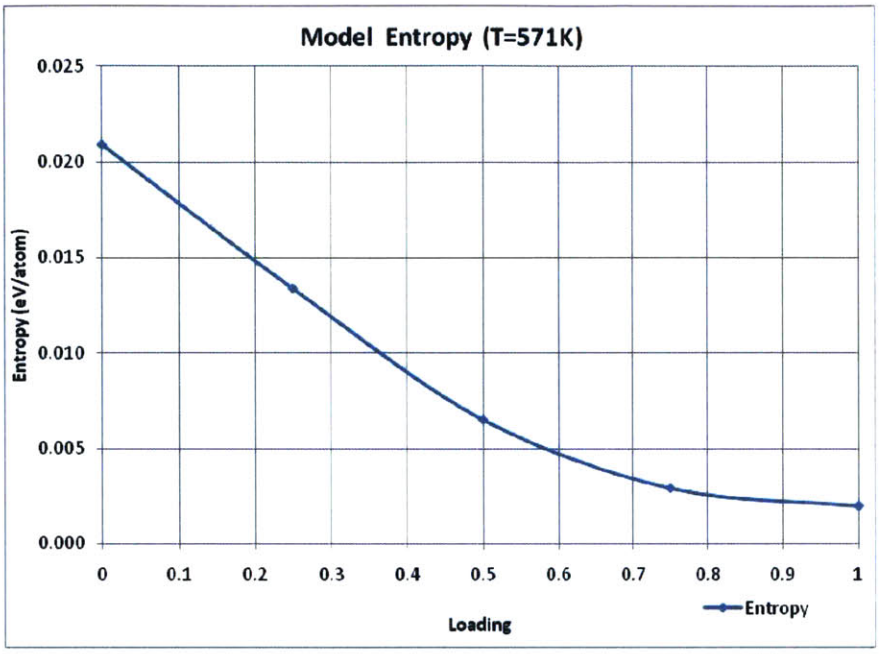

Figure 135: Model Electronic Entropy at 571K

A Re-Examination of Configurational Entropy

The results of the previous sections, starting with the more approximate result in section *An Improved Electronic Model* above, followed by more exact *ab initio* results just presented above make it clear that electronic contributions to entropy are negligible. This is supported by other workers, for example, (Oates & Flanagan, 1981), (Kuji, Oates, Bowerman, & Flanagan, 1983) and (Wuttig, 1974). The consequence is that the entropy at high loading, specifically the change in slope around a loading of 0.65 from negative to positive, must have a non-ideal configurational origin - see (Flanagan, Luo, & Clewley, 1991) and (Kuji, Oates, Bowerman, & Flanagan, 1983), for example.

We set out to investigate this in the context of our clumped model.

Clumped Model Without Exclusion and Non-Ideal Configuration Entropy

The obvious question is whether any of our models here can predict the high loading entropy result.

First, we already dismissed the Clumped Model with Exclusion since it yields worse fit to experiment. Second, we note that our clumping model without nearest neighbor exclusions appears to show a correlation between strong clumping and the miscibility gap (see Figures 6 and 7 of Chapter 9). We may use these results as foundation, except that instead of making assumptions regarding the clumping factor, we numerically solve the "Orondo Isotherm" generally (it is relatively simple in this model).

Allowing Clumping at High Loading

We previously attempted to exclude clumping at high loading on the basis that no clumps would form in adjacent interstitials. This assumption, however, does not appear to be correct. Specifically, if we allow an interpretation of the binding energy as a simple energetically favored configuration within a clump, then there is no practical or theoretical difficulty in having adjacent clump configuration, and there appears to be some support for it in the literature, e.g., (Lacher, 1937), (Simons & Flanagan, 1965) or (Makrides, 1964). There could certainly be some higher order binding energy between neighboring clumps, but as long as the clumped binding energy is lower, there clump quasi-molecules would still be more stable and hence favored energetically.

We use those results to derive the phase diagram in the next chapter.

Chapter 11 - Phase Diagram of the Clumped Model and Analysis of Temperature Dependence

Summary

This is a summary chapter uses the results from prior chapters to derive the phase diagram of PdH.

Phase Diagram Model I

As you may recall from Chapter 2, the original phase diagram was based on the initial statistical model, which contained the following model elements:

- A statistical description of H loading Pd in the mold of (Lacher, 1937), following treatment of (Christensen, Stoltze, Jacobsen, & Norskov, 1990).
- The model treats absorbed hydrogen as a harmonic oscillator (Chapter 2, Equation 53)

$$z = \left(2sinh\frac{\epsilon_{0v}}{2\tau}\right)^{-3}$$

687

- The model finds an expression for the chemical potential of absorbed hydrogen as (Equation 50, Chapter 2)

$$\mu_H(\tau,\theta) = \tau\, ln\frac{\theta}{1-\theta} - \tau\, ln\, z + \theta\frac{\partial}{\partial\theta}\varepsilon_h(\theta) + \varepsilon_h(\theta)$$

688

- The model includes tetrahedral site occupation, based on an ab initio determination of an O-to-T Excitation model (Equations 86, 89, Chapter 2)

$$e^{-\Delta\varepsilon_{O-T}(\theta)/\tau} = \frac{\theta_t(1-\theta_o)}{\theta_o(1-\theta_t)}$$

689

$$\Delta\varepsilon_{O-T}(\theta) = \frac{1}{2}\theta\frac{\partial\varepsilon_h(\theta_o,\theta_t)}{\partial\theta_t} - \theta\frac{\partial\varepsilon_h(\theta_o,\theta_t)}{\partial\theta_o}$$

690

- The state energies above are determined according to (Equation 94, Chapter 2), and are corrected via a simple offset to match experimental pressure.

$$\varepsilon_h(n) = \varepsilon^{Pd}_{(n+1)H} - \left(\varepsilon^{Pd}_{nH} + \frac{1}{2}\varepsilon^{Vac}_{2H}\right)$$

691

- The gas phase Hydrogen is treated as non-ideal, with the non-ideal corrections added via the fugacity model of (Tkacz & Litwiniuk, 2002) (Equations 138, 152, Chapter 2)

$$\mu_{H_2} = -\tau\, ln\left[\left(\frac{2\pi m\tau}{h^2}\right)^{\frac{3}{2}}\frac{\tau}{f}\right] - \tau\, ln\frac{e^{-\frac{\epsilon_{0v}}{2\tau}}}{1-e^{-\frac{\epsilon_{0v}}{\tau}}} - \tau\, ln\frac{8\pi^2 I\tau}{\sigma h^2} - \epsilon_D$$

692

$$ln(f) = \frac{\left\{1.5 * A * P^{2/3} + 3 * B * P^{1/3} + (D + E * T) * ln(P) - 3 * C * P^{-1/3}\right\}}{R * T}$$

693

- The final pressure model, to be compared to experimental data, was then modeled by a continuity between individual site potentials and the gas phase (Equations 160-162, Chapter 2)

$$f(\theta) = Ae^{\frac{B(\theta)}{\tau}}$$

694

$$A = \tau\left(\frac{2\pi m\tau}{h^2}\right)^{\frac{3}{2}}$$

695

$$B(\theta) = 2\tau\, ln\frac{\theta_o}{1-\theta_o} - 2\tau\, ln(z) + 2\theta\frac{\partial\varepsilon_h(\theta)}{\partial\theta} + 2\varepsilon_h(\theta) + \tau ln\frac{e^{-\frac{\epsilon_{0v}}{2\tau}}}{1-e^{-\frac{\epsilon_{0v}}{\tau}}} + \tau ln\frac{8\pi^2 I\tau}{\sigma h^2} + \epsilon_D$$

696

- Using these results, together with the Rule of Equal Areas (Lacher, 1937), we derived the following phase diagram [Figure 54, Chapter 3]

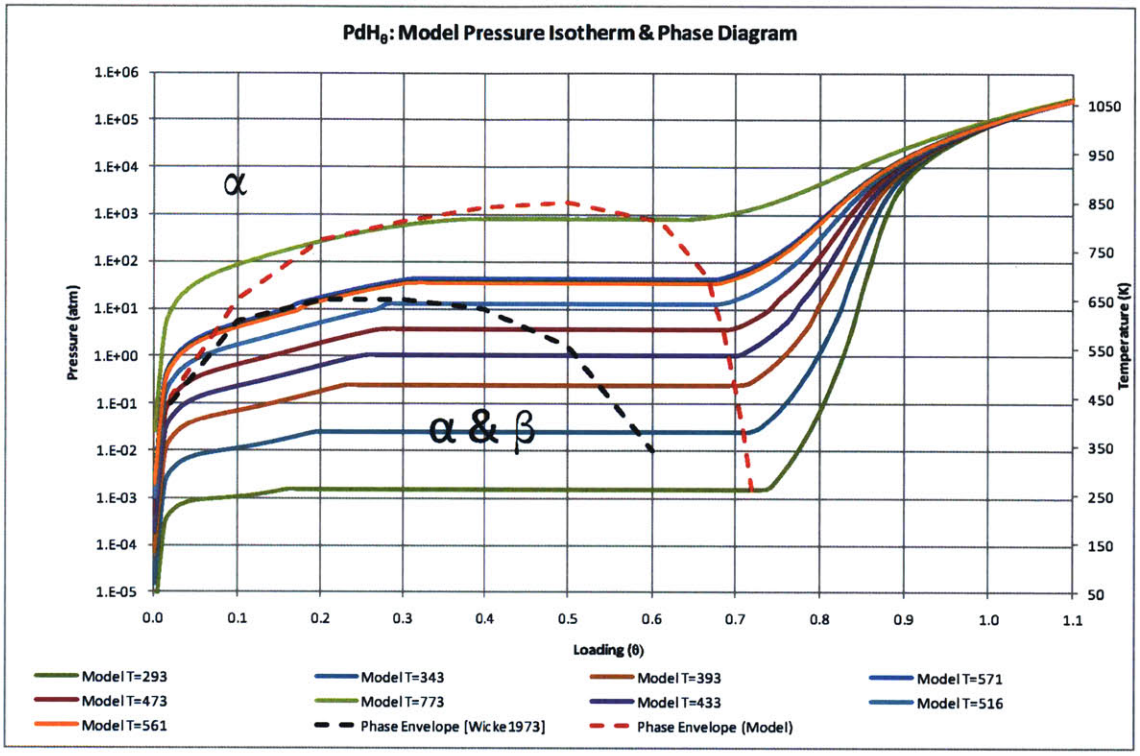

Figure 136: Model vs. Experimental Phase Diagram (After (Wicke & Brodowsky, 1978)). Model Phase diagram is derived graphically based on alpha/beta phase boundary, and is approximate.

Phase Diagram Model II

We would like to improve on the above results based on subsequent model improvements. In particular,

- We added a clumping model to account for the mixed phase (Equation 394, Chapter 9)

$$Z_H(\tau,\mu) = \sum_{n_{nc}=0}^{N_o} \sum_{n_c=0}^{N_o-n_{nc}} \sum_{n_t=0}^{N_t} \sum_{ASN} e^{\frac{(n_{nc}+n_t+n_c)\mu-\varepsilon_h(n_{nc},n_t,n_c)}{\tau}} z_o^{n_{nc}} z_t^{n_t} z_c^{n_c} z_{e,o}^{n_{nc}} z_{e,t}^{n_t} z_{e,c}^{n_c} \quad (697)$$

- Clumping was then assumed to lower configurational energy (relative to non-clumped states) according to a simple binding energy model correction to the single particle partition function (Equation 409, Chapter 9)

$$z_c(n) = e^{-\left(\frac{3\epsilon_{0V}}{2\tau}+\frac{E_B^c(n)}{\tau}\right)} \quad (698)$$

- We also modeled electronic contributions to the partition function explicitly; thus, the non-clumped configuration was modeled as a doublet while the clumped configuration was deemed to be a singlet (Equations 411 and 413, Chapter 9)

$$z_{e,t} = \sum_{j,e} g_j^t e^{-\frac{\varepsilon_{j,e,t}}{\kappa_B T}} = g_0^o = g_0^t = 2 \quad (699)$$

$$z_{e,c} = \sum_{j,e} g_j^c e^{-\frac{\varepsilon_{j,e,c}}{\kappa_B T}} \approx g_0^c = 1 \quad (700)$$

- We phenomenologically added the interaction and binding energies to the model as free parameters, thus (Equations 414, 415, Chapter 9)

$$\varepsilon_h(\theta) \to \varepsilon_h(\theta) + \varepsilon_\delta^0 + \varepsilon_\delta^1\theta + \varepsilon_\delta^2\theta^2 + \mathcal{O}(\theta^3) \quad (701)$$

$$E_B^c(\theta) \to \varepsilon_c^0 + \theta\varepsilon_c^1 + \theta^2\varepsilon_c^2 + \mathcal{O}(\theta^3)$$

702

- The results were a clumping-type isotherm that we christened "Orondo Isotherm" (Equation 503, Chapter 9)

$$\frac{\theta_c}{\theta_{nc}{}^{\gamma}(\Theta_o - \theta_{nc})^{1-\gamma}} = \frac{1}{2^{\gamma}}\left(1 - e^{-\frac{\epsilon_{0v}}{\kappa_B T}}\right)^{3\gamma} e^{-\gamma\frac{E_B^c(n)}{\kappa_B T}}$$

703

- The "Orondo Isotherm" needs to be solved in consistency with thermodynamic molar quantities from experiment (Equations 504, 505, Chapter 9)

$$\bar{H}_H^E(\theta,T) = -\frac{RT^2}{2}\frac{A'(T)}{A(T)} + \frac{R}{\kappa_B}\left(\theta\frac{\partial}{\partial\theta}\varepsilon_h(\theta) + \varepsilon_h(\theta) + \varepsilon_\delta^0 + 2\varepsilon_\delta^1\theta + 3\varepsilon_\delta^2\theta^2\right)$$
$$+\frac{R}{\kappa_B}[\varepsilon_c^0 + \varepsilon_c^1(\theta_c + \theta) + \varepsilon_c^2(2\theta_c\theta + \theta^2)] + \frac{3R\epsilon_{0v}}{2\kappa_B} - \frac{R\epsilon_{0v}}{4\kappa_B}coth\frac{\epsilon_{0v}}{2\kappa_B T} - \frac{RT}{2} + \frac{R\epsilon_D}{2\kappa_B} - \Delta\bar{H}_H^0$$

704

$$\bar{S}_H^E(\theta,T) = -\frac{RT}{2}\frac{A'(T)}{A(T)} - \frac{R}{2}lnA(T) - \frac{R}{\gamma}ln\frac{\theta_c}{\Theta_o - \theta_o} - \frac{1}{4}\frac{R\epsilon_{0v}}{\kappa_B T}coth\frac{\epsilon_{0v}}{2\kappa_B T} + \frac{R}{2}ln\left(2\,sinh\frac{\epsilon_{0v}}{2\kappa_B T}\right) - \frac{R}{2}$$
$$-\frac{R}{2}ln\frac{8\pi^2 I\kappa_B T}{\sigma h^2} + Rln\frac{\theta}{1-\theta} - \Delta\bar{S}_H^0$$

705

- In this model, fugacity is given as above, Equation 694, except $B(\theta,T)$ is now (Equation 488, Chapter 9)

$$B(\theta,T) = \left[\frac{2\kappa_B T}{\gamma}ln\frac{\theta_c}{\Theta_o - \theta_o} + 2\left(\theta\frac{\partial}{\partial\theta}\varepsilon_h(\theta) + \varepsilon_h(\theta) + \varepsilon_\delta^0 + 2\varepsilon_\delta^1\theta + 3\varepsilon_\delta^2\theta^2\right)\right.$$
$$+2[\varepsilon_c^0 + \varepsilon_c^1(\theta_c + \theta) + \varepsilon_c^2(2\theta_c\theta + \theta^2)] + 3\epsilon_{0v} - \kappa_B T ln\left(2sinh\frac{\epsilon_{0v}}{2\kappa_B T}\right) + \kappa_B T ln\frac{8\pi^2 I\kappa_B T}{\sigma h^2}$$
$$\left.+\epsilon_D\right]$$

706

The results were found to be, respectively, fractional occupations, enthalpy, and entropy

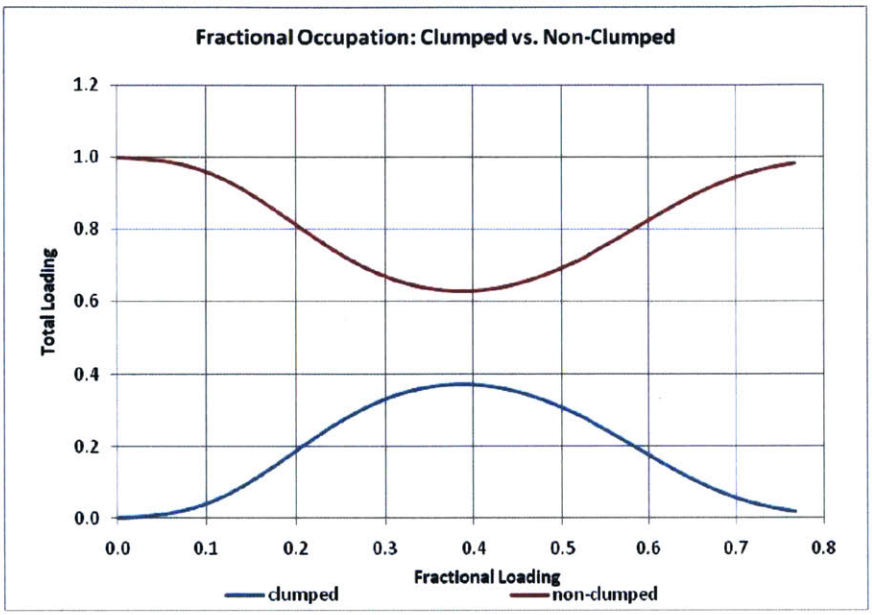

Figure 137: Fractional clumped and non-clumped populations

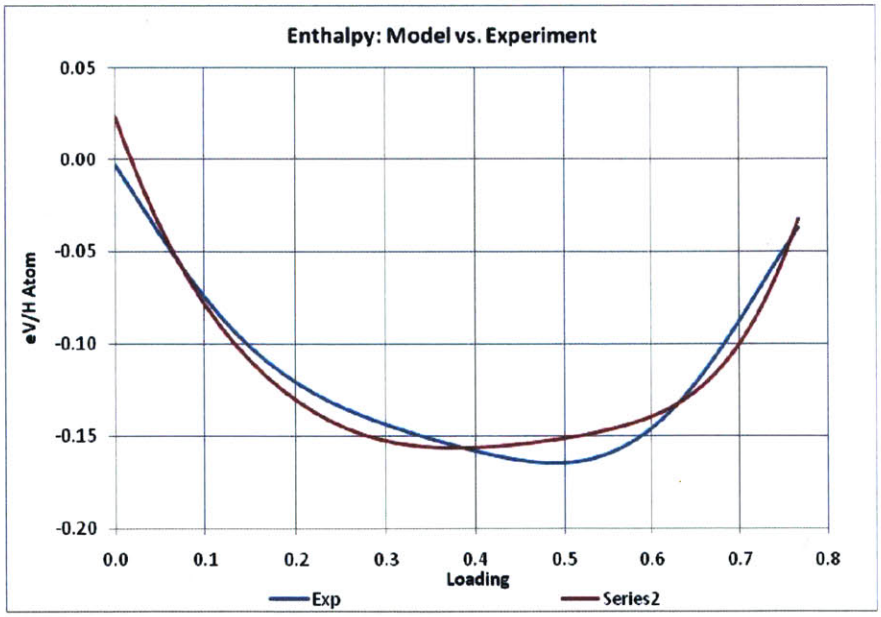

Figure 138: Enthalpy vs. Experiment. Experiment is from [Kuji1983]

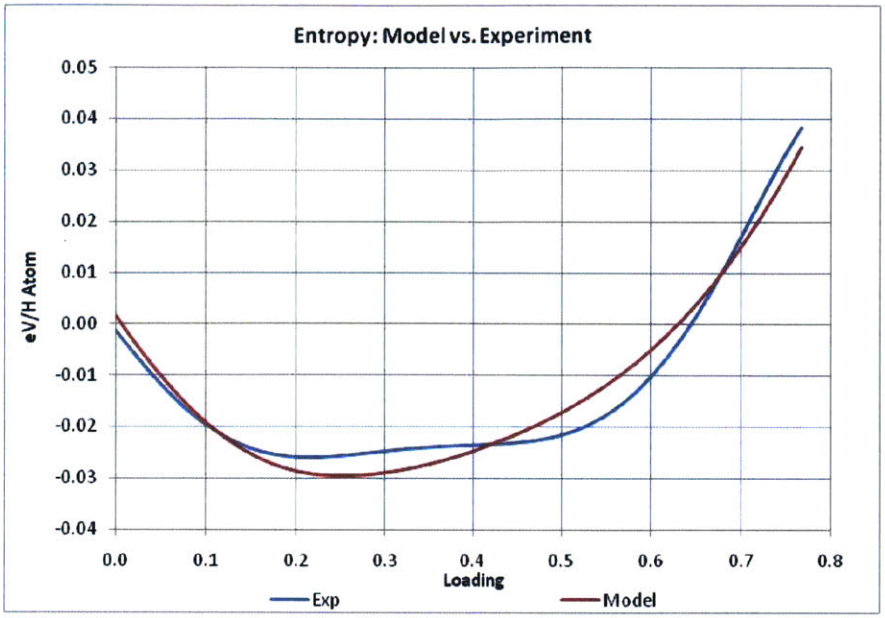

Figure 139: Model Entropy vs. Experiment. Experimentis from [Kuji1983]

Phase Diagram Model III

While the prior model matched the enthalpy and entropy data very well, we attempted an even further refinement of the model by a phenomenological treatment of the electronic contributions to thermodynamic quantities (Chapter 10) whereby

- The miscibility gap was modeled to contain clumps with nearest neighbor exclusions, designed to approximate a physical picture where singlets are only formed by isolated H quasi-molecule clumps (Equation 553, Chapter 10)

$$Z_H(\tau,\mu) = \sum_{n_{nc}=0}^{N_o} \sum_{k=0}^{\frac{N_o-n_{nc}}{\alpha+\gamma}} \sum_{n_t=0}^{N_t} \sum_{ASN} e^{\frac{(n_{nc}+n_t+k\gamma)\mu-\varepsilon_h(n_{nc},n_t,k\gamma)}{\tau}} z_o^{n_{nc}} z_t^{n_t} z_c^{k\gamma} z_{e,o}^{n_{nc}} z_{e,t}^{n_t} z_{e,c}^{k\gamma}$$

707

- The new Enthalpy, Entropy and "Orondo Isotherm" expressions were found to be, respectively, (Equations 608-610, Chapter 10)

$$\bar{H}_H^E(\theta,T) = -\frac{RT^2}{2}\frac{A'(T)}{A(T)} + \frac{R}{\kappa_B}\left(\theta\frac{\partial}{\partial\theta}\varepsilon_h(\theta) + \varepsilon_h(\theta) + \varepsilon_\delta^0 + 2\varepsilon_\delta^1\theta + 3\varepsilon_\delta^2\theta^2\right)$$
$$+\frac{R}{\kappa_B}[\varepsilon_c^0 + \varepsilon_c^1(\theta_c+\theta) + \varepsilon_c^2(2\theta_c\theta+\theta^2)] + \frac{3R}{2\kappa_B}\epsilon_{0v} - \frac{R}{4}\frac{\epsilon_{0v}}{\kappa_B}coth\frac{\epsilon_{0v}}{2\kappa_BT} - \frac{RT}{2} + \frac{R}{2\kappa_B}\epsilon_D$$
$$-\Delta\bar{H}_H^0(T)$$

708

$$\bar{S}_H^E(\theta,T) = -\frac{RT}{2}\frac{A'(T)}{A(T)} - \frac{R}{2}lnA(T) - \frac{R}{\gamma}ln\frac{\varphi\theta_c}{\Theta_o-\theta_{nc}-\varphi\theta_c} - \frac{R\epsilon_{0v}}{4\kappa_BT}coth\frac{\epsilon_{0v}}{2\kappa_BT} + \frac{R}{2}ln\left(2\,sinh\frac{\epsilon_{0v}}{2\kappa_BT}\right) - \frac{R}{2}$$
$$-\frac{R}{2}ln\frac{8\pi^2I\kappa_BT}{\sigma h^2} + Rln\frac{\theta}{1-\theta} - \Delta\bar{S}_H^0(T)$$

709

$$\varphi^{\frac{1}{\gamma}}\frac{\theta_c^{\frac{1}{\gamma}}(1-\theta_{nc})^{\frac{\gamma\varphi-1}{\gamma\varphi}}}{\theta_{nc}(1-\theta_{nc}-\varphi\theta_c)^{\frac{\varphi-1}{\gamma\varphi}}} = \frac{1}{2}\left(1-e^{-\frac{\epsilon_{0v}}{\kappa_BT}}\right)^3 e^{-\frac{E_B^c(n)}{\kappa_BT}}$$

710

- The results were, respectively for fractional clumped occupations, entropy and enthalpy, respectively (Figure 121, Figure 125, Figure 126, Chapter 10):

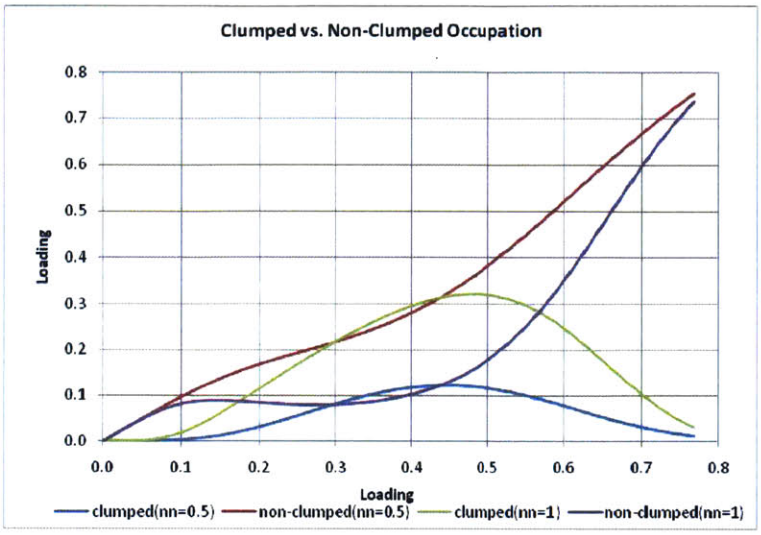

Figure 140: Clumped and non-clumped Fractional Occupation

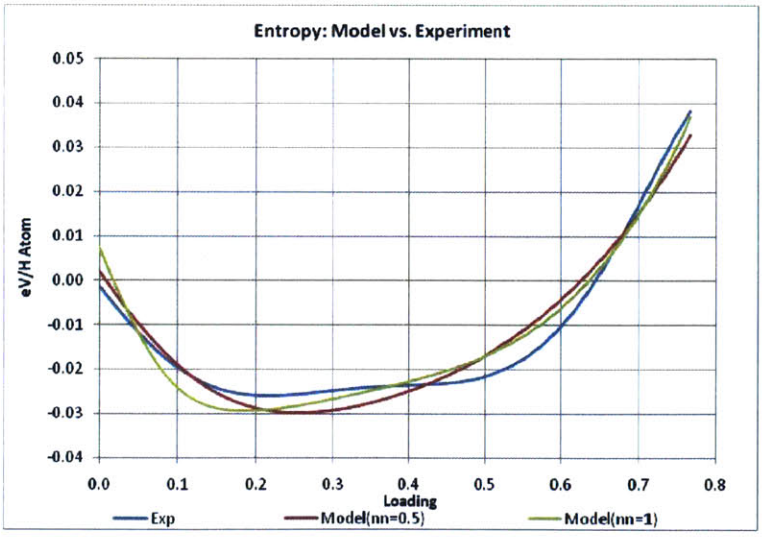

Figure 141: Entropy: Model vs. Experiment

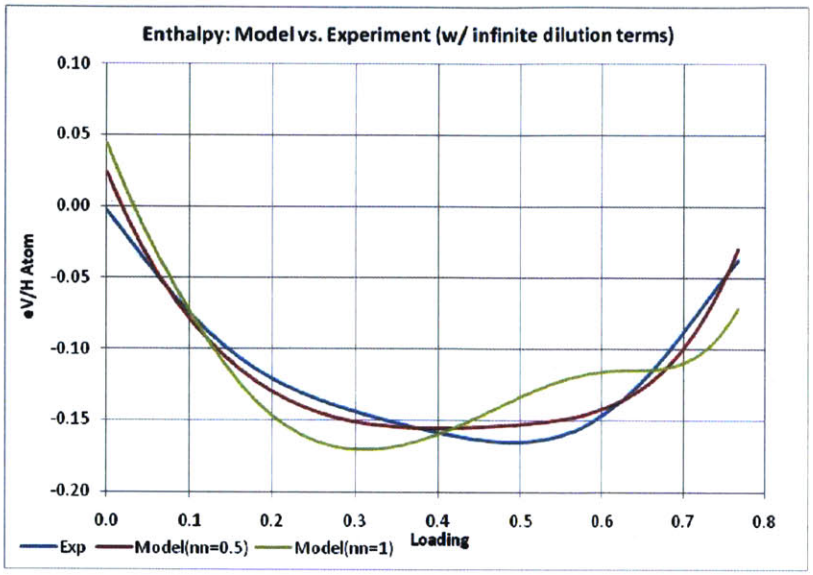

Figure 142: Enthalpy vs. Experiment

- We noted an inadequacy in the model for electronic contributions to thermodynamic quantities. To that end, we attempted an improved electronic model where we did away with prior approximations in the non-clumped electrons and instead assumed a full band energy model leading to the partition function of the non-clumped electrons being (Equation 617, Chapter 10)

$$z_{e,o} = \sum_{\kappa}\sum_{\sigma} g_{\kappa}^{\sigma} e^{-\frac{\varepsilon_{\sigma}(n,\kappa)-\mu_F(n,T)}{\kappa_B T}}$$

711

- This resulted in negligible correction since the terms were of the order $\frac{1}{N}$.

- We next separated the loading process into protonic and electronic contributions. The protonic contribution was found to be captured in the statistical model, while the electronic contributions to entropy was found to be (Equation 679, Chapter 10):

$$S_E(T,x) = -\int g(\varepsilon)d\varepsilon\left(f_{FD}\log f_{FD} + (1-f_{FD})\log(1-f_{FD})\right)$$

712

- An *ab initio* evaluation of Equation 679, however, led to the conclusion that electronic contributions to entropy were about an order of magnitude smaller than those from configuration, a result confirming other workers (Wallace, 1992).

- Based on these results, we base our phase calculations on the Clumped model, with no exclusions.

Overall Phase Diagram (Based on Clumped Model)

We may derive a phase diagram from the clumped model by calculating the Pressure-Composition-Temperature profiles as before (Equations 694, 695 and 706 above)

The initial results are shown below for three temperatures, T=293K, T=433K and T=571K. We also shown two experimental profiles (one at T=293K and the other at T=571K)

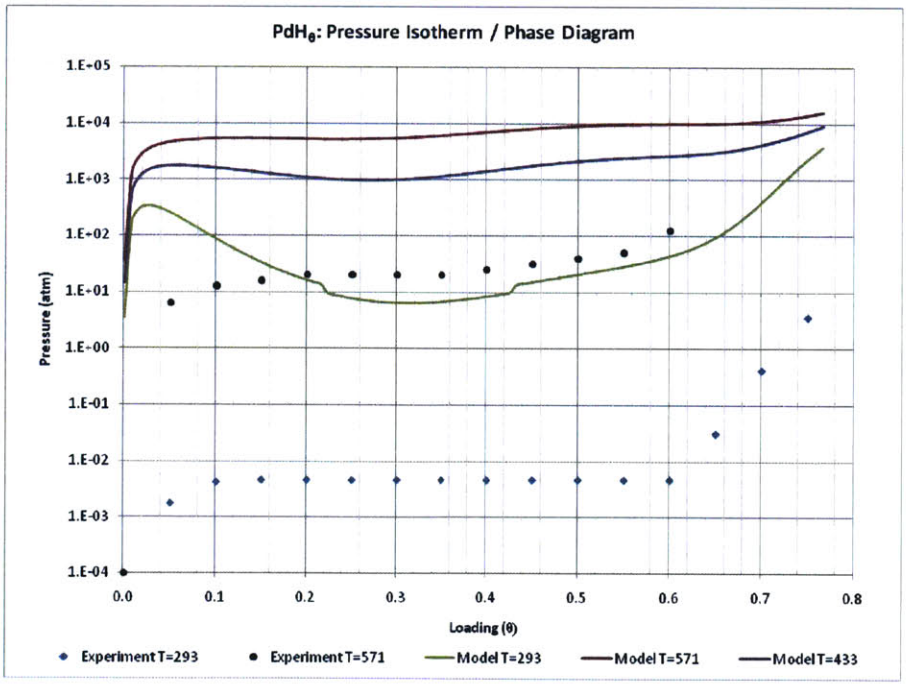

Figure 143: Model PCT vs Experiment based on Enthalpy and Entropy least squares fit to [Kuji1983]

Obviously the match is not good – there is a large constant offset which we address in the next section. We however note that our model correctly predicts the disappearance of the miscibility above the critical temperature.

Below, we plot the corresponding molar quantity matches together with the matched parameters, where we also note that the clumping population increases with temperature, albeit modestly.

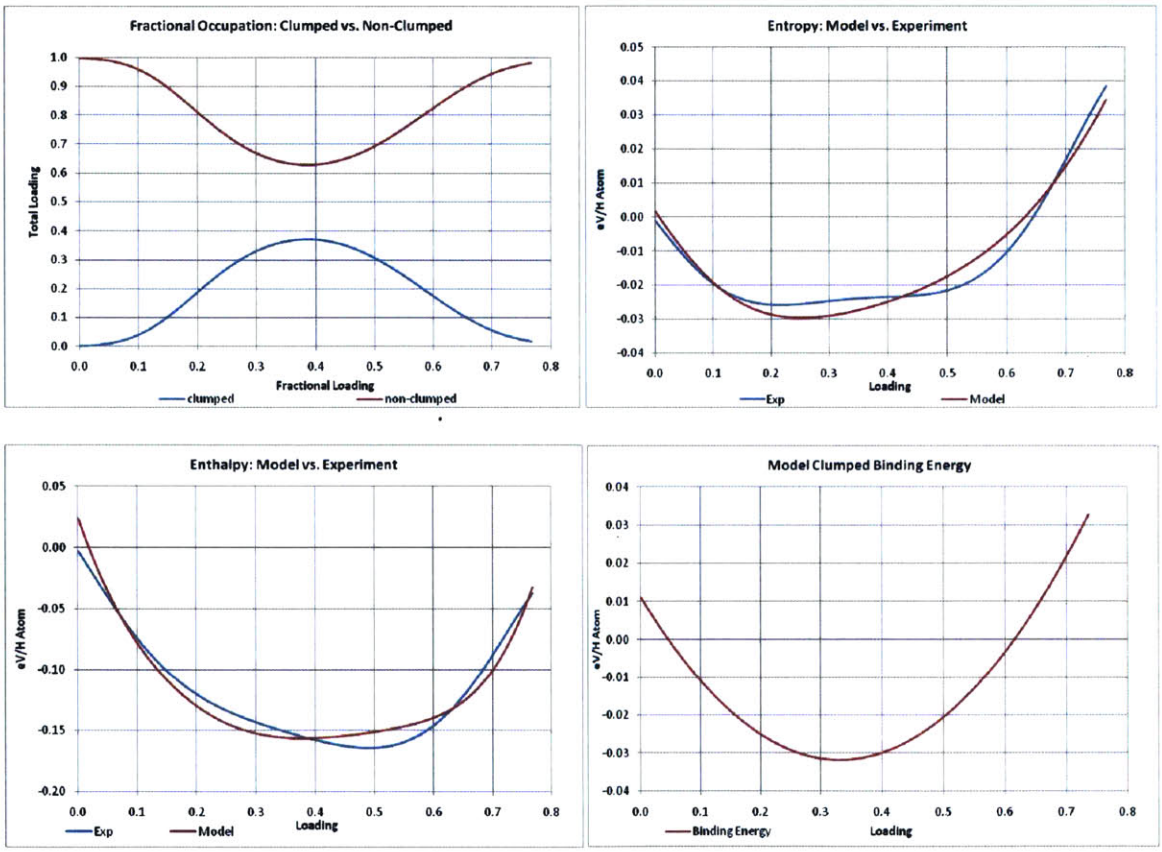

Figure 144: Fractional Clumping (top left), Entropy (top right), enthalpy (bottom left), and model binding energy (bottom right) T=293K

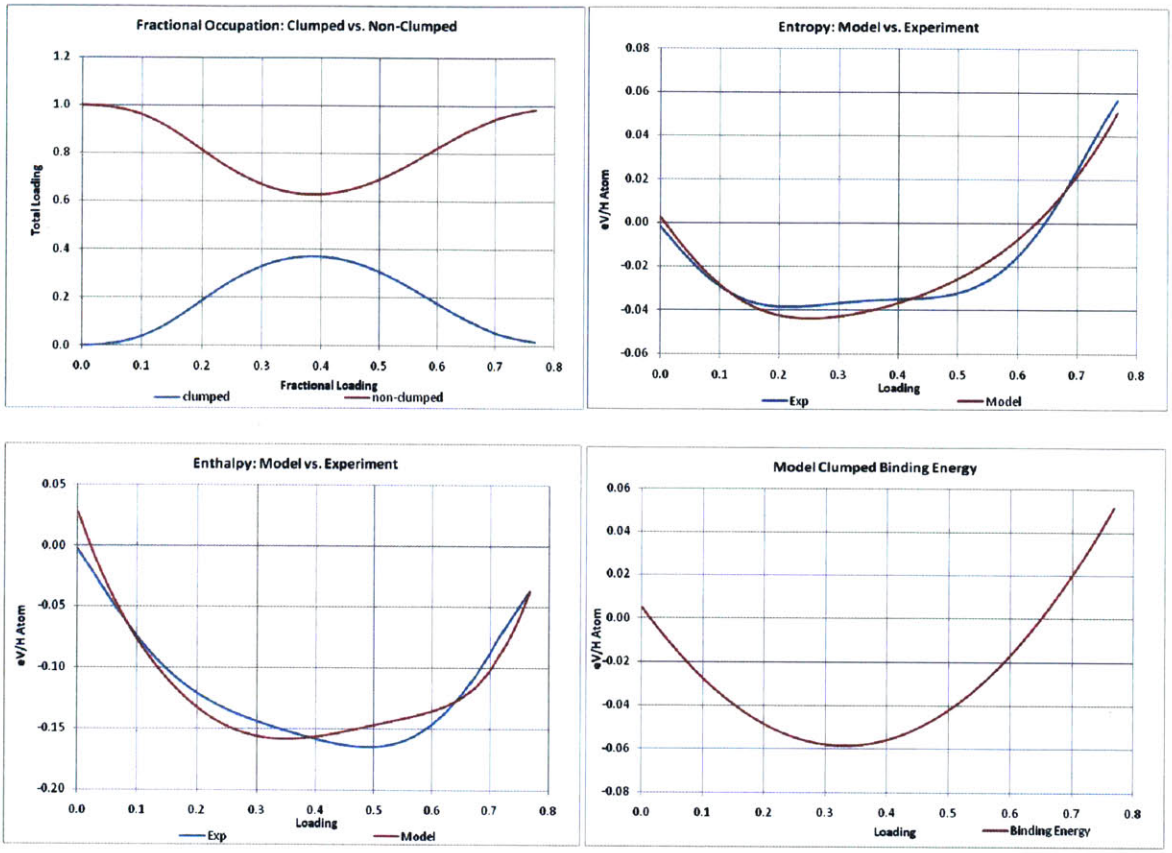

Figure 145: Fractional Clumping (top left), Entropy (top right), enthalpy (bottom left), and model binding energy (bottom right) T=433K

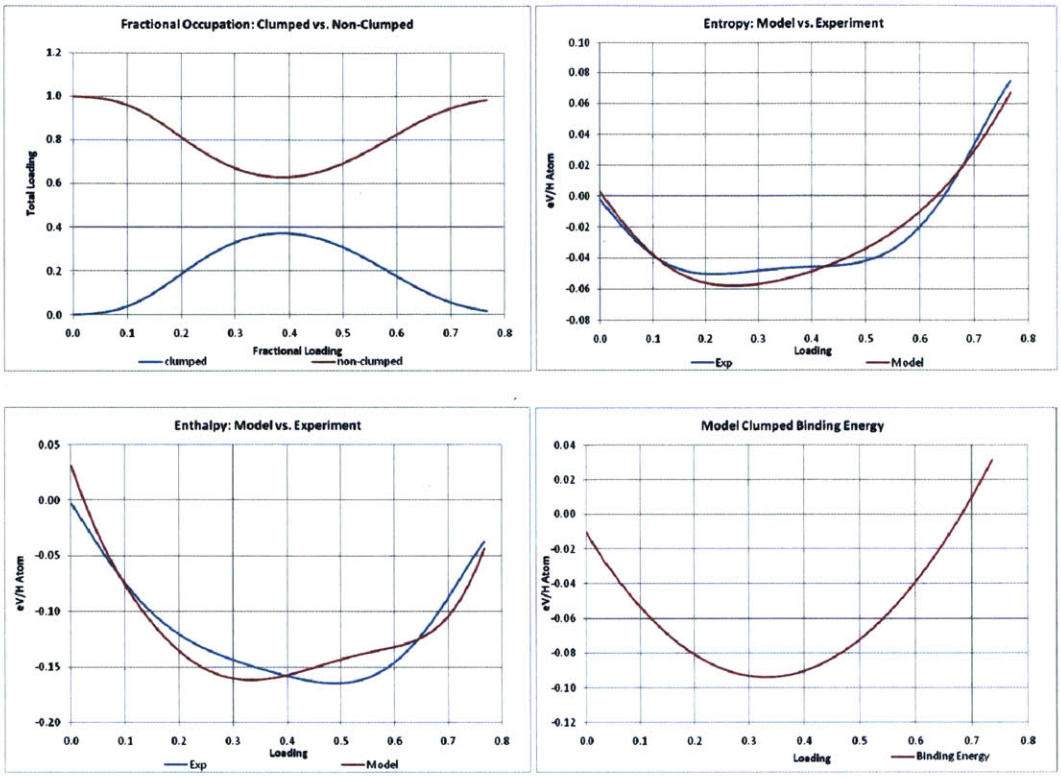

Figure 146: Fractional Clumping (top left), Entropy (top right), enthalpy (bottom left), and model binding energy (bottom right) T=571K

Free Parameters

Enthalpy Fitting parameters

Temperature (K)	$\varepsilon_\delta^0\ (eV)$	$\varepsilon_\delta^1(eV/atom)$	$\varepsilon_\delta^2(eV/atom\text{^}2)$
293	2.638319E-01	-1.849281E-01	1.721260E-01
433	1.624982E-01	-2.881014E-01	2.932991E-01
571	1.785568E-01	-2.881014E-01	2.932991E-01

Binding Energy Fitting Parameters

Temperature (K)	$\varepsilon_c^0\ (eV)$	$\varepsilon_c^1(eV/atom)$	$\varepsilon_c^2(eV/atom\text{^}2)$
293	1.131048E-02	-2.595355E-01	3.918549E-01
433	8.15E-02	0	0
571	8.15E-02	0	0

Entropy Constant Offset Fitting parameters

Temperature (K)	$S_\delta^0\ (eV)$	$S_\delta^1(eV/atom)$	$S_\delta^2(eV/atom\text{^}2)$
293	1.401763E-001	0	0
433	1.8E-01	0	0
571	2.5E-01	0	0

P-C-T Fitting Parameter

Temperature (K)	$P_\delta^0\ (atm)$		
All	(-)5 decades		

Connecting Enthalpy & Entropy Fitting Parameters to P-C-T

From the previous section, it is clear that we cannot simply use enthalpy and entropy fitting parameters with the PCT model. To understand why not, we need to go back to the relationship between pressure and enthalpy (Equation 270, Chapter 7), which we rewrite as

$$\bar{H}_H^E(\theta,T) = -T^2\left(\frac{\partial\left(\frac{RTln(P)}{T}\right)}{\partial T}\right)_n = -RT^2\left(\frac{\partial\left(lnP(\theta,T)\right)}{\partial T}\right)_n$$

713

We use the expression for enthalpy, Equation 708 above, to write

$$-\frac{\bar{H}_H^E(\theta,T)}{RT^2} \rightarrow \frac{1}{2}\frac{A'(T)}{A(T)} - \frac{1}{\kappa_B T^2}\left(\theta\frac{\partial}{\partial\theta}\varepsilon_h(\theta) + \varepsilon_h(\theta) + \varepsilon_\delta^0 + 2\varepsilon_\delta^1\theta + 3\varepsilon_\delta^2\theta^2\right)$$
$$-\frac{1}{\kappa_B T^2}[\varepsilon_c^0 + \varepsilon_c^1(\theta_c+\theta) + \varepsilon_c^2(2\theta_c\theta+\theta^2)] - \frac{3}{2\kappa_B T^2}\epsilon_{0v} + \frac{1}{4}\frac{\epsilon_{0v}}{\kappa_B T^2}coth\frac{\epsilon_{0v}}{2\kappa_B T} + \frac{1}{2T}$$
$$-\frac{1}{2\kappa_B T^2}\epsilon_D + \frac{\Delta\bar{H}_H^0(T)}{RT^2}$$

714

and

$$\left(\frac{\partial\left(lnP(\theta,T)\right)}{\partial T}\right)_n = \frac{1}{2}\frac{A'(T)}{A(T)} - \frac{1}{\kappa_B T^2}\left(\theta\frac{\partial}{\partial\theta}\varepsilon_h(\theta) + \varepsilon_h(\theta) + \varepsilon_\delta^0 + 2\varepsilon_\delta^1\theta + 3\varepsilon_\delta^2\theta^2\right)$$
$$-\frac{1}{\kappa_B T^2}[\varepsilon_c^0 + \varepsilon_c^1(\theta_c+\theta) + \varepsilon_c^2(2\theta_c\theta+\theta^2)] - \frac{3}{2\kappa_B T^2}\epsilon_{0v} + \frac{1}{4}\frac{\epsilon_{0v}}{\kappa_B T^2}coth\frac{\epsilon_{0v}}{2\kappa_B T} + \frac{1}{2T}$$
$$-\frac{1}{2\kappa_B T^2}\epsilon_D + \frac{\Delta\bar{H}_H^0(T)}{RT^2}$$

715

Integrating both sides at constant loading yields

$$lnP(\theta,T) = \int \left[\frac{1}{2}\frac{A'(T)}{A(T)} - \frac{1}{\kappa_B T^2}\left(\theta\frac{\partial}{\partial\theta}\varepsilon_h(\theta) + \varepsilon_h(\theta) + \varepsilon_\delta^0 + 2\varepsilon_\delta^1\theta + 3\varepsilon_\delta^2\theta^2\right)\right.$$
$$-\frac{1}{\kappa_B T^2}[\varepsilon_c^0 + \varepsilon_c^1(\theta_c+\theta) + \varepsilon_c^2(2\theta_c\theta+\theta^2)] - \frac{3}{2\kappa_B T^2}\epsilon_{0v} + \frac{1}{4}\frac{\epsilon_{0v}}{\kappa_B T^2}coth\frac{\epsilon_{0v}}{2\kappa_B T} + \frac{1}{2T}$$
$$\left. -\frac{1}{2\kappa_B T^2}\epsilon_D + \frac{\Delta\bar{H}_H^0(T)}{RT^2}\right] dT$$

716

The result is

$$P(\theta,T) = \frac{1}{2}lnA(T) + \frac{1}{\kappa_B T}\left(\theta\frac{\partial}{\partial\theta}\varepsilon_h(\theta) + \varepsilon_h(\theta) + \varepsilon_\delta^0 + 2\varepsilon_\delta^1\theta + 3\varepsilon_\delta^2\theta^2\right)$$
$$+\frac{1}{\kappa_B T}[\varepsilon_c^0 + \varepsilon_c^1(\theta_c+\theta) + \varepsilon_c^2(2\theta_c\theta+\theta^2)] + \frac{3}{2\kappa_B T}\epsilon_{0v} - \frac{1}{2}ln\left(2sinh\frac{\epsilon_{0v}}{2\kappa_B T}\right)$$
$$+\frac{1}{2}ln\frac{8\pi^2 I\kappa_B T}{\sigma h^2} + \frac{1}{2\kappa_B T}\epsilon_D + \int\frac{\Delta\bar{H}_H^0(T)}{RT^2}dT + C(\theta)$$

717

where $C(\theta)$ is an integration constant independent of temperature but may depend on loading.

Setting

$$C(\theta) \rightarrow ln\,(P_0)$$

718

allows us to set the level of model P-C-T isotherm to be consistent with experiment.

A consistent correction should also be available via entropy formulation (Equation 271, Chapter 7), which is rewritten as

$$-\bar{S}_H^E(\theta,T) = Rln(P) + RT\left(\frac{\partial(lnP)}{\partial T}\right)_n$$

719

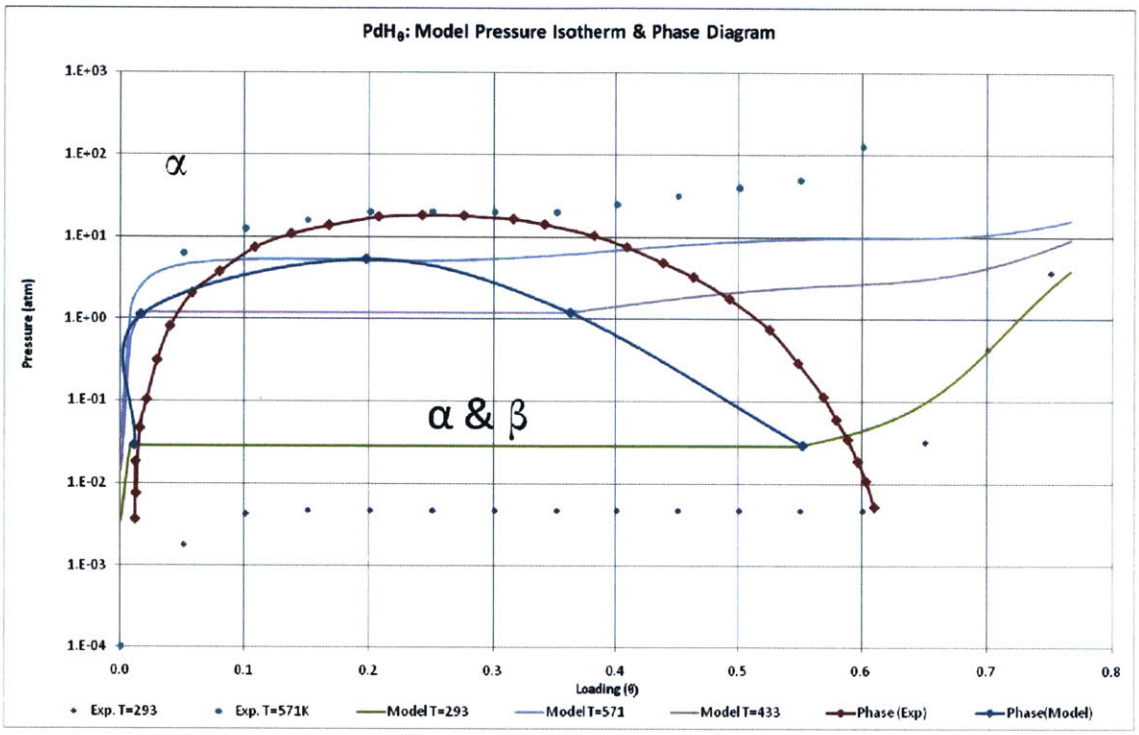

Figure 147: Phase Diagram for the Clumped Model

The results of Figure 147 do not compare well to experiment. However they also suggest a solution, namely that the binding energy should depend on temperature. We attempt such a model improvement below.

Temperature Dependent Binding Energy Model

Formulation

It is expected that the binding energy will be temperature dependent, in addition to being loading dependent – see for example, (Stern & Sarma, 1984). In addition, this dependence is expected to be approximately linear [ibid]. The result is that Equation **415** may be corrected as follows, with constants δ_c^0, δ_c^1 and δ_c^2 to be determined based on experimental fit (in a manner described below)

$$E_B^c(\theta) \to \varepsilon_c^0 + \delta_c^0(T - T_c) + \left(\varepsilon_c^1 + \delta_c^1(T - T_c)\right)\theta + \left(\varepsilon_c^2 + \delta_c^2(T - T_c)\right)\theta^2 + \mathcal{O}(\theta^3) \tag{720}$$

Equation 720 is designed to reproduce the previous model results at the critical temperature, T_c, and make temperature dependent corrections away from it.

The previous results for the clumped model apply, Equations 466-468, 480 and 483:

$$\mu_t(\tau,\theta) = \tau\, ln\frac{\theta_t}{\Theta_t - \theta_t} + \theta\frac{\partial}{\partial\theta}\varepsilon_h(\theta) + \varepsilon_h(\theta) - \tau lnz_{o,t} - \tau lng_{o,t} + \theta_c\frac{\partial}{\partial\theta}E_B^c(\theta) \tag{721}$$

$$\mu_{nc}(\tau,\theta) = \tau ln\frac{\theta_{nc}}{\Theta_o - \theta_{nc}} + \frac{\tau}{\gamma} ln\frac{\Theta_o - \theta_{nc}}{\Theta_o - \theta_o} + \theta\frac{\partial}{\partial\theta}\varepsilon_h(\theta) + \varepsilon_h(\theta) - \tau lnz_{o,t} - \tau lng_{o,t} + \theta_c\frac{\partial}{\partial\theta}E_B^c(\theta) \tag{722}$$

$$\mu_c(\tau,\theta) = \frac{\tau}{\gamma} ln\frac{\theta_c}{\Theta_o - \theta_o} + \theta\frac{\partial}{\partial\theta}\varepsilon_h(\theta) + \varepsilon_h(\theta) + \theta_c\frac{\partial}{\partial\theta}E_B^c(\theta) + \frac{3}{2}\epsilon_{0v} + E_B^c(\theta) \tag{723}$$

$$\frac{\theta_c}{\theta_{nc}{}^{\gamma}(\Theta_o - \theta_{nc})^{1-\gamma}} = \frac{1}{2^{\gamma}}\left(1 - e^{-\frac{\epsilon_{0v}}{\kappa_B T}}\right)^{3\gamma} e^{-\gamma\frac{E_B^c(n)}{\kappa_B T}} \tag{724}$$

$$f(\tau,\theta) = A(\tau)e^{\frac{B(\tau,\theta)}{\tau}} \tag{725}$$

but with Equation 488 modified according to Equation 720 above:

$$B(\theta,T)=\left[\frac{2\kappa_B T}{\gamma}ln\frac{\theta_c}{\Theta_o-\theta_o}+2\left(\theta\frac{\partial}{\partial\theta}[\varepsilon_h(\theta)+\varepsilon_\delta^0+\varepsilon_\delta^1\theta+\varepsilon_\delta^2\theta^2]+[\varepsilon_h(\theta)+\varepsilon_\delta^0+\varepsilon_\delta^1\theta+\varepsilon_\delta^2\theta^2]\right)\right.$$
$$+2\left(\theta_c\frac{\partial}{\partial\theta}[\varepsilon_c^0+\varepsilon_c^1\theta+\varepsilon_c^2\theta^2+\delta_c^0(T-T_c)+\delta_c^1(T-T_c)\theta+\delta_c^2(T-T_c)\theta^2]\right.$$
$$\left.+[\varepsilon_c^0+\varepsilon_c^1\theta+\varepsilon_c^2\theta^2+\delta_c^0(T-T_c)+\delta_c^1(T-T_c)\theta+\delta_c^2(T-T_c)\theta^2]\right)+3\epsilon_{0v}$$
$$\left.-\kappa_B T\,ln\left(2sinh\frac{\epsilon_{0v}}{2\kappa_B T}\right)+\kappa_B T\,ln\frac{8\pi^2 I\kappa_B T}{\sigma h^2}+\epsilon_D\right]$$

726

or

$$B(\theta,T)=\left[\frac{2\kappa_B T}{\gamma}ln\frac{\theta_c}{\Theta_o-\theta_o}+2\left(\left[\theta\frac{\partial}{\partial\theta}\varepsilon_h(\theta)+\varepsilon_h(\theta)+\varepsilon_\delta^0+2\varepsilon_\delta^1\theta+3\varepsilon_\delta^2\theta^2\right]\right)\right.$$
$$+2\left(\left[\frac{1}{1}\varepsilon_c^1\theta_c+2\varepsilon_c^2\theta_c\theta+\delta_c^1(T-T_c)\theta_c+2\delta_c^2(T-T_c)\theta_c\theta\right]\right.$$
$$\left.\left.+\left[\frac{1}{1}\varepsilon_c^0+\varepsilon_c^1\theta+\varepsilon_c^2\theta^2+\delta_c^0(T-T_c)+\delta_c^1(T-T_c)\theta+\delta_c^2(T-T_c)\theta^2\right]\right)+3\epsilon_{0v}\right.$$
$$\left.-\kappa_B T ln\left(2sinh\frac{\epsilon_{0v}}{2\kappa_B T}\right)+\kappa_B T ln\frac{8\pi^2 I\kappa_B T}{\sigma h^2}+\epsilon_D\right]$$
$$=\frac{2\kappa_B T}{\gamma}ln\frac{\theta_c}{\Theta_o-\theta_o}+2\left(\left[\theta\frac{\partial}{\partial\theta}\varepsilon_h(\theta)+\varepsilon_h(\theta)+\varepsilon_\delta^0+2\varepsilon_\delta^1\theta+3\varepsilon_\delta^2\theta^2\right]\right)$$
$$+2\left(\frac{1}{1}\varepsilon_c^0+\delta_c^0(T-T_c)+\left(\varepsilon_c^1+\delta_c^1(T-T_c)\right)\theta+\left(\varepsilon_c^1+\delta_c^1(T-T_c)\right)\theta_c\right.$$
$$\left.+2\left(\varepsilon_c^2+\delta_c^2(T-T_c)\right)\theta_c\theta+\left(\varepsilon_c^2+\delta_c^2(T-T_c)\right)\theta^2\right)+3\epsilon_{0v}-\kappa_B T ln\left(2sinh\frac{\epsilon_{0v}}{2\kappa_B T}\right)$$
$$+\kappa_B T ln\frac{8\pi^2 I\kappa_B T}{\sigma h^2}+\epsilon_D$$
$$=\frac{2\kappa_B T}{\gamma}ln\frac{\theta_c}{\Theta_o-\theta_o}+2\left(\left[\theta\frac{\partial}{\partial\theta}\varepsilon_h(\theta)+\varepsilon_h(\theta)+\varepsilon_\delta^0+2\varepsilon_\delta^1\theta+3\varepsilon_\delta^2\theta^2\right]\right)$$
$$+2\left(\frac{1}{1}\varepsilon_c^0+\delta_c^0(T-T_c)+\left(\varepsilon_c^1+\delta_c^1(T-T_c)\right)(\theta+\theta_c)+\left(\varepsilon_c^2+\delta_c^2(T-T_c)\right)(2\theta_c\theta+\theta^2)\right)$$
$$+3\epsilon_{0v}-\kappa_B T ln\left(2sinh\frac{\epsilon_{0v}}{2\kappa_B T}\right)+\kappa_B T ln\frac{8\pi^2 I\kappa_B T}{\sigma h^2}+\epsilon_D$$

727

The relative Gibbs energy and other related quantities are then given by, similar to Equations 493-499:

$$\Delta\bar{G}_H^E(\theta,T) = \frac{RT}{2}lnA(T) + \frac{RT}{\gamma}ln\frac{\theta_c}{\Theta_o-\theta_o} + \frac{R}{\kappa_B}\left(\left[\theta\frac{\partial}{\partial\theta}\varepsilon_h(\theta) + \varepsilon_h(\theta) + \varepsilon_\delta^0 + 2\varepsilon_\delta^1\theta + 3\varepsilon_\delta^2\theta^2\right]\right)$$
$$+\frac{R}{\kappa_B}\left(\frac{1}{1}\varepsilon_c^0 + \delta_c^0(T-T_c) + \left(\varepsilon_c^1 + \delta_c^1(T-T_c)\right)\theta + \left(\varepsilon_c^1 + \delta_c^1(T-T_c)\right)\theta_c\right.$$
$$\left.+2\left(\varepsilon_c^2 + \delta_c^2(T-T_c)\right)\theta_c\theta + \left(\varepsilon_c^2 + \delta_c^2(T-T_c)\right)\theta^2\right) + \frac{3R}{2\kappa_B}\epsilon_{0v} - \frac{RT}{2}ln\left(2sinh\frac{\epsilon_{0v}}{2\kappa_BT}\right)$$
$$+\frac{RT}{2}ln\frac{8\pi^2I\kappa_BT}{\sigma h^2} + \frac{1}{2}\frac{R}{\kappa_B}\epsilon_D - RTln\frac{\theta}{1-\theta}$$

728

$$\frac{\Delta\bar{G}_H^E(\theta,T)}{T} \rightarrow \frac{R}{2}lnA(T) + \frac{R}{\gamma}ln\frac{\theta_c}{\Theta_o-\theta_o} + \frac{R}{\kappa_BT}\left(\theta\frac{\partial}{\partial\theta}\varepsilon_h(\theta) + \varepsilon_h(\theta) + \varepsilon_\delta^0 + 2\varepsilon_\delta^1\theta + 3\varepsilon_\delta^2\theta^2\right)$$
$$+\frac{R}{\kappa_BT}\left[\frac{1}{1}\varepsilon_c^0 + \delta_c^0(T-T_c) + \left(\varepsilon_c^1 + \delta_c^1(T-T_c)\right)\theta + \left(\varepsilon_c^1 + \delta_c^1(T-T_c)\right)\theta_c\right.$$
$$\left.+2\left(\varepsilon_c^2 + \delta_c^2(T-T_c)\right)\theta_c\theta + \left(\varepsilon_c^2 + \delta_c^2(T-T_c)\right)\theta^2\right] + \frac{3R}{2\kappa_BT}\epsilon_{0v} - \frac{R}{2}ln\left(2sinh\frac{\epsilon_{0v}}{2\kappa_BT}\right)$$
$$+\frac{R}{2}ln\frac{8\pi^2I\kappa_BT}{\sigma h^2} + \frac{1}{2}\frac{R}{\kappa_BT}\epsilon_D - Rln\frac{\theta}{1-\theta}$$
$$=\frac{R}{2}lnA(T) + \frac{R}{\gamma}ln\frac{\theta_c}{\Theta_o-\theta_o} + \frac{R}{\kappa_BT}\left(\theta\frac{\partial}{\partial\theta}\varepsilon_h(\theta) + \varepsilon_h(\theta) + \varepsilon_\delta^0 + 2\varepsilon_\delta^1\theta + 3\varepsilon_\delta^2\theta^2\right)$$
$$+\frac{R}{\kappa_BT}\left[\frac{1}{1}\varepsilon_c^0 + \delta_c^0(T-T_c) + \left(\varepsilon_c^1 + \delta_c^1(T-T_c)\right)(\theta+\theta_c) + \left(\varepsilon_c^2 + \delta_c^2(T-T_c)\right)(2\theta_c\theta+\theta^2)\right]$$
$$+\frac{3R}{2\kappa_BT}\epsilon_{0v} - \frac{R}{2}ln\left(2sinh\frac{\epsilon_{0v}}{2\kappa_BT}\right) + \frac{R}{2}ln\frac{8\pi^2I\kappa_BT}{\sigma h^2} + \frac{1}{2}\frac{R}{\kappa_BT}\epsilon_D - Rln\frac{\theta}{1-\theta}$$

729

$$\Delta\bar{H}_H^E(\theta,T) = -T^2\left(\frac{\partial\left(\frac{\Delta\bar{G}_H^E(\theta,T)}{T}\right)}{\partial T}\right)_{P,n}$$

$$= -T^2\left(\frac{R}{2}\frac{A'(T)}{A(T)} - \frac{R}{\kappa_B T^2}\left(\theta\frac{\partial}{\partial\theta}\varepsilon_h(\theta) + \varepsilon_h(\theta) + \varepsilon_\delta^0 + 2\varepsilon_\delta^1\theta + 3\varepsilon_\delta^2\theta^2\right)\right.$$

$$- \frac{R}{\kappa_B T^2}\left[\frac{1}{1}\varepsilon_c^0 + \delta_c^0(T-T_c) + \left(\varepsilon_c^1 + \delta_c^1(T-T_c)\right)(\theta+\theta_c)\right.$$

$$\left.\left. + \left(\varepsilon_c^2 + \delta_c^2(T-T_c)\right)(2\theta_c\theta+\theta^2)\right] + \frac{R}{\kappa_B T}\left[\frac{1}{1}\delta_c^0 + \delta_c^1(\theta+\theta_c) + \delta_c^2(2\theta_c\theta+\theta^2)\right]\right.$$

$$\left. - \frac{3R}{2\kappa_B T^2}\epsilon_{0v} + \frac{R}{4}\frac{\epsilon_{0v}}{\kappa_B T^2}coth\frac{\epsilon_{0v}}{2\kappa_B T} + \frac{R}{2T} - \frac{R}{2\kappa_B T^2}\epsilon_D\right)$$

730

or

$$\Delta\bar{H}_H^E(\theta,T) = -\frac{RT^2}{2}\frac{A'(T)}{A(T)} + \frac{R}{\kappa_B}\left(\theta\frac{\partial}{\partial\theta}\varepsilon_h(\theta) + \varepsilon_h(\theta) + \varepsilon_\delta^0 + 2\varepsilon_\delta^1\theta + 3\varepsilon_\delta^2\theta^2\right)$$

$$+ \frac{R}{\kappa_B}\left[\frac{1}{1}\varepsilon_c^0 + \delta_c^0(T-T_c) + \left(\varepsilon_c^1 + \delta_c^1(T-T_c)\right)(\theta+\theta_c) + \left(\varepsilon_c^2 + \delta_c^2(T-T_c)\right)(2\theta_c\theta+\theta^2)\right]$$

$$- \frac{RT}{\kappa_B}\left[\frac{1}{1}\delta_c^0 + \delta_c^1(\theta+\theta_c) + \delta_c^2(2\theta_c\theta+\theta^2)\right] + \frac{3R}{2\kappa_B}\epsilon_{0v} - \frac{R}{4}\frac{\epsilon_{0v}}{\kappa_B}coth\frac{\epsilon_{0v}}{2\kappa_B T} - \frac{RT}{2} + \frac{R}{2\kappa_B}\epsilon_D$$

731

$$\Delta\bar{S}_H^E(\theta,T) = -\frac{RT}{2}\frac{A'(T)}{A(T)} - \frac{R}{2}lnA(T) - \frac{R}{\gamma}ln\frac{\theta_c}{\theta_o-\theta_o} - \frac{R}{\kappa_B}\left(\frac{1}{1}\delta_c^0 + \delta_c^1(\theta+\theta_c) + \delta_c^2(2\theta_c\theta+\theta^2)\right)$$

$$- \frac{1}{4}\frac{R\epsilon_{0v}}{\kappa_B T}coth\frac{\epsilon_{0v}}{2\kappa_B T} + \frac{R}{2}ln\left(2\,sinh\frac{\epsilon_{0v}}{2\kappa_B T}\right) - \frac{R}{2} - \frac{R}{2}ln\frac{8\pi^2 I\kappa_B T}{\sigma h^2} + Rln\frac{\theta}{1-\theta}$$

732

Similarly, (Equations 713-**716**),

$$-\frac{\bar{H}_H^E(\theta,T)}{RT^2}\rightarrow\frac{1}{2}\frac{A'(T)}{A(T)}-\frac{1}{\kappa_B T^2}\left(\theta\frac{\partial}{\partial\theta}\varepsilon_h(\theta)+\varepsilon_h(\theta)+\varepsilon_\delta^0+2\varepsilon_\delta^1\theta+3\varepsilon_\delta^2\theta^2\right)$$
$$-\frac{1}{\kappa_B T^2}\left[\frac{1}{1}\varepsilon_c^0+\delta_c^0(T-T_c)+\left(\varepsilon_c^1+\delta_c^1(T-T_c)\right)(\theta+\theta_c)\right.$$
$$\left.+\left(\varepsilon_c^2+\delta_c^2(T-T_c)\right)(2\theta_c\theta+\theta^2)\right]+\frac{1}{\kappa_B T}\left[\frac{1}{1}\delta_c^0+\delta_c^1(\theta+\theta_c)+\delta_c^2(2\theta_c\theta+\theta^2)\right]$$
$$-\frac{3}{2\kappa_B T^2}\epsilon_{0v}+\frac{1}{4}\frac{\epsilon_{0v}}{\kappa_B T^2}coth\frac{\epsilon_{0v}}{2\kappa_B T}+\frac{1}{2T}-\frac{1}{2\kappa_B T^2}\epsilon_D+\frac{\Delta\bar{H}_H^0(T)}{RT^2}$$

733

$$\left(\frac{\partial\left(lnP(\theta,T)\right)}{\partial T}\right)_n=\frac{1}{2}\frac{A'(T)}{A(T)}-\frac{1}{\kappa_B T^2}\left(\theta\frac{\partial}{\partial\theta}\varepsilon_h(\theta)+\varepsilon_h(\theta)+\varepsilon_\delta^0+2\varepsilon_\delta^1\theta+3\varepsilon_\delta^2\theta^2\right)$$
$$-\frac{1}{\kappa_B T^2}\left[\frac{1}{1}\varepsilon_c^0+\delta_c^0(T-T_c)+\left(\varepsilon_c^1+\delta_c^1(T-T_c)\right)(\theta+\theta_c)\right.$$
$$\left.+\left(\varepsilon_c^2+\delta_c^2(T-T_c)\right)(2\theta_c\theta+\theta^2)\right]+\frac{1}{\kappa_B T}\left[\frac{1}{1}\delta_c^0+\delta_c^1(\theta+\theta_c)+\delta_c^2(2\theta_c\theta+\theta^2)\right]$$
$$-\frac{3}{2\kappa_B T^2}\epsilon_{0v}+\frac{1}{4}\frac{\epsilon_{0v}}{\kappa_B T^2}coth\frac{\epsilon_{0v}}{2\kappa_B T}+\frac{1}{2T}-\frac{1}{2\kappa_B T^2}\epsilon_D+\frac{\Delta\bar{H}_H^0(T)}{RT^2}$$

734

or

$$P(\theta,T)=\frac{1}{2}lnA(T)+\frac{1}{\kappa_B T}\left(\theta\frac{\partial}{\partial\theta}\varepsilon_h(\theta)+\varepsilon_h(\theta)+\varepsilon_\delta^0+2\varepsilon_\delta^1\theta+3\varepsilon_\delta^2\theta^2\right)$$
$$+\frac{1}{\kappa_B T}\left[\frac{1}{1}\varepsilon_c^0+\delta_c^0(T-T_c)+\left(\varepsilon_c^1+\delta_c^1(T-T_c)\right)(\theta+\theta_c)+\left(\varepsilon_c^2+\delta_c^2(T-T_c)\right)(2\theta_c\theta+\theta^2)\right]$$
$$+\frac{3}{2\kappa_B T}\epsilon_{0v}-\frac{1}{2}ln\left(2sinh\frac{\epsilon_{0v}}{2\kappa_B T}\right)+\frac{1}{2}ln\frac{8\pi^2 I\kappa_B T}{\sigma h^2}+\frac{1}{2\kappa_B T}\epsilon_D+\int\frac{\Delta\bar{H}_H^0(T)}{RT^2}dT+C(\theta)$$

735

Methodology and Results

There are probably several ways to proceed from here. One way is to use Kuji's data (Kuji, Oates, Bowerman, & Flanagan, 1983) for entropy and enthalpy in the single phase regime where our model is valid (at $T = T_c$).

To do this, we used the earlier results as starting point for the optimization of Equations 731 and 732 to experiment. To our surprise, the new model converged to a bound state as before that matched the pressure isotherm reasonably well – other schemes including constraining the optimization around prior results or using setting some of δ_c^0, δ_c^1 or δ_c^2 to zero did not yield any physically meaningful results.

Once we get critical point results, we can derive the other isotherms by assuming piece-wise solutions within the mixed phase region. The results are quite reasonable and provide a consistent model for the entire phase – as can be seen from a much improved estimated phase. We present the results below.

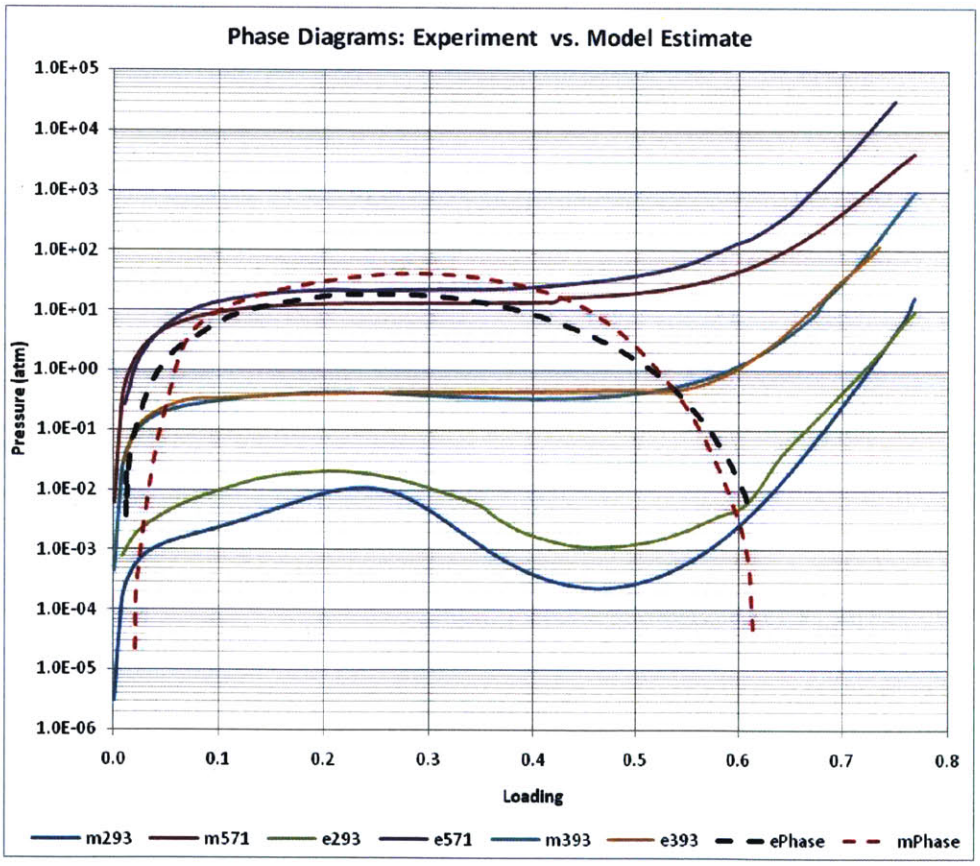

Figure 148: Estimated Phase Model (Temperature dependent binding energy)

The excess molar quantities, matched at the critical temperature are also fairly reasonable.

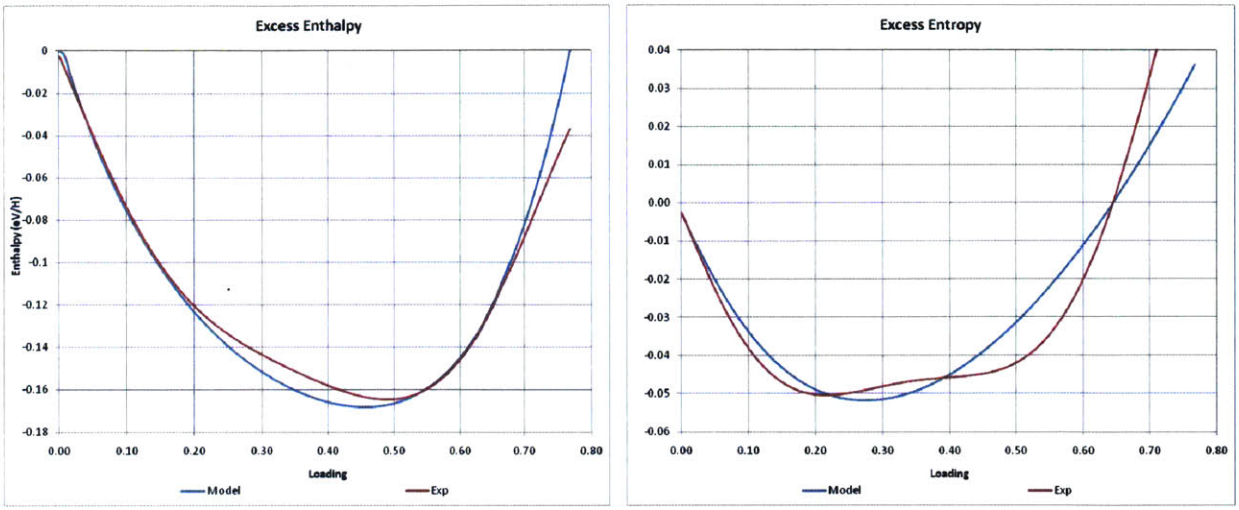

Figure 149: Excess Molar Quantities (Temperature dependent binding)

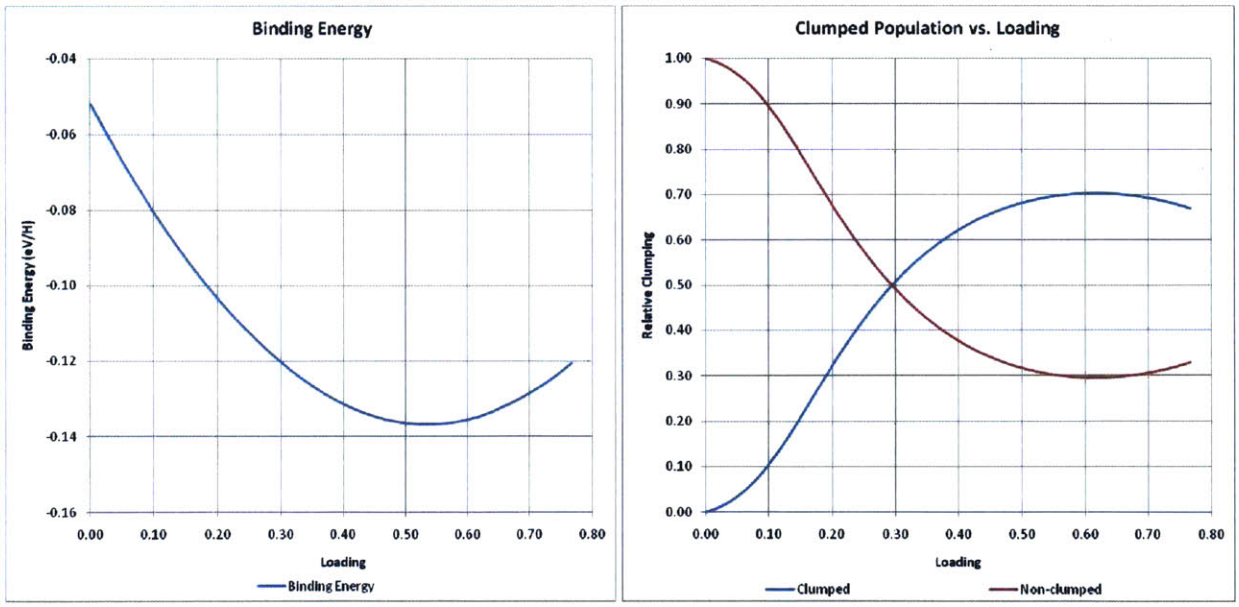

Figure 150: Binding Energy (at T=Tc) and Clumping Population as a function of loading

We notice that there is a somewhat tighter binding energy when we include temperature dependence (90 meV vs. 136 meV per H atom). The result is a higher clumped population as expected.

Temperature Dependent Interaction Energy

Analysis and Motivation

The above results, while very encouraging, still consist of a set of parameters at each temperature. In other words, each isotherm in Figure 148 is arrived at using a different value of the parameter set $\varepsilon_\delta^0, \varepsilon_\delta^1, \varepsilon_\delta^2, \varepsilon_c^0, \varepsilon_c^1, \varepsilon_c^2, \delta_c^0, \delta_c^1, \delta_c^2$ and the entropy and chemical potential offsets.

It would seem like a universal model should be accessible, especially when we notice that the temperature dependence of the interaction energy parameters appears linear:

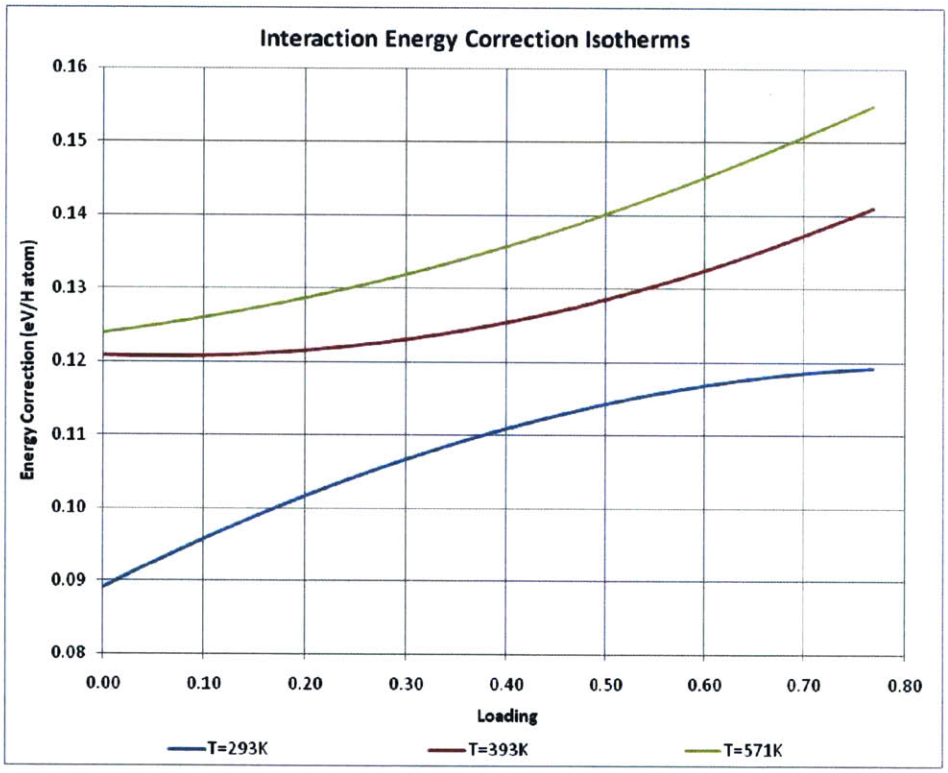

Figure 151: Interaction Energy Correction terms vs. Loading. The figure is arrived at by evaluating the model Interaction Energy Corrections along the loading scale.

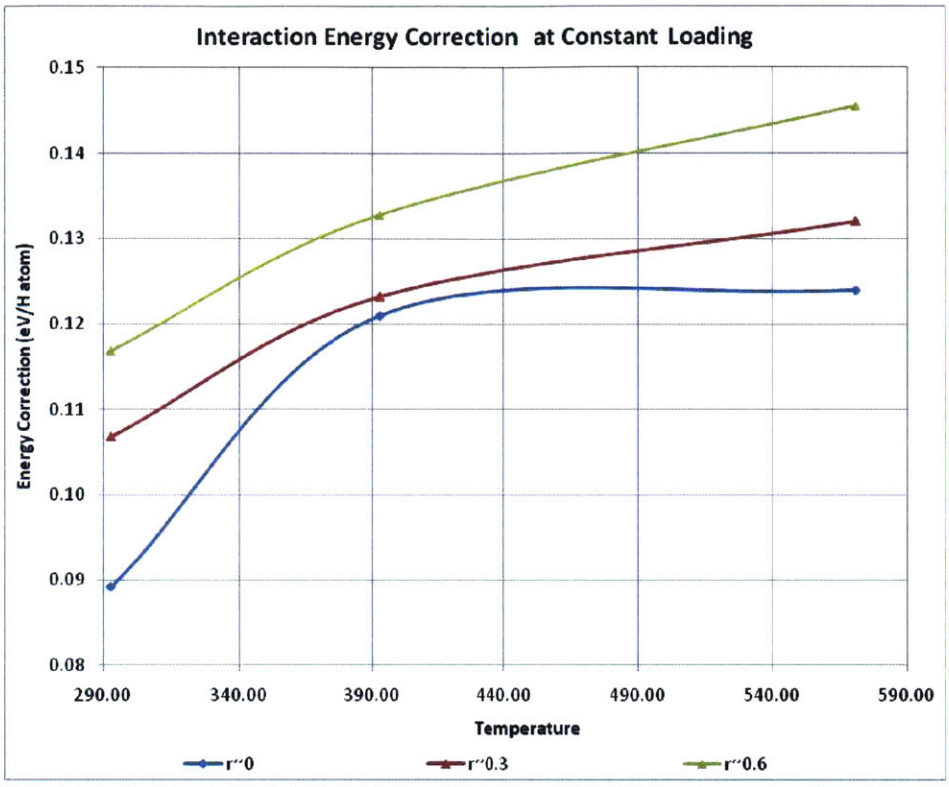

Figure 152: Interaction Energy Correction at constant loading

Figure 152, especially, suggests that we may reprise the argument behind Equation **720** to write the Interaction energy as

$$\varepsilon_h(\theta,T) \to \varepsilon_h(\theta) + \varepsilon_\delta^0 + \epsilon_\delta^0(T-T_c) + \left(\varepsilon_\delta^1 + \epsilon_\delta^1(T-T_c)\right)\theta + \left(\varepsilon_\delta^2 + \epsilon_\delta^2(T-T_c)\right)\theta^2 + \mathcal{O}(\theta^3) \tag{736}$$

whereupon

$$B(\theta,T)=\left[\frac{2\kappa_B T}{\gamma}ln\frac{\theta_c}{\Theta_o-\theta_o}\right.$$

$$+2\left(\theta\frac{\partial}{\partial\theta}\left[\frac{1}{1}\varepsilon_h(\theta)+\varepsilon_\delta^0+\varepsilon_\delta^1\theta+\varepsilon_\delta^2\theta^2+\epsilon_\delta^0(T-T_c)+\epsilon_\delta^1(T-T_c)\theta+\epsilon_\delta^2(T-T_c)\theta^2\right]\right.$$

$$\left.+\left[\frac{1}{1}\varepsilon_h(\theta)+\varepsilon_\delta^0+\varepsilon_\delta^1\theta+\varepsilon_\delta^2\theta^2+\epsilon_\delta^0(T-T_c)+\epsilon_\delta^1(T-T_c)\theta+\epsilon_\delta^2(T-T_c)\theta^2\right]\right)$$

$$+2\left(\theta_c\frac{\partial}{\partial\theta}[\varepsilon_c^0+\varepsilon_c^1\theta+\varepsilon_c^2\theta^2+\delta_c^0(T-T_c)+\delta_c^1(T-T_c)\theta+\delta_c^2(T-T_c)\theta^2]\right.$$

$$\left.+[\varepsilon_c^0+\varepsilon_c^1\theta+\varepsilon_c^2\theta^2+\delta_c^0(T-T_c)+\delta_c^1(T-T_c)\theta+\delta_c^2(T-T_c)\theta^2]\right)+3\epsilon_{0v}$$

$$\left.-\kappa_B T\,ln\left(2sinh\frac{\epsilon_{0v}}{2\kappa_B T}\right)+\kappa_B T\,ln\frac{8\pi^2 I\kappa_B T}{\sigma h^2}+\epsilon_D\right]$$

$$=\left[\frac{2\kappa_B T}{\gamma}ln\frac{\theta_c}{\Theta_o-\theta_o}\right.$$

$$+2\left(\theta\frac{\partial}{\partial\theta}\varepsilon_h(\theta)+\varepsilon_h(\theta)+\varepsilon_\delta^0+\epsilon_\delta^0(T-T_c)+2\left(\varepsilon_\delta^1+\epsilon_\delta^1(T-T_c)\right)\theta\right.$$

$$\left.+3\left(\varepsilon_\delta^2+\epsilon_\delta^2(T-T_c)\right)\theta^2\right)$$

$$+2\left(\frac{1}{1}\varepsilon_c^0+\delta_c^0(T-T_c)+\left(\varepsilon_c^1+\delta_c^1(T-T_c)\right)(\theta+\theta_c)+\left(\varepsilon_c^2+\delta_c^2(T-T_c)\right)(2\theta_c\theta+\theta^2)\right)$$

$$\left.+3\epsilon_{0v}-\kappa_B T\,ln\left(2sinh\frac{\epsilon_{0v}}{2\kappa_B T}\right)+\kappa_B T\,ln\frac{8\pi^2 I\kappa_B T}{\sigma h^2}+\epsilon_D\right]$$

737

and

$$\Delta\bar{G}_H^E(\theta,T)=\frac{RT}{2}lnA(T)+\frac{RT}{\gamma}ln\frac{\theta_c}{\Theta_o-\theta_o}$$

$$+\frac{R}{\kappa_B}\left(\frac{\partial}{\partial\theta}\varepsilon_h(\theta)+\varepsilon_h(\theta)+\varepsilon_\delta^0+\epsilon_\delta^0(T-T_c)+2\left(\varepsilon_\delta^1+\epsilon_\delta^1(T-T_c)\right)\theta\right.$$

$$\left.+3\left(\varepsilon_\delta^2+\epsilon_\delta^2(T-T_c)\right)\theta^2\right)$$

$$+\frac{R}{\kappa_B}\left(\varepsilon_c^0+\delta_c^0(T-T_c)+\left(\varepsilon_c^1+\delta_c^1(T-T_c)\right)(\theta+\theta_c)+\left(\varepsilon_c^2+\delta_c^2(T-T_c)\right)(2\theta_c\theta+\theta^2)\right)$$

$$+\frac{3}{2}\frac{R}{\kappa_B}\epsilon_{0v}-\frac{RT}{2}ln\left(2sinh\frac{\epsilon_{0v}}{2\kappa_B T}\right)+\frac{RT}{2}\,ln\frac{8\pi^2 I\kappa_B T}{\sigma h^2}+\frac{1}{2}\frac{R}{\kappa_B}\epsilon_D-RTln\frac{\theta}{1-\theta}$$

738

$$\frac{\Delta\bar{G}_H^E(\theta,T)}{T} \to \frac{R}{2}lnA(T) + \frac{R}{\gamma}ln\frac{\theta_c}{\Theta_o-\theta_o}$$

$$+\frac{R}{\kappa_B T}\left(\frac{\partial}{\partial\theta}\varepsilon_h(\theta)+\varepsilon_h(\theta)+\varepsilon_\delta^0+\epsilon_\delta^0(T-T_c)+2\left(\varepsilon_\delta^1+\epsilon_\delta^1(T-T_c)\right)\theta\right.$$

$$\left.+3\left(\varepsilon_\delta^2+\epsilon_\delta^2(T-T_c)\right)\theta^2\right)$$

$$+\frac{R}{\kappa_B T}\left(\varepsilon_c^0+\delta_c^0(T-T_c)+\left(\varepsilon_c^1+\delta_c^1(T-T_c)\right)(\theta+\theta_c)+\left(\varepsilon_c^2+\delta_c^2(T-T_c)\right)(2\theta_c\theta+\theta^2)\right)$$

$$+\frac{3}{2}\frac{R}{\kappa_B T}\epsilon_{0v}-\frac{R}{2}ln\left(2sinh\frac{\epsilon_{0v}}{2\kappa_B T}\right)+\frac{R}{2}ln\frac{8\pi^2 I\kappa_B T}{\sigma h^2}+\frac{1}{2}\frac{R}{\kappa_B T}\epsilon_D-Rln\frac{\theta}{1-\theta}$$

739

$$\Delta\bar{H}_H^E(\theta,T) = -T^2\left(\frac{\partial\left(\frac{\Delta\bar{G}_H^E(\theta,T)}{T}\right)}{\partial T}\right)_{P,n}$$

$$= -T^2\left(\frac{R}{2}\frac{A'(T)}{A(T)}-\frac{R}{\kappa_B T^2}\left(\frac{\partial}{\partial\theta}\varepsilon_h(\theta)+\varepsilon_h(\theta)+\varepsilon_\delta^0+\epsilon_\delta^0(T-T_c)+2\left(\varepsilon_\delta^1+\epsilon_\delta^1(T-T_c)\right)\theta\right.\right.$$

$$\left.\left.+3\left(\varepsilon_\delta^2+\epsilon_\delta^2(T-T_c)\right)\theta^2\right)+\frac{R}{\kappa_B T}\left(\epsilon_\delta^0+2\epsilon_\delta^1\theta+3\epsilon_\delta^2\theta^2\right)\right.$$

$$-\frac{R}{\kappa_B T^2}\left[\frac{1}{1}\varepsilon_c^0+\delta_c^0(T-T_c)+\left(\varepsilon_c^1+\delta_c^1(T-T_c)\right)(\theta+\theta_c)\right.$$

$$\left.+\left(\varepsilon_c^2+\delta_c^2(T-T_c)\right)(2\theta_c\theta+\theta^2)\right]+\frac{R}{\kappa_B T}\left[\frac{1}{1}\delta_c^0+\delta_c^1(\theta+\theta_c)+\delta_c^2(2\theta_c\theta+\theta^2)\right]$$

$$\left.-\frac{3R}{2\kappa_B T^2}\epsilon_{0v}+\frac{R}{4}\frac{\epsilon_{0v}}{\kappa_B T^2}coth\frac{\epsilon_{0v}}{2\kappa_B T}+\frac{R}{2T}-\frac{R}{2\kappa_B T^2}\epsilon_D\right)$$

740

or

$$\Delta\bar{H}_H^E(\theta,T) = -\frac{RT^2}{2}\frac{A'(T)}{A(T)}$$
$$+\frac{R}{\kappa_B}\left(\frac{\partial}{\partial\theta}\varepsilon_h(\theta)+\varepsilon_h(\theta)+\varepsilon_\delta^0+\epsilon_\delta^0(T-T_c)+2\left(\varepsilon_\delta^1+\epsilon_\delta^1(T-T_c)\right)\theta\right.$$
$$\left.+3\left(\varepsilon_\delta^2+\epsilon_\delta^2(T-T_c)\right)\theta^2\right)-\frac{RT}{\kappa_B}\left(\epsilon_\delta^0+2\epsilon_\delta^1\theta+3\epsilon_\delta^2\theta^2\right)$$
$$+\frac{R}{\kappa_B}\left[\frac{1}{1}\varepsilon_c^0+\delta_c^0(T-T_c)+\left(\varepsilon_c^1+\delta_c^1(T-T_c)\right)(\theta+\theta_c)+\left(\varepsilon_c^2+\delta_c^2(T-T_c)\right)(2\theta_c\theta+\theta^2)\right]$$
$$-\frac{RT}{\kappa_B}\left[\frac{1}{1}\delta_c^0+\delta_c^1(\theta+\theta_c)+\delta_c^2(2\theta_c\theta+\theta^2)\right]+\frac{3R}{2\kappa_B}\epsilon_{0v}-\frac{R}{4}\frac{\epsilon_{0v}}{\kappa_B}coth\frac{\epsilon_{0v}}{2\kappa_BT}-\frac{RT}{2}+\frac{R}{2\kappa_B}\epsilon_D$$

741

$$\Delta\bar{S}_H^E(\theta,T) = -\frac{RT}{2}\frac{A'(T)}{A(T)}-\frac{R}{2}lnA(T)-\frac{R}{\gamma}ln\frac{\theta_c}{\theta_o-\theta_o}-\frac{R}{\kappa_B}\left(\epsilon_\delta^0+2\epsilon_\delta^1\theta+3\epsilon_\delta^2\theta^2\right)$$
$$-\frac{R}{\kappa_B}\left(\delta_c^0+\delta_c^1(\theta+\theta_c)+\delta_c^2(2\theta_c\theta+\theta^2)\right)-\frac{1}{4}\frac{R\epsilon_{0v}}{\kappa_BT}coth\frac{\epsilon_{0v}}{2\kappa_BT}+\frac{R}{2}ln\left(2\,sinh\frac{\epsilon_{0v}}{2\kappa_BT}\right)-\frac{R}{2}$$
$$-\frac{R}{2}ln\frac{8\pi^2I\kappa_BT}{\sigma h^2}+Rln\frac{\theta}{1-\theta}$$

742

Finally, the model is completed with

$$f(T,\theta) = A(T)e^{\frac{B(T,\theta)}{\kappa_BT}}$$

743

Results

We carried out the above analysis. We first present the interaction energy as a function of loading and temperature. We know the latter should be approximately linear and a confirmation of this would indicate if the model is on the right path.

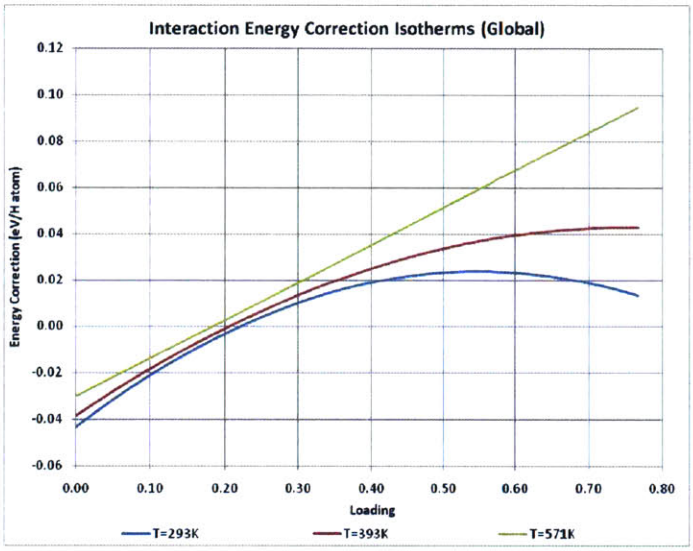

Figure 153: Interaction Correction Based on a global fit to enthalpy, entropy and three pressure isotherms

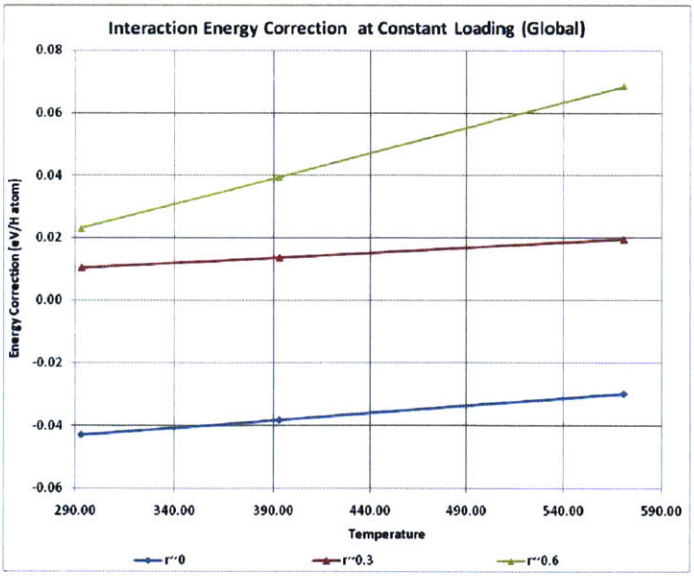

Figure 154: Same as Figure 153 but at constant loading

We present next the thermodynamic quantities and chemical potential. All show very good match.

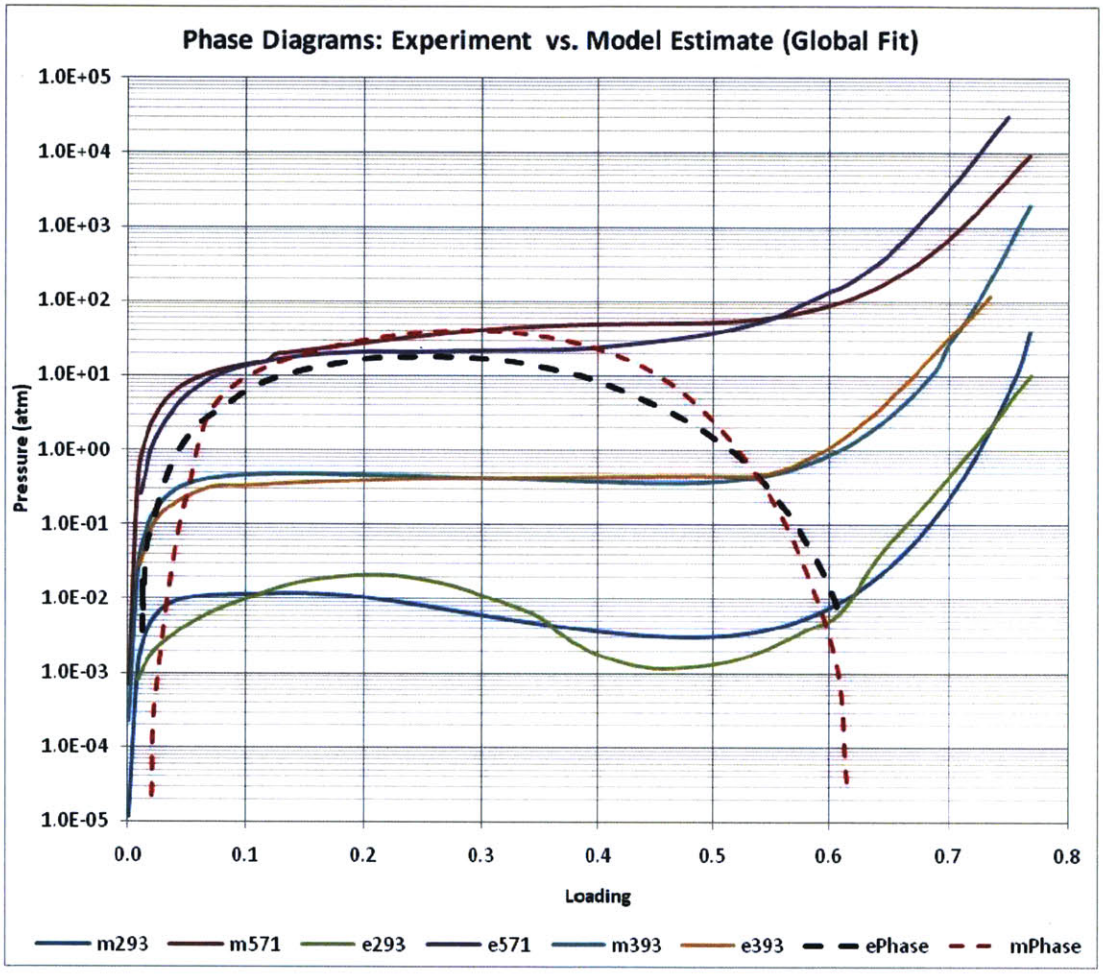

Figure 155: Chemical Potential and Estimated Phase Diagram for the Global Fit

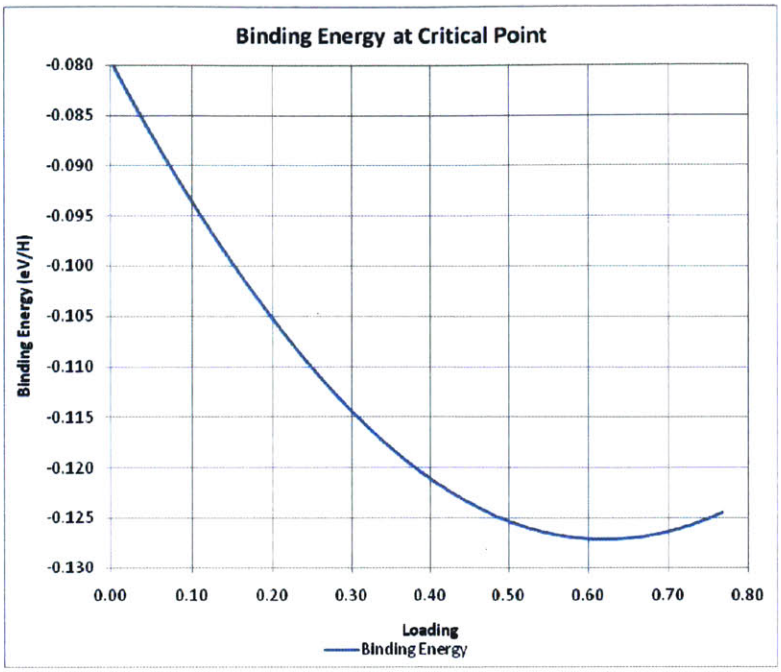

Figure 156: Binding Energy Based on Global Fit

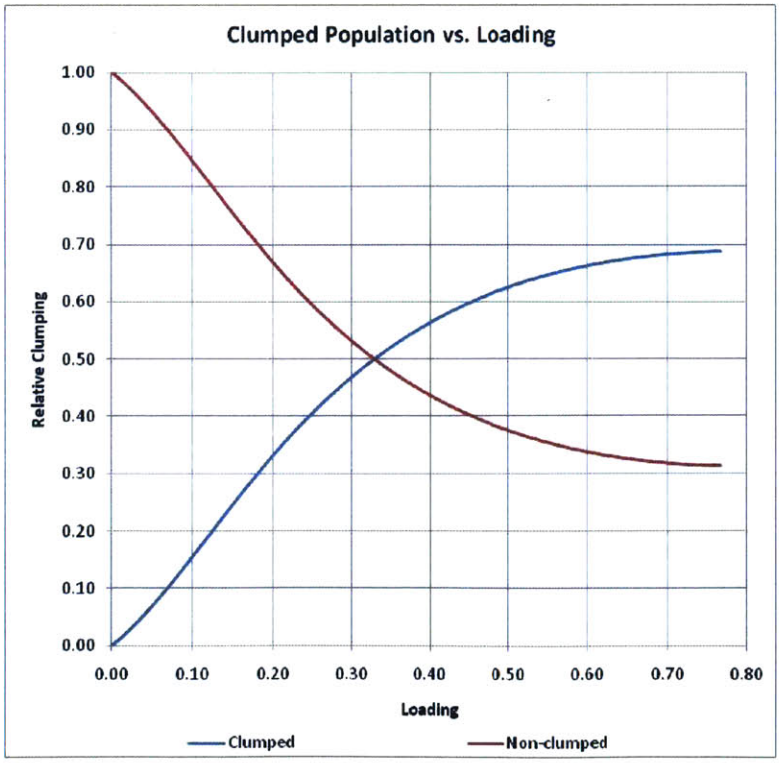

Figure 157: Clumped Population

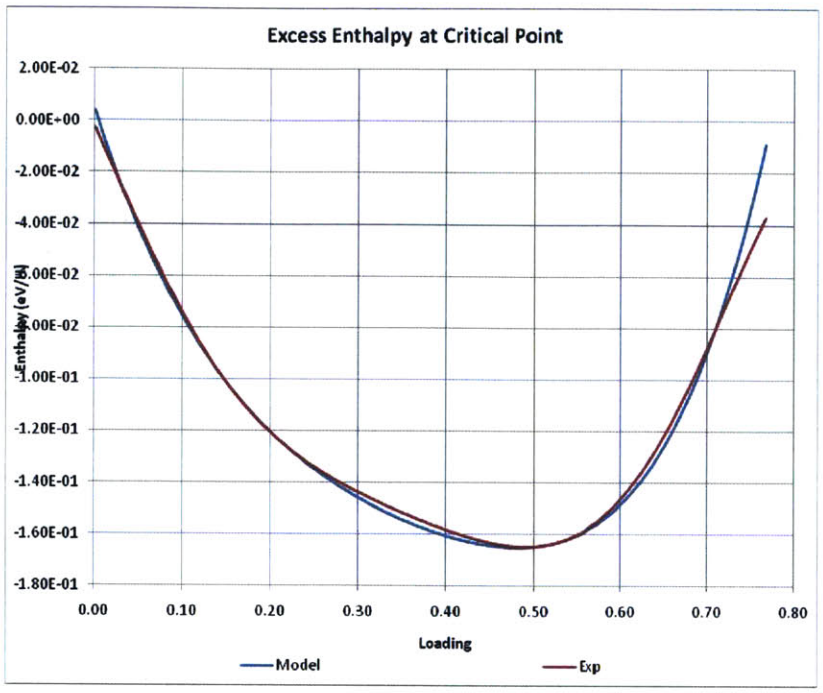

Figure 158: Excess Enthalpy Based on Global Fit

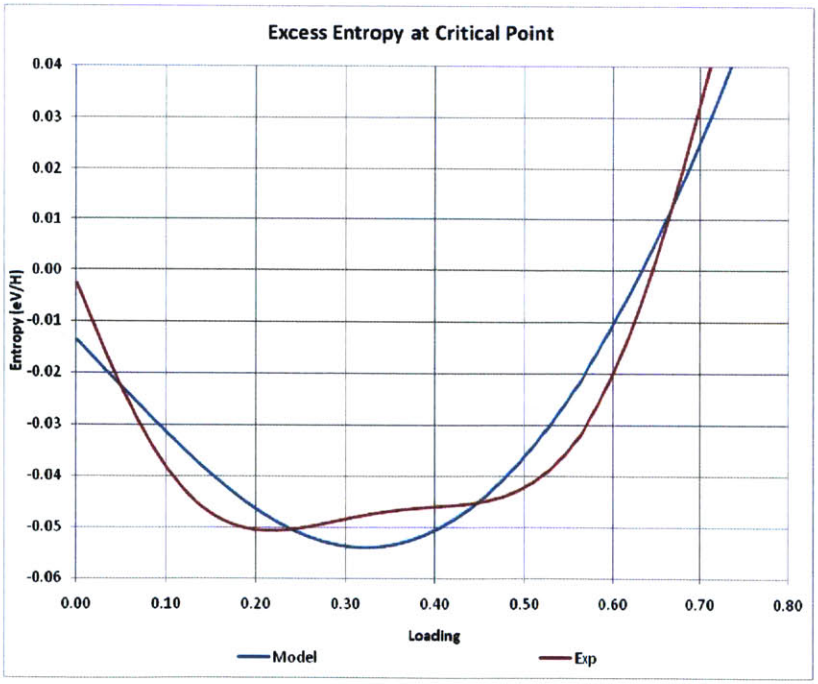

Figure 159: Excess Entropy Based on Global Fit.

Discussion of the Results

The following table shows the final values of the free parameters.

Parameter	Value (eV/H atom)	Description
ε_δ^0	$-9.9601 * 10^{-2}$	Interaction Energy Correction – 0^{th} Order
ε_δ^1	$-1.5285 * 10^{-1}$	Interaction Energy Correction – 1^{st} Order
ε_δ^2	$+1.2307 * 10^{-1}$	Interaction Energy Correction – 2^{nd} Order
ε_c^0	$+1.4182 * 10^{-1}$	Binding Energy Correction – 0^{th} Order
ε_c^1	$-3.0024 * 10^{-2}$	Binding Energy Correction –1^{st} Order
ε_c^2	$+8.1793 * 10^{-2}$	Binding Energy Correction –2^{nd} Order
ϵ_δ^0	$+4.7136 * 10^{-5}$	Interaction Energy Correction -0^{th} Order (Temperature)
ϵ_δ^1	$-1.4423 * 10^{-4}$	Interaction Energy Correction -1^{st} Order (Temperature)
ϵ_δ^2	$+2.6481 * 10^{-4}$	Interaction Energy Correction -2^{nd} Order (Temperature)
δ_c^0	$-3.4818 * 10^{-4}$	Binding Energy Correction – 0^{th} Order (Temperature)
δ_c^1	$+4.4300 * 10^{-4}$	Binding Energy Correction –1^{st} Order (Temperature)
δ_c^2	$-6.2001 * 10^{-4}$	Binding Energy Correction –2^{nd} Order (Temperature)
s_0	$+2.7783 * 10^{-1}$	Entropy Offset (at 571K)
μ_0	$-1.2068 * 10^{-2}$	Chemical Potential Offset (see Above)

These parameters may be reduced from the above 14 to 8 as suggested by Equations **720** and **736**:

$$E_B^c(\theta) \to \varepsilon_c^0 + \delta_c^0(T - T_c) + \left(\varepsilon_c^1 + \delta_c^1(T - T_c)\right)\theta + \left(\varepsilon_c^2 + \delta_c^2(T - T_c)\right)\theta^2 + O(\theta^3)$$
$$= \varepsilon_B^0(T - T_c) + \varepsilon_B^1(T - T_c)\theta + \varepsilon_B^2(T - T_c)\theta^2$$

744

$$\varepsilon_h(\theta, T) \to \varepsilon_h(\theta) + \varepsilon_\delta^0 + \epsilon_\delta^0(T - T_c) + \left(\varepsilon_\delta^1 + \epsilon_\delta^1(T - T_c)\right)\theta + \left(\varepsilon_\delta^2 + \epsilon_\delta^2(T - T_c)\right)\theta^2 + O(\theta^3)$$
$$= \varepsilon_h^0(T - T_c) + \varepsilon_h^1(T - T_c)\theta + \varepsilon_h^2(T - T_c)\theta^2$$

745

As before, the results were obtained by performing a least squares fit for enthalpy and entropy at the critical point, and simultaneously fitting the three pressure isotherms. The resulting 8 temperature dependent fitting parameters describe the loading process at any temperature, and provide a reasonable model of the physics and thermodynamics of the loading process. Other than setting the initial conditions at the critical point, the optimization is otherwise unconstrained. Following this process remarkably yields a bound state of the system as can be seen in Figure 156.

The first confirmation that the results are correct is in the temperature dependence of the interaction energy, which shows a positive slope, Figure 153 & Figure 154, consistent with experiment (Stern & Sarma, 1984). This is a validation of the model because we did not restrict the slope in any way.

The other validation point is in the binding energy, which we also did not constrain. The interpretation is that a preferred binding state exists that matches experimental data. The model now predicts the highest binding closer to beta phase boundary (compared to the middle of the miscibility gap as we would have expected), and the clumped population does not appear to be decreasing with loading; rather it levels off. One possible interpretation of this result is that once they are created, clumps persist even as loading increases. This would mean that the bound states are deeper than the interaction with non-clumped H-atoms.

In the next section, we explore some limits of clumping in the model.

Is Clumping Essential to the Model?

Analysis and Motivation

With the introduction of temperature dependence, it may be worthwhile to explore if clumping is still a critical factor in the model. To do this, we run the prior model by setting a large constant binding energy in an attempt to remove any clumping. However, it is soon realized that no solutions exist (in a least squares sense) above about 80 meV. This seems to suggest that some binding or clumping, however small, is a necessary ingredient in the model. Specifically, the binding is responsible for the non-ideal entropy, as can be seen by examining the expression for entropy, Equation 742. We therefore need to remove clumping completely from the model.

In addition, we revisit the Clumped Model with Nearest neighbor exclusion

Model with No Clumps

We assume here that there is no clumping, but the interaction energy depends on Temperature according to Equation 745. To do this, it may be easier to rewrite Equation 419 as

$$Z_H(\tau,\mu) = \sum_{n_o=0}^{N_o}\sum_{n_t=0}^{N_t}\sum_{ASN} e^{\frac{(n_o+n_t)\mu-\varepsilon_h(n_o,n_t)}{\tau}} z_{o,t}^{n_o+n_t} g_{o,t}^{n_{nc}+n_t} \tag{746}$$

and we can derive the chemical potential simply as

$$\mu_o(\tau,\theta) = \tau\, ln\frac{\theta_o}{\theta_o-\theta_o} + \theta\frac{\partial}{\partial\theta}\varepsilon_h(\theta) + \varepsilon_h(\theta) - \tau ln z_{o,t} - \tau ln g_{o,t} \tag{747}$$

The boundary condition becomes

$$\tau\, ln\frac{\theta_o}{\Theta_o-\theta_o}+\theta\frac{\partial}{\partial\theta}\varepsilon_h(\theta)+\varepsilon_h(\theta)-\tau lnz_{o,t}-\tau lng_{o,t}$$

$$=-\frac{\tau}{2}\left[ln\left[\left(\frac{2\pi m\tau}{h^2}\right)^{\frac{3}{2}}\frac{\tau}{f}\right]+ln\frac{e^{-\frac{\epsilon_{0v}}{2\tau}}}{1-e^{-\frac{\epsilon_{0v}}{\tau}}}+\ ln\frac{8\pi^2 I\tau}{\sigma h^2}+\frac{\epsilon_D}{\tau}\right]$$

748

from which we get fugacity, except now (Equations 499):

$$B(\tau,\theta)=2\left(\tau\, ln\frac{\theta_o}{\Theta_o-\theta_o}+\theta\frac{\partial}{\partial\theta}\varepsilon_h(\theta)+\varepsilon_h(\theta)+\varepsilon_\delta^0+\epsilon_\delta^0(T-T_c)+2\left(\varepsilon_\delta^1+\epsilon_\delta^1(T-T_c)\right)\theta\right.$$

$$\left.+3\left(\varepsilon_\delta^2+\epsilon_\delta^2(T-T_c)\right)\theta^2+\frac{5}{2}\tau ln\left(2sinh\frac{\epsilon_{0v}}{2\tau}\right)-\tau lng_{o,t}\right)+\ \tau ln\frac{8\pi^2 I\tau}{\sigma h^2}+\epsilon_D$$

749

such that

$$\Delta\bar{G}_H^E(\theta,T)=\frac{1}{2}RT\left(lnA(T)+ln\frac{8\pi^2 I\kappa_B T}{\sigma h^2}+5ln\left(2sinh\frac{\epsilon_{0v}}{2\kappa_B T}\right)-2lng_{o,t}\right)+\frac{R}{\kappa_B}\left(\theta\frac{\partial}{\partial\theta}\varepsilon_h(\theta)+\varepsilon_h(\theta)+\frac{1}{2}\epsilon_D\right)$$

750

and

$$\Delta\bar{H}_H^E(\theta,T)=-\frac{1}{2}RT^2\left(\frac{A'(T)}{A(T)}+\frac{1}{T}-\frac{5}{2}\frac{\epsilon_{0v}}{\kappa_B T^2}coth\frac{\epsilon_{0v}}{2\kappa_B T}\right)-\frac{RT}{\kappa_B}\left(\epsilon_\delta^0+2\epsilon_\delta^1\theta+3\epsilon_\delta^2\theta^2\right)$$

$$+\frac{R}{\kappa_B}\left(\theta\frac{\partial}{\partial\theta}\varepsilon_h(\theta)+\varepsilon_h(\theta)+\varepsilon_\delta^0+\epsilon_\delta^0(T-T_c)+2\left(\varepsilon_\delta^1+\epsilon_\delta^1(T-T_c)\right)\theta\right.$$

$$\left.+3\left(\varepsilon_\delta^2+\epsilon_\delta^2(T-T_c)\right)\theta^2+\frac{1}{2}\epsilon_D\right)$$

751

$$\Delta\bar{S}_H^E(\theta,T) = -\frac{RT}{2}\frac{A'(T)}{A(T)} - \frac{R}{2}lnA(T) - \frac{R}{2} - \frac{1}{2}Rln\frac{8\pi^2 I\kappa_B T}{\sigma h^2} + \frac{5}{4}\frac{R\epsilon_{0v}}{\kappa_B T}coth\frac{\epsilon_{0v}}{2\kappa_B T} - \frac{5}{2}Rln\left(2sinh\frac{\epsilon_{0v}}{2\kappa_B T}\right)$$
$$+ Rlng_{o,t} - \frac{R}{\kappa_B}\left(\epsilon_\delta^0 + 2\epsilon_\delta^1\theta + 3\epsilon_\delta^2\theta^2\right)$$

752

Clumps with Nearest Neighbor Exclusion

For the clumped configuration with nearest neighbor exclusion, we start with Equation 592, from whence:

$$B(\theta,T) = \frac{2\kappa_B T}{\gamma}ln\frac{\varphi\theta_c}{\theta_o - \theta_{nc} - \varphi\theta_c}$$
$$+ 2\left(\theta\frac{\partial}{\partial\theta}\varepsilon_h(\theta) + \varepsilon_h(\theta) + \varepsilon_\delta^0 + \epsilon_\delta^0(T - T_c) + 2\left(\varepsilon_\delta^1 + \epsilon_\delta^1(T - T_c)\right)\theta\right.$$
$$\left. + 3\left(\varepsilon_\delta^2 + \epsilon_\delta^2(T - T_c)\right)\theta^2\right)$$
$$+ 2\left(\frac{1}{1}\varepsilon_c^0 + \delta_c^0(T - T_c) + \left(\varepsilon_c^1 + \delta_c^1(T - T_c)\right)(\theta + \theta_c) + \left(\varepsilon_c^2 + \delta_c^2(T - T_c)\right)(\theta^2 + 2\theta\theta_c)\right)$$
$$+ 3\epsilon_{0v} - \kappa_B T ln\left(2\,sinh\frac{\epsilon_{0v}}{2\kappa_B T}\right) + \kappa_B T ln\frac{8\pi^2 I\kappa_B T}{\sigma h^2} + \epsilon_D$$

753

and

$$\Delta\bar{G}_H^E(\theta,T)=\frac{1}{2}RTlnA(T)+\frac{1}{\gamma}RT\,ln\frac{\varphi\theta_c}{\Theta_o-\theta_{nc}-\varphi\theta_c}$$
$$+\frac{R}{\kappa_B}\Big(\theta\frac{\partial}{\partial\theta}\varepsilon_h(\theta)+\varepsilon_h(\theta)+\varepsilon_\delta^0+\epsilon_\delta^0(T-T_c)+2\left(\varepsilon_\delta^1+\epsilon_\delta^1(T-T_c)\right)\theta$$
$$+3\left(\varepsilon_\delta^2+\epsilon_\delta^2(T-T_c)\right)\theta^2\Big)$$
$$+\frac{R}{\kappa_B}\left(\frac{1}{1}\varepsilon_c^0+\delta_c^0(T-T_c)+\left(\varepsilon_c^1+\delta_c^1(T-T_c)\right)(\theta+\theta_c)+\left(\varepsilon_c^2+\delta_c^2(T-T_c)\right)(\theta^2+2\theta\theta_c)\right)$$
$$+\frac{3}{2}\frac{R}{\kappa_B}\epsilon_{0v}-\frac{1}{2}RTln\left(2\,sinh\frac{\epsilon_{0v}}{2\kappa_BT}\right)+\frac{1}{2}RTln\frac{8\pi^2I\kappa_BT}{\sigma h^2}+\frac{1}{2}\frac{\mathrm{R}}{\kappa_B}\epsilon_D-RTln\frac{\theta}{1-\theta}$$

754

$$\Delta\bar{H}_H^E(\theta,T)=-\frac{RT^2}{2}\frac{A'(T)}{A(T)}-\frac{RT}{\kappa_B}\left(\epsilon_\delta^0+2\epsilon_\delta^1\theta+3\epsilon_\delta^2\theta^2\right)$$
$$+\frac{R}{\kappa_B}\Big(\theta\frac{\partial}{\partial\theta}\varepsilon_h(\theta)+\varepsilon_h(\theta)+\varepsilon_\delta^0+\epsilon_\delta^0(T-T_c)+2\left(\varepsilon_\delta^1+\epsilon_\delta^1(T-T_c)\right)\theta$$
$$+3\left(\varepsilon_\delta^2+\epsilon_\delta^2(T-T_c)\right)\theta^2\Big)-\frac{RT}{\kappa_B}\left(\delta_c^0+\delta_c^1(\theta+\theta_c)+\delta_c^2(\theta^2+2\theta\theta_c)\right)$$
$$+\frac{R}{\kappa_B}\left(\frac{1}{1}\varepsilon_c^0+\delta_c^0(T-T_c)+\left(\varepsilon_c^1+\delta_c^1(T-T_c)\right)(\theta+\theta_c)+\left(\varepsilon_c^2+\delta_c^2(T-T_c)\right)(\theta^2+\theta\theta_c)\right)$$
$$+\frac{3}{2}\frac{R}{\kappa_B}\epsilon_{0v}-\frac{1}{4}\frac{R\epsilon_{0v}}{\kappa_B}\coth\left(\frac{\epsilon_{0v}}{2\kappa_BT}\right)-\frac{1}{2}RT+\frac{1}{2}\frac{R}{\kappa_B}\epsilon_D$$

755

$$\Delta\bar{S}_H^E(\theta,T)=-\frac{RT}{2}\frac{A'(T)}{A(T)}-\frac{R}{2}lnA(T)-\frac{R}{\gamma}ln\frac{\varphi\theta_c}{\Theta_o-\theta_{nc}-\varphi\theta_c}-\frac{R}{\kappa_B}\left(\epsilon_\delta^0+2\epsilon_\delta^1\theta+3\epsilon_\delta^2\theta^2\right)$$
$$-\frac{R}{\kappa_B}\left(\frac{1}{1}\delta_c^0+\delta_c^1(\theta+\theta_c)+\delta_c^2(\theta^2+2\theta\theta_c)\right)-\frac{R\epsilon_{0v}}{4\kappa_BT}coth\frac{\epsilon_{0v}}{2\kappa_BT}+\frac{R}{2}ln\left(2\,sinh\frac{\epsilon_{0v}}{2\kappa_BT}\right)-\frac{R}{2}$$
$$-\frac{R}{2}ln\frac{8\pi^2I\kappa_BT}{\sigma h^2}+Rln\frac{\theta}{1-\theta}$$

756

With Equation 589 rewritten with the temperature dependent binding energy model:

$$\frac{{\theta_c}^{\varphi}(\Theta_o - \theta_{nc})^{\gamma\varphi-1}}{{\theta_{nc}}^{\gamma\varphi}(\Theta_o - \theta_{nc} - \varphi\theta_c)^{\varphi-1}} = \frac{1}{\varphi^{\varphi}}\left[\frac{1}{2}\left(1 - e^{\frac{\epsilon_{0v}}{\kappa_B T}}\right)^3 e^{\frac{E_B^c(\theta)}{\kappa_B T}}\right]^{\gamma\varphi}$$

757

The results are shown below:

Results

Model with no Binding

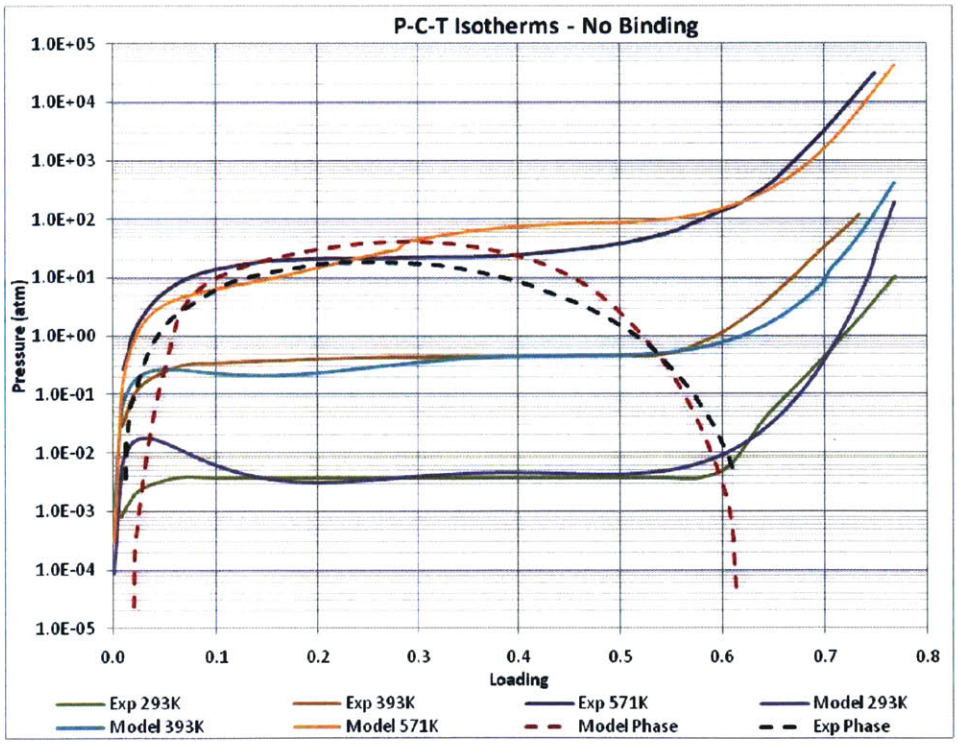

Figure 160: No Binding Model: Pressure Isotherms and Phase Envelope

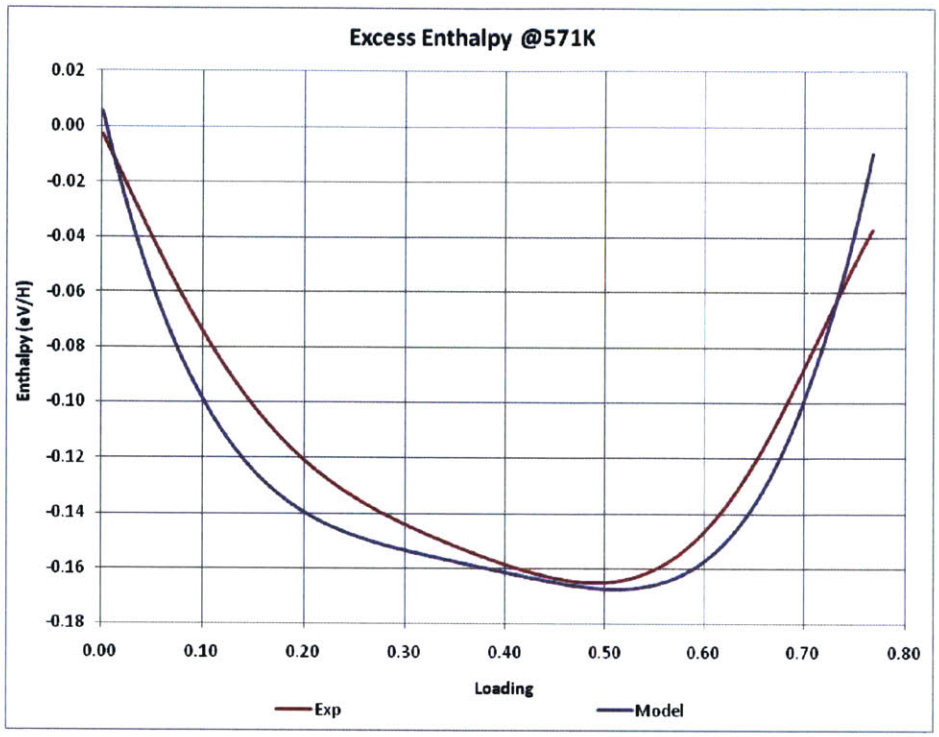

Figure 161: No Binding Model - Excess Enthalpy

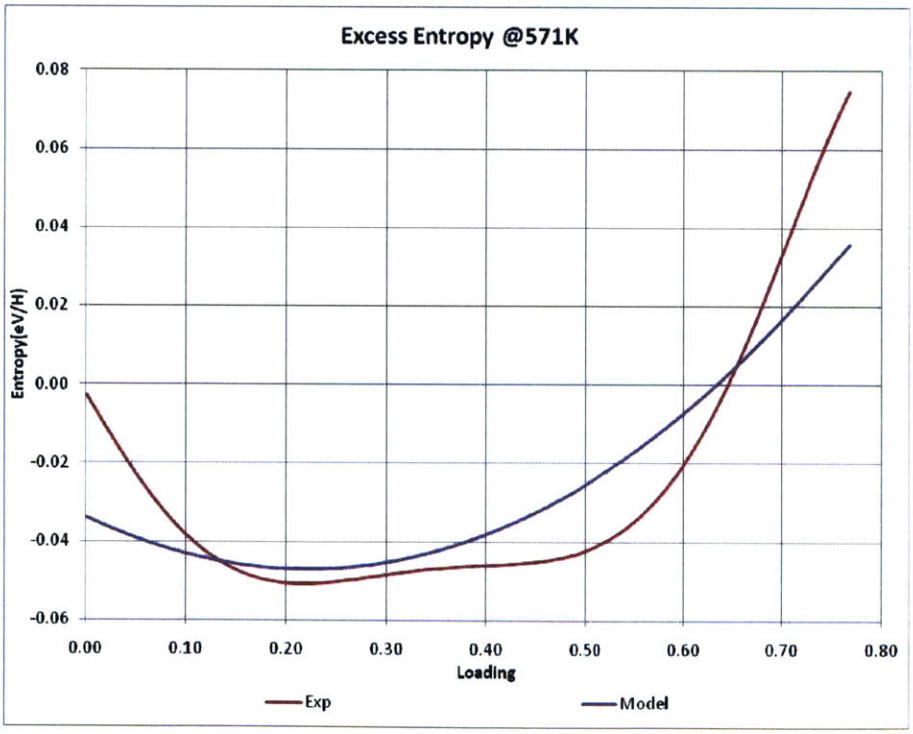

Figure 162: No Binding Model: Excess Entropy

Model with Binding

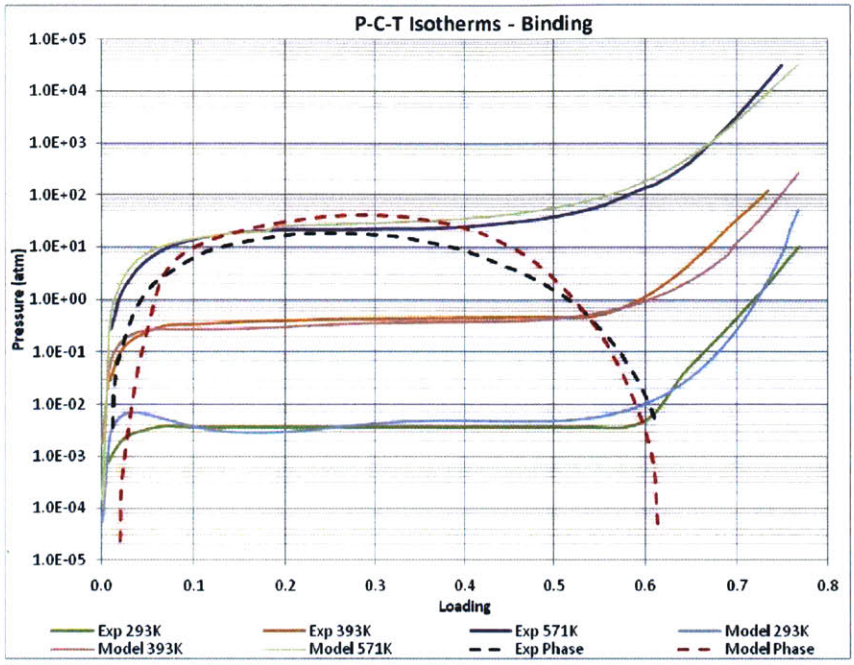

Figure 163: Model with Binding: Pressure Isotherms and Phase

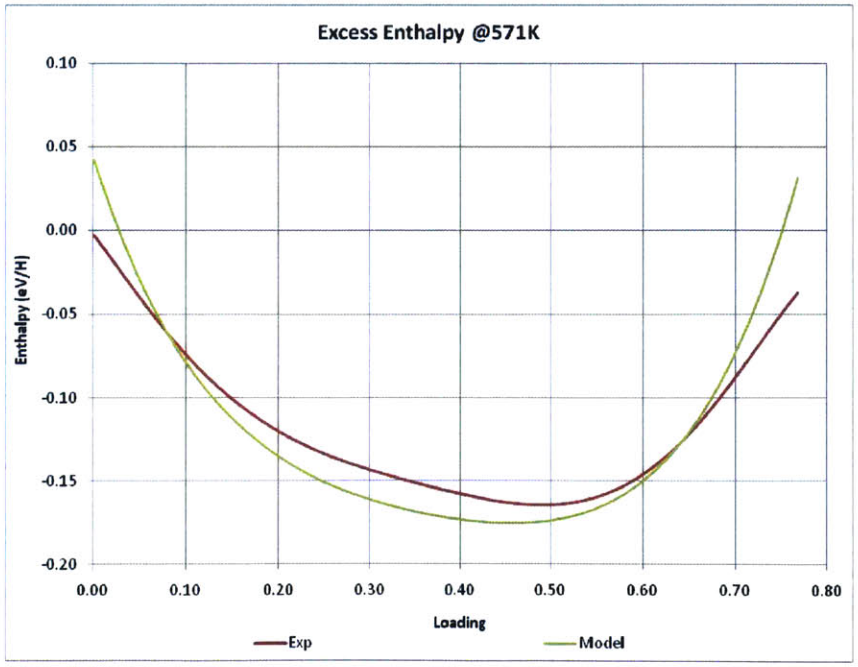

Figure 164: Model with Binding: Excess Enthalpy

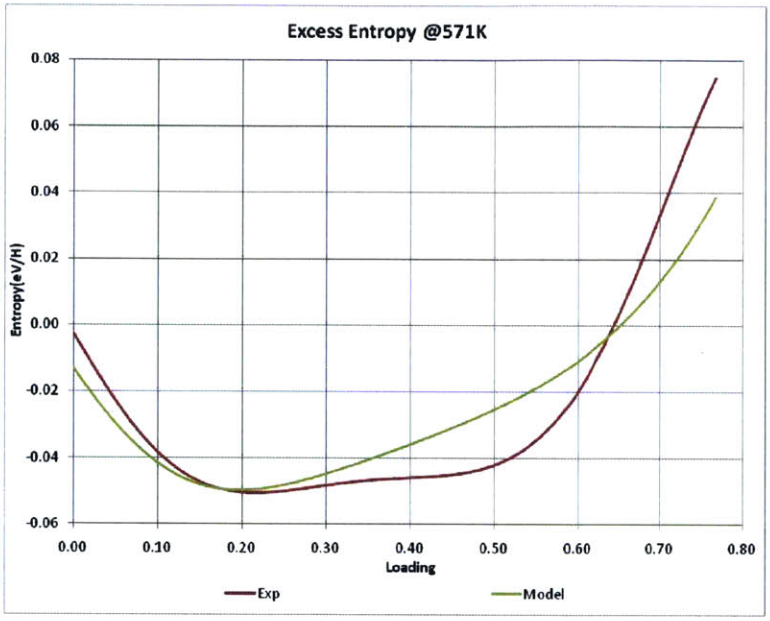

Figure 165: Model with Binding: Excess Entropy

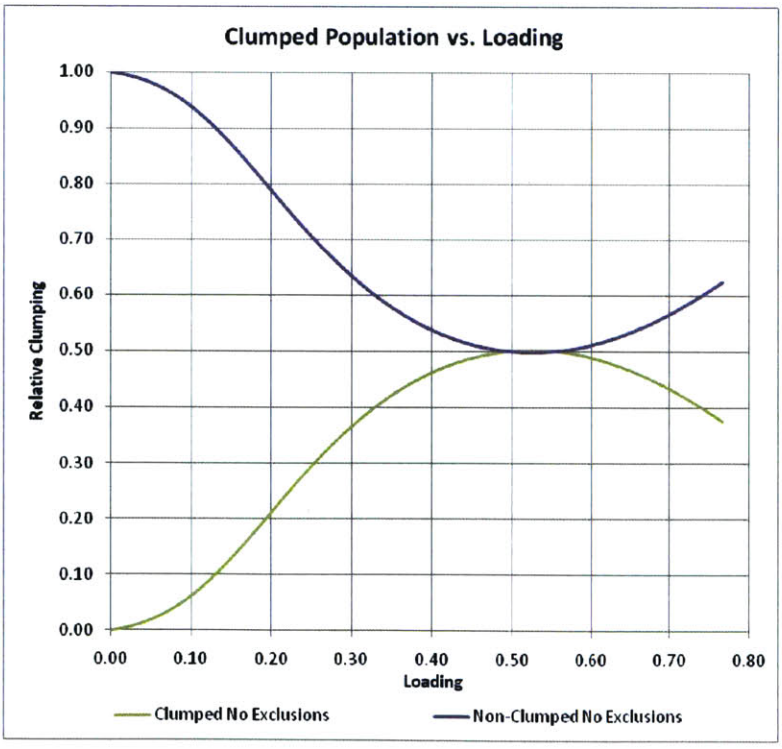

Figure 166: Model with Binding: Clumped vs. Non-Clumped Population

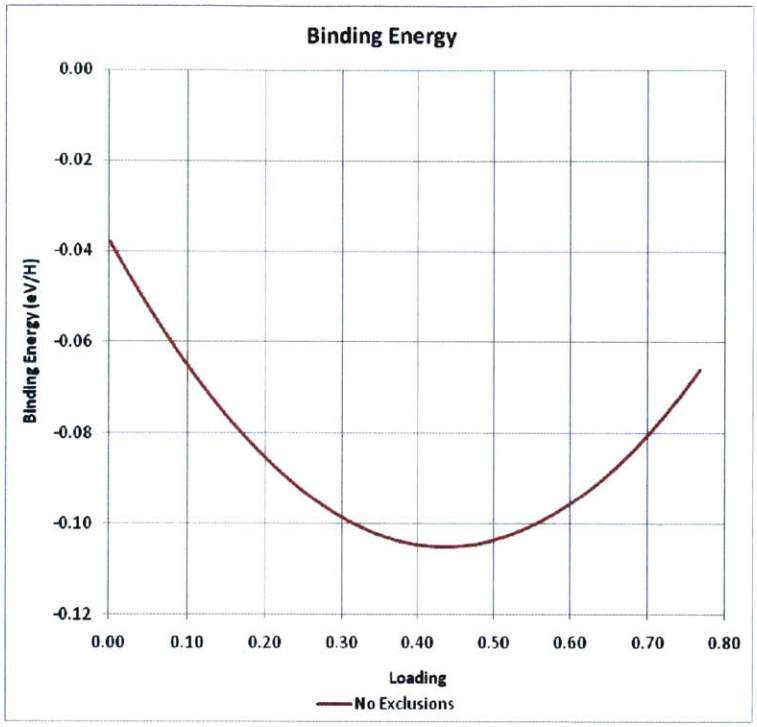

Figure 167: Model with Binding: Binding Energy

Model with Binding and Nearest Neighbor Exclusion

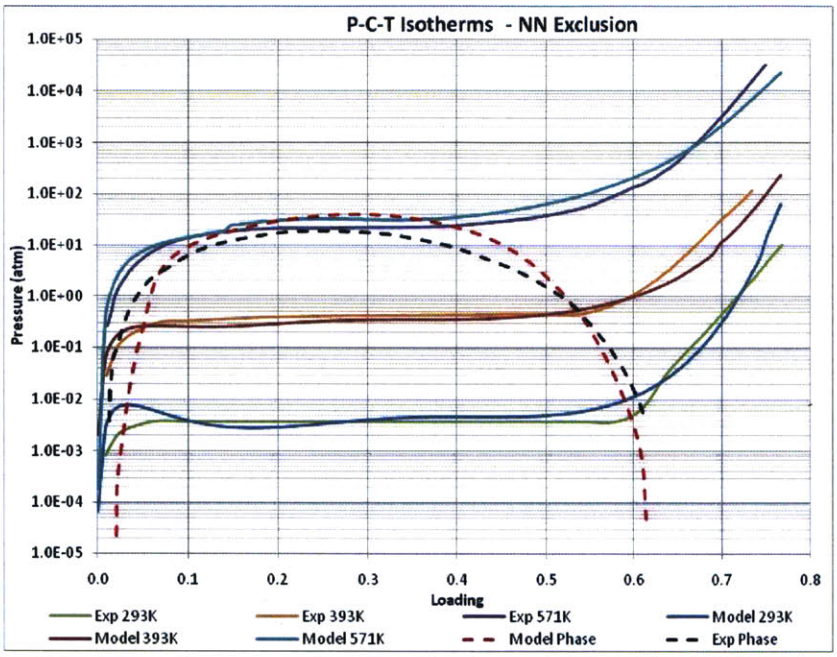

Figure 168: Model with NN Exclusion: Pressure Isotherm and Phase

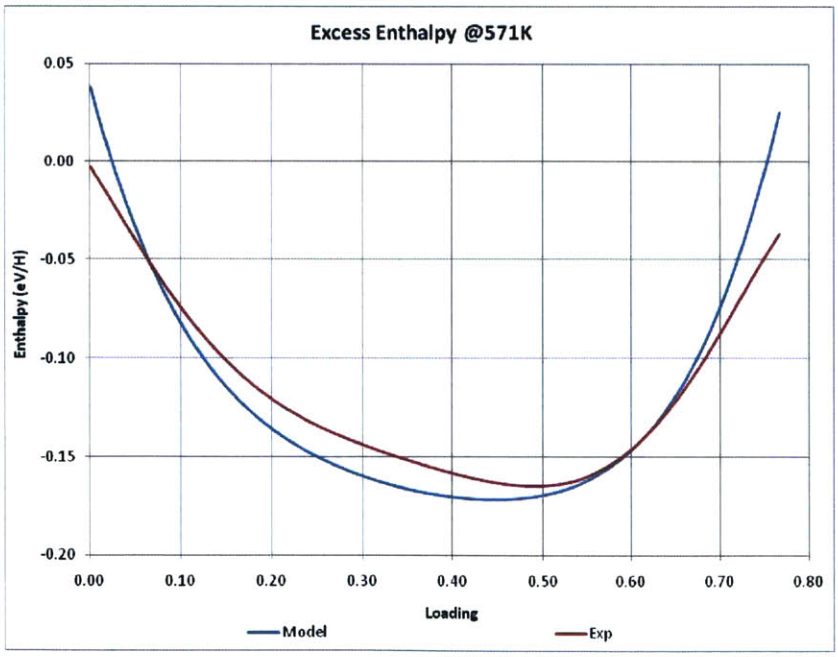

Figure 169: Model with NN Exclusion: Excess Enthalpy

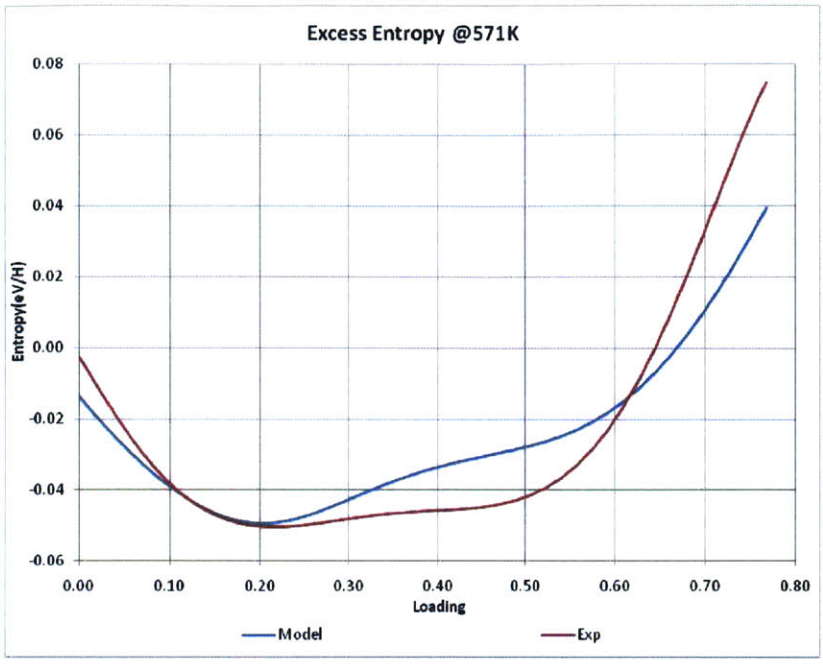

Figure 170: Model with NN Exclusion: Excess Entropy

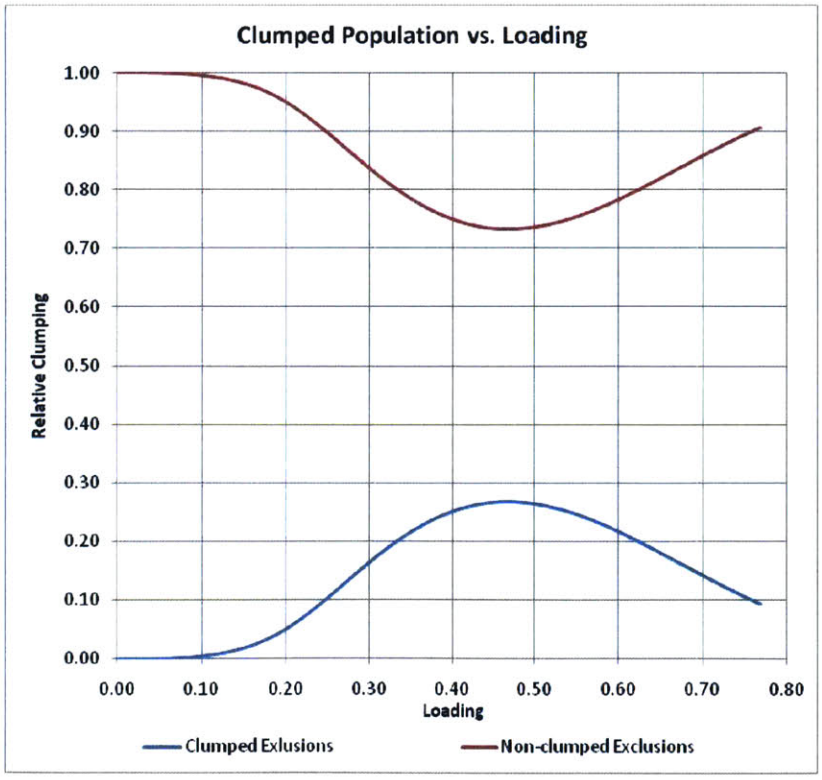

Figure 171: Model with NN Exclusion: Clumped Population.

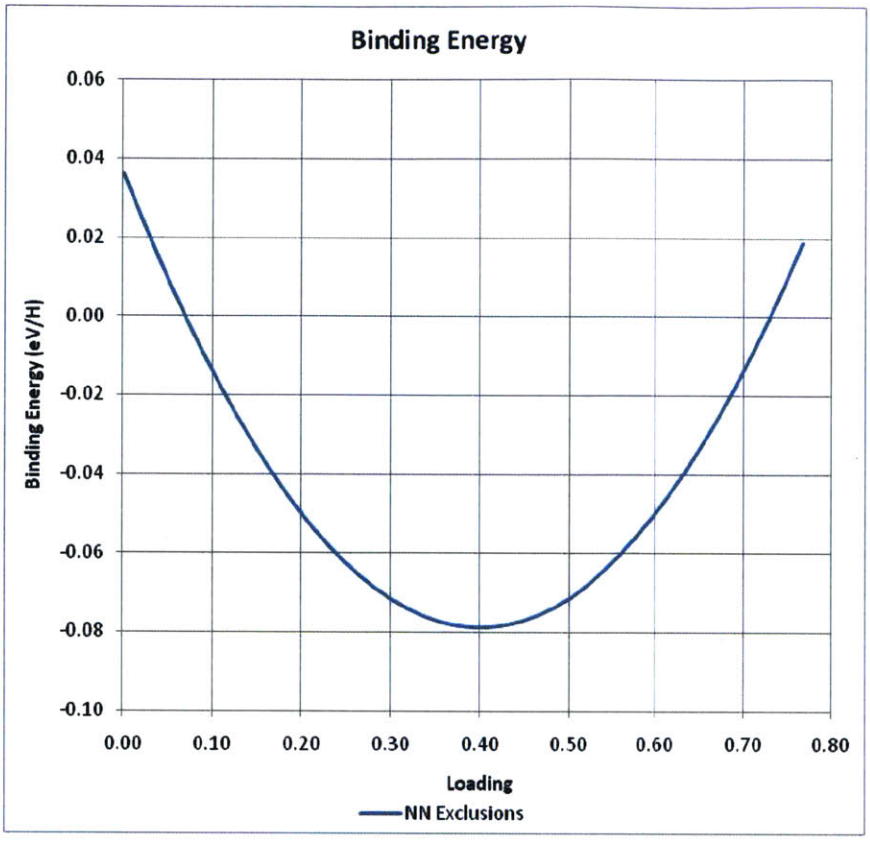

Figure 172: Model with NN Exclusion: Binding Energy

Does Temperature Correction Contain Any Physics?

We would like to evaluate if the temperature dependence is reasonable physically. We therefore plot the corrections to the interaction energy, i.e.,

$$\Delta\varepsilon_h(\theta,T) = \varepsilon_\delta^0 + \epsilon_\delta^0(T-T_c) + \left(\varepsilon_\delta^1 + \epsilon_\delta^1(T-T_c)\right)\theta + \left(\varepsilon_\delta^2 + \epsilon_\delta^2(T-T_c)\right)\theta^2 \quad (758)$$

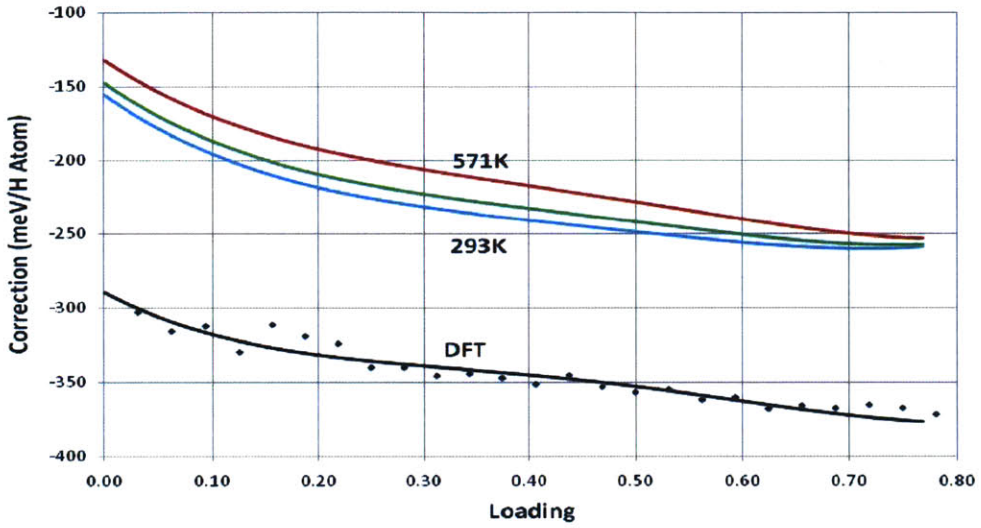

Figure 173: Temperature corrections vs. Loading (No Clumping)

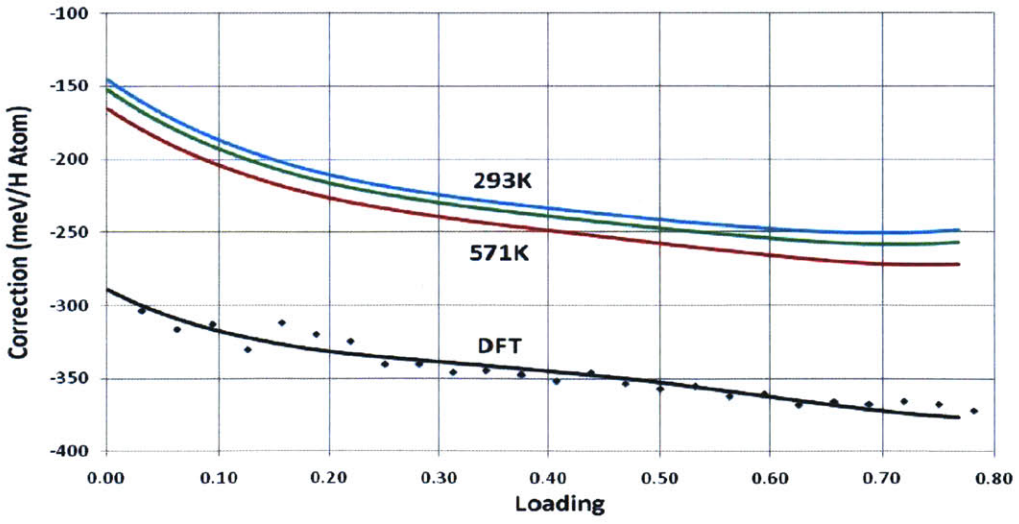

Figure 174: Temperature corrections vs. Loading (Clumping with NN Exclusion)

We note that there is a big (150 meV) constant DFT offset as expected. Even more remarkably, we note that the temperature dependence is weak, as would be expected from solid state physics. This weak dependence is seen in both the model with no binding (Figure 173) and that with binding (Figure 174). Of note is the inversion in temperature dependence of the corrections going from no binding to binding. A possible explanation could be that occupation probabilities increase with temperature, in which case, the model with binding provides a physically more plausible model.

Summary

Overall, all three models show reasonable match with experiment. However, the nearest neighbor exclusion appears to capture the physics of the problem. The exclusion model shows the clumped population peaking around the middle of the miscibility gap, which corresponds to our physical intuition of the miscibility gap. Additionally, it provides the best match with entropy data. The model is hereby proposed for experimental verification.

Chapter 11 - Summary and Conclusions

In this work, we have attempted a physics-based model that describes the hydrogen absorption into palladium lattice. Using a statistical analysis and the grand partition function formalism, we are able to obtain a theoretical expression for basic properties of the absorption process in equilibrium.

To calculate the state energies, we solved the Time Independent Schrodinger's Equation for the many body problem using Density Functional Theory (DFT). We know that we can only hope for an approximate solution – (if we could solve the TISE exactly, the physics of the absorption would be completely specified!). It is noticed that the gross DFT results are able to capture some basic physics of the absorption process in an approximate manner. For example, we are able to derive a phase envelope, P-C-T isotherms, and thermodynamic quantities that bear some semblance to experiments.

We have also connected the various properties of the equilibrium loading process in a fundamental way from first principles. Even though this is not new, the particular analysis is novel, especially the interpretation of the entropy in terms of accessible microstates at low loading.

The miscibility gap is analyzed by introducing a clumping model that posits a weak binding between adjacent absorbed hydrogen atoms. We propose that the resulting quasi-molecule may, for the first time, provide a physical explanation for the miscibility gap in palladium. The resulting analysis leads to the Orondo Isotherm, which is a key theoretical result.

Electronic contributions to entropy have long been postulated, but not demonstrated nor much understood. We show here that these contributions are not significant through an *ab initio* calculation, and provide the theoretical foundation for some further investigations.

Another key contribution of this thesis is the analysis and methodology surrounding the interpretation and correction of the calculated state energies. We are able to show that a physics-based correction of interaction energies leads to results that are consistent with Solid State Physics, namely, a weak dependence of band energies on temperature.

Finally, we invite experimentalists to conduct investigation of palladium hydride in the middle of the miscibility gap and look for any evidence of pairings between absorbed hydrogen atoms.

Bibliography

Alefeld, G. (1972). *Ber. Bunsenges Phys. Chem. , 76*, 746.

Baer, R. (2009). *Electronic Function Density Theory.* Hebrew University.

Balasubramanian, K., Feng, F., & Liao, M. (1987). *J. Chem. Phys. , 7*, 3981.

Baranowski, B., Filipek, S., Szustakowski, M., & Woryna, W. (1990). *Journal of Less Common Metals , 158*, 347.

Benzinger, J. (1980). *App. Surf. Sci. , 6*, 106.

Bockris, J., Chien, C., Hodko, D., & Minevski, Z. (1992). *Int. J. Hydrogen Energy , 17*, 445.

Boureau, G., & Kleppa, O. (1976). *The Journal of Chemical Physics , 65*, 3915.

Boureau, G., Kleppa, O., & Dantzer, P. (1976). *The Journal of Chemical Physics , 64*, 5247.

Bragg, W., & Williams, E. (1934). *Proc. Roy. Soc. A , 145*, 699.

Buckley, C., Dobson, J., & Poyser, M. (1995). *J. Phys. Cond. Matter , 7*, 5815.

Cao, Y., & Chen, Z. (2006). *Surf. Sci. , 600*, 4572.

Chan, C., & Louie, G. (1983). *Phys. Rev. B , 27*, 3325.

Christensen, O., Stoltze, P., Jacobsen, W., & Norskov, J. (1990). *Phys. Rev. B , 41*, 12413.

Eriksson, O., Wills, J., & Wallace, D. (1992). *Phys. Rev. B , 46*, 5221.

Fall, C. (1999). *PhD Thesis.* Ecole Polytechnique Federale Lausanne.

Flanagan, T., & Oates, W. (1991). *Annu. Rev. Mater. Sci. , 21*, 269.

Flanagan, T., Luo, W., & Clewley, J. (1991). *Journal of the Less-Common Metals , 172*, 42.

Fowler, R. (1936). *Proc. Camb. Phil. Soc. , 32*, 144.

Fukai, Y. (2005). *The Metal-Hydrogen System: Basic Bulk Properties.* Springer.

Geerken, B., & Griessen, R. (1983). *J. Phys. F.: Met. Phys. , 13*, 963.

Giannozzi, P. e. (2010). *http://www.quantum-espresso.org.*

Green, T., & Britz, D. (1996). *Journal of Electroanalytical Chemistry , 412*, 59.

Hagelstein, P. (2010). *Private Communication.*

Hagelstein, P. (2009). *Private Conversation.*

Hagelstein, P., & deChiaro, L. (2009). *Unpublished* .

Hagelstein, P., Senturia, S., & Orlando, T. (2004). *Introductory Quantum Physics and Statistical Mechanics.* Wiley.

Hagelstein, Senturia, & Orlando. (2004). *Introductory Quantum Physics and Statistical Mechanics.* Wiley.

Haus, H., & Melcher, J. (1989). *Electromagnetic Fields and Energy.* Prentice Hall.

Hemmes, H., Driessen, A., & Griessen, R. (1986). *J. Phys. C: Solid State Physics , 19*, 3571.

Herzberg, G. (1970). *Journal of Molecular Spectroscopy , 33*, 147.

Hohenberg, P., & Kohn, W. (1964). *Phys. Rev. 3B , 136*, B864.

Kittel, C. (1996). *Introduction to Solid State Physics, 7th Edition.* John Wiley.

Kittel, C. (1980). *Thermal Physics.* John Wiley.

Klein, B., & Pickett, W. (1984). *Journal of the Less-Common Metals , 103*, 185.

Kohn, W., & Sham, J. (1965). *Phys. Rev. 4A , 140*, A1133.

Kolos, W., & Wolniewicz, L. (1964). *The Journal of Chemical Physics , 41*, 3663.

Kuji, T., Oates, W., Bowerman, B., & Flanagan, T. (1983). *J. Phys. F: Met. Phys. , 13*, 1785.

Lacher, J. (1937). *Proc. R. Soc. Lond. A , 161*, 525.

Lagerquist, A., Neuhaus, H., & Scullman, R. (1964). *Proc. Phys. Soc. , 83*, 498.

Lewis, F. (1967). *The Palladium Hydrogen System.* New York: Academic.

Makrides, A. (1964). *The Journal Physical Chemistry , 68*, 2160.

Malmberg, C., Scullman, R., & Nylen, P. (1969). *Ark. Phys. , 83*, 495.

Martin, R. (2004). *Electronic Structure.* Cambridge University Press.

Matlab. (2011). Mathworks.

McKubre, M., & Tanzella, F. (2006). SRI.

Meng, S., Wang, E., & Gao, S. (2004). *Phys. Rev. B , 69*, 195404.

Michaelides, A., Alavi, A., & King, D. (2003). *J. Am. Chem. Soc. , 125*, 2746.

Michaelides, A., Alavi, A., & King, D. (2004). *Phys. Rev. B , 69*, 113404.

Mitsui, T., Rose, M., Fomin, R., Ogletree, F., & Salmeron, M. (2002). *Science , 297*, 1850.

Mueller, F., Freeman, A., Dimmock, J., & Furdyna, A. (1970). *Phys. Rev. B , 1*, 4617.

Oates, W. (1982). *Journal of the Less-Common Metals , 88*, 411.

Oates, W., & Flanagan, T. (1971). *Solid State Communications , 9*, 1841.

Oates, W., & Flanagan, T. (1981). *Prog. Solid St. Chem , 13*, 193.

Oates, W., & Stoneham, A. (1983). *J. Phys. F.: Met. Phys. , 13*, 2427.

Ogasawara, H., Brena, B., Nordlund, D., Nyberg, M., Pelmenschikov, A., Petterson, L., et al. (2002). *Phys. Rev. Lett. , 89*, 276102.

Powell, G. (1976). *The Journal of Physical Chemistry , 80*, 375.

Purcell. (1985). *Electricity and Magnetism, 2nd Edition.*

Rush, J. (1982). *Proc. Int. Symp. on the Electronic Structures and Properties of Hydrogen in Metals .*

Rush, J., Rowe, J., & Richter, D. (1984). *Z. Phys. B: Condensed Matter , 55*, 283.

Sakamoto, Y., Imoto, M., Takai, K., Yanaru, T., & Ohshima, K. (1996). *J. Phys.: Condens. Matter , 8*, 3229.

Salomons, E. (1990). *J. Phys: Condensed Matter , 2*, 845.

Schirber, J., & Morosin, B. (1975). *Phys. Rev. B , 12*, 117.

Silbey, Alberty, & Bawendi. (2004). *Physical Chemistry.* Wiley.

Simons, J., & Flanagan, T. (1965). *Canadian Journal of Chemistry , 65*, 1665.

Starr, P. (1982). *J. Am. Chem. Soc. , 104*, 4044.

Stern, F., & Sarma, S. (1984). *Phys. Rev. B* , 840.

Thiel, P., & Madey, T. (1987). *Surf. Sci. Rep. , 7*, 211.

Tkacz, M., & Litwiniuk, A. (2002). *Journal of Alloys and Compounds* , 330.

Tripodi. (2000). *Physics Letters A , 276*, 122.

Wallace, D. (1992). *Phys. Rev. B , 46*, 5242.

Wicke, E., & Brodowsky, F. (1978). *Hydrogen in Metals II.*

Wuttig, M. (1974). *Scripta Metallurgica , 8*, 1089.

Zhang, W., Zhang, Z., & Zhang, Z. (2004). *J. Electroanal. Chem , 571*, 81.